RIGA TECHNICAL UNIVERSITY

Armands Maļeckis

JAUNU ANTRONA FLUOROFORU SINTĒZE UN ĪPAŠĪBAS

Promocijas darbs

SYNTHESIS AND PROPERTIES OF NOVEL ANTHRONE FLUOROPHORES

Doctoral Thesis

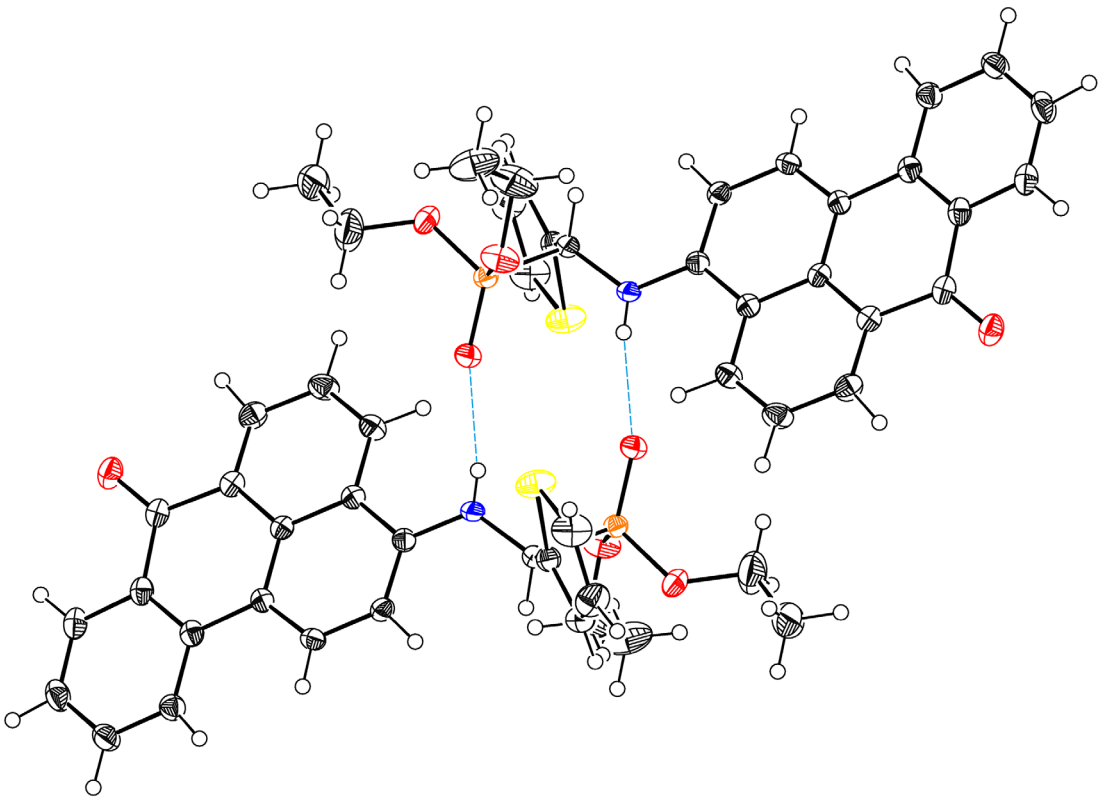

RTU Izdevniecība
RTU Press
Rīga 2025

RĪGAS TEHNISKĀ UNIVERSITĀTE
Dabaszinātņu un tehnoloģiju fakultāte
Ķīmijas un ķīmijas tehnoloģijas institūts

RIGA TECHNICAL UNIVERSITY
Faculty of Natural Sciences and Technology
Institute of Chemistry and Chemical Technology

Armands Maļeckis
Doktora studiju programmas "Ķīmija, materiālzinātne un tehnoloģijas" doktorants
Doctoral Student of the Study Programme "Chemistry, Materials Science and Engineering"

JAUNU ANTRONA FLUOROFORU SINTĒZE UN ĪPAŠĪBAS

Promocijas darbs

SYNTHESIS AND PROPERTIES OF NOVEL ANTHRONE FLUOROPHORES

Doctoral Thesis

Zinātniskā vadītāja / Scientific supervisor
docente, vadošā pētniece / Docent, Senior Researcher *Dr. chem.* JEĻENA KIRILOVA

Konsultants / Consultant
profesors / Professor *Dr. chem.* MĀRIS TURKS

RTU Izdevniecība / RTU Press
Rīga 2025

Maļeckis, A. Jaunu antrona fluoroforu sintēze un īpašības. Promocijas darbs. – Rīga: RTU Izdevniecība, 2025. – 166 lpp.

Maļeckis, A. Synthesis and Properties of Novel Anthrone Fluorophores. Doctoral Thesis. – Riga: RTU Press, 2025. – 166 p.

Iespiests saskaņā ar promocijas padomes "RTU P-01" 2025. gada 13. februāra lēmumu, protokols Nr. 04030-9.1/67.

Published in accordance with the decision of the Promotion Council "RTU P-01" of 13 February 2025, Minutes No. 04030-9.1/67.

Promocijas darbs izstrādāts ar Eiropas Sociālā fonda atbalstu darbības programmas "Izaugsme un nodarbinātība" 8.2.2. specifiskā atbalsta mērķa "Stiprināt augstākās izglītības institūciju akadēmisko personālu stratēģiskās specializācijas jomās" projektā Nr. 8.2.2.0/20/I/008 "Rīgas Tehniskās universitātes un Banku augstskolas doktorantu un akadēmiskā personāla stiprināšana stratēģiskās specializācijas jomās" un Rīgas Tehniskās universitātes Doktorantūras grantu programmas atbalstu.

This work has been supported by the European Social Fund within Project No. 8.2.2.0/20/I/008, "Strengthening of PhD students and academic personnel of Riga Technical University and BA School of Business and Finance in the strategic fields of specialization" of the Specific Objective 8.2.2 "To Strengthen Academic Staff of Higher Education Institutions in Strategic Specialization Areas" of the Operational Programme "Growth and Employment" and by Riga Technical University's Doctoral Grant programme.

PROMOCIJAS DARBS IZVIRZĪTS ZINĀTNES DOKTORA GRĀDA IEGŪŠANAI RĪGAS TEHNISKAJĀ UNIVERSITĀTĒ

Promocijas darbs zinātnes doktora (*Ph. D.*) grāda ķīmijas nozares organiskās ķīmijas apakšnozarē iegūšanai tiek publiski aizstāvēts 2025. gada 17. jūnijā Rīgas Tehniskās universitātes Dabaszinātņu un tehnoloģiju fakultātē, Paula Valdena ielā 3, Rīgā, 272. auditorijā ar attālinātās pieslēgšanās iespēju *Zoom*: https://rtucloud1.zoom.us/j/9352086644.

OFICIĀLIE RECENZENTI

Vadošā pētniece *Dr. chem.* Aiva Plotniece,
Latvijas Organiskās sintēzes institūts, Latvija

Latvijas Zinātņu akadēmijas korespondētājlocekle *Dr. chem.* Māra Jure,
Latvijas Zinātņu akadēmija, Latvija

Asociētais profesors *Dr. chem.* Artis Kinēns,
Latvijas Universitāte, Latvija

APSTIPRINĀJUMS

Apstiprinu, ka esmu izstrādājis šo promocijas darbu, kas iesniegts izskatīšanai Rīgas Tehniskajā universitātē zinātnes doktora (*Ph. D.*) grāda iegūšanai. Promocijas darbs zinātniskā grāda iegūšanai nav iesniegts nevienā citā universitātē.
Armands Maļeckis ……. (paraksts)
Datums: ……

Promocijas darbs ir sagatavots kā tematiski vienotu zinātnisko publikāciju kopa ar kopsavilkumu latviešu un angļu valodā. Tas ietver sešus zinātniskos oriģinālrakstus. Publikācijas zinātniskajos žurnālos uzrakstītas angļu valodā, to kopējais apjoms, ieskaitot pielikumus, ir 328 lpp.

SATURS

Pielikums VI Maļeckis, A.; Cvetinska, M.; Griškjāns, E.; Kirilova, E. Exploring Dual Solvatochromic Traits in Novel Fluorescent Benzanthrone Ethynyl Derivatives. *J. Solution. Chem.* **2024**.

PROMOCIJAS DARBA VISPĀRĒJS RAKSTUROJUMS

Tēmas aktualitāte

Fluorescence notiek, kad viela absorbē gaismu un gandrīz uzreiz to atkal izstaro pie garāka viļņa garuma, parasti dažu nanosekunžu laikā. Šī atkārtoti izstarotā gaisma ir ar mazāku enerģiju nekā absorbētā gaisma, kas izraisa pāreju uz garāku viļņa garumu. Izciliem fluorescējošajiem materiāliem raksturīgas unikālas optiskās īpašības, tiem ir augsti absorbcijas koeficienti efektīvai ierosināšanai, ievērojamas Stoksa nobīdes paaugstinātai jutībai, augsti kvantu iznākumi efektīvai gaismas izstarošanai un augsta fotostabilitāte ilgstošai darbībai, kas ir būtiski tādiem lietojumiem kā bioloģiskā attēlveidošana, diagnostikas testi un optiskie sensori, jo fotodegradācijas procesā veidojas nevēlami blakusprodukti, kas var radīt kļūdas mērījumos un samazināt rezultātu precizitāti un ticamību [1].

Starp daudziem poliaromātiskajiem savienojumiem benzantroni (7*H*-benzo[*de*]antracēn-7-oni) ieņem nozīmīgu vietu krāsvielu rūpniecībā, pateicoties to unikālajām īpašībām un daudzveidīgajām lietošanas iespējām. Šīs antrona krāsvielas izceļas ar efektīvu lādiņa pārnesi, ko veicina mijiedarbība starp elektrondonorajām grupām un elektronakceptoro karbonilgrupu aromātiskajā struktūrā. Pateicoties spēcīgajam slāpekļa elektrondonorajam efektam, šī mijiedarbība ir īpaši izteikta slāpekli saturošajos atvasinājumos. Tāpēc 3-aminoaizvietotie benzantroni ir izpelnījušies ievērojamu uzmanību un ir plaši pētīti. Piemēram, nukleofīlās aizvietošanas reakcijās, kurās iesaistīti 3-nitrobenzantrons un 3-brombenzantrons ar pirmējiem un otrējiem alifātiskajiem amīniem, tiek iegūti aizvietoti 3-aminobenzantroni. Pētījumi liecina, ka šie savienojumi ir piemēroti polimēru masveida krāsošanai, šķidro kristālu sistēmu ražošanai un uzrāda nelineārās optiskās (NLO) īpašības [2]–[5]. Papildus tam imīni, kas sintezēti 3-aminobenzantrona kondensācijas reakcijā ar piemērotiem aromātiskiem aldehīdiem, ir efektīvi dažādu metālu katjonu noteikšanai, tos var izmantot arī šķidro kristālu sistēmās un polimēros kā fluorescējošas krāsvielas un spilgtinātājus [6]–[9]. Kad šie imīni tiek reducēti ar $NaBH_4$, veidojas amīni, kuriem ir vēl izteiktāka luminiscence nekā sākotnējiem imīniem [10], [11]. 3-Aminobenzantrona acilēšana ar hloroacetilhlorīdu, kam seko hlora atoma nukleofīlā aizvietošana ar amīniem, radot trešējos amīnus vai amonija savienojumus, kas ir ideāli piemēroti dažādiem sensoru lietojumiem [12]–[14]. Līdzīgi, amidinoatvasinājumi ir plaši pētīti un sintezēti, izmantojot Vilsmeijera-Hāka tipa reakciju [15]. Šie solvatohromie savienojumi galvenokārt tiek izmantoti konfokālajā lāzera skenēšanas mikroskopijā (KLSM) bioloģiskiem paraugiem [16], [17]. Aromātiskās aizvietošanas reakcijās 3-brombenzantrons ar spirtiem rada fluorescējošus 3-oksibenzantronus, kas tāpat kā amīni un imīni ir piemēroti polimēru un šķidro kristālu sistēmām [18]. 3-Brombenzantrona Bakvalda-Hartviga aminēšanas reakcijā ar aromātiskiem amīniem, piemēram, fenoksazīnu un fenotiazīnu, tika iegūti savienojumi ar emisiju dziļi sarkanajā/tuvā infrasarkanajā reģionā un termiski aktivētu aizkavēto fluorescenci, kas der izgatavošanai ierīcēm ar kvantitatīvām skābekļa noteikšanas spējām gaisā [19]. Karbazola atvasinājumi savukārt izceļas ar pašregulējošu mehanohromismu, kas palielina to daudzveidību dažādos modernajos lietojumos [20].

Kopumā plašā benzantronu un to atvasinājumu izpēte ne tikai attēlo to iespējamo lietojumu dažādās nozarēs, bet arī izgaismo ceļu, kā attīstīt fluorescences tehnoloģijas un tās daudzveidīgos lietojumus, sākot no materiālzinātnes līdz biomedicīnas pētījumiem.

Pētījuma mērķis un uzdevumi

Promocijas darba mērķis bija jaunu benzantrona un antrahinona atvasinājumu sintēzes metožu izstrāde un to luminiscento īpašību un potenciālo lietojumu izpēte.

Tika definēti šādi uzdevumi:

1) izpētīt jaunu benzantrona un antrahinona atvasinājumu sintēzes metodes, izmantojot nukleofīlo aromātisko aizvietošanu, Kabačnika-Fīldsa un Sonogaširas reakcijas, paplašinot fluorescējošo savienojumu kopu;
2) iegūt absorbcijas un emisijas spektrus dažādos šķīdinātājos, izvērtēt molārās ekstinkcijas koeficientus, Stoksa nobīdes un fluorescences kvantu iznākumus iegūto krāsvielu fotofizikālo īpašību visaptverošai izpētei;
3) pamatojoties uz fotofizikālajiem parametriem, izvērtēt potenciālos lietojumus.

Zinātniskā novitāte un galvenie rezultāti

Iepriekšējie pētījumi par benzantrona savienojumiem lielākoties bija veltīti aizvietotu 3-aminobenzantrona atvasinājumu analīzei. Šajā darbā apskatīta citu heteroatomu papildu funkcionālo grupu ievades un konjugācijas virknes pagarināšanas ietekme uz šo savienojumu īpašībām, kas līdz šim nebija izpētīta.

Promocijas darbā, pirmkārt, tika ietverta aizvietotu 3-amino-9-nitrobenzantrona atvasinājumu sintēze; uzmanība tika pievērsta tam, kā papildu elektronakceptorā grupa ietekmē molekulu uzvedību gaismas absorbcijas un izstarošanas procesos. Papildus tika pētīta un salīdzināta jaunu α-aminofosfonātu, kas iegūti no 1-aminoantrahinona un 3-aminobenzantrona, sintēze un īpašības, izpētot to potenciālo bioloģisko aktivitāti un fotofizikālos parametrus. Turklāt pētījumā tika izstrādāta alkil- un aril-3-tiobenzantronu sintēzes metode un izpētīti iegūto savienojumu raksturlielumi, kas atspoguļo to luminiscentās īpašības un struktūras. Visbeidzot, tika pētīta 3-alkinilbenzantronu sintēze un īpašības, mērķējot uz to fluorescences īpašību uzlabošanu.

Kopumā pētījums veicina jaunu antronu atvasinājumu struktūras un īpašību attiecību izpratni un apskata to potenciālo lietojumu tādās jomās kā bioattēlveidošana, nelineārā optika un fluorescences tehnoloģijas.

Darba struktūra un apjoms

Promocijas darbs ir sagatavots kā tematiski saistītu zinātnisko publikāciju kopa, kas veltīta benzantronu un antrahinonu funkcionalizācijai un to fotofizikālo īpašību analīzei. Promocijas darbā apkopoti seši zinātniskie oriģinālraksti.

Darba aprobācija un publikācijas

Promocijas darba galvenie rezultāti publicēti sešos zinātniskajos oriģinālrakstos. Pētījumu rezultāti prezentēti starptautiskajās konferencēs.

Zinātniskās publikācijas

1. **Maļeckis, A.**; Griškjāns, E.; Cvetinska, M.; Savicka, M.; Belyakov, S.; Kirilova, E. Synthesis, Characterization, Spectroscopic Studies and Evaluation of Toxicological Effect on Growth of Wheat Sprouts (*Triticum Aestivum*) of New Benzanthrone α-Aryl-α-Aminophosphonates. *J. Mol. Struct.* **2023**, *1277*, 134838. https://doi.org/10.1016/j.molstruc.2022.134838.
2. **Maļeckis, A.**; Cvetinska, M.; Griškjāns, E.; Mežaraupe, L.; Kirjušina, M.; Pavlova, V.; Kirilova, E. Novel Anthraquinone α-Aryl-α-Aminophosphonates: Synthesis, Spectroscopy and Imaging by Confocal Laser Scanning Microscopy of Trematode *Opisthioglyphe Ranae*. *J. Photochem. Photobiol. A Chem.* **2023**, *444*, 114918. https://doi.org/10.1016/j.jphotochem.2023.114918.
3. **Maļeckis, A.**; Cvetinska, M.; Puckins, A.; Osipovs, S.; Sirokova, J.; Belyakov, S.; Kirilova, E. Synthesis and Properties of New 3-Heterylamino-Substituted 9-Nitrobenzanthrone Derivatives. *Molecules* **2023**, *28* (13), 5171. https://doi.org/10.3390/molecules28135171.
4. **Maļeckis, A.**; Cvetinska, M.; Griškjāns, E.; Dmitrijevs, K.; Traskovskis, K.; Belyakov, S.; Kirilova, E. Benzanthrone Sulfides: Synthesis, Solvatochromism Characterization and Analysis of Experimental Photophysical Parameters and Theoretical Calculations. *Dyes and Pigments* **2023**, *219*, 111599. https://doi.org/10.1016/j.dyepig.2023.111599.
5. **Maļeckis, A.**; Cvetinska, M.; Kirjušina, M.; Mežaraupe, L.; Kecko, S.; Gavarāne, I.; Kiyan, V.; Lider, L.; Pavlova, V.; Savicka, M.; Belyakov, S.; Kirilova, E. A Comparative Study of New Fluorescent Anthraquinone and Benzanthrone α-Aminophosphonates: Synthesis, Spectroscopy, Toxicology, X-Ray Crystallography, and Microscopy of *Opisthorchis Felineus*. *Molecules* **2024**, *29* (5), 1143. https://doi.org/10.3390/molecules29051143.
6. **Maļeckis, A.**; Cvetinska, M.; Griškjāns, E.; Kirilova, E. Exploring Dual Solvatochromic Traits in Novel Fluorescent Benzanthrone Ethynyl Derivatives. *J. Solution. Chem.* **2024**. https://doi.org/10.1007/s10953-024-01363-x.

Citas tēmai atbilstošas publikācijas, kas nav iekļautas promocijas darbā

1. **Maļeckis, A.**; Griškjāns, E.; Cvetinska, M.; Kirilova, E. 3-(Phenylethynyl)-7H-Benzo[de]Anthracen-7-One. *Molbank* **2022**, *2022* (3), M1442. https://doi.org/10.3390/M1442.
2. Olipova, M.; **Maleckis, A.**; Puckins, A.; Kirilova, A.; Romanovska, E.; Kirilova, E. Spectroscopic Investigation of New Benzanthrone Luminescent Dyes. *Bulgarian Chemical Communications* 2022, 54 (3), 253–257. https://doi.org/10.34049/bcc.54.3.F006.

Konferences, kurā prezentēti pētījumu rezultāti

1. Kirilova, J.; **Maleckis, A.**; Puckins, A.; Kirilova, A.; Grigorjeva, T. (2022). Spectroscopic Investigation of New Benzanthrone Luminescent Dyes. *8th International Conference on New Trends in Chemistry*, Istanbul, Turkey, p. 57. https://icntcconference.com/wp-content/uploads/2024/06/ICNTC-2022-ABSTRACT-BOOK.pdf.
2. Sirokova, J.; **Maleckis, A.**; Kirilova, J. (2023). Effect of the Nitro Group on Nucleophilic Substitution in Benzanthrone. *The 65th International Scientific Conference of Daugavpils University*, Daugavpils, Latvia, p. 21. https://dukonference.lv/files/Tezes_65.konf_publicesanai_gala_versija.pdf.
3. **Maļeckis, A.**; Griškjāns, E.; Cvetinska, M.; Kirilova, E. (2023). Synthesis and Examination of Photophysical Properties of Benzanthrone Ethynyl Derivatives. *The 65th International Scientific Conference of Daugavpils University*, Daugavpils, Latvia, p. 23. https://dukonference.lv/files/Tezes_65.konf_publicesanai_gala_versija.pdf.
4. Kirilova, J.; Savicka, M.; Kirilova, A.; **Maleckis, A.**; Grigorjeva, T. (2023). Study of the Toxicity of Benzanthrone Luminescent Dyes. *9th International Conference On New Trends in Chemistry*, Istanbul, Turkey, p. 43. https://icntcconference.com/wp-content/uploads/2024/06/9th-ICNTC-BOOK-OF-ABSTRACTS.pdf.
5. **Maļeckis, A.**; Kirilova, E. (2024). Advancements in Fluorescent α-aminophosphonates. *The 66th International Scientific Conference Of Daugavpils University*, Daugavpils, Latvia, p. 13. https://dukonference.lv/files/Tezes_66_konf_2024_gala.pdf.

PROMOCIJAS DARBA GALVENIE REZULTĀTI

Antronu atvasinājumi ir kļuvuši ievērojami ar savām izcilajām luminiscentajām īpašībām un regulējamu fluorescences emisiju, kas ļauj tos izmantot dažādās jomās. Atzīstot to potenciālu, pēdējos gados ir pieaudzis pētījumu skaits, kas vērsti uz antronu atvasinājumu sintēzi un funkcionalizēšanu. Šī pieaugošā interese izriet no vajadzības izpētīt jaunas molekulārās struktūras ar uzlabotām optiskajām īpašībām specifiskiem nolūkiem, lai apmierinātu mainīgos tehnoloģiskos un zinātniskos izaicinājumus. Līdz ar to bija nepieciešami papildu pētījumi, lai noskaidrotu antrona atvasinājumu struktūru un īpašību sakarības un izstrādātu efektīvas sintētiskās stratēģijas, lai paplašinātu to lietojamību, atklātu pilnu antronu atvasinājumu potenciālu un veicinātu inovācijas fluorescences materiālzinātnē.

Promocijas darba galvenais mērķis ir jaunu benzantrona un antrahinona fluoroforu sintēze, papildināta ar plašiem fotofizikālo īpašību mērījumiem un to potenciālo lietojumu noteikšanu.

1. Aizvietotu 3-amino-9-nitrobenzantronu sintēze un īpašības

Benzantrona krāsvielām novērotā fluorescence galvenokārt rodas ierosinātā stāvoklī iekšmolekulārās lādiņa pārneses (ILP) dēļ. Tas notiek, pateicoties mijiedarbībai starp elektrondonorām grupām un elektronakceptoro karbonilgrupu benzantrona aromātiskajā sistēmā (D-π-A arhitektūras tips). Ievērības cienīgi ir aizvietotie 3-aminobenzantrona atvasinājumi, kas demonstrē nelineārās optiskās īpašības [21]; ar nitrogrupas pievienošanu būtiski uzlabojot to nelineārās optiskās (NLO) īpašības [22]. Tādēļ bija interesanti izpētīt papildu elektronakceptoras grupas ietekmi uz aizvietoto 3-aminobenzantrona atvasinājumu fotofizikālajām īpašībām.

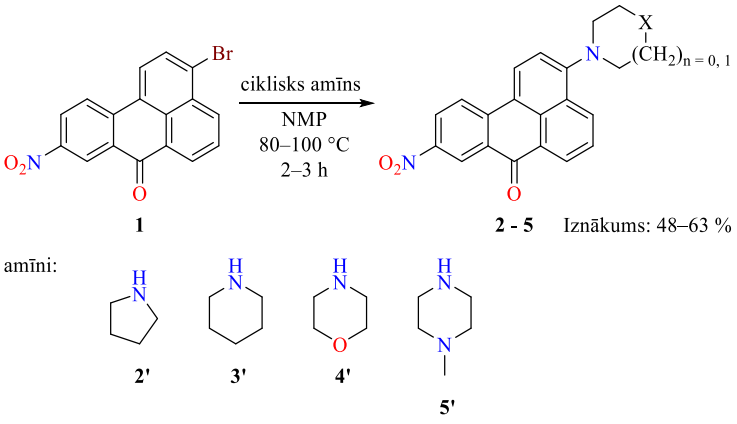

1. shēma. Aizvietotu 3-amino-9-nitrobenzantrona atvasinājumu **2**–**5** sintēze.

Šim mērķim komerciālais 3-brombenzantrons tika nitrēts ar nitrējošo maisījumu (HNO_3/H_2SO_4 (4:1/ v:v)) ledus etiķskābē saskaņā ar iepriekš publicētu pētījumu, lai elektrofīlās aizvietošanās reakcijā iegūtu savienojumu **1** [23], kas pēc tam stājās sekojošā nukleofīlās aromātiskās aizvietošanas reakcijā ar cikliskiem amīniem 1-metilpirolidīn-2-onā (NMP), kā parādīts 1. shēmā. Salīdzinot ar atbilstošo aizvietošanas reakciju nenitrētam 3-brombenzantronam, kur reakcija norit amīnos bez papildu šķīdinātāja, broma atomu aizvietošana nitroatvasinājumā **1** notiek zemākā temperatūrā (80–100 °C pret 86–138 °C) un ātrāk (2–3 stundas pret 8 stundām). Paaugstinātā reaģētspēja izriet no spēcīgā elektronakceptorā nitrogrupas rakstura, kas ievērojami samazina elektronu blīvumu benzantrona *C*(3) atoma pozīcijā, veicinot nukleofīlo uzbrukumu. Tā rezultātā mērķproduktu **2**–**5** iznākumi bija vidēji par 10 % augstāki, salīdzinot ar analogiem savienojumiem bez nitrogrupas [2]. Šie iegūtie savienojumi cietā stāvoklī ir tumši sarkanā krāsā un izrāda intensīvu luminiscenci šķīdumos.

Šo savienojumu struktūras tika apstiprinātas un noraksturotas, izmantojot Furjē transformācijas infrasarkano spektroskopiju (*FTIR*), ^{1}H, ^{13}C kodolu magnētiskās rezonanses (KMR) spektroskopiju, 2D-KMR (*COSY* un *HSQC*) spektroskopiju un augstas izšķirtspējas masas spektrometriju. Papildus tam, izmantojot lēnās iztvaicēšanas tehniku, tika iegūti savienojumu **2** un **3** kristāli. Rentgenstaru kristalogrāfiskās analīzes rezultātā tika novērota ūdeņraža saišu klātbūtne abos savienojumos un π–π mijiedarbības, kas noved pie molekulu pakošanos (1. un 2. attēls). Rentgenstaru kristalogrāfiskā analīze visiem šajā darbā minētajiem savienojumiem tika veikta sadarbībā ar *Dr. sc. phys.* Sergeju Beļakovu.

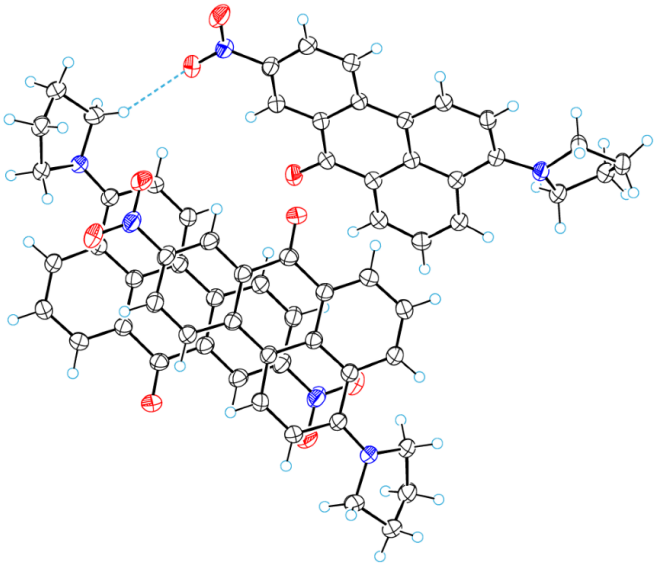

1. attēls. Savienojuma **2** molekulu pakojums kristālā ar N–O···H–C ūdeņraža saitēm.

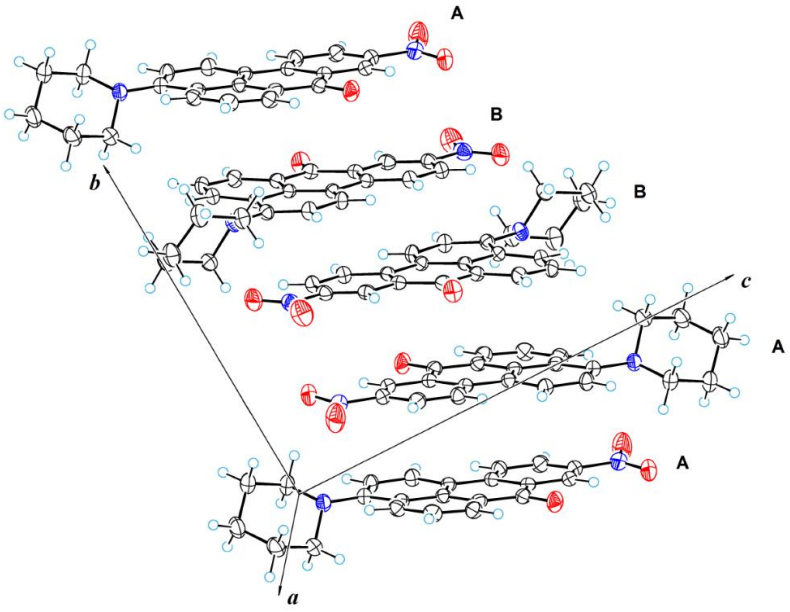

2. attēls. Savienojuma **3** molekulārā sakārtojuma perspektīvais skats.

Iegūtajām krāsvielām ir izcilas luminiscences īpašības dažādos organiskajos šķīdinātājos. Saistībā ar faktu tika pētītas sintezēto atvasinājumu fotofizikālās īpašības, iegūstot absorbcijas un emisijas spektrus septiņos organiskajos šķīdinātājos (benzolā, etilacetātā (EtOAc), hloroformā ($CHCl_3$), acetonā, etanolā (EtOH), *N*,*N*-dimetilformamīdā (DMF) un dimetilsulfoksīdā (DMSO)) ar plašu polaritāšu variāciju (1. tabula). Iegūtie spektrālie dati apkopoti 1. un 2. tabulā, 3. attēlā vizuāli parādīti savienojuma **3** UV–Vis absorbcijas un fluorescences emisijas spektri dažādos organiskajos šķīdinātājos.

1. tabula

Izmantoto šķīdinātāju empīriskās polaritātes vērtības $E_T(30)$ [24]; savienojumu **2**–**5** absorbcijas maksimumi (nm) un molārās absorbcijas koeficientu logaritmiskās vērtības organiskajos šķīdinātājos (koncentrācija 10^{-5} M)

Šķīdinātājs	$E_T(30)$	Absorbcija λ_{abs}, nm; (lgε)			
		2	**3**	**4**	**5**
Benzols	34,3	498 (3,94)	460 (4,55)	447 (4,47)	453 (4,26)
EtOAc	38,1	493 (3,92)	459 (4,53)	447 (4,49)	454 (4,15)
Hloroforms	39,1	505 (4,01)	474 (4,62)	449 (4,56)	462 (4,26)
Acetons	42,2	512 (4,08)	467 (4,51)	448 (4,60)	462 (4,11)
Etanols	51,9	526 (3,97)	471 (4,50)	449 (4,49)	455 (3,99)
DMF	43,2	519 (4,18)	475 (4,50)	460 (4,54)	467 (4,17)
DMSO	45,1	531 (4,06)	478 (4,49)	466 (4,43)	472 (4,11)

2. tabula

Savienojumu **2**–**5** emisijas maksimumi (nm) un Stoksa nobīdes organiskajos šķīdinātājos (koncentrācija 10^{-5} M)

Šķīdinātājs	Emisija λ_{em}, nm un Stoksa nobīdes, cm^{-1}							
	2		**3**		**4**		**5**	
Benzols	584	2957	578	4438	570	4564	574	4653
Hloroforms	613	3489	606	4596	592	4827	598	4923
EtOAc	598	3562	598	5064	592	5380	592	5135
Acetons	621	3428	620	5284	612	5479	612	5305
Etanols	661	3882	661	6103	652	5981	645	6474
DMF	630	3395	632	5230	624	6935	622	5336
DMSO	641	3231	643	5368	650	5713	634	5413

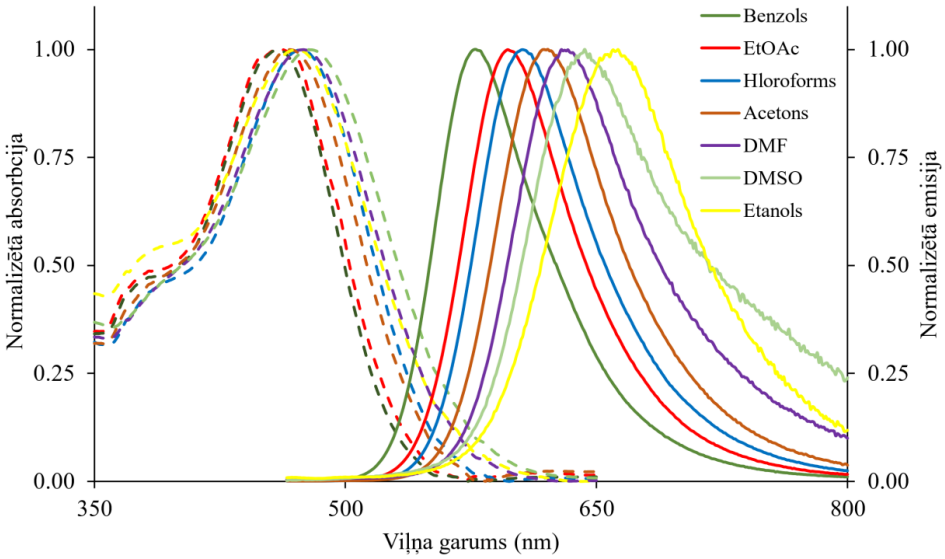

3. attēls. Savienojuma **3** normalizēti UV-Vis absorbcijas un fluorescences emisijas spektri dažādos organiskajos šķīdinātājos.

Atvasinājums **2** absorbē gaismu 498–531 nm diapazonā un parāda batohromo nobīdi par 33 nm, skatot no nepolārā benzola uz polāro DMSO, savukārt amīni **3** un **5** absorbē īsākā viļņu garuma diapazonā, precīzi, 453–478 nm, un parāda mazāku batohromo nobīdi, kas ir 18–19 nm.

Iepriekš iegūtais nenitrētais pirolidīna atvasinājums demonstrē absorbciju visplašākajā viļņu garuma spektrā (525–558 nm), salīdzinot ar visiem pārējiem pētītajiem savienojumiem [3]. Iepriekšējā gadījumā stiprāka mijiedarbība starp donoru un akceptoru grupām izraisa elektroniskās pārejas enerģijas pazemināšanos un lādiņa pārneses palielināšanos pēc fotona absorbcijas. Savienojuma **2** absorbcijas joslas hipsohromā nobīde un absorbcijas maksimālās vērtības samazināta jutība pret šķīdinātāja polaritāti liecina par intramolekulārās lādiņa

pārneses (ILP) rakstura samazināšanos elektroniskajā pārejā. Tādējādi elektronegatīvās nitrogrupas iekļaušana molekulā rada konkurenci starp šo aizvietotāju un molekulas karbonilgrupu, kas rezultējās jaunā elektronu blīvuma sadalījumā pamata stāvoklī.

Salīdzinot ar nenitrētajiem amīniem, savienojumi **2**–**5** uzrāda stiprāku absorbciju; vidējais lgε ir 4,30 savienojumiem **2**–**5**, savukārt nenitrētajiem analogiem tas ir ap 4,19. Sintezēto atvasinājumu luminiscences maksimālās vērtības batohromā nobīde (no benzola uz DMSO) ir līdzīga nenitrēto atvasinājumu batohromajai nobīdei – 60–85 nm.

Nitrētie savienojumi **2** un **3** parāda absorbcijas maksimālās vērtības nobīdi uz garākiem viļņu garumiem, kas ir no 15 nm līdz 35 nm, salīdzinot ar to nenitrētajiem analogiem, tomēr to emisijas maksimālās vērtības parāda nobīdi uz īsākiem viļņu garumiem, kas ir no 3 nm līdz 14 nm, salīdzinot ar monoaizvietoto atvasinājumu luminiscences spektriem. Rezultātā nitrēto atvasinājumu spektru Stoksa nobīdes ir samazinātas, salīdzinot ar nenitrēto atvasinājumu nobīdēm.

2. Benzantrona α-aminofosfonātu sintēze un īpašības

α-Aminofosfonāti ir analogi aminoskābēm ($N\text{-}C\text{-}PO_3H_2$ un $N\text{-}C\text{-}CO_2H$ strukturālie fragmenti attiecīgi) un tādējādi uzrāda dažādas bioloģiskās aktivitātes, jo spēj inhibēt fermentus, kas iesaistīti aminoskābju metabolismā, darbojoties kā antagonisti [25]. Tāpēc jauni α-aminofosfonāti tiek pētīti kā potenciālie antibiotiskie [26], pretsēnīšu [27] un ķīmijterapeitiskie līdzekļi [28], herbicīdi [29] un neiromodulatori [30]. Papildus tam šos savienojumus var potenciāli izmantot kā antioksidantus [31], sorbentus [32], [33], korozijas inhibitorus [34] un smērvielu piedevas [35].

Lai gan α-aminofosfonātu atvasinājumiem ir plašas lietojuma iespējas, šādi fluorescējoši savienojumi ir maz pētīti, pētījumi ir veikti tikai ar benzola, naftalīna, antracēna un pirēna atvasinājumiem [36]–[40].

Ņemot vērā iepriekš minēto, tika secināts, ka ir nepieciešams sintezēt un izpētīt 3-aminobenzantrona α-aril-α-aminofosfonātu atvasinājumu īpašības.

Sintētiski α-aminofosfonāti parasti tiek iegūti Kabačnika-Fīldsa reakcijā. Tā ir savienošanās reakcija starp karbonilsavienojumu – ketonu vai aldehīdu, amīnu un fosfonātu (saukts arī par fosfītu) (2. shēma). Kopš šīs sintētiskās pieejas atklāšanas ir ieviestas vairākas modifikācijas, kurās izmanto katalizatorus, dehidratējošos aģentus, jonu šķidrumus un mikroviļņu starojumu [41]. Vispirms sākotnējais savienojums **6** tika sintezēts, reducējot 3-nitrobenzantronu ar nātrija sulfīdu, kas savukārt tika iegūts, nitrējot komerciāli pieejamo benzantronu, kā aprakstīts iepriekšējos pētījumos [42]. Tad tika izvēlēta ērtākā un efektīvākā metode – vienpakāpes reakcija bez katalizatora un atsevišķa šķīdinātāja. Dialkilfosfonāts tiek izmantots gan kā reaģents, gan kā šķīdinātājs. 120 °C temperatūrā reakcijas rezultātā tika iegūti oranžas – sarkanas krāsas savienojumi ar 55–81 % iznākumu (3. shēma). Tādējādi tika iegūti 22 savienojumi – neliela bibliotēka (3. tabula), rezultātā izpētot gan aromātiskā aizvietotāja rakstura (ar elektronakceptorām un elektrondonorām grupām dažādās pozīcijās benzola gredzenā un citas dabas aizvietotāju – 2-tienilatvasinājumus) pie alfa oglekļa, gan fosfonāta grupas aizvietotāju (metil-, etil- un izopropil-) ietekmi uz jauno benzantrona fluoroforu īpašībām.

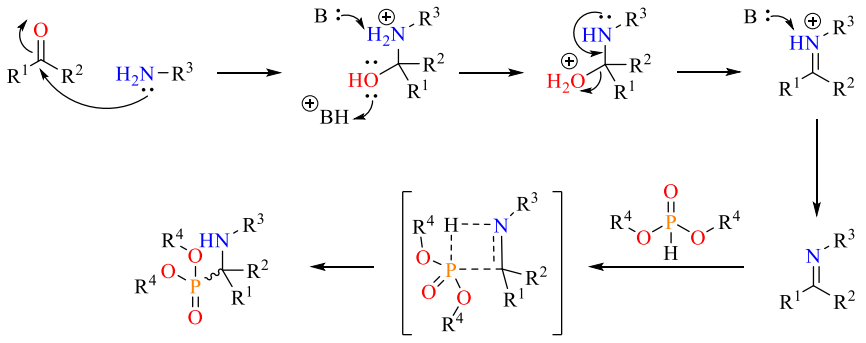

2. shēma. Piedāvātais Kabačnika-Fīldsa reakcijas mehānisms [43].

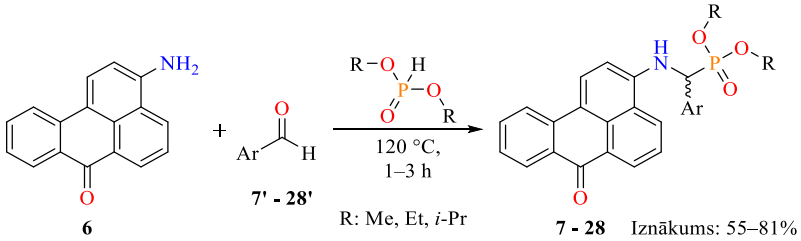

3. shēma. Benzantrona α-aminofosfonātu **7** – **28** atvasinājumu sintēze.

3. tabula

Iegūto savienojumu **7**–**28** struktūras.

R \ Ar	C_6H_5-	C_6H_4-(4-Me)	C_6H_4-(4-F)	C_6H_4-(4-Cl)	C_6H_4-(4-Br)	C_6H_4-(4-SMe)	C_6H_4-(4-OMe)	C_6H_4-(2-OMe)	C_6H_3-(3-CN-4-F)	2-tienil
Me	**7**	**8**	**9**	**10**	**11**	**12**	**13**	**14**	**15**	**16**
Et	**17**	**18**	**19**	**20**	–	–	–	**21**	–	**22**
i-Pr	**23**	**24**	**25**	–	–	–	**26**	**27**	–	**28**

FTIR, ^{1}H-, ^{13}C- un ^{31}P-KMR spektri un masas spektrometriskā analīze apstiprina iegūto savienojumu struktūras. Benzantrona α-aminofosfonātu rentgenstaru kristalogrāfiskais pētījums papildus sniedza ieskatu šo savienojumu molekulārajā izkārtojumā un starpmolekulārajās mijiedarbībās kristāliskajā stāvoklī (4.–7. attēli). Visu molekulu struktūrās ir asimetrisks oglekļa atoms, tomēr to kristālstruktūras ir ahirālas, tādēļ šie savienojumi ir īsti racemāti. Savienojuma **17** kristālstruktūrā starp benzantrona sistēmām pastāv spēcīgas π-π mijiedarbības. Savukārt savienojumu **22** un **23** kristālstruktūrās pastāv spēcīgas starpmolekulāras NH···O tipa saites. Savienojums **11** izceļas ar spēcīgu iekšmolekulāru NH···O ūdeņraža saiti starp aminogrupu un dimetilfosfonātu, kas veido papildu pieclocekļu ciklu.

Savienojumu **7**–**17** un **23** absorbcijas un emisijas spektri tika iegūti šķīdinātājos ar dažādu polaritāti, lai izpētītu iegūto savienojumu fotofizikālās īpašības. Visas pārbaudītās krāsvielas uzrādīja fluorescenci un nozīmīgu solvatohromisko uzvedību, izstarojot gaismu no zaļas heksānā līdz sarkanai etanolā. Fenilgrupas aizvietotāji, aromātiskā aizvietotāja daba (fenil- vai tienil-) pie α-oglekļa, kā arī fosfonāta alkilgrupu veids (metil-, etil- vai izopropil-) kopumā neietekmē iegūto hromoforu fotofizikālās īpašībās. Pirmais izņēmums ir savienojums **23** ar apjomīgām izopropilgrupām – tā nedaudz paaugstinātie molārie absorbcijas koeficienti (4,60 (benzolā) un 4,65 (DMSO), logaritmiskā vērtība), salīdzinot ar savienojumiem **7** (4,10 (benzolā), 4,08 (DMSO)), **17** (4,05 (benzolā) un 4,03 (DMSO)), liecina par izteiktāku elektromagnētiskā starojuma absorbciju. Otrs izņēmums ir savienojums **15** ar spēcīgām elektronakceptorām grupām pie benzola gredzena, kas samazina ekstinkcijas koeficientus un

kvantu iznākumus. Kā piemēru izmantojot savienojumu **11**, ir novērots, ka benzantrona α-aminofosfonāti šķīdumos uzrāda plašas joslas absorbciju aptuveni starp 458 nm un 500 nm un emisiju no 534 nm (heksānā) līdz 636 nm (etanolā) (8. attēls), kas attiecīgi rezultējas 42 nm un 102 nm batohromiskās nobīdēs. Tas liecina, ka polaritātes efekts uz fluorescenci ir izteiktāks nekā uz absorbciju. Lielākā Stoksa nobīde 4963 cm^{-1} starp pārbaudītajām krāsvielām tika novērota savienojumam **16** etanolā. Iepriekš pētīti benzantrona amidīni absorbē diapazonā no 410 nm līdz 495 nm [15], [44], absorbējot īsāku viļņu garumu apgabalā. Savukārt 3-aizvietoto benzantrona aminoatvasinājumu absorbcija ir diapazonā no 430 nm līdz 520 nm [2], [10], absorbējot garāku viļņu garumu apgabalā. Tādējādi benzantrona aminogrupa, kurai pievienota fosforilgrupa (savienojumi **7**–**28**), izrāda nedaudz vājāku donorefektu nekā alkilaminogrupa, bet spēcīgāku nekā amidinogrupa.

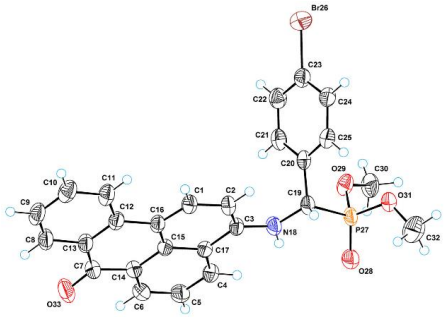

4. attēls. Savienojuma **11** *ORTEP* diagramma. Monoklīnā singonija.

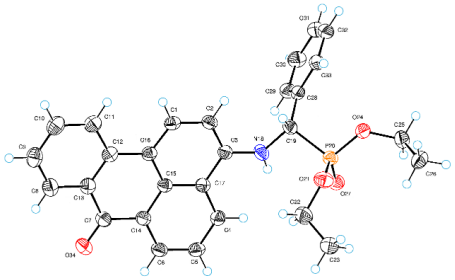

5. attēls. Savienojuma **17** *ORTEP* diagramma. Rombiskā singonija.

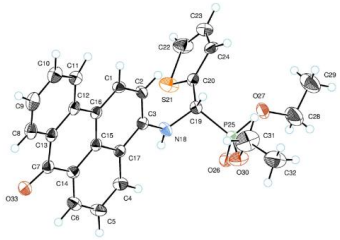

6. attēls. Savienojuma **22** *ORTEP* diagramma. Monoklīnā singonija.

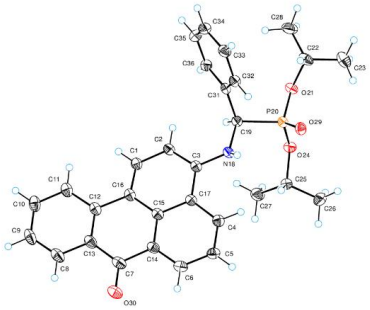

7. attēls. Savienojuma **23** *ORTEP* diagramma. Triklīnā singonija.

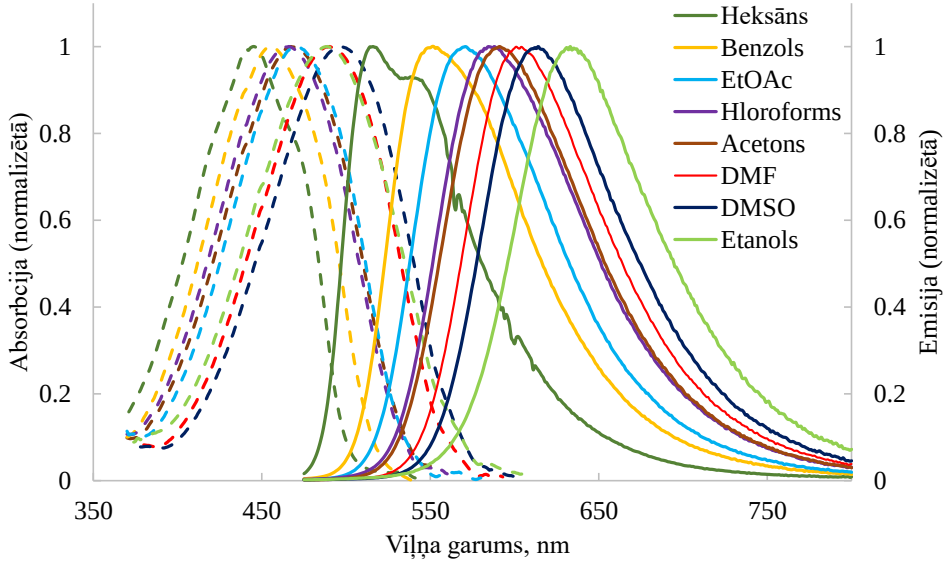

8. attēls. Savienojuma **11** normalizēti UV-Vis absorbcijas un fluorescences emisijas spektri dažādos organiskajos šķīdinātājos.

Izmantojot luminiscējošas krāsvielas, kas jutīgas uz vides polaritāti, bioloģisko sugu iekrāsošana konfokālajā lāzera skenējošajā mikroskopijā kļūst arvien efektīvāka. Fosforilgrupas klātbūtne molekulā palielina savienojumu lipofilitāti, tādējādi uzlabojot to spēju saistīties ar audiem, tāpēc benzantrona krāsvielas **12** un **15** tika izmantotas trematodes *Opisthorchis felineus* parazīta bioattēlošanai (9. attēls). Šīs sugas parazītu izpēte un analīze ir svarīga, jo tie inficē dažādu zīdītāju, tostarp cilvēku, aknas [45].

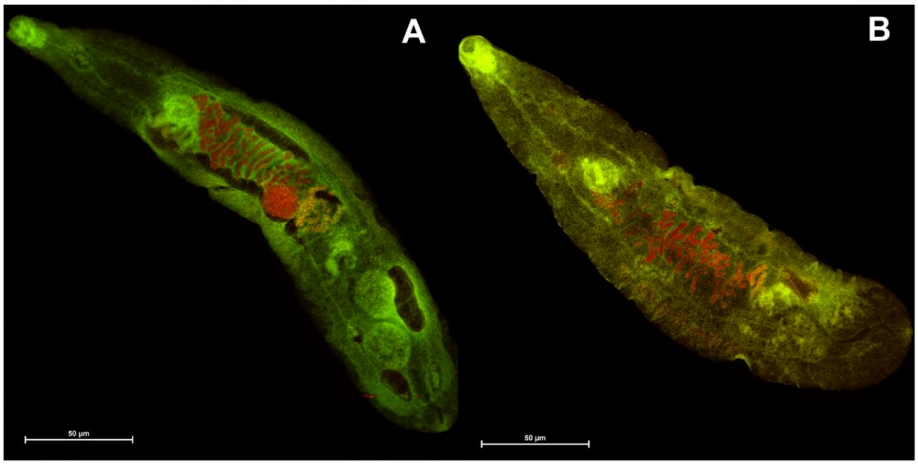

9. attēls. Pieaugušais *Opisthorchis felineus*, kas iekrāsots ar pētītajām krāsvielām: (A) – **12**; (B) – **15**.

Lai novērtētu iegūto savienojumu toksicitāti un aromātiskā aizvietotāja pie α-oglekļa atoma ietekmi, tika veikti kviešu dīgstu morfoloģijas, elektrolītu noplūdes, malondialdehīda un pigmentu kvantificēšanas eksperimenti. Tika izmantoti savienojumi ar vienādiem fosfonātgrupas aizvietotājiem (R = Me) un dažādām aromātiskajām grupām (Ar) – fenilgrupa bez aizvietotājiem (**7**), fenilgrupa ar halogēna atomu, bromu, para-pozīcijā (**11**) un tienilgrupu (**16**). Kopumā benzantrona α-aminofosfonāti uzrāda dažāda līmeņa toksisko efektu – fitotoksicitāte svārstās no 37 % (**7**) līdz 83 % (**16**) atkarībā no koncentrācijas un aromātiskā aizvietotāja pie α-oglekļa atoma. Parazītisko sugu iekrāsošana un toksikoloģija tika veikta sadarbībā ar Daugavpils Universitātes Dzīvības zinātņu un tehnoloģiju institūta pētniekiem.

Termiskā stabilitāte nosaka, vai savienojums var ilgtermiņā izturēt praktiskajā lietojumā nepieciešamos temperatūras apstākļus. Tā tika pārbaudīta, izmantojot savienojuma **17** piemēru, izmantojot diferenciālo termisko analīzi (DTA) un termogravimetrijas (TG) metodi. Saskaņā ar TG līkni termiskā degradācija notiek divos galvenajos posmos – starp 270–330 °C (rezultējoties aptuveni 20 % masas zudumā) un starp 630–950 °C (rezultējoties aptuveni 30 % masas zudumā). Kopumā analizējamais savienojums uzrāda termisko stabilitāti līdz aptuveni 270 °C, kad paraugs zaudē 5 % no sākotnējās masas un tā stabilitāte ir salīdzināma ar iepriekš pētītajiem benzantrona aminoatvasinājumiem. Lai izvērtētu aizvietotāju ietekmi uz savienojumu termisko stabilitāti, pētījumu būtu vērts turpināt.

3. Antrahinona α-aminofosfonātu sintēze un īpašības

Ņemot vērā ierobežoto pētījumu skaitu par fluorescentajiem α-aminofosfonātu atvasinājumiem, tika pieņemts lēmums spert soli tālāk un iegūt antrahinona savienojumus, lai tos salīdzinātu ar līdzīgiem benzantrona savienojumiem. Antrahinona atvasinājumi ir plaši pētīti kā fluorescenti sensori [46], emiteri un šūnu attēlveidošanas aģenti [47], [48]. Atsevišķiem antrahinona atvasinājumiem piemīt medicīniskas īpašības – antibiotiskās, antiparazitārās, insekticīdās, fungicīdās un pretvīrusu; tos var izmantot arī kā ķīmijterapijas līdzekļus [49], [50]. Antrahinona α-aminofosfonāti līdz šim nebija iegūti. Sintēze (4. shēma) tika veikta benzantroniem (2. nodaļa) identiskos apstākļos. Sintezēto savienojumu struktūras apkopotas 4. tabulā.

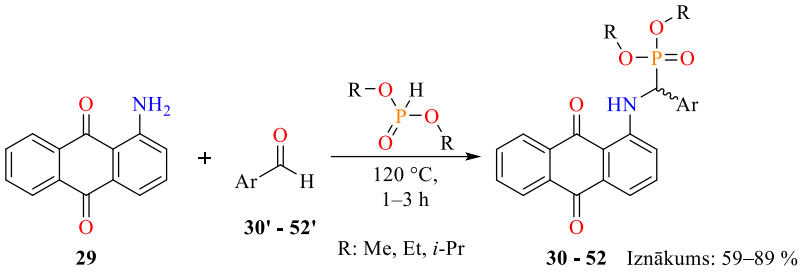

4. shēma. Antrahinona α-aminofosfonātu **30** – **52** atvasinājumu sintēze.

4. tabula

Iegūto savienojumu **30**–**52** struktūras

R \ Ar	C_6H_5-	C_6H_4-(4-Me)	C_6H_4-(4-F)	C_6H_4-(4-Cl)	C_6H_4-(4-Br)	C_6H_4-(4-SMe)	C_6H_4-(4-OMe)	C_6H_4-(2-OMe)	C_6H_3-(3-CN-4-F)	2-tienil
Me	**30**	**31**	**32**	**33**	**34**	**35**	**36**	**37**	**38**	**39**
Et	**40**	**41**	**42**	**43**	–	–	**44**	**45**	–	–
i-Pr	**46**	**47**	**48**	**49**	–	–	**50**	**51**	–	**52**

Šķīdumos antrahinona α-aril-α-aminofosfonāti absorbē gaismu ar maksimumiem ap 465–488 nm ar nelielu batohromo nobīdi no benzola uz DMSO šķīdumu (5–8 nm) pretstatā neaizvietotajam savienojumam **29**, kuram absorbcijas maksimuma batohromā nobīde starp heksāna un etanola šķīdumiem ir 30 nm. Visi pētītie savienojumi fluorescē. Emisijas spektru maksimumi ir no 585 nm (EtOAc) līdz 628 nm (DMSO), sasniedzot fluorescences batohromo nobīdi līdz pat 30 nm. Šķīdinātāja polaritātes efekts uz fluorescenci ir daudz izteiktāks nekā uz absorbciju. Var secināt, ka šķīdinātāja polaritātes ietekme uz absorbcijas un emisijas viļņu garuma maksimumiem ir izteiktāka benzantrona savienojumiem **7**–**28**. Novērojams ir arī tas, ka fluorescences kvantu iznākumi ir augstāki analogiem benzantrona savienojumiem **11**, **12** un **15** (0,10–0,57) nekā antrahinona atvasinājumiem **34**, **35** un **38** (< 0,01–0,14).

Lai iegūtu dziļāku izpratni par jauno krāsvielu fotostabilitāti, tika veikts fotoizbalēšanas tests vielas etanola šķīdumam (koncentrācija 10^{-4} M). Lai noskaidrotu fosfonātgrupas aizvietotāju R ietekmi uz savienojumu fotostabilitāti, eksperiments tika veikts savienojumiem ar metil- (**30**), etil- (**40**) un izopropilgrupām (**46**) un vienu un to pašu aromātisko aizvietotāju (fenilgrupu) pie α-oglekļa atoma. Rezultāti tika salīdzināti ar izejvielas, 1-aminoantrahinona (**29**) un plaši izmantotas testēšanas krāsvielas fluoresceīna (FL) fotostabilitātes datiem (11. attēls). Pēc četru stundu apstarojuma fluoresceīns saglabāja 71 % no sākotnējās absorbcijas, savukārt savienojums **30** saglabāja tikai 27 %. Savienojumi ar etil- (**40**) un izopropilgrupām (**46**) uzrādīja visaugstāko fotostabilitāti ar absorbcijas samazinājumu par 40 %. Šie rezultāti liecina, ka sintezētās krāsvielas uzrāda lielāku fotostabilitāti, salīdzinot ar neaizvietotu amīnu **29**.

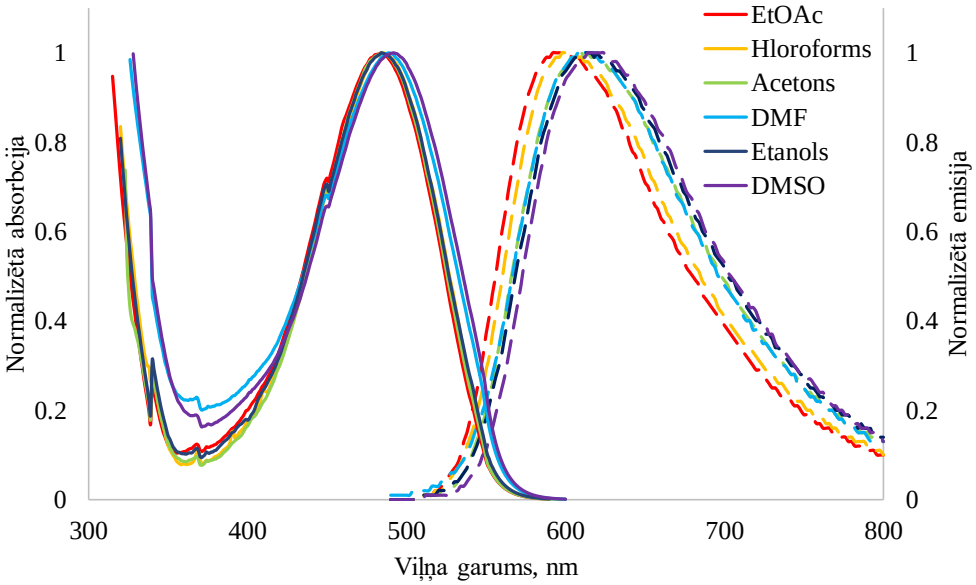

10. attēls. Savienojuma **49** normalizēti UV-Vis absorbcijas un fluorescences emisijas spektri dažādos organiskajos šķīdinātājos.

Antrahinona α-aril-α-aminofosfonāti ar elektrondonoro grupu pie benzola gredzena (4-tiometil-) **35** un stiprām elektronakceptorām grupām (3-ciāno-4-fluor-) **38** tika lietoti parazīta *Opisthorchis felineus* iekrāsošanai (12. attēls). Pamatojoties uz sākotnējiem datiem, benzantrona krāsvielas **12** un **15** ar tiem pašiem aizvietotājiem attiecīgi nodrošināja nedaudz skaidrāku parazīta struktūras un muskulatūras vizualizāciju. Tādējādi var secināt, ka benzantrona krāsvielas **12** un **15** ir efektīvākas *Opisthorchis felineus* parazītu vizualizēšanai nekā antrahinona krāsvielas **35** un **38**. To var izskaidrot ar lipofīlāku benzantrona dabu, kas būtiski ietekmē šo bioloģisko objektu vizualizāciju. Krāsviela **49** tika izmantota arī tāpēc, lai iekrāsotu Eirāzijā izplatītu dzīvnieku parazītu – *Opisthioglyphe ranae* [51] (13. attēls). Kopumā

visas pārbaudītās krāsvielas – **12**, **15**, **35**, **38** un **49** – uzrādīja labus sākotnējos rezultātus un ir piemērotas detalizētai un ātrai bioattēlu iegūšanai.

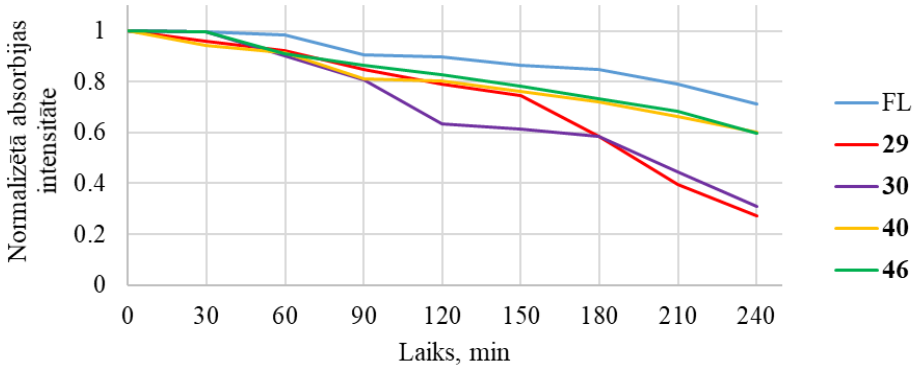

11. attēls. Normalizētas absorbcijas intensitātes atkarība no apstarošanas laika pie 365 nm fluoresceīnam (FL) un savienojumiem **29**, **30**, **40** un **46**.

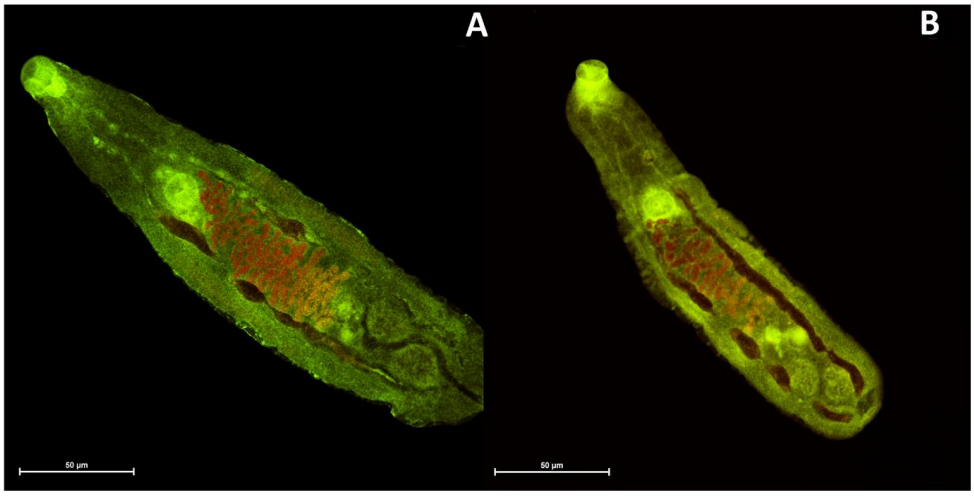

12. attēls. Pieaugušais *Opisthorchis felineus*, kas iekrāsots ar krāsvielām: (A) – **35**; (B) – **38**.

13. attēls. Pieaugušais *Opisthioglyphe ranae*, kas iekrāsots ar krāsvielu **49**.

4. 3-Tiobenzantronu sintēze un īpašības

Lai sasniegtu darba mērķi, pēc slāpekli saturošo antrona atvasinājumu īpašību analīzes pētījumi tika turpināti ar citu heteroatomu ieviešanu benzantrona molekulā. Sēru saturošie savienojumi ir ieguvuši ievērojamu uzmanību zinātnieku aprindās. Nesenajos pētījumos īpaša uzmanība bija pievērsta pirēna sulfīdiem un sulfoksīdiem [52], savienojumiem ar ditiofulvēna grupām [53], 1,5-bis-(4-alkilfeniltio)antrahinona krāsvielām ar potenciālu lietojumu šķidro kristālu sistēmās [54], [55], kā arī triarilciklopentadiēna savienojumiem, kas iekļauj tiofēna un dibenzotiofēna grupas [56]. Šo un līdzīgu sēru saturošu savienojumu sintēzes un lietojuma iespējas tika detalizēti apkopotas nesen publicētā rakstā [57]. Iepriekš iegūtie benzantrona savienojumi, kas satur sēru ir 3-merkaptobenzantrons [58], 14*H*-antra[2,1,9-*mna*]tioksantēn-14-ons ar pusvadītāja īpašībām [59] un fenotiazīnaizvietots benzantrona atvasinājums ar termiski aktivētu atliktu fluorescenci [19]. Slāpekli un skābekli saturoši benzantrona savienojumi ar elektrondonorām grupām ir plaši raksturoti un aprakstīti literatūrā, un ir pierādīts, ka tiem ir izcilas luminiscentās īpašības [18]. Savukārt, ņemot vērā ierobežoto pieejamo informāciju par benzantrona sēru un selēnu saturošiem savienojumiem, tika nolemts pievērsties benzantrona tioalkil-, tiofenil- un selanilfenilatvasinājumu sintēzei un analīzei.

Iepriekš daudzos apskatrakstos plaši tika apspriesta alifātisko un aromātisko sulfīdu sintēze un šīs nukleofīlās aromātiskās aizvietošanas reakcijas mehānisms [60]–[62]. Šajā pētījumā tika ieviesta praktiska pieeja, lai sintezētu benzantronu sulfīdus **54**–**62** (5. tabula), izmantojot nukleofīlo aromātisko aizvietošanas reakciju, kuras pamatā ir 3-brombenzantrons kā elektrofīlā izejviela un alifātiskie dažāda telpiskā apjomīguma tioli un aromātiskie tioli ar elektrondonorām un elektronakceptorām grupām kā nukleofīli.

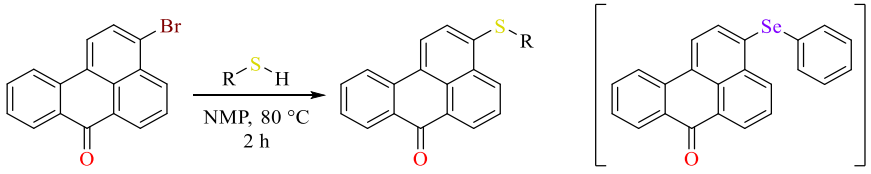

53 **54 - 62** **63**

Iznākums: 59–86 % Iznākums: 60 %

5. shēma. Benzantrona tioatvasinājumu **54** – **62** sintēze un savienojuma **63** struktūra.

5. tabula

Iegūto savienojumu **54**–**62** struktūru kopsavilkums

R	Me	*i*-Pr	cikloheksil	*t*-Bu	-$(CH_2)_2$-Ph	C_6H_5-	C_6H_4-(4-Me)	C_6H_4-(4-F)	C_6H_4-(4-OMe)
Nr.	**54**	**55**	**56**	**57**	**58**	**59**	**60**	**61**	**62**

Reakcijas tika veiktas bāziskos apstākļos (NaOH) *N*-metil-2-pirolidonā (NMP) (5. shēma). Papildus tam analoģiski bez bāzes klātbūtnes tika iegūts 3-(fenilselanil)-7*H*-benzo[*de*]antracēn-7-ons (**63**), kā nukleofīlu izmantojot nātrija benzoselenolātu. Teorētiski alifātiskie tioli ar lielāku telpisko apjomīgumu būtu mazāk reaģētspējīgi stērisku traucējumu dēļ; aromātisko tiolu gadījumā ar elektrondonorām grupām būtu sagaidāma lielāka reaģētspēja lielākas nukleofilitātes dēļ nekā ar elektronakceptorām [63], taču sakarība starp izejvielu struktūrām un to reaģētspēju netika novērota.

FTIR, ^{1}H- un ^{13}C-KMR spektri un augstas izšķirtspējas masas spektrometriskā analīze apstiprināja iegūto savienojumu ķīmiskās struktūras. Kā aizvietotu 3-aminobenzantronu kristālu struktūrās, arī savienojumā **55** starp benzantrona sistēmām ir π-π paketēšanas mijiedarbības un ūdeņraža saites (14. attēls).

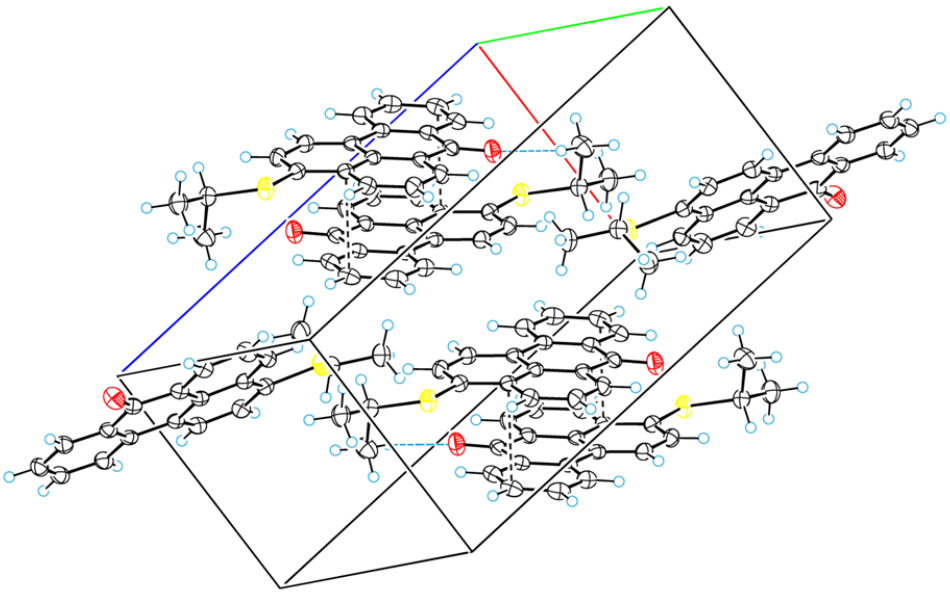

14. attēls. Molekulu paketēšana savienojuma **55** elementāršūnā ar saīsinātu starpmolekulāro saskarsmi.

Tioatvasinājumu ar alifātisko aizvietotāju (R = Me) **54** un aromātisko aizvietotāju (R = C_6H_5-) **59**, kā arī 3-(fenilselanil)benzantrona **63** fotofizikālie parametri apkopoti 6. tabulā. Benzantrona alkil- un arilsulfīdi, kā arī 3-(fenilselanil)benzantrons šķīdumos uzrāda absorbcijas joslas ar maksimumiem no 403 nm līdz 448 nm un to garāko viļņu nobīdi no 10 nm līdz 20 nm starp maksimumiem benzolā un DMSO. Salīdzinot ar absorbciju, šķīdinātāju polaritātes ietekme uz vielu emisijas spektru maksimumiem ir izteiktāka. Gan alkil-, gan arilsulfīdi izstaro gaismu pēc ierosināšanas no aptuveni 507 nm benzolā līdz 591 nm etanolā (15. attēls). Sēra atomu aizstājot ar lielāku selēna atomu, novērojama neliela emisijas batohromā nobīde; nedaudz palielinās arī Stoksa nobīdes, savukārt ekstinkcijas koeficienti un absorbcijas maksimumi lielā mērā paliek nemainīgi. Visaugstākais fluorescences kvantu iznākums visiem

pētītajiem savienojumiem tika novērots hloroformā. Precīzi, 3-(metiltio)benzantrons uzrādīja visaugstāko emisijas iznākumu (0,31–0,52), tam seko 3-(feniltio)benzantrons ar nedaudz zemāku iznākumu (0,08–0,24), savukārt 3-(fenilselanil)benzantrons bija ar viszemāko emisijas iznākumu (0,001–0,07). Šī tendence, visticamāk, ir saistīta ar lādiņa pārneses efektivitātes samazināšanos dotajā secībā.

6. tabula

Savienojumu **54**, **59** un **63** (koncentrācija 10^{-5} M) absorbcijas spektru maksimumi un molārās absorbcijas koeficientu logaritmiskās vērtības, fluorescences spektru maksimumi, Stoksa nobīdes vērtības, fluorescences kvantu iznākumu vērtības (Φ_F) un fluorescences dzīves laika (τ) vērtības organiskajos šķīdinātājos

Nr.	Šķīdinātājs	Absorbcija λ_{abs}, nm; (lgε)	Emisija λ_{em}, nm	Stoksa nobīde, cm^{-1}	Φ_F	τ, ns
54	Benzols	429 (4,18)	508	3625	0,31	3,5
	$CHCl_3$	444 (4,16)	533	3761	0,52	10,0
	DMF	446 (4,06)	552	4306	0,40	10,7
	EtOH	448 (4,15)	587	5286	0,32	10,6
59	Benzols	413 (4,16)	504	4372	0,08	2,3
	$CHCl_3$	421 (4,18)	538	5166	0,24	9,3
	DMF	417 (4,15)	541	5497	0,14	5,6
	EtOH	423 (4,09)	583	6488	0,11	7,1
63	Benzols	416 (4,14)	510	4431	0,05	1,0
	$CHCl_3$	423 (4,14)	543	5224	0,07	3,7
	DMF	419 (4,11)	562	6073	0,001	–[a]
	EtOH	423 (4,04)	595	6834	0,001	–[a]

[a] Vērtību nav iespējams noteikt zemas fluorescences intensitātes dēļ.

Iepriekš analizētie benzantrona amidīni absorbē pie 410–495 nm [15], [44], savukārt 3-aizvietoto benzantrona amīni absorbē pie 430–520 nm [2], [10]. Runājot par benzantrona 3-metoksi- un 3-fenoksiatvasinājumiem, to absorbcijas spektru maksimumi svārstās no 417 nm līdz 436 nm [18]. Kopumā sēra un selēna atvasinājumos gan emisijas, gan absorbcijas maksimumi ir nobīdīti uz īsāku viļņu pusi, kas liecina par nedaudz vājāku donora efektu, salīdzinot ar slāpekli un skābekli saturošiem savienojumiem, ko apstiprina arī Hammeta aizvietotāju konstantes, kas aminogrupai (-NH_2) ir −0,66, hidroksilgrupai (-OH) −0,37, tiolgrupai (-SH) −0,10 un selenolgrupai (-SeH) −0,05 [64]. Iegūto atvasinājumu fotofizikālās īpašības pārsvarā tomēr ir līdzīgas iepriekš pētītajiem benzantrona savienojumiem. Iegūto fluoroforu ILP raksturs un nanosekunžu mēroga gaismas izstarošanas process liecina par fluorescences emisijas mehānismu.

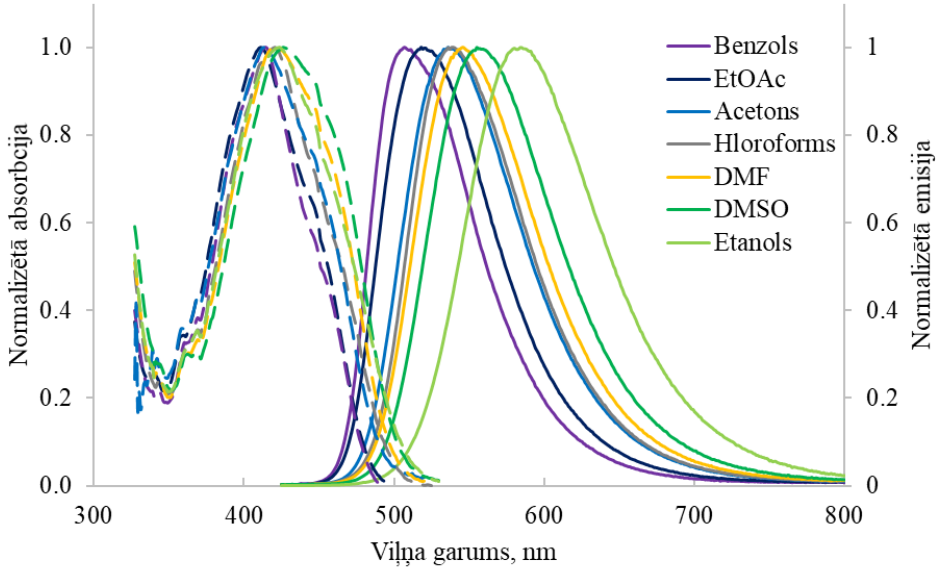

15. attēls. Savienojuma **59** normalizēti UV-Vis absorbcijas un fluorescences emisijas spektri dažādos organiskajos šķīdinātājos.

5. 3-Alkinilbenzantronu sintēze un īpašības

Vēl viens svarīgs paņēmiens fluoroforu modifikācijai papildus iepriekš aplūkotajām funkcionālo grupu un heteroatomu ieviešanas metodēm ir konjugētās sistēmas pagarināšana molekulā.

Vairāki teorētiskie un praktiskie pētījumi liecina, ka fenilacetilēngrupu tieša pievienošana luminiscentām molekulām maina to fotofizikālās īpašības un uzlabo fluorescences raksturlielumus. Kā piemēru var minēt pirēna [65], karbazola [66], antrahinona [67], naftalimīda [68] un hinoliniltiazola [69] atvasinājumus. Šāda veida savienojumus var lietot sensoru tehnoloģijās, organisko gaismu izstarojošo diožu ražošanā un fluorescentajai iezīmēšanai [70]–[72]. Turklāt pētījumi liecina, ka elektrondonoru vai elektronakceptoru grupu ievadīšana fenilacetilēna molekulā un π-konjugācijas garuma pielāgošana var mainīt fluorescences iznākumu, Stoksa nobīdes lielumu, kā arī absorbcijas un emisijas maksimumus [73], tāpēc tika nolemts veikt iepriekš neizpētītu benzantrona alkīnu sintēzi un analīzi.

Runājot par palādija katalizētajām reakcijām, patlaban vienīgās literatūrā aprakstītās metodes jaunu benzantrona atvasinājumu sintēzei ir arilcianēšana un Bakvalda-Hartviga aminēšanas reakcijas [19], [74]. Sonogaširas reakcija, kas pirmo reizi tika aprakstīta 1975. gadā, ir sametināšanas reakcija, ko izmanto alkīnu sintēzei. Reakcija norit vairākos posmos, sākot ar palādija katalizatora oksidatīvo pievienošanos aril- vai vinilhalogenīdam un beidzot ar vēlamā alkīna produkta izdalīšanos reduktīvās eliminēšanās rezultātā. Vara(I) līdzkatalizators ir būtisks, lai veicinātu transmetalēšanās posmu [75], [76]. Šie apstākļi tika izmantoti, lai sintezētu savienojumus **64**–**68** (7. tabula) no 3-brombenzantrona (**53**) *N*,*N*-dimetilacetamīdā, kā bāzi lietojot trietilamīnu (6. shēma). Lai noskaidrotu aizvietotāju R rakstura ietekmi uz savienojumu īpašībām, sintēze tika veikta ar terminālajiem alkīniem, kas satur dažāda spēka elektrondonorās un elektronakceptorās grupas.

Sonogaširas reakcijā produkti rodas, izveidojoties jaunajai C-C saitei starp diviem kovalentajiem ligandiem reduktīvās eliminēšanās rezultātā. Ir zināms, ka reduktīvā eliminēšanās norit lēnāk elektronu bagātos kompleksos nekā elektronu nabadzīgos [77]. Tāpēc varēja sagaidīt augstākus reakciju iznākumus ar alkīniem, kas satur elektronakceptorās grupas, tomēr korelācija starp substrātu struktūrām un reakciju iznākumiem nepastāv.

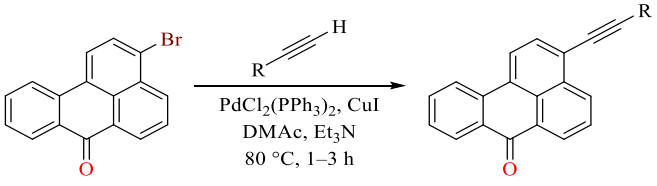

53 **64 - 69** Iznākums: 43–89 %

6. shēma. Benzantrona alkinilatvasinājumu **64**–**69** sintēze.

7. tabula

Iegūto savienojumu **64**–**69** struktūras

R	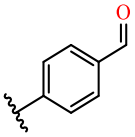	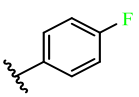	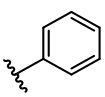	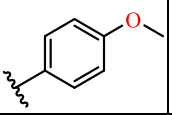	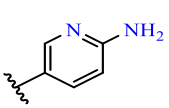	
Nr.	**64**	**65**	**66**	**67**	**68**	**69**

8. tabula

Savienojumu **64**–**69** absorbcijas spektru maksimumi (nm) un molārās absorbcijas koeficientu logaritmiskās vērtības organiskajos šķīdinātājos (koncentrācija 10^{-5} M)

Šķīdinātājs	Absorbcija λ_{abs}, nm; (lgε)				
	64	**65**	**67**	**68**	**69**
Benzols	416 (4,65)	423 (4,55)	427 (4,51)	432 (4,32)	423 (4,24)
EtOAc	412 (4,68)	416 (4,56)	425 (4,51)	437 (4,29)	419 (4,29)
$CHCl_3$	420 (4,72)	425 (4,52)	436 (4,46)	438 (4,49)	427 (4,22)
Acetons	414 (4,65)	419 (4,55)	432 (4,49)	445 (4,41)	419 (4,27)
DMF	419 (4,71)	423 (4,58)	437 (4,48)	455 (4,54)	422 (4,25)
DMSO	422 (4,68)	435 (4,50)	440 (4,42)	462 (4,55)	424 (4,26)
Etanols	430 (4,25)	429 (4,57)	442 (4,45)	446 (4,36)	419 (4,19)

9. tabula

Savienojumu **64**–**69** emisijas spektru maksimumi (nm) un Stoksa nobīdes vērtības organiskajos šķīdinātājos (koncentrācija 10^{-5} M)

Šķīdinātājs	Emisija λ_{em}, nm un Stoksa nobīde, cm^{-1}				
	64	**65**	**67**	**68**	**69**
Benzols	463 (2440)	466 (2181)	502 (3499)	530 (4280)	482 (2894)
$CHCl_3$	462 (2627)	473 (2897)	510 (3922)	576 (5522)	479 (2990)
EtOAc	479 (2933)	498 (3449)	534 (4209)	574 (5409)	491 (3053)
Acetons	475 (3102)	492 (3541)	565 (5449)	641 (6871)	488 (3375)
DMF	481 (3076)	497 (3520)	553 (4800)	691 (7506)	495 (3495)
DMSO	489 (3247)	506 (3226)	570 (5183)	720 (7756)	494 (3342)
Etanols	515 (3838)	531 (4478)	598 (5902)	701 (8156)	495 (3664)

Visas pētītās krāsvielas ir fluorescentas un uzrāda ievērojamu solvatohromisko efektu (8. un 9. tabula). 16. attēlā redzami savienojuma **67** normalizēti UV–Vis absorbcijas un fluorescences emisijas spektri dažādos organiskos šķīdinātājos. Benzantrona alkīni šķīdumos uzrāda divas absorbcijas joslas ap 310–330 nm un 420–450 nm ar batohromo nobīdi 12–30 nm garo viļņu absorbcijas joslā starp maksimumiem benzolā un DMSO. Šķīdinātāju polaritātes ietekme uz fluorescenci ir izteiktāka nekā uz absorbciju. Sintezētie savienojumi ir fluorescējoši ar emisiju no 462 nm (**64**, EtOAc) līdz 701 nm (**68**, EtOH). Iegūtie savienojumi uzrāda divkāršu solvatohromismu – ne tikai katra atsevišķa savienojuma emisijas maksimums ir atkarīgs no šķīdinātāja polaritātes, bet pastāv arī ievērojama korelācija starp aizvietotāju elektronisko dabu

un fotofizikālajiem parametriem; elektronakceptorie aizvietotāji nobīda emisiju hipsohromi, bet spēcīgi elektrondonorie aizvietotāji – batohromi tajā pašā šķīdinātājā (17. attēls). Elektrondonoru un elektronakceptoru grupu daba ietekmē pētīto vielu emisijas efektivitāti. Atvasinājumiem ar elektronakceptorām grupām (**64** un **65**) etanolā ir augstāks fluorescences kvantu iznākums (0,67 un 0,74 attiecīgi), salīdzinot ar mazāk polāriem šķīdinātājiem (0,01–0,41). Pretstatā tam atvasinājumi ar donorām grupām intensīvāk luminiscē hloroformā nekā etanolā. Savukārt trimetilsililgrupas klātbūtne izraisa ievērojamu emisijas efektivitātes samazinājumu. Fotofizikālo parametru izmaiņas ietekmē arī Stoksa nobīdes vērtības. Stoksa nobīžu diapazons svārstās no 2181 cm^{-1} savienojumam **65** mazāk polārā šķīdinātājā (benzols) līdz 8156 cm^{-1} savienojumam **68** polārā etanolā. Tādējādi elektrondonorā aizvietotāja klātbūtne izraisa lielāku Stoksa nobīdi.

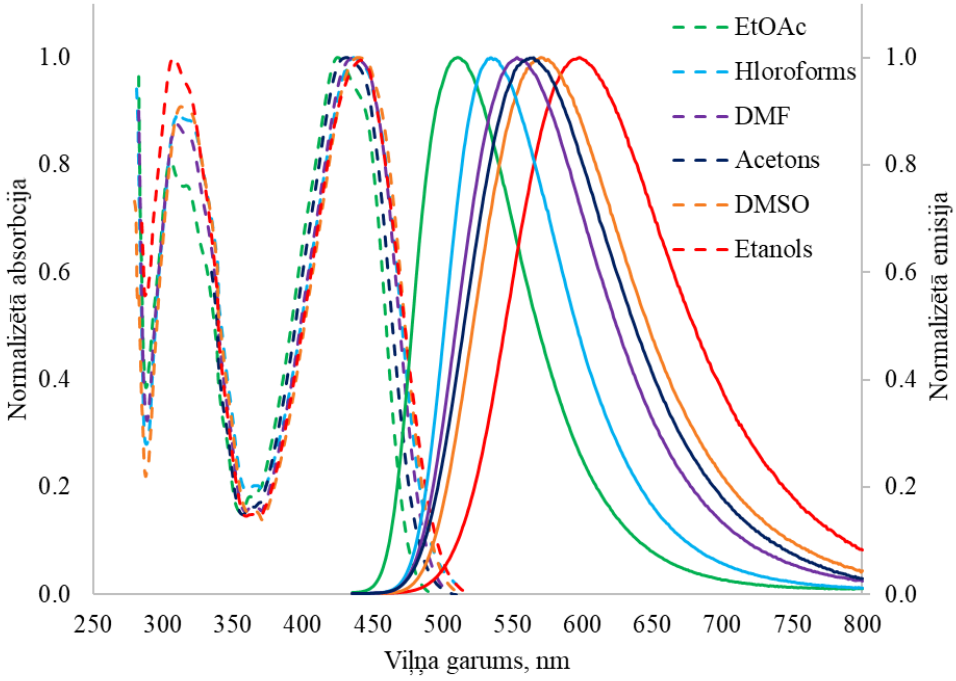

16. attēls. Savienojuma **67** normalizēti UV-Vis absorbcijas un fluorescences emisijas spektri dažādos organiskajos savienojumos.

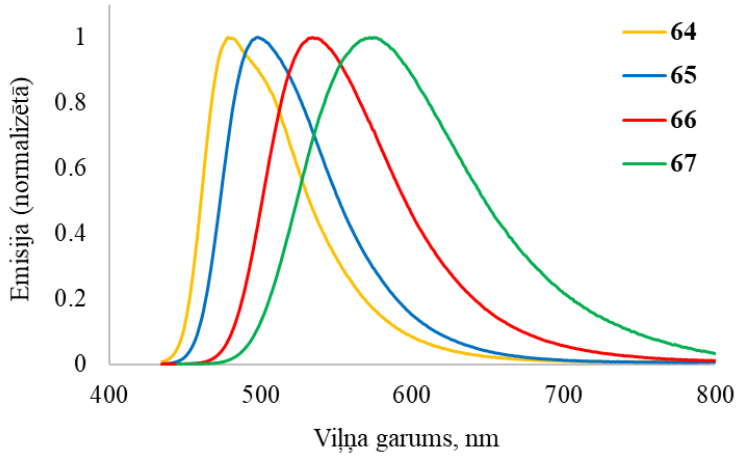

17. attēls. Savienojumu **64**–**67** normalizēti fluorescences emisijas spektri hloroforma šķīdumā.

Lai novērtētu krāsvielu **64**–**69** fotostabilitāti, sintezēto atvasinājumu fotoizbalēšanās process tika veikts etanolā (koncentrācijā 10^{-4} M) un salīdzināts ar plaši izmantoto testa krāsvielu fluoresceīnu. Rezultāti apkopoti 18. attēlā. Pēc četru stundu ilgas apstarošanas fluoresceīna absorbcija bija 71 % no sākotnējā līmeņa. Starp sintezētajiem savienojumiem visaugstāko fotostabilitāti uzrādīja atvasinājums **65**, saglabājot 96 % no sākotnējās absorbcijas. Tam sekoja savienojums **64** ar fotostabilitāti 82 %. Savukārt atvasinājums **67** parādīja viszemāko stabilitāti, zaudējot vairāk nekā pusi no savas absorbcijas intensitātes (57 %) eksperimenta beigās. Šie rezultāti liecina, ka trīs no sintezētajām vielām – **64**, **65** un **69** – uzrāda lielāku fotostabilitāti nekā fluoresceīns.

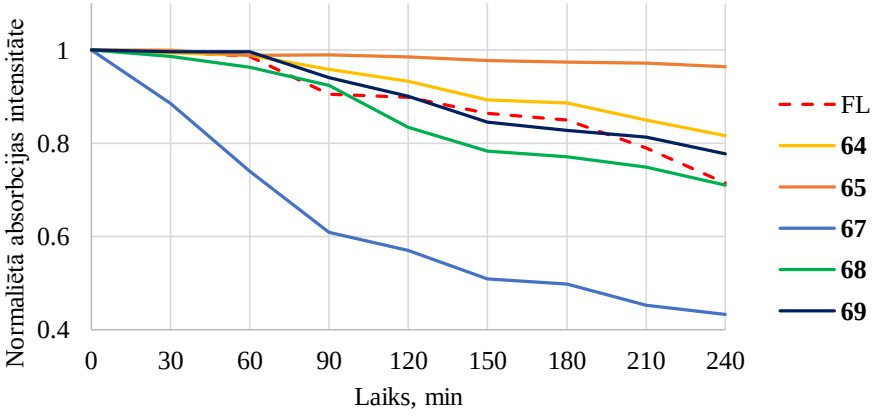

18. attēls. Fluoresceīna (FL) un savienojumu **64**–**69** normalizētās absorbcijas intensitātes atkarība no apstarošanas laika pie 365 nm viļņa garuma.

Ņemot vērā dažu benzantronu pierādītās nelineārās optiskās īpašības un izpratni, ka π-konjugācijas pagarināšana var uzlabot šīs īpašības, nelineāro optisko īpašību noteikšanai patlaban tiek pētīti gan šie benzantrona alkīni, gan savienojumi, kas nav apskatīti šajā darbā; atvasinājumi, kas iegūti reakcijā ar 4-etinil-*N*,*N*-dimetilanilīnu, 1-etinil-4-(trifluormetil)benzolu, 3-etiniltiofēnu un metilpropiolātu.

Darba rezultātā tika paplašināta benzantrona un antrahinona fluorescējošo savienojumu kopa. Stoksa nobīdes atkarība no absorbcijas maksimuma acetonā darbā izpētītajiem savienojumiem redzama 19. attēlā. Benzantrona un antrahinona aminoatvasinājumiem raksturīga absorbcija un arī emisija pie garākiem viļņiem, kas ļauj tos lietot mikroskopijā bioloģisko objektu iekrāsošanai, jo tiek samazināta paraugu autofluorescence un panākts palielināts attēlu kontrasts. Tioalkil- un tiofenilaizvietotājiem ir vājāks elektrondonorais efekts, kas palielina nepieciešamo enerģiju benzantrona pārējai ierosinātā stāvoklī. Lai gan kopumā benzantrona tioatvasinājumiem ir lielākas Stoksa nobīdes (no 4089 cm^{-1} līdz 6052 cm^{-1}) nekā α-aminofosfonātiem (no 3798 cm^{-1} līdz 4170 cm^{-1}), to emisijas viļņu garums ir pārāk mazs, lai efektīvi lietotu konfokālajā lāzera skenējošajā mikroskopijā. Arī benzantrona alkinilatvasinājumiem absorbcijas un emisijas maksimumi palielinās, pastiprinoties aizvietotāju elektrondonorajam efektam, taču pretēji pārējiem savienojumiem, palielinoties absorbcijas maksimumam, palielinās arī Stoksa nobīde. Piemēram, savienojums **64** ar spēcīgu elektronakceptoro aizvietotāju absorbē gaismu ar absorbcijas maksimumu 414 nm, un tā Stoksa nobīde ir 3102 cm^{-1}. Savukārt savienojums **68** ar spēcīgu elektrondonoro aizvietotāju absorbē gaismu ar maksimumu 445 nm, un tā Stoksa nobīde ir 6871 cm^{-1}. Lai pamatoti pierādītu šīs sakarības dabu, būtu nepieciešams turpināt pētījumus.

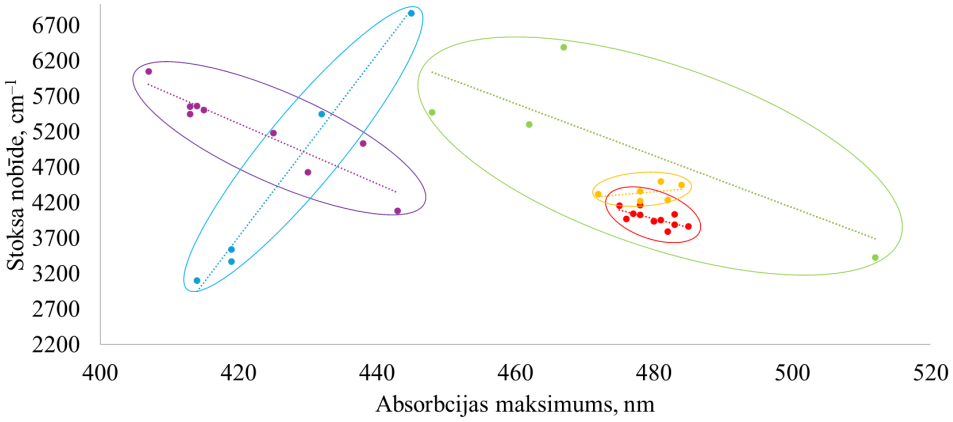

19. attēls. Darbā izpētīto savienojumu Stoksa nobīdes atkarība no absorbcijas maksimuma acetonā. Zaļā krāsā: benzantrona 3-amino-9-nitroatvasinājumi; sarkanā krāsā: benzantrona α-aminofosfonāti; oranžā krāsā: antrahinona α-aminofosfonāti; violetā krāsā: benzantrona tioatvasinājumi; zilā krāsā: benzantrona alkinilatvasinājumi.

SECINĀJUMI

1. Darba rezultātā izdevās izpētīt jaunas benzantrona un antrahinona atvasinājumu sintēzes metodes. Fluorescējošo savienojumu klāsts tika paplašināts ar atvasinājumiem, kas iegūti nukleofīlās aromātiskās aizvietošanas, Kabačnika-Fīldsa un Sonogaširas reakcijās. Iegūtajiem savienojumiem paveikta spektrālā analīze un to fotofizikālo īpašību izpēte. Tika nodemonstrēta jauno savienojumu ar uzlabotām īpašībām praktiskā lietojuma iespēja mikroskopijā.

2. 3-Brom-9-nitrobenzantrona nukleofīlās aromātiskās aizvietošanas reakcijā ar iznākumu no 48 % līdz 63 % tika iegūti aizvietoti 3-amino-9-nitrobenzantroni, kas absorbē gaismu diapazonā no 447 nm līdz 531 nm un izstaro gaismu diapazonā no 570 nm līdz 650 nm. 3-Brom-9-nitrobenzantrona reakcijas spēja ir palielināta, salīdzinot ar nenitrētajiem analogiem, un augstāki molārie absorbcijas koeficienti padara tos par labākiem kandidātiem nelineārajai optikai.

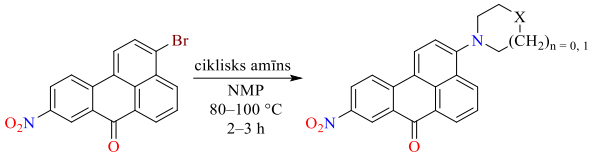

3. Kabačnika-Fīldsa reakcijas apstākļos tika iegūti fluorescenti 3-aminobenzantrona un 1-aminoantrahinona α-aminofosfonāti ar iznākumu no 55 % līdz 89 %. Emisijas joslā novērojama batohromā nobīde, pārejot no heksāna uz DMSO; benzantrona atvasinājumiem tā sasniedz 100 nm, savukārt antrahinona atvasinājumiem tā ir tikai 40 nm. Benzantrona α-aminofosfonātu fluorescences kvantu iznākumi ir līdz 10 reizēm augstāki, antrahinona atvasinājumiem no < 0,01 līdz 0,17 un benzantrona atvasinājumiem no 0,10 līdz 0,57.

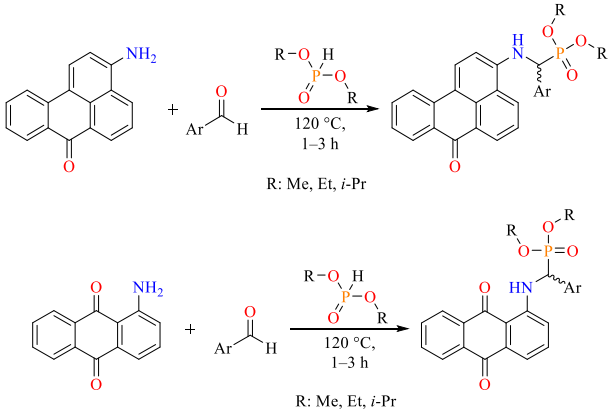

4. Gan benzantrona, gan antrahinona α-aminofosfonāti (savienojumi **12**, **15**, **35**, **38** un **49**) ir piemēroti bioloģisko paraugu, it īpaši parazītisko trematodu, iekrāsošanai un pētījumiem, izmantojot konfokālās lāzerskenēšanas mikroskopiju.

5. 3-Brombenzantrona aromātiskās aizvietošanās reakcijā ar tioliem tika iegūtas alkil- un arilaizvietotas 3-tiobenzantrona krāsvielas ar iznākumu no 59 % līdz 86 %. Pētītie savienojumi izrāda fluorescenci un solvatohromismu ar kvantu iznākumu līdz 52 %, absorbē gaismu diapazonā no 403 nm līdz 448 nm un izstaro gaismu diapazonā no 507 nm līdz 591 nm.

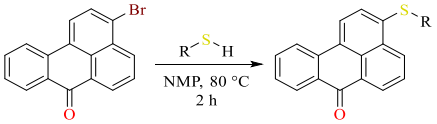

6. 3-Brombenzantrona Sonogaširas reakcijā ar terminālajiem alkīniem ar 43–89 % iznākumu tika iegūti aizvietoti 3-alkinilbenzantroni, kas absorbē gaismu diapazonā no 420 nm līdz 450 nm un izstaro gaismu no 462 nm līdz 701 nm. Elektrondonorās grupas alkīnu aromātiskajos gredzenos izraisa absorbcijas un emisijas maksimumu batohromo nobīdi, savukārt elektronakceptorās grupas – hipsohromo nobīdi. Augsta fotostabilitāte un pagarināta π-konjugācija padara šos savienojumus potenciāli lietojamus nelineārajās optiskajās tehnoloģijās.

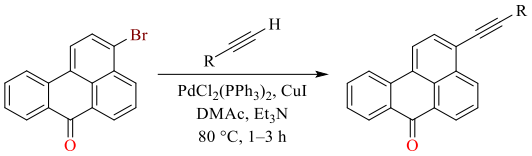

LITERATŪRAS SARAKSTS

1. Introduction to Fluorescence. In *Principles of Fluorescence Spectroscopy*; Springer US: Boston, MA, 2006; pp. 1–26.
2. Grabchev, I.; Bojinov, V.; Moneva, I. The Synthesis and Application of Fluorescent Dyes Based on 3-Amino Benzanthrone. *Dyes and Pigments* **2001**, *48*, 143–150, doi:10.1016/S0143-7208(00)00098-X.
3. Kirilova, E. M.; Meirovics, I.; Belyakov, S. V. Preparation and Properties of Nitrogen Derivatives of Benzanthrone with Heterocyclic Fragments. *Chem. Heterocycl. Compd. (N Y)* **2002**, *38*, 789–792, doi:10.1023/A:1020621418164.
4. Siddlingeshwar, B.; Hanagodimath, S. M.; Kirilova, E. M.; Kirilov, G. K. Photophysical Characteristics of Three Novel Benzanthrone Derivatives: Experimental and Theoretical Estimation of Dipole Moments. *J. Quant. Spectrosc. Radiat. Transf.* **2011**, *112*, 448–456, doi:10.1016/j.jqsrt.2010.09.001.
5. Thomas, A.; Kirilova, E. M.; Nagesh, B. V.; Manohara, S. R.; Siddlingeshwar, B.; Belyakov, S. V. Synthesis, Solvatochromism and DFT Study of Pyridine Substituted Benzanthrone with ICT Characteristics. *J. Mol. Struct.* **2022**, *1262*, 132971, doi:10.1016/j.molstruc.2022.132971.
6. Grabchev, I.; Moneva, I. Synthesis and Properties of Benzanthrone Derivatives as Luminophore Dyes for Liquid Crystals. *Dyes and Pigments.* **1998**, *37*, 155–164, doi:10.1016/S0143-7208(97)00050-8.
7. Grabtchev, I. K.; Bojinov, V. B.; Moneva, I. T. Functional Properties of Azomethine Substituted Benzanthrone Dyes for Use in Nematic Liquid Crystals. *J. Mol. Struct.* **1998**, *471*, 19–25, doi:10.1016/S0022-2860(98)00400-1.
8. Grabchev, I.; Mykowska, E.; Moneva, I.; Bauman, D. Molecular Orientation of Some Fluorescent Dichroic Dyes in Nematic Liquid Crystal. *Zeitschrift für Naturforschung A.* **2004**, *59*, 368–374, doi:10.1515/zna-2004-0610.
9. Almalki, A. S. A.; Alhadhrami, A.; Obaid, R. J.; Alsharif, M. A.; Adam, A. M. A.; Grabchev, I.; Refat, M. S. Preparation of Some Compounds and Study Their Thermal Stability for Use in Dye Sensitized Solar Cells. *J. Mol. Liq.* **2018**, *261*, 565–582, doi:10.1016/j.molliq.2018.04.057.
10. Orlova, N.; Nikolajeva, I.; Pučkins, A.; Belyakov, S.; Kirilova, E. Heterocyclic Schiff Bases of 3-Aminobenzanthrone and Their Reduced Analogues: Synthesis, Properties and Spectroscopy. *Molecules.* **2021**, *26*, 2570, doi:10.3390/molecules26092570.
11. Kirilova, A.; Pučkins, A.; Belyakov, S.; Kirilova, E. 3-[N-(4-Methoxybenzyl)Amino]Benzo[de]Anthracen-7-One. *Molbank.* **2021**, *2021*, M1287, doi:10.3390/M1287.
12. Staneva, D.; Betcheva, R. Synthesis and Functional Properties of New Optical PH Sensor Based on Benzo[de]Anthracen-7-One Immobilized on the Viscose. *Dyes and Pigments.* **2007**, *74*, 148–153, doi:10.1016/j.dyepig.2006.01.029.
13. Staneva, D.; Grabchev, I. Heterogeneous Sensors for Ammonia, Amines and Metal Ions Based on a Dendrimer Modified Fluorescent Viscose Fabric. *Dyes and Pigments.* **2018**, *155*, 164–170, doi:10.1016/j.dyepig.2018.03.044.
14. Staneva, D.; Vasileva-Tonkova, E.; Makki, M. S. I.; Sobahi, T. R.; Abdel-Rahman, R. M.; Asiri, A. M.; Grabchev, I. Synthesis, Photophysical and Antimicrobial Activity of New Water Soluble Ammonium Quaternary Benzanthrone in Solution and in

Polylactide Film. *J. Photochem. Photobiol. B.* **2015**, *143*, 44–51, doi:10.1016/j.jphotobiol.2014.12.024.
15. Gonta, S.; Utinans, M.; Kirilov, G.; Belyakov, S.; Ivanova, I.; Fleisher, M.; Savenkov, V.; Kirilova, E. Fluorescent Substituted Amidines of Benzanthrone: Synthesis, Spectroscopy and Quantum Chemical Calculations. *Spectrochim Acta A Mol. Biomol. Spectrosc.* **2013**, *101*, 325–334, doi:10.1016/j.saa.2012.09.104.
16. Kirilova, E.; Kecko, S.; Mežaraupe, L.; Gavarāne, I.; Pučkins, A.; Mickeviča, I.; Rubeniņa, I.; Osipovs, S.; Bulanovs, A.; Pupiņš, M.; et al. Novel Luminescent Dyes for Confocal Laser Scanning Microscopy Used in Trematoda Parasite Diagnostics. *Acta Biochim. Pol.* **2018**, *65*, 449–454, doi:10.18388/abp.2018_2574.
17. Rubenina, I.; Gavarane, I.; Kirilova, E.; Mezaraupe, L.; Kirjusina, M. Comparison of the Benzanthrone Luminophores: They Are Not Equal for Rapid Examination of Parafasciolopsis Fasciolaemorpha (Trematoda: Digenea). *Biomolecules.* **2021**, *11*, 598, doi:10.3390/biom11040598.
18. Grabchev, I.; Moneva, I.; Wolarz, E.; Bauman, D. Fluorescent 3-Oxy Benzanthrone Dyes in Liquid Crystalline Media. *Dyes and Pigments.* **2003**, *58*, 1–6, doi:10.1016/S0143-7208(03)00033-0.
19. Tsiko, U.; Bezvikonnyi, O.; Volyniuk, D.; Minaev, B. F.; Keruckas, J.; Cekaviciute, M.; Jatautiene, E.; Andruleviciene, V.; Dabuliene, A.; Grazulevicius, J.V. TADF Quenching Properties of Phenothiazine or Phenoxazine-Substituted Benzanthrones Emitting in Deep-Red/near-Infrared Region towards Oxygen Sensing. *Dyes and Pigments.* **2022**, *197*, 109952, doi:10.1016/j.dyepig.2021.109952.
20. Tsiko, U.; Sych, G.; Volyniuk, D.; Bezvikonnyi, O.; Keruckiene, R.; Lazauskas, A.; Grazulevicius, J. V. Self-Recovering Mechanochromic Luminescence of the Derivatives of Benzanthrone and Carbazole: Towards Damage-Resistive Information Recording and Security Probes. *Dyes and Pigments.* **2022**, *199*, 110082, doi:10.1016/j.dyepig.2022.110082.
21. Thomas, A.; Patil, P. S.; Siddlingeshwar, B.; Manohara, S. R.; Gummagol, N. B.; Krishna Chaitanya, G.; Kirilova, E. M. Nonlinear Optical Properties of Benzanthrone Derivatives with N'-Methylpiperazin-1-Yl and N'-Phenylpiperazin-1-Yl Substituents: Experimental and Quantum Chemical Study. *Opt. Laser Technol.* **2022**, *156*, 108616, doi:10.1016/j.optlastec.2022.108616.
22. Thomas, A.; Kirilova, E. M.; Nagesh, B. V.; Krishna Chaitanya, G.; Philip, R.; Manohara, S. R.; Sudeeksha, H. C.; Siddlingeshwar, B. Influence of Nitro Group on Solvatochromism, Nonlinear Optical Properties of 3-Morpholinobenzanthrone: Experimental and Theoretical Study. *J. Photochem. Photobiol. A. Chem.* **2023**, *437*, 114434, doi:10.1016/j.jphotochem.2022.114434.
23. Day, F. H. Nitration of the 13-Halogenobenzanthrones. *Journal of the Chemical Society (Resumed)* **1940**, 1474, doi:10.1039/jr9400001474.
24. Cerón-Carrasco, J. P.; Jacquemin, D.; Laurence, C.; Planchat, A.; Reichardt, C.; Sraïdi, K. Solvent Polarity Scales: Determination of New ET(30) Values for 84 Organic Solvents. *J. Phys. Org. Chem.* **2014**, *27*, 512–518, doi:10.1002/poc.3293.
25. Mucha, A.; Kafarski, P.; Berlicki, Ł. Remarkable Potential of the α-Aminophosphonate/Phosphinate Structural Motif in Medicinal Chemistry. *J. Med. Chem.* **2011**, *54*, 5955–5980, doi:10.1021/jm200587f.
26. Litim, B.; Djahoudi, A.; Meliani, S.; Boukhari, A. Synthesis and Potential Antimicrobial Activity of Novel α-Aminophosphonates Derivatives Bearing Substituted Quinoline or

Quinolone and Thiazole Moieties. *Medicinal Chemistry Research.* **2022**, *31*, 60–74, doi:10.1007/s00044-021-02815-5.
27. Rezaei, Z.; Khabnadideh, S.; Zomorodian, K.; Pakshir, K.; Nadali, S.; Mohtashami, N.; Faghih Mirzaei, E. Design, Synthesis, and Antifungal Activity of New α -Aminophosphonates. *Int. J. Med. Chem.* **2011**, *2011*, 1–11, doi:10.1155/2011/678101.
28. Varga, P. R.; Szabó, R. O.; Dormán, G.; Bősze, S.; Keglevich, G. Cytotoxic Activity of α-Aminophosphonic Derivatives Coming from the Tandem Kabachnik-Fields Reaction and Acylation. *Pharmaceuticals.* **2023**, *16*, 506, doi:10.3390/ph16040506.
29. Grzyś, E.; Bielecki, K.; Sarapuk, J. Aminophosphonate-Induced Changes of Betacyanine and Ionic Efflux. *Zeitschrift für Naturforschung C.* **2001**, *56*, 349–352, doi:10.1515/znc-2001-5-605.
30. Kafarski, P.; Lejczak, B. Biological Activity of Aminophosphonic Acids. *Phosphorus Sulfur Silicon Relat. Elem.* **1991**, *63*, 193–215, doi:10.1080/10426509108029443.
31. Reddy, N. B.; Sundar, C. S.; Krishna, B. S.; Santhisudha, S.; Sreelakshmi, P.; Nayak, S. K.; Reddy, C. S. Cellulose-SO3H Catalyzed Synthesis of Bis(α-Aminophosphonates) and Their Antioxidant Activity. *Organic Communications.* **2017**, *10*, 46–55, doi:10.25135/acg.oc.8.16.06.422.
32. Fouda, S. R.; El-Sayed, I. E.; Attia, N. F.; Abdeen, M. M.; Abdel Aleem, A. A. H.; Nassar, I. F.; Mira, H. I.; Gawad, E. A.; Kalam, A.; Al-Ghamdi, A. A.; et al. Mechanistic Study of Hg(II) Interaction with Three Different α-Aminophosphonate Adsorbents: Insights from Batch Experiments and Theoretical Calculations. *Chemosphere.* **2022**, *304*, 135253, doi:10.1016/j.chemosphere.2022.135253.
33. Imam, E. A.; Hashem, A. I.; Tolba, A. A.; Mahfouz, M. G.; El-Sayed, I. E.-T.; El-Tantawy, A. I.; Galhoum, A. A.; Guibal, E. Effect of Mono- vs. Bi-Functionality of Aminophosphonate Derivatives on the Enhancement of U(VI) Sorption: Physicochemical Properties and Sorption Performance. *J. Environ. Chem. Eng.* **2023**, *11*, 109951, doi:10.1016/j.jece.2023.109951.
34. Moumeni, O.; Mehri, M.; Kerkour, R.; Boublia, A.; Mihoub, F.; Rebai, K.; Khan, A. A.; Erto, A.; Darwish, A. S.; Lemaoui, T.; et al. Experimental and Detailed DFT/MD Simulation of α-Aminophosphonates as Promising Corrosion Inhibitor for XC48 Carbon Steel in HCl Environment. *J. Taiwan Inst. Chem. Eng.* **2023**, *147*, 104918, doi:10.1016/j.jtice.2023.104918.
35. Li, S.; Liu, R.; Han, X.; Ge, C.; Zhang, X. Diethyl α-Aminophosphonate Containing Lubricating Additives Synthesized from (3-Aminophenyl)Boronic Acid Pinacol Ester. *Inorg. Chem. Commun.* **2022**, *140*, 109477, doi:10.1016/j.inoche.2022.109477.
36. Górny vel Górniak, M.; Kafarski, P. Preparation of the Library of Fluorescent Aromatic Aminophosphonate Phenyl and Benzyl Esters. *Phosphorus Sulfur Silicon Relat. Elem.* **2016**, *191*, 511–519, doi:10.1080/10426507.2015.1094658.
37. Kuśnierz, A.; Chmielewska, E. Synthesis of Fluorescent Aminophosphonates by Green Chemistry Procedures. *Phosphorus Sulfur Silicon Relat. Elem.* **2017**, *192*, 700–705, doi:10.1080/10426507.2017.1308934.
38. Wang, Q.-M.; Gao, W.; Song, J.-L.; Liu, Y.; Qi, H.; Tang, X.-H. Synthesis, X-Ray Crystallographic Analysis and BSA Interaction of a New α-Aminophosphonate. *J. Appl. Spectrosc.* **2016**, *83*, 703–709, doi:10.1007/s10812-016-0351-9.
39. Lewkowski, J.; Rodriguez Moya, M.; Wrona-Piotrowicz, A.; Zakrzewski, J.; Kontek, R.; Gajek, G. Synthesis, Fluorescence Properties and the Promising

Cytotoxicity of Pyrene–Derived Aminophosphonates. *Beilstein Journal of Organic Chemistry.* **2016**, *12*, 1229–1235, doi:10.3762/bjoc.12.117.
40. Kraicheva, I.; Vodenicharova, E.; Tashev, E.; Tosheva, T.; Tsacheva, I.; Troev, K. Synthesis and NMR Characterization of Two Novel Anthracene-Derived BIS-Aminophosphonates. Basic Hydrolysis of Some Aminophosphonate Derivatives. *Phosphorus Sulfur Silicon Relat. Elem* **2012**, *187*, 660–667, doi:10.1080/10426507.2011.638349.
41. Varga, P. R.; Keglevich, G. Synthesis of α-Aminophosphonates and Related Derivatives; The Last Decade of the Kabachnik-Fields Reaction. *Molecules.* **2021**, *26*, 2511, doi:10.3390/molecules26092511.
42. Lüttringhaus, A.; Neresheimer, H. Zur Kenntnis Des Benzanthrons. *Justus Liebigs Ann. Chem.* **1929**, *473*, 259–289, doi:10.1002/jlac.19294730115.
43. Keglevich, G.; Bálint, E. The Kabachnik-Fields Reaction: Mechanism and Synthetic Use. *Molecules.* **2012**, *17*, 12821–12835, doi:10.3390/molecules171112821.
44. Kirilova, E. M.; Puckins, A. I.; Romanovska, E.; Fleisher, M.; Belyakov, S. V. Novel Amidine Derivatives of Benzanthrone: Effect of Bromine Atom on the Spectral Parameters. *Spectrochim. Acta A Mol. Biomol. Spectrosc.* **2018**, *202*, 41–49, doi:10.1016/j.saa.2018.05.029.
45. Armignacco, O.; Caterini, L.; Marucci, G.; Ferri, F.; Bernardini, G.; Raponi, G. N.; Ludovisi, A.; Bossù, T.; Morales, M. A. G.; Pozio, E. Human Illnesses Caused by Opisthorchis Felineus Flukes, Italy. *Emerg. Infect. Dis.* **2008**, *14*, 1902–1905, doi:10.3201/eid1412.080782.
46. Kaur, N.; Gauri Anthraquinone Appended Chemosensors for Fluorescence Monitoring of Anions and/or Metal Ions. *Inorganica Chim. Acta.* **2022**, *536*, 120917, doi:10.1016/j.ica.2022.120917.
47. Bin Huang; Ji, Y.; Li, Z.; Zhou, N.; Jiang, W.; Feng, Y.; Lin, B.; Sun, Y. Simple Aggregation-Induced Delayed Fluorescence Materials Based on Anthraquinone Derivatives for Highly Efficient Solution-Processed Red OLEDs. *J. Lumin.* **2017**, *187*, 414–420, doi:10.1016/j.jlumin.2017.03.038.
48. Yang, L.; Fu, Z.; Niu, X.; Zhang, G.; Cui, F.; Zhou, C. Probing the Interaction of Anthraquinone with DNA by Spectroscopy, Molecular Modeling and Cancer Cell Imaging Technique. *Chem. Biol. Interact.* **2015**, *233*, 65–70, doi:10.1016/j.cbi.2015.03.026.
49. Malik, M. S.; Alsantali, R. I.; Jassas, R. S.; Alsimaree, A. A.; Syed, R.; Alsharif, M. A.; Kalpana, K.; Morad, M.; Althagafi, I. I.; Ahmed, S. A. Journey of Anthraquinones as Anticancer Agents – a Systematic Review of Recent Literature. *RSC Adv.* **2021**, *11*, 35806–35827, doi:10.1039/D1RA05686G.
50. Zhao, L.; Zheng, L. A Review on Bioactive Anthraquinone and Derivatives as the Regulators for ROS. *Molecules.* **2023**, *28*, 8139, doi:10.3390/molecules28248139.
51. Bespalaya, Y. V.; Kondakov, A. V.; Travina, O. V.; Khrebtova, I. S.; Kropotin, A. V.; Aksenova, O. V.; Gofarov, M. Yu.; Lyubas, A. A.; Tomilova, A. A.; Vikhrev, I. V. First Record of Metacercariae Trematodes Opisthioglyphe Ranae (Digenea: Telorchiidae) and Echinostoma Bolschewense (Digenea: Echinostomatidae) in Dreissena Polymorpha (Bivalvia: Dreissenidae) from the Don and Volga River Basins, Russia. *Ecol Montenegrina.* **2022**, *54*, 57–76, doi:10.37828/em.2022.54.8.
52. Monçalves, M.; Zanotto, G. M.; Toldo, J. M.; Rampon, D. S.; Schneider, P. H.; Gonçalves, P. F. B.; Rodembusch, F. S.; Silveira, C. C. Dipolar Vinyl Sulfur Fluorescent

Dyes. Synthesis and Photophysics of Sulfide, Sulfoxide and Sulfone Based D–π–A Compounds. *RSC Adv.* **2017**, *7*, 8832–8842, doi:10.1039/C6RA27989A.
53. Rachi, Y.; Yamakado, R.; Okada, S. Synthesis of Dyes with a Sulfur-Containing Heterocyclic Donor and a Pyrroline-Type Acceptor. *Dyes and Pigments.* **2018**, *159*, 345–351, doi:10.1016/j.dyepig.2018.06.032.
54. Sims, M. T.; Abbott, L. C.; Cowling, S. J.; Goodby, J. W.; Moore, J. N. Molecular Design Parameters of Anthraquinone Dyes for Guest-Host Liquid-Crystal Applications: Experimental and Computational Studies of Spectroscopy, Structure, and Stability. *The Journal of Physical Chemistry C.* **2016**, *120*, 11151–11162, doi:10.1021/acs.jpcc.6b03607.
55. Cowling, S. J.; Ellis, C.; Goodby, J. W. Anthraquinone Liquid Crystal Dichroic Dyes – a New Form of Chromonic Dye? *Liq. Cryst.* **2011**, *38*, 1683–1698, doi:10.1080/02678292.2011.620181.
56. Ye, J.; Gao, Y.; He, L.; Tan, T.; Chen, W.; Liu, Y.; Wang, Y.; Ning, G. Efficient Blue-Emitting Molecules by Incorporating Sulfur-Containing Moieties into Triarylcyclopentadiene: Synthesis, Crystal Structures and Photophysical Properties. *Dyes and Pigments.* **2016**, *124*, 145–155, doi:10.1016/j.dyepig.2015.09.018.
57. Liu, Y.; Yu, Y.; Zhao, Q.; Tang, C.; Zhang, H.; Qin, Y.; Feng, X.; Zhang, J. Fluorescent Probes Based on Nucleophilic Aromatic Substitution Reactions for Reactive Sulfur and Selenium Species: Recent Progress, Applications, and Design Strategies. *Coord. Chem. Rev.* **2021**, *427*, 213601, doi:10.1016/j.ccr.2020.213601.
58. Vaidyanathan, T.; Seshadri, S. Nucleophilic Substitution Reactions on 3-Bromo- and 3-Nitrobenzanthrones. *Dyes and Pigments.* **1984**, *5*, 431–436, doi:10.1016/0143-7208(84)80035-2.
59. Melville, O. A.; Grant, T. M.; Rice, N. A.; Wang, B.; Josse, P.; Lessard, B. H. Functionalization of Commercial Pigment Hostasol Red GG for Incorporation into Organic Thin-Film Transistors. *New Journal of Chemistry.* **2020**, *44*, 845–851, doi:10.1039/C9NJ04851K.
60. Montanari, S.; Paradisi, C.; Scorrano, G. Thiol Anions in Nucleophilic Aromatic Substitution Reactions with Activated Aryl Halides. Attack on Carbon vs Attack on Halogen. *J. Org. Chem.* **1993**, *58*, 5628–5631, doi:10.1021/jo00073a020.
61. Campodónico, P. R.; Alarcón-Espósito, J.; Olivares, B. Kinetics and Reaction Mechanism of Biothiols Involved in SNAr Reactions: An Experimental Study. *Front. Chem.* **2022**, *10*, doi:10.3389/fchem.2022.854918.
62. Rohrbach, S.; Smith, A. J.; Pang, J. H.; Poole, D. L.; Tuttle, T.; Chiba, S.; Murphy, J. A. Concerted Nucleophilic Aromatic Substitution Reactions. *Angewandte Chemie International Edition.* **2019**, *58*, 16368–16388, doi:10.1002/anie.201902216.
63. Kunda, G.; Akhmadullin, R. M.; Zakirov, R. K.; Akhmadullina, F. Y.; Gizyatullov, R. N.; Madaminov, N. V.; Musin, L. I. Thiol Synthesis Methods: A Review. *Journal of Sulfur Chemistry.* **2024**, 1–34, doi:10.1080/17415993.2024.2428607.
64. Hansch, C.; Leo, A.; Taft, R. W. A Survey of Hammett Substituent Constants and Resonance and Field Parameters. *Chem. Rev.* **1991**, *91*, 165–195, doi:10.1021/cr00002a004.
65. Maeda, H.; Maeda, T.; Mizuno, K.; Fujimoto, K.; Shimizu, H.; Inouye, M. Alkynylpyrenes as Improved Pyrene-Based Biomolecular Probes with the Advantages of High Fluorescence Quantum Yields and Long Absorption/Emission Wavelengths. *Chemistry – A European Journal.* **2006**, *12*, 824–831, doi:10.1002/chem.200500638.

66. Chen, M.; Wei, J.; Zhang, Y.; Wu, L.; Tan, L.; Shi, S.; Shi, J.; Ji, L. 2,7-Carbazole Derived Organoboron Compounds: Synthesis and Molecular Fluorescence. *Front. Chem.* **2021**, *9*, doi:10.3389/fchem.2021.754298.
67. Yang, J.; Dass, A.; Rawashdeh, A.-M. M.; Sotiriou-Leventis, C.; Panzner, M. J.; Tyson, D. S.; Kinder, J. D.; Leventis, N. Arylethynyl Substituted 9,10-Anthraquinones: Tunable Stokes Shifts by Substitution and Solvent Polarity. *Chemistry of Materials.* **2004**, *16*, 3457–3468, doi:10.1021/cm049590g.
68. Yang, J.-X.; Wang, X.-L.; Wang, X.-M.; Xu, L.-H. The Synthesis and Spectral Properties of Novel 4-Phenylacetylene-1,8-Naphthalimide Derivatives. *Dyes and Pigments.* **2005**, *66*, 83–87, doi:10.1016/j.dyepig.2004.07.015.
69. Bai, J.-Y.; Xie, Y.-Z.; Wang, C.-J.; Fang, S.-Q.; Cao, L.-N.; Wang, L.-L.; Jin, J.-Y. A Quninolylthiazole Derivatives as an ICT-Based Fluorescent Probe of Hg(II) and Its Application in Ratiometric Imaging in Live HeLa Cells. *J. Fluoresc.* **2018**, *28*, 795–800, doi:10.1007/s10895-018-2241-4.
70. Altınok, E.; Smith, Z. C.; Thomas, S. W. Two-Dimensional, Acene-Containing Conjugated Polymers That Show Ratiometric Fluorescent Response to Singlet Oxygen. *Macromolecules.* **2015**, *48*, 6825–6831, doi:10.1021/acs.macromol.5b01076.
71. Tlach, B. C.; Tomlinson, A. L.; Bhuwalka, A.; Jeffries-EL, M. Tuning the Optical and Electronic Properties of 4,8-Disubstituted Benzobisoxazoles via Alkyne Substitution. *J. Org. Chem.* **2011**, *76*, 8670–8681, doi:10.1021/jo201078w.
72. Saeed, M. A.; Le, H. T. M.; Miljanić, O. Š. Benzobisoxazole Cruciforms as Fluorescent Sensors. *Acc. Chem. Res.* **2014**, *47*, 2074–2083, doi:10.1021/ar500099z.
73. Yamaguchi, Y.; Matsubara, Y.; Ochi, T.; Wakamiya, T.; Yoshida, Z. How the π Conjugation Length Affects the Fluorescence Emission Efficiency. *J. Am. Chem. Soc.* **2008**, *130*, 13867–13869, doi:10.1021/ja8040493.
74. Maļeckis, A.; Avotiņa, L.; Ķizāne, G.; Pučkins, A.; Osipovs, S.; Kirilova, E. New Fluorescent Heterocyclic Compounds Derived From 3-Cyanobenzanthrone. *Polycycl. Aromat. Compd.* **2022**, *42*, 5508–5520, doi:10.1080/10406638.2021.1939068.
75. Sonogashira, K.; Tohda, Y.; Hagihara, N. A Convenient Synthesis of Acetylenes: Catalytic Substitutions of Acetylenic Hydrogen with Bromoalkenes, Iodoarenes and Bromopyridines. *Tetrahedron Lett.* **1975**, *16*, 4467–4470, doi:10.1016/S0040-4039(00)91094-3.
76. Kanwal, I.; Mujahid, A.; Rasool, N.; Rizwan, K.; Malik, A.; Ahmad, G.; Shah, S. A. A.; Rashid, U.; Nasir, N. M. Palladium and Copper-Catalyzed Sonogashira Cross-Coupling an Excellent Methodology for C-C Bond Formation over 17 Years: A Review. *Catalyst.s* **2020**, *10*, 443, doi:10.3390/catal10040443.
77. Hartwig, J. F. Electronic Effects on Reductive Elimination To Form Carbon−Carbon and Carbon−Heteroatom Bonds from Palladium(II) Complexes. *Inorg. Chem.* **2007**, *46*, 1936–1947, doi:10.1021/ic061926w.

DOCTORAL THESIS PROPOSED TO RIGA TECHNICAL UNIVERSITY FOR PROMOTION TO THE SCIENTIFIC DEGREE OF DOCTOR OF SCIENCE

To be granted the scientific degree of Doctor of Science (Ph. D.), the present Doctoral Thesis has been submitted for defence at the open meeting of RTU Promotion Council on 17 June 2025 at the Faculty of Natural Sciences and Technology of Riga Technical University, 3 Paula Valdena Street, Room 272 with online participation option at zoom link https://rtucloud1.zoom.us/j/9352086644.

OFFICIAL REVIEWERS

Senior Researcher Dr. chem. Aiva Plotniece
Latvian Institute of Organic Synthesis, Latvia

Corresponding member of the Latvian Academy of Sciences, Dr. chem. Māra Jure
Latvian Academy of Sciences, Latvia

Associate Professor Dr. chem. Artis Kinēns
University of Latvia, Latvia

DECLARATION OF ACADEMIC INTEGRITY

I hereby declare that the Doctoral Thesis submitted for review to Riga Technical University for promotion to the scientific degree of Doctor of Science (Ph. D) is my own. I confirm that this Doctoral Thesis has not been submitted to any other university for promotion to a scientific degree.

Armands Maļeckis ……. (signature)
Date: ……

The Doctoral Thesis has been prepared as a collection of thematically related scientific publications complemented by summaries in both Latvian and English. The Doctoral Thesis unites eight scientific publications. The scientific publications have been written in English, with a total volume of 328 pages, including supplementary data.

CONTENTS

Appendix VI Maļeckis, A.; Cvetinska, M.; Griškjāns, E.; Kirilova, E. Exploring Dual Solvatochromic Traits in Novel Fluorescent Benzanthrone Ethynyl Derivatives. *J. Solution. Chem.* **2024**.

GENERAL OVERVIEW OF THE THESIS

Introduction

Fluorescence occurs when a substance absorbs light and almost instantly reemits it at a longer wavelength, typically within a few nanoseconds. This reemitted light has less energy than the absorbed light, resulting in a shift to a longer wavelength. Excellent fluorescent materials are characterized by their unique optical properties: they have high absorption coefficients for effective excitation, significant Stokes shifts for increased sensitivity, high quantum yields for efficient light emission, and strong photostability for enduring performance. These properties are crucial for applications such as biological imaging, diagnostic assays and optical sensors, as the photodegradation process can produce undesirable by-products that may cause measurement errors and reduce the accuracy and reliability of results [1].

Among the myriad polyaromatic compounds, benzanthrones (7*H*-benzo[*de*]anthracen-7-ones) have long held a significant position in the dye industry due to their unique properties and versatile applications. These anthraquinoid dyes exhibit efficient charge transfer, facilitated by the interaction between electron-donating groups and the electron-accepting carbonyl group within the aromatic structure. This interaction is particularly pronounced in nitrogen-substituted derivatives. Consequently, 3-amino substituted benzanthrones have garnered considerable attention and have been the focus of extensive research owing to the strong electron-donating effects of nitrogen. For instance, nucleophilic substitution reactions involving 3-nitrobenzanthrone and 3-bromobenzanthrone with primary and secondary aliphatic amines produce substituted 3-aminobenzanthrones. Research indicates that these compounds are well-suited for the mass coloration of polymers and the production of liquid-crystal systems and exhibit nonlinear optical (NLO) properties [2]–[5]. Additionally, imines synthesized through the condensation reaction of 3-aminobenzanthrone with suitable aromatic aldehydes are effective for detecting various metal cationic species and can also be used in liquid crystal systems and polymers as fluorescent dyes and brighteners [6]–[9]. When these imines are reduced with $NaBH_4$, they yield amines that exhibit even more pronounced luminescence than the original imines [10], [11]. Acylation of 3-aminobenzanthrone with chloroacetyl chloride followed by nucleophilic substitution of the chlorine atom with amines yields tertiary or quaternary ammonium compounds, which are ideal for diverse sensing applications [12]–[14]. Similarly, amidino derivatives have been extensively studied, synthesized via the Vilsmeier–Haack type reaction [15]. These solvatochromic compounds are primarily used in confocal laser scanning microscopy (CLSM) for biological specimens [16], [17]. Aromatic substitution reactions of 3-bromobenzanthrone with alcohols produce fluorescent 3-oxybenzanthrones, which, like amines and imines, are suitable for polymer and liquid crystal systems [18]. The Buchwald-Hartwig amination of 3-bromobenzanthrone with aromatic amines such as phenoxazine and phenothiazine results in compounds emitting in the deep-red/near-infrared region with thermally activated delayed fluorescence properties, suitable for fabrication of devices with quantitative oxygen sensing capabilities in air [19]. Carbazole derivatives, on the other hand, exhibit self-regulating mechanochromism, adding to their versatility in various advanced applications [20].

In essence, the extensive exploration of benzanthrones and their derivatives not only underscores their potential role in various industries but also illuminates a promising avenue for advancing fluorescence technology and its multifaceted applications in fields ranging from materials science to biomedical research.

Aims and objectives

The aim of the Thesis was the synthesis of new benzanthrone and anthraquinone derivatives and the examination of their luminescent properties and potential applications.

The following tasks were defined:

1. to research methods for synthesizing novel benzanthrone and anthraquinone derivatives through nucleophilic aromatic substitution, Kabachnik-Fields and Sonogashira reactions, expanding the library of fluorescent compounds;
2. obtain absorption and emission spectra in various solvents and analyze molar extinction coefficients, Stokes shifts and fluorescence quantum yields of the obtained dyes to comprehensively examine photophysical properties;
3. based on the photophysical parameters, outline potential applications.

Scientific novelty and main results

Previous studies on benzanthrone derivatives have been mostly limited to the analysis of substituted 3-aminobenzanthrone derivatives. In this work, the impact of other heteroatoms, additional functional group introductions and elongation of conjugation on the properties of these compounds has been investigated, which up to this point has not been investigated.

The Doctoral Thesis encompasses, firstly, the synthesis of substituted 3-amino-9-nitrobenzanthrone derivatives, with a focus on understanding how additional electron-withdrawing groups influence molecular behavior during light absorption and emission processes. Additionally, the synthesis and properties of novel α-aminophosphonates derived from 1-aminoanthraquinone and 3-aminobenzanthrone were investigated in a comparative fashion, exploring their potential biological activities and photophysical behaviors. Furthermore, the research investigates the synthesis and properties of alkyl and aryl 3-thiobenzanthrones, shedding light on their luminescent properties and structural characteristics. Lastly, the synthesis and properties of 3-alkynylbenzanthrones, aiming to enhance their fluorescent characteristics, were explored.

Overall, the research contributes to the understanding of novel anthrone derivatives' structure-property relationships and their potential applications in such fields as bioimaging, nonlinear optics, and fluorescence-based technologies.

Structure and volume of the Thesis

The Doctoral Thesis has been prepared as a collection of thematically related scientific publications related to the functionalization and photophysical properties of benzanthrones and anthraquinones with applications in bioimaging. The Thesis unites six original research publications.

Publications and approbation of the Thesis

The results of the Thesis are reported in six original experimental publications. The main results were presented at international conferences.

Scientific publications

1. **Maļeckis, A.**; Griškjāns, E.; Cvetinska, M.; Savicka, M.; Belyakov, S.; Kirilova, E. Synthesis, Characterization, Spectroscopic Studies and Evaluation of Toxicological Effect on Growth of Wheat Sprouts (*Triticum Aestivum*) of New Benzanthrone α-Aryl-α-Aminophosphonates. *J. Mol. Struct.* **2023**, *1277*, 134838. https://doi.org/10.1016/j.molstruc.2022.134838.
2. **Maļeckis, A.**; Cvetinska, M.; Griškjāns, E.; Mežaraupe, L.; Kirjušina, M.; Pavlova, V.; Kirilova, E. Novel Anthraquinone α-Aryl-α-Aminophosphonates: Synthesis, Spectroscopy and Imaging by Confocal Laser Scanning Microscopy of Trematode *Opisthioglyphe Ranae*. *J. Photochem. Photobiol. A Chem.* **2023**, *444*, 114918. https://doi.org/10.1016/j.jphotochem.2023.114918.
3. **Maļeckis, A.**; Cvetinska, M.; Puckins, A.; Osipovs, S.; Sirokova, J.; Belyakov, S.; Kirilova, E. Synthesis and Properties of New 3-Heterylamino-Substituted 9-Nitrobenzanthrone Derivatives. *Molecules* **2023**, *28* (13), 5171. https://doi.org/10.3390/molecules28135171.
4. **Maļeckis, A.**; Cvetinska, M.; Griškjāns, E.; Dmitrijevs, K.; Traskovskis, K.; Belyakov, S.; Kirilova, E. Benzanthrone Sulfides: Synthesis, Solvatochromism Characterization and Analysis of Experimental Photophysical Parameters and Theoretical Calculations. *Dyes and Pigments* **2023**, *219*, 111599. https://doi.org/10.1016/j.dyepig.2023.111599.
5. **Maļeckis, A.**; Cvetinska, M.; Kirjušina, M.; Mežaraupe, L.; Kecko, S.; Gavarāne, I.; Kiyan, V.; Lider, L.; Pavlova, V.; Savicka, M.; Belyakov, S.; Kirilova, E. A Comparative Study of New Fluorescent Anthraquinone and Benzanthrone α-Aminophosphonates: Synthesis, Spectroscopy, Toxicology, X-Ray Crystallography, and Microscopy of *Opisthorchis Felineus*. *Molecules* **2024**, *29* (5), 1143. https://doi.org/10.3390/molecules29051143.
6. **Maļeckis, A.**; Cvetinska, M.; Griškjāns, E.; Kirilova, E. Exploring Dual Solvatochromic Traits in Novel Fluorescent Benzanthrone Ethynyl Derivatives. *J. Solution. Chem.* **2024**. https://doi.org/10.1007/s10953-024-01363-x.

Other publications on the topic not included in the Doctoral Thesis

1. **Maļeckis, A.**; Griškjāns, E.; Cvetinska, M.; Kirilova, E. 3-(Phenylethynyl)-7H-Benzo[de]Anthracen-7-one. Molbank 2022, *2022* (3), M1442. https://doi.org/10.3390/M1442.
2. Olipova, M.; **Maleckis, A.**; Puckins, A.; Kirilova, A.; Romanovska, E.; Kirilova, E. Spectroscopic Investigation of New Benzanthrone Luminescent Dyes. *Bulgarian Chemical Communications* **2022**, *54* (3), 253–257. https://doi.org/10.34049/bcc.54.3.F006.

The results of the Thesis were presented at the following conferences

1. Kirilova, J.; **Maleckis, A.**; Puckins, A.; Kirilova, A.; Grigorjeva, T. (2022). Spectroscopic Investigation of New Benzanthrone Luminescent Dyes. *8th International Conference on New Trends in Chemistry*, Istanbul, Turkey, pp. 57. https://icntcconference.com/wp-content/uploads/2024/06/ICNTC-2022-ABSTRACT-BOOK.pdf
2. Sirokova, J.; **Maleckis, A.**; Kirilova, J. (2023). Effect of the Nitro Group on Nucleophilic Substitution in Benzanthrone. *The 65th International Scientific Conference of Daugavpils University*, Daugavpils, Latvia, p. 21. https://dukonference.lv/files/Tezes_65.konf_publicesanai_gala_versija.pdf
3. **Maļeckis, A.**; Griškjāns, E.; Cvetinska, M.; Kirilova, E. (2023). Synthesis and Examination of Photophysical Properties of Benzanthrone Ethynyl Derivatives. *The 65th International Scientific Conference of Daugavpils University*, Daugavpils, Latvia, p. 23. https://dukonference.lv/files/Tezes_65.konf_publicesanai_gala_versija.pdf
4. Kirilova, J.; Savicka, M.; Kirilova, A.; **Maleckis, A.**; Grigorjeva, T. (2023). Study of the Toxicity of Benzanthrone Luminescent Dyes. *9th International Conference On New Trends in Chemistry*, Istanbul, Turkey, p. 43. https://icntcconference.com/wp-content/uploads/2024/06/9th-ICNTC-BOOK-OF-ABSTRACTS.pdf
5. **Maļeckis, A.**; Kirilova, E. (2024). Advancements in Fluorescent α-aminophosphonates. *The 66th International Scientific Conference of Daugavpils University*, Daugavpils, Latvia, p. 13. https://dukonference.lv/files/Tezes_66_konf_2024_gala.pdf

MAIN RESULTS OF THE THESIS

Anthrone derivatives have gained prominence for their remarkable luminescent attributes and tunable fluorescence emission, which enable diverse applications. Recognizing their potential, recent years have seen a surge in research focused on the synthesis and functionalization of anthrone derivatives. This growing interest stems from the need to explore new molecular structures with enhanced optical properties and tailor-made functionalities to meet the demands of evolving technological and scientific challenges. Consequently, further investigation was required to elucidate the structure-property relationships of anthrone derivatives and devise efficient synthetic strategies to expand their applicability further to unlock the full potential of anthrone derivatives and drive innovation in fluorescent materials science.

In this Thesis, the primary objective centered on the synthesis of new benzanthrone and anthraquinone fluorophores, accompanied by comprehensive measurements of the photophysical properties and the determination of their potential applications.

1. Synthesis and properties of substituted 3-amino-9-nitrobenzanthrone derivatives

The fluorescence observed in benzanthrone dyes primarily occurs due to intramolecular charge transfer (ICT) taking place upon excitation. This happens due to the interaction between electron-donating groups and the electron-accepting carbonyl group within the aromatic system of benzanthrone (D-π-A architecture type). Noteworthy, substituted 3-aminobenzanthrone derivatives display nonlinear optical properties [21]; with the addition of a nitro group notably augmenting their NLO (nonlinear optical) response [22], therefore, it was of interest to investigate the impact of an additional electron-withdrawing group on photophysical attributes of substituted 3-aminobenzanthrone derivatives of benzanthrone.

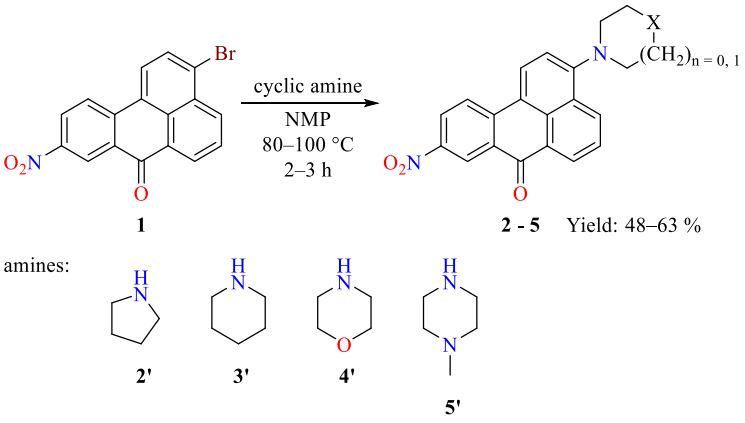

Scheme 1. Synthesis of substituted 3-amino-9-nitrobenzanthrone derivatives **2**–**5**.

For this objective, commercial 3-bromobenzanthrone was nitrated with a nitrating mixture (HNO_3/H_2SO_4 (4:1 v/v)) in glacial acetic acid, according to a previously published study, to obtain compound **1** via an electrophilic substitution reaction [23], which then underwent following nucleophilic aromatic substitution with cyclic amines in 1-methylpyrrolidin-2-one (NMP) as depicted in Scheme 1. Compared to the corresponding substitution reaction involving non-nitrated 3-bromobenzanthrone, the substitution of the bromine atom in nitro derivative **1** occurs at a lower temperature (80–100 °C versus 86–138 °C) and more rapidly (2–3 hours versus 8 hours). The enhanced reactivity stems from the potent electron-withdrawing character of the nitro group, leading to a significant reduction in electron density at the *C*(3) atom of the benzanthrone core, promoting the nucleophilic attack. Consequently, the yields of the desired products **2**–**5** were, on average, 10 % higher compared to equivalent derivatives lacking a nitro group [2]. These resulting compounds are dark red colored in their solid state and display intense luminescence in solutions.

While structures of these compounds were confirmed and characterized by Fourier transform infrared spectroscopy (FTIR), ^{1}H, ^{13}C nuclear magnetic resonance (NMR) spectroscopy and 2D-NMR (COSY and HSQC) spectroscopy and high-resolution mass spectrometry, in addition, slow evaporation technique provided crystals of **2** and **3**. X-ray crystallographic analysis, besides providing clear confirmation of the structures, also unveiled the presence of hydrogen bonds for both compounds and π–π interactions leading to molecular stacking (Figs. 1 and 2). The X-ray crystallographic analysis for all compounds mentioned in this work was carried out in collaboration with Dr. sc. phys. Sergey Belyakov.

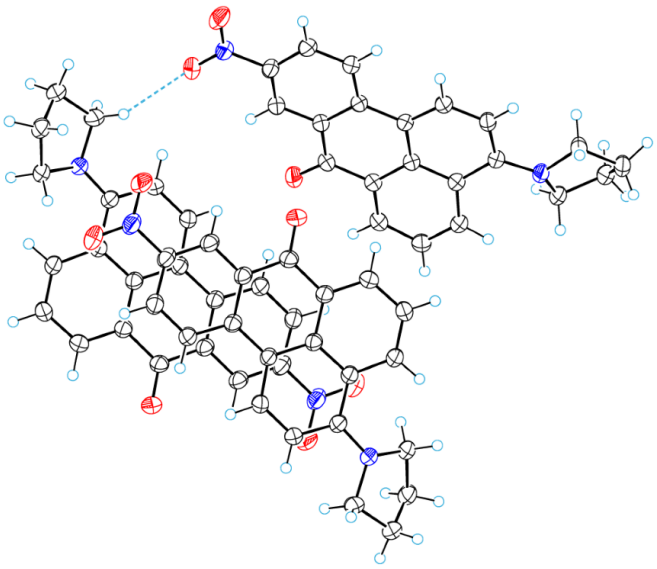

Fig. 1. A fragment of molecular packing of **2** with N–O···H–C hydrogen bonds.

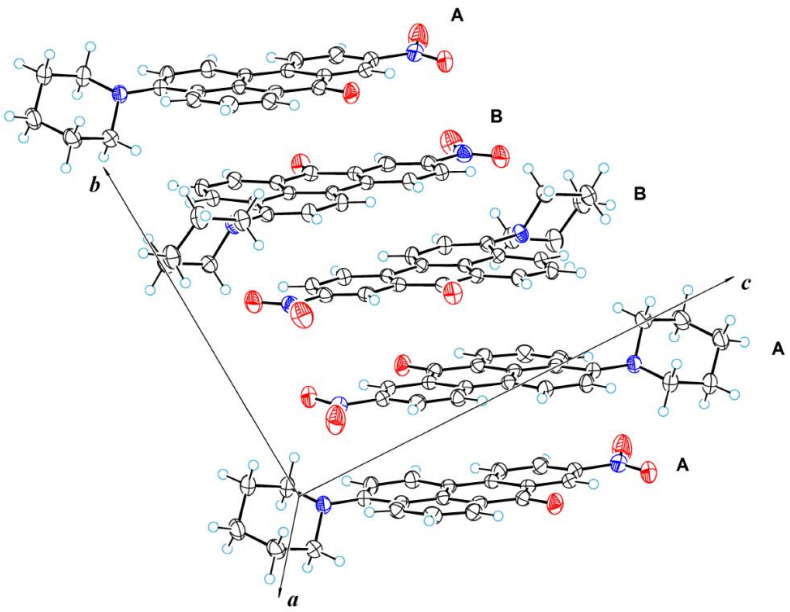

Fig. 2. A perspective view of the molecular stack of compound **3**.

The obtained dyes exhibit remarkable luminescent characteristics in different organic solvents. In this connection, the photophysical properties of the synthesized derivatives were examined, acquiring the absorption and emission spectra in seven organic solvents (benzene, ethyl acetate (EtOAc), chloroform ($CHCl_3$), acetone, ethanol (EtOH), *N*,*N*-dimethylformamide (DMF) and dimethyl sulfoxide (DMSO)) with a vast selection of polarities. The obtained spectral data are summarized in Tables 1 and 2, and Fig. 3 visually represents ultraviolet-visible (UV-Vis) absorption and fluorescence emission spectra of compound **3** in various organic solvents.

Table 1

Values of empirical polarity solvent parameter $E_T(30)$ [24]; absorption maxima and logarithmic value of molar absorption coefficient of compounds **2**–**5** in organic solvents (concentration 10^{-5} M)

Solvent	$E_T(30)$	Absorption λ_{abs}, nm; (lgε)			
		2	**3**	**4**	**5**
Benzene	34.3	498 (3.94)	460 (4.55)	447 (4.47)	453 (4.26)
EtOAc	38.1	493 (3.92)	459 (4.53)	447 (4.49)	454 (4.15)
$CHCl_3$	39.1	505 (4.01)	474 (4.62)	449 (4.56)	462 (4.26)
Acetone	42.2	512 (4.08)	467 (4.51)	448 (4.60)	462 (4.11)
EtOH	51.9	526 (3.97)	471 (4.50)	449 (4.49)	455 (3.99)
DMF	43.2	519 (4.18)	475 (4.50)	460 (4.54)	467 (4.17)
DMSO	45.1	531 (4.06)	478 (4.49)	466 (4.43)	472 (4.11)

Table 2

Fluorescence maxima and Stokes shifts of compounds **2**–**5** in organic solvents (concentration 10^{-5} M)

Solvent	Emission λ_{em}, nm, and Stokes shift, cm^{-1}							
	2		**3**		**4**		**5**	
Benzene	584	2957	578	4438	570	4564	574	4653
$CHCl_3$	613	3489	606	4596	592	4827	598	4923
EtOAc	598	3562	598	5064	592	5380	592	5135
Acetone	621	3428	620	5284	612	5479	612	5305
EtOH	661	3882	661	6103	652	5981	645	6474
DMF	630	3395	632	5230	624	6935	622	5336
DMSO	641	3231	643	5368	650	5713	634	5413

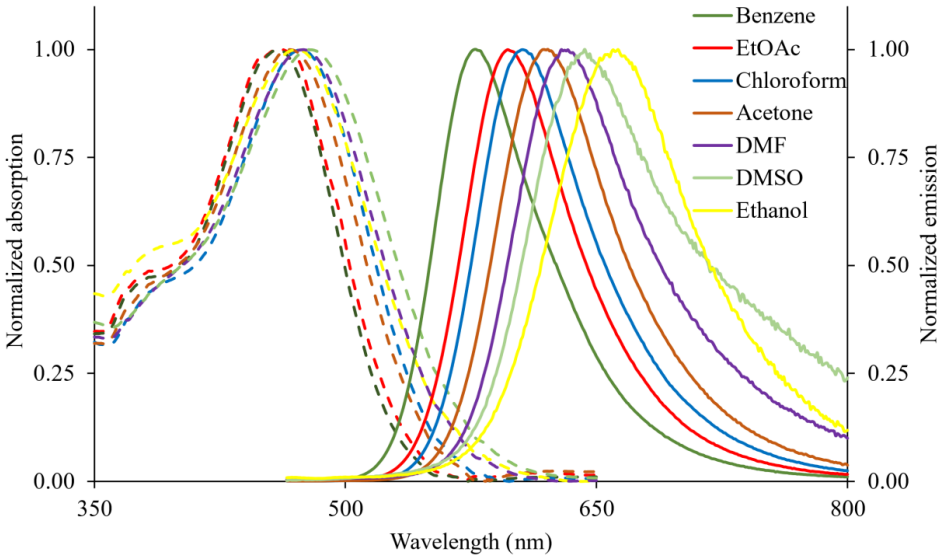

Fig. 3. Normalized UV-Vis absorption and fluorescence emission spectra of compound **3** in various organic solvents.

Derivative **2** absorbs light at 498–531 nm and exhibits a bathochromic shift of 33 nm from nonpolar benzene to polar DMSO, while amines **3** and **5** have shorter wavelength absorption band at 453–478 nm and shorter bathochromic shift of 18–19 nm.

The non-nitrated pyrrolidine derivative obtained earlier demonstrates absorption in the most extensive wavelength spectrum (525–558 nm) compared to all other compounds examined [3]. In the case of the prior, stronger interaction between the donor and the acceptor groups leads to a lowered electronic transition energy and an increase in the charge transfer once the photon is absorbed. The hypsochromic shift of the absorption band of compound **2** and the reduced sensitivity of the absorption maxima to the solvent polarity suggest a decrease in the ICT nature of the electronic transition. Thus, incorporating an electronegative nitro group into

the molecule leads to competition between this substituent and the molecule's carbonyl group, resulting in a new electron density distribution in the ground state.

In comparison to non-nitrated amines, compounds **2**–**5** exhibit stronger absorption; the average lgε is 4.30 for compounds **2**–**5**, whereas it is around 4.19 for non-nitrated counterpart compounds. The bathochromic shift of luminescence maxima (from benzene to DMSO) of the synthesized derivatives is similar to the bathochromic shift of non-nitrated derivatives: 60–85 nm.

Nitrated compounds **2** and **3** exhibit a shift in absorption maxima towards longer wavelengths, ranging from 15 nm to 35 nm, compared to their non-nitrated counterparts. However, their emission maxima display a shift towards shorter wavelengths, ranging from 3 nm to 14 nm, in comparison to the luminescence spectra of monosubstituted derivatives. Consequently, the Stokes shifts of the spectra of nitro derivatives are reduced compared to those of non-nitrated derivatives.

2. Synthesis and properties of α-aminophosphonates derived from 3-aminobenzanthrone

α-Aminophosphonates are analogous to amino acids (N-C-PO_3H_2 and N-C-CO_2H structural fragments accordingly) and thus possess a variety of biological activities due to their ability to inhibit enzymes involved in the metabolism of amino acids – acting as antagonists [25]. Thus, novel α-aminophosphonates are studied as potential antibiotics [26], antifungal [27] and chemotherapeutic agents [28], herbicides [29] and neuromodulators [30]. Additionally, these compounds have the potential to be used as antioxidants [31], sorbents [32], [33], corrosion inhibitors [34] and lubricating additives [35].

While many derivatives of α-aminophosphonates were obtained for diverse purposes, up to now, such fluorescent compounds have been scarcely studied, and the research is limited to benzene, naphthalene, anthracene and pyrene derivatives [36]–[40].

With the above mentioned in mind, it was concluded to be worth synthesizing and investigating the properties of 3-aminobenzanthrone α-aryl-α-aminophosphonate derivatives.

Synthetically α-aminophosphonates are usually obtained through Kabachnik-Fields reaction. This is a tricomponent coupling reaction of a carbonyl compound – a ketone or an aldehyde, an amine and a phosphonate (also referred to as a phosphite) (Scheme 2). Several modifications of this reaction were introduced since the discovery of this synthetic approach; among these are catalyzed variations, uncatalyzed ones and those employing dehydrating agents, ionic liquids and microwave irradiation [41]. Firstly, starting compound **6** was synthesized by reduction of 3-nitrobenzanthrone with sodium sulfide, which in turn was obtained by nitration of commercially available benzanthrone as described in previous research [42]. Then, it was decided on the most convenient and efficient method – a one-pot catalyst and solvent free one, where dialkyl phosphonate acts as a reactant and as a solvent. At 120 °C, the reaction yields orange to red compounds in 55–81% yield (Scheme 3). Thus, 22 compounds were obtained –a small library (Table 3), resulting from the investigation of both the nature of the aromatic substituent (with electron-accepting and electron-donating groups in various positions on the benzene ring and other types of substituents, such as 2-thienyl derivatives) on the alpha carbon, and the influence of phosphonate group substituents (methyl, ethyl, and isopropyl) on the properties of the new benzanthrone fluorophores.

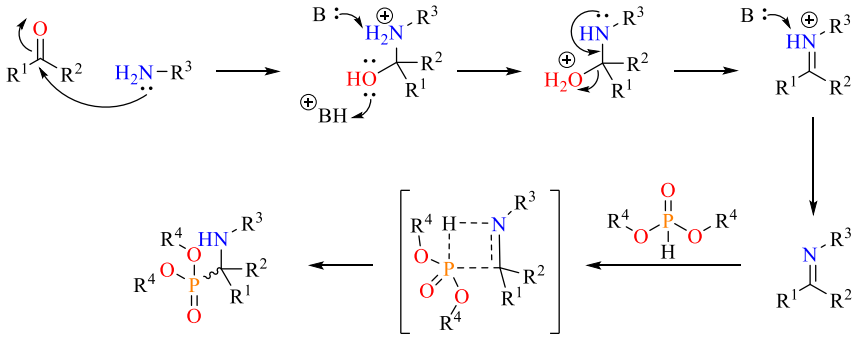

Scheme 2. Proposed mechanism of the Kabachnik-Fields reaction [43].

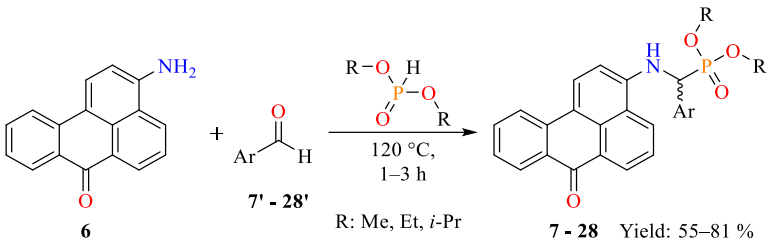

Scheme 3. Synthesis of benzanthrone α-aminophosphonate derivatives **7**–**28**.

Table 3

Structures of the obtained compounds **7**–**28**

R \ Ar	C_6H_5-	C_6H_4-(4-Me)	C_6H_4-(4-F)	C_6H_4-(4-Cl)	C_6H_4-(4-Br)	C_6H_4-(4-SMe)	C_6H_4-(4-OMe)	C_6H_4-(2-OMe)	C_6H_3-(3-CN-4-F)	2-thienyl
Me	**7**	**8**	**9**	**10**	**11**	**12**	**13**	**14**	**15**	**16**
Et	**17**	**18**	**19**	**20**	–	–	–	**21**	–	**22**
i-Pr	**23**	**24**	**25**	–	–	–	**26**	**27**	–	**28**

FTIR, ^{1}H-, ^{13}C- and ^{31}P-NMR spectra and mass spectrometric analysis confirm the chemical structures of prepared compounds. The X-ray crystallographic study of benzanthrone α-aminophosphonates additionally provided insights into the molecular arrangement and intermolecular interactions of these compounds in the crystalline state (Figs. 4–7). All molecular structures possess an asymmetric carbon atom, yet their crystal structures are achiral, therefore, these compounds represent true racemates. In the crystal structure of compound **17**, strong π-π stacking interactions occur between benzanthrone systems. In contrast, both compounds **22** and **23** exhibit strong intermolecular bonds of NH···O type in their crystal structure. Notably, the molecular structure of compound **11** features a strong intramolecular NH···O hydrogen bond between the amino group and the dimethyl phosphonate, forming an additional five-membered ring.

Absorbance and emission spectra of compounds **7**–**17** and **23** were acquired in solvents of varying polarity to investigate the photophysical properties of the obtained compounds. All the examined dyes exhibited fluorescence and displayed significant solvatochromic behavior, emitting light ranging from green in hexane to red in ethanol. No notable impact of substituents on the phenyl group or the type of aromatic substituent on the α-carbon (phenyl or thienyl), nor of phosphonate alkyl groups (methyl, ethyl, or isopropyl), was observed on the photophysical characteristics of the resulting chromophores. The first exception is the slightly elevated molar attenuation coefficients (4.60 (benzene) and 4.65 (DMSO)) observed in compound **23**, which bears bulkier isopropyl groups, in contrast to compounds **7** (4.10 (benzene) and 4.08 (DMSO)) and **17** (4.05 (benzene) and 4.03 (DMSO)), indicating a more pronounced absorption of

electromagnetic radiation. The second one is compound **15**, which bears strong electron-accepting groups, which decrease the extinction coefficients and quantum yields. Using compound **11** as an example, it is noted that benzanthrone α-aminophosphonates in solutions display a wide-band absorbance approximately between 458 nm and 500 nm and fluoresce from 534 nm (in hexane) to 636 nm (in ethanol) (Fig. 8), resulting in bathochromic shifts of 42 nm and 102 nm, respectively. This indicates that the polarity effect of the medium on fluorescence is more pronounced than on absorption. The highest Stokes shift among the examined dyes, measuring 4963 cm^{-1}, was noted for compound **16** in ethanol. The absorption spectra of previously investigated benzanthrone amidines fall within the range of 410 nm to 495 nm [15], [44], having absorption in the shorter wavelength region. In contrast, 3-substituted benzanthrone amino derivatives demonstrate absorption in the range of 430 nm to 520 nm [2], [10], having absorption in the longer wavelength region. It appears that the benzanthrone amino group, when attached to a phosphoryl group (compounds **7**–**28**), exhibits a donating effect slightly weaker than that of an alkyl amino group yet stronger than an amidino group.

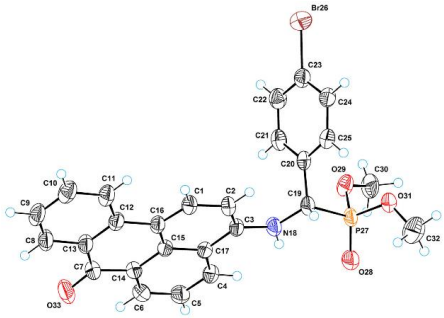

Fig. 4. ORTEP diagram of **11**. Crystal system: monoclinic.

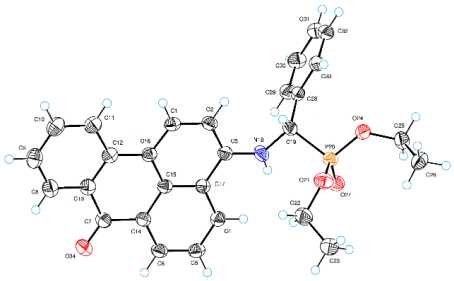

Fig. 5. ORTEP diagram of **17**. Crystal system: orthorhombic.

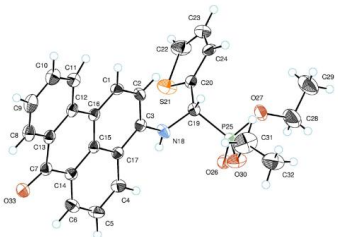

Fig. 6. ORTEP diagram of **22**. Crystal system: monoclinic.

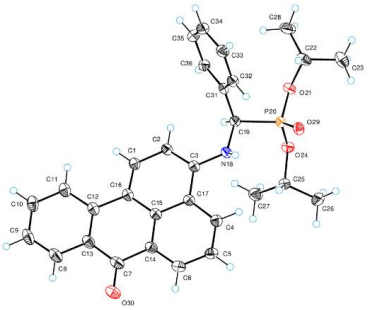

Fig. 7. ORTEP diagram of **23**. Crystal system: triclinic.

.

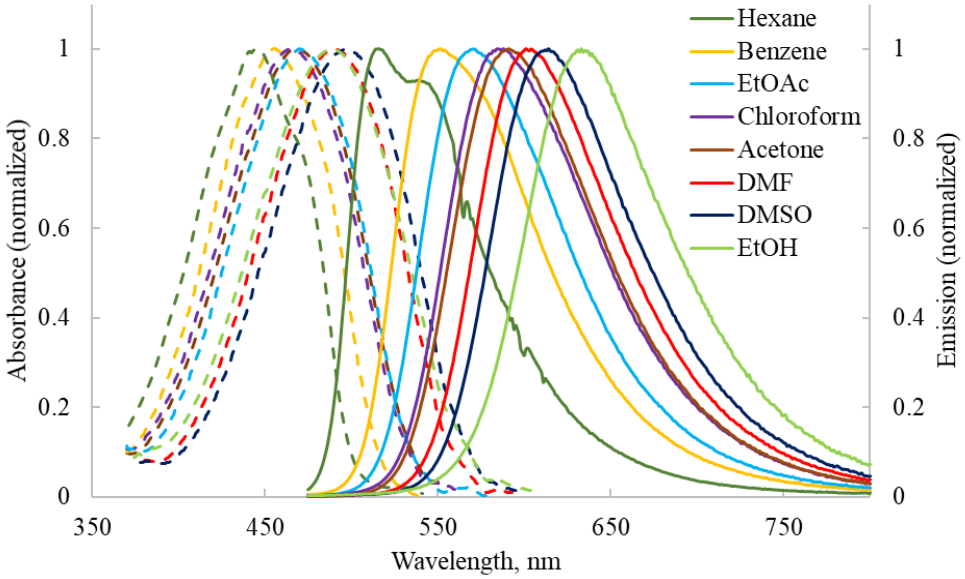

Fig. 8. Normalized UV-Vis absorption and fluorescence emission spectra of compound **11** in various organic solvents.

Using polarity-sensitive luminescent dyes is becoming more efficient in staining biological species in confocal laser scanning microscopy. Benzanthrone dyes **12** and **15,** enhanced by attached phosphoryl group lipophilicity, were utilized to bioimage the trematode *Opisthorchis felineus*, a parasite that mainly infects the livers of different mammals, including humans (Fig. 9) [45].

Fig. 9. Adult *Opisthorchis felineus* stained with the examined dyes: A – **12**;B – **15**.

To evaluate the toxicity of the obtained compounds and the impact of the aromatic substituent on the α-carbon atom, experiments were conducted on wheat sprout morphology, electrolyte leakage, malondialdehyde levels, and pigment quantification. Compounds with identical phosphonate group substituents (R = Me) and various aromatic groups (Ar) were used: a phenyl group without substituents (**7**), a phenyl group with a halogen atom, bromine, in the para position (**11**), and a thienyl group (**16**). Overall, benzanthrone α-aminophosphonates exhibit varying levels of toxic effects – phytotoxicity ranges from 37 % (**7**) to 83 % (**16**), depending on the concentration and the aromatic substituent on the α-carbon atom. The staining and toxicology of parasitic species were carried out in collaboration with researchers from the Institute of Life Sciences and Technology at Daugavpils University.

Thermal stability determines whether a compound can withstand the temperature conditions required for practical use over the long term. This was examined on the example of compound **17**, using differential thermal analysis (DTA) and thermogravimetry (TG) methods. According to the TG curve, thermal degradation occurs in two primary phases: between 270–330 °C (resulting in around 20 wt. % loss) and 630–950 °C (resulting in approximately 30 wt. % loss). Overall, the compound under analysis exhibits thermal stability up to roughly 270 °C, experiencing a 5 wt. % loss in initial mass, showing stability comparable to benzanthrone amino derivatives studied previously. To evaluate the impact of substituents on the thermal stability of the compounds, it would be worthwhile to continue the study.

3. Synthesis and properties of α-aminophosphonates derived from 1-aminoanthraquinone

Considering the scarcity of research on fluorescent α-aminophosphonate derivatives, a decision was made to take a step further and synthesize derivatives of anthraquinone for comparison with analogous benzanthrone compounds. Anthraquinone compounds are widely studied for use as fluorescent sensors [46], emitters and cell imaging agents [47], [48]. Some anthraquinone derivatives possess medicinal properties, including antibiotic, antiparasitic, insecticidal, fungicidal, and antiviral activities; they can also be used as chemotherapeutic agents [49], [50]. No anthraquinone α-aminophosphonates have been synthesized yet. The synthesis (Scheme 4) was carried out under the same conditions as for benzanthrones (Chapter 2). The structures of synthesized compounds are summarized in Table 4.

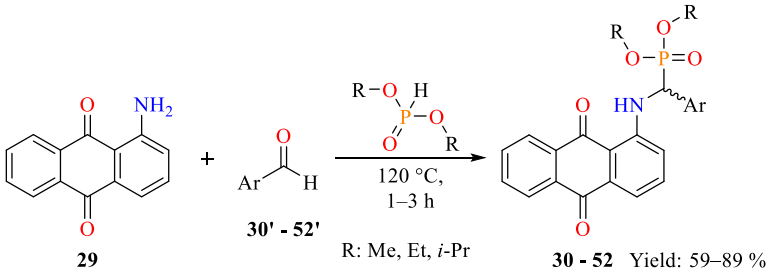

Scheme 4. Synthesis of anthraquinone α-aminophosphonate derivatives **30**–**52**.

Table 4

Structures of the obtained compounds **30**–**52**

R \ Ar	C_6H_5-	C_6H_4-(4-Me)	C_6H_4-(4-F)	C_6H_4-(4-Cl)	C_6H_4-(4-Br)	C_6H_4-(4-SMe)	C_6H_4-(4-OMe)	C_6H_4-(2-OMe)	C_6H_3-(3-CN-4-F)	2-thienyl
Me	**30**	**31**	**32**	**33**	**34**	**35**	**36**	**37**	**38**	**39**
Et	**40**	**41**	**42**	**43**	–	–	**44**	**45**	–	–
i-Pr	**46**	**47**	**48**	**49**	–	–	**50**	**51**	–	**52**

It is observed that in solutions, anthraquinone α-aryl-α-aminophosphonates exhibit broad band absorbance with maxima at around 465–488 nm showing small bathochromic shift from benzene to DMSO solution (5–8 nm) in contrast to unsubstituted compound **29**, for which the bathochromic shift of the absorption maximum between solutions in hexane and ethanol is 30 nm. Studied compounds show fluorescence with maxima from 585 nm (EtOAc) to 628 nm (DMSO), attaining fluorescence bathochromic shifts of up to 30 nm. The polarity effect of the medium on fluorescence is much more pronounced than on the absorption. It may be concluded that the impact of solvent polarity on the absorption and emission wavelength maxima is more pronounced for benzanthrone compounds. It is also observed that fluorescence quantum yields

are higher for the analogous benzanthrone compounds **11**, **12** and **15** (0.10–0.57) compared to the anthraquinone derivatives **34**, **35** and **38** (< 0.01–0.14).

To gain a deeper understanding of the photostability of new dyes, the photofading behavior of the derived compounds was assessed in ethanol (at a concentration of 10^{-4} M). To determine the effect of the phosphonate group substituent R on the photostability of the compounds, an experiment was conducted with compounds containing methyl (**30**), ethyl (**40**) and isopropyl groups (**46**) and the same aromatic substituent (phenyl group) on the α-carbon atom. The results were compared with the photostability of the starting material, 1-aminoanthraquinone (**29**), and the widely used test dye fluorescein (FL) (Fig. 11). Following a 4-hour irradiation period, fluorescein retained 71 % of its initial absorbance, whereas compound **30** retained only 27 %. Among the obtained compounds, those with ethyl (**40**) and isopropyl (**46**) groups displayed the highest photostability, with a decrease in absorption of 40 %. These findings indicate that the synthesized dyes exhibit greater photostability compared to the unsubstituted amine **29**.

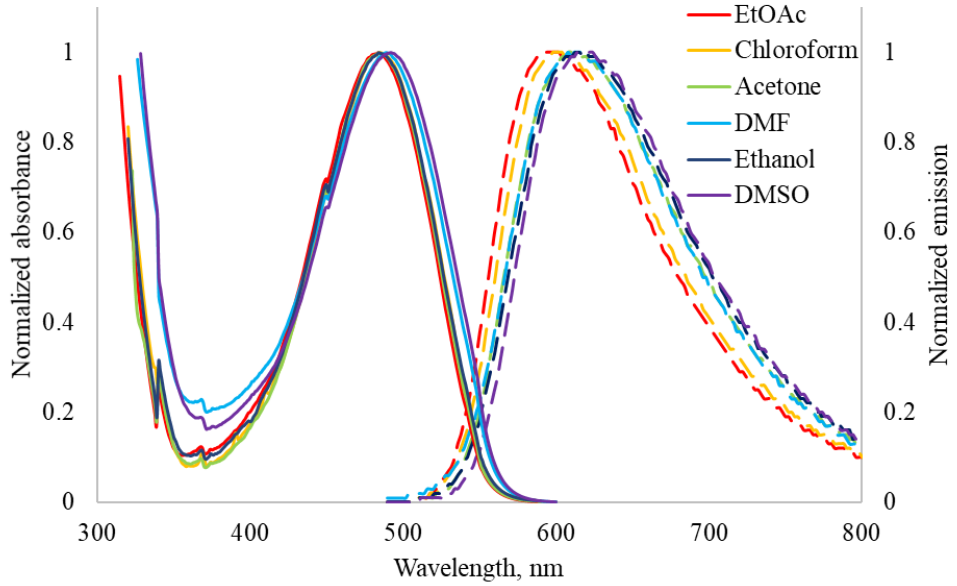

Fig. 10. Normalized UV-Vis absorption and fluorescence emission spectra of compound **49** in various organic solvents.

Anthraquinone α-aryl-α-aminophosphonates with an electron-donating group on benzene ring (4-thiomethyl) **35** and strong electron-withdrawing groups (3-cyano-4-fluoro) **38** were also subjected to testing for *Opisthorchis felineus*. Based on the initial data, benzanthrone dyes **12** and **15** with the same substituents, respectively, provided slightly clearer visualization of the structure and musculature of the parasite (Fig. 12). Consequently, it can be inferred that benzanthrone dyes **12** and **15** are more effective for visualizing *Opisthorchis felineus* flukes than anthraquinone dyes **35** and **38**. This can be attributed to a more lipophilic nature of the

latter, which has a significant impact on the visualization of these biological objects. Dye **49** was also used to stain a common parasite of the Eurasian amphibians – *Opisthioglyphe ranae* (Fig. 13) [51]. Overall, all tested dyes – **12**, **15**, **35**, **38** and **49** – demonstrated promising initial outcomes and are applicable for detailed and rapid bioimaging.

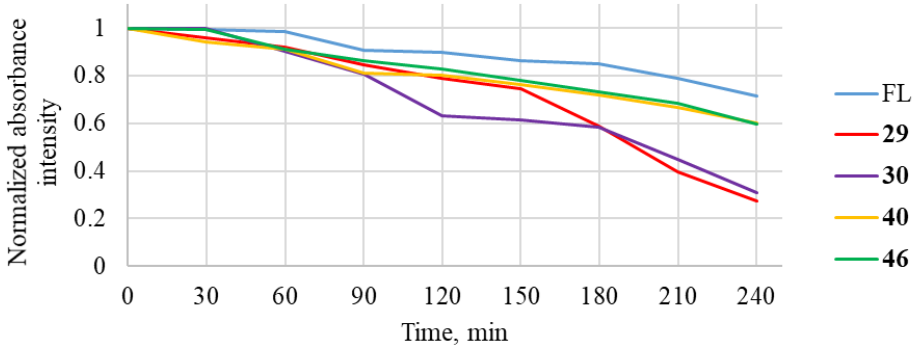

Fig. 11. Normalized absorbance intensities as a function of irradiation time upon 365 nm of fluoresceine (FL) and compounds **29**, **30**, **40** and **46**.

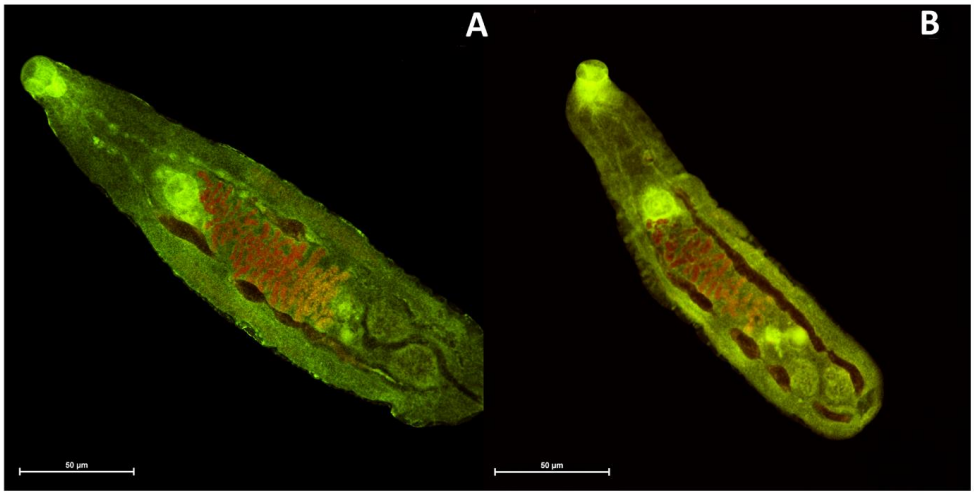

Fig. 12. Adult *Opisthorchis felineus* stained with the examined dyes: A – **35**;B – **38**.

Fig. 13. Adult *Opisthioglyphe ranae* stained with examined dye **49**.

4. Synthesis and properties of 3-thiobenzanthrones

To achieve the objective of the study, following the analysis of the properties of nitrogen-containing anthrone derivatives, the research was continued by introducing other heteroatoms into the benzanthrone molecule. Sulfur-containing compounds have garnered considerable attention within the scientific community. Notably, recent research has focused on various derivatives, including pyrene sulfides and sulfoxides [52], compounds featuring the dithiafulvene moiety [53], 1,5-bis-(4-alkylphenylthio)anthraquinone dyes with potential applications in liquid crystal systems [54], [55], as well as triarylcyclopentadiene compounds incorporating thiophene rings and dibenzothiophene groups [56]. These and other related compounds, along with their diverse applications, have been comprehensively reviewed in a recently published paper [57]. Previously, 3-mercaptobenzanthrone had been documented [58], and 14*H*-anthra[2,1,9-*mna*]thioxanthen-14-one was investigated as a semiconducting compound [59]. Additionally, benzanthrone compounds based on phenothiazine with thermally activated delayed fluorescence have been discussed [19]. Benzanthrone compounds featuring electron-donating substituents such as nitrogen and oxygen have been recorded and demonstrated to exhibit remarkable luminescent properties [18]. However, due to limited available data concerning thioalkyl and thiophenyl derivatives of benzanthrone, we have opted to pursue the synthesis and analysis of benzanthrone compounds incorporating sulfur and selenium.

Previously, numerous review articles extensively discussed the mechanism and synthesis of aliphatic and aromatic sulfides via nucleophilic aromatic substitution reactions [60]–[62]. This study introduces a practical approach to synthesize benzanthrone sulfides **54**–**62** (Table 5) through nucleophilic aromatic substitution reactions, utilizing 3-bromobenzanthrone as the principal electrophile and aliphatic thiols with varying steric bulk and aromatic thiols with electron-donating and electron-accepting groups as nucleophiles.

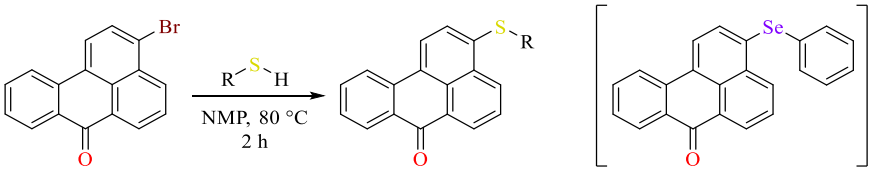

53 **54 - 62** Yield: 59–86 % **63** Yield: 60 %

Scheme 5. Synthesis of benzanthrone thio-derivatives **54**–**62** and structure of phenylselanyl derivative **63**.

Table 5

Summary of the structures of the obtained compounds **54**–**62**.

R	Me	*i*-Pr	cyclohexyl	*t*-Bu	-$(CH_2)_2$-Ph	C_6H_5-	C_6H_4-(4-Me)	C_6H_4-(4-F)	C_6H_4-(4-OMe)
Nr.	**54**	**55**	**56**	**57**	**58**	**59**	**60**	**61**	**62**

The reactions were conducted under basic conditions (NaOH) in *N*-methyl-2-pyrrolidone (NMP) (Scheme 5). Additionally, 3-(phenylselanyl)-7*H*-benzo[*de*]anthracen-7-one (**63**) was synthesized using the same method as aliphatic and aromatic sulfides, starting from sodium benzeneselenolate without the presence of a base, following a previously reported procedure. Theoretically, aliphatic thiols with larger steric bulk would be less reactive due to steric hindrance; in the case of aromatic thiols, those with electron-donating groups would be expected to exhibit greater reactivity due to increased nucleophilicity than those with electron-accepting groups [63], but a correlation between structures of substrates and reactivity has not been found.

FTIR, ^{1}H- and ^{13}C-NMR spectra and high-resolution mass spectrometric analysis confirmed the chemical structures of newly prepared compounds. Like in the crystal structures of 3-aminobenzanthrones, in the case of **15**, there also are π-π stacking interactions between benzanthrone systems and hydrogen bonds (Fig. 14).

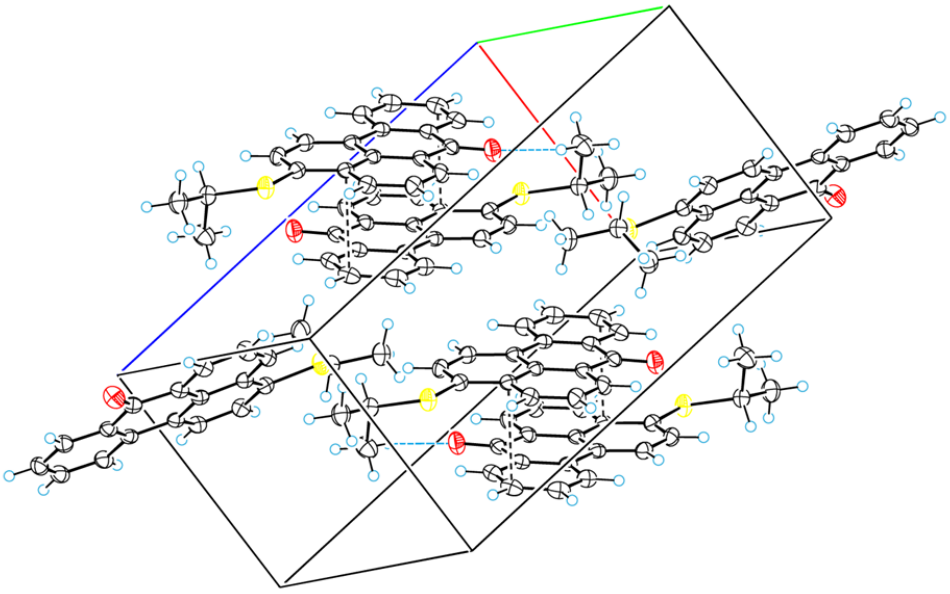

Fig. 14. Molecular packing in the unit cell of **55** showing the intermolecular shortened contacts.

Table 6 outlines the photophysical parameters of the thio derivatives with an aliphatic substituent (R = Me) **54** and an aromatic substituent (R = C_6H_5-) **59**, as well as 3-(phenylselanyl)benzanthrone **63**. The benzanthrone alkyl and aryl sulfides, along with 3-(phenylselanyl)benzanthrone in solutions, exhibited absorption bands ranging from 403 nm to 448 nm, with a shift towards longer wavelengths of 10 nm to 20 nm between the maxima in benzene and DMSO. Both alkyl and aryl sulfides emit light upon excitation from approximately

507 nm in benzene to 591 nm in ethanol (Fig. 15). Substituting the sulfur atom with the larger selenium atom slightly shifts the emission bathochromically and increases the Stokes shifts to some extent while extinction coefficients and absorption maxima remain largely unchanged. The highest fluorescence quantum yield for all studied compounds was observed in chloroform. Specifically, 3-(methylthio)benzanthrone exhibited the highest emission yield (0.31–0.52), followed by 3-(phenylthio)benzanthrone with slightly lower yields (0.08–0.24), while 3-(phenylselanyl)benzanthrone had the lowest emission yield (0.001–0.07). This trend is likely to be due to decreasing efficiency of charge transfer in the sequence.

Table 6

Absorption maxima and logarithmic value of molar absorption coefficient, fluorescence maxima, Stokes shifts, fluorescence quantum yields (Φ_F) and fluorescence lifetime values (τ) of compounds **54**, **59** and **63** in organic solvents (concentration 10^{-5} M)

Nr.	Solvent	Absorption λ_{abs}, nm; (lgε)	Emission λ_{em}, nm	Stokes shift, cm^{-1}	Φ_F	τ, ns
54	Benzene	429 (4.18)	508	3625	0.31	3.5
	$CHCl_3$	444 (4.16)	533	3761	0.52	10.0
	DMF	446 (4.06)	552	4306	0.40	10.7
	EtOH	448 (4.15)	587	5286	0.32	10.6
59	Benzene	413 (4.16)	504	4372	0.08	2.3
	$CHCl_3$	421 (4.18)	538	5166	0.24	9.3
	DMF	417 (4.15)	541	5497	0.14	5.6
	EtOH	423 (4.09)	583	6488	0.11	7.1
63	Benzene	416 (4.14)	510	4431	0.05	1.0
	$CHCl_3$	423 (4.14)	543	5224	0.07	3.7
	DMF	419 (4.11)	562	6073	0.001	-[a]
	EtOH	423 (4.04)	595	6834	0.001	-[a]

[a] The value could not be determined due to the low intensity of fluorescence.

Previously analyzed benzanthrone amidines absorb at 410–495 nm [15], [44], while 3-substituted benzanthrone amino derivatives absorb at 430–520 nm [2], [10]. As for the 3-methoxy and 3-phenoxy derivatives of benzanthrone, their absorption spectra range from 417 nm to 436 nm [18]. Interestingly, in sulfur and selenium derivatives, both the peaks of emission and absorption shift towards shorter wavelengths, indicating a slightly weaker donating effect compared to nitrogen and oxygen-containing species, which is also confirmed by the Hammett substituent constants, where the value for the amino group (-NH_2) is −0.66, −0.37 for the hydroxyl group (-OH), −0.10 for the thiol group (-SH), and −0.05 for the selenol group (-SeH) [64]. The ICT character and the nanosecond-scale light emission process of the dyes are indicative of the fluorescence emission mechanism.

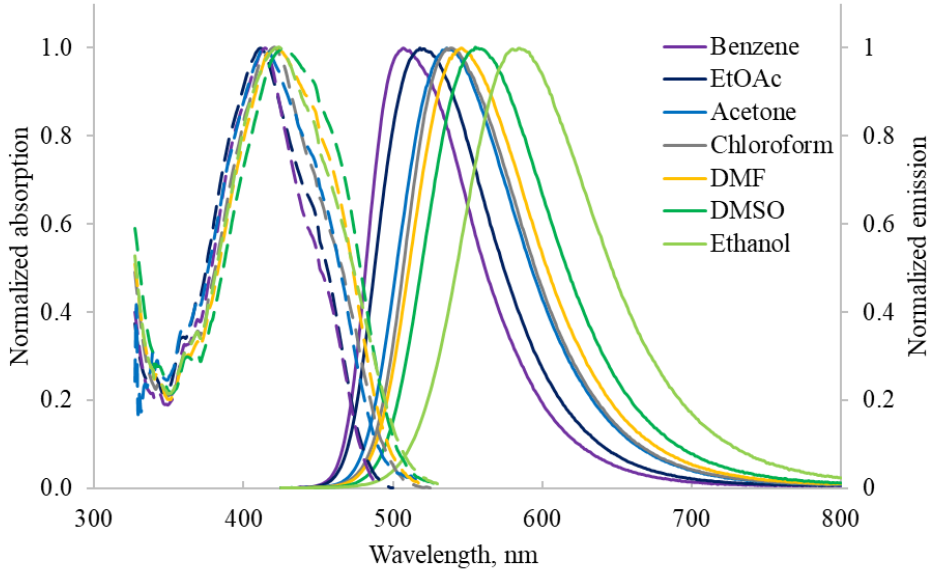

Fig. 15. Normalized UV-Vis absorption and fluorescence emission spectra of compound **59** in various organic solvents.

5. Synthesis and properties of 3-alkynylbenzanthrones

Another approach to fluorophore modification, in addition to the previously discussed methods of introducing functional groups and heteroatoms, is the extension of the conjugated system within the molecule.

Several theoretical and practical investigations indicate that directly attaching phenylacetylene groups to luminescent molecules alters their photophysical properties, enhancing fluorescent characteristics and enabling various applications. These molecules encompass pyrene [65], carbazole [66], anthraquinone [67], naphthalimide [68], and quninolylthiazole [69]. Such compounds can be applied in sensor technologies, organic light-emitting diode production, and fluorescent labeling [70]–[72]. Moreover, studies suggest that introducing electron-donating or electron-withdrawing groups to the phenyl rings of phenylacetylene moieties and adjusting the π-conjugation length can modify fluorescence yields, Stokes shift sizes, and absorption and emission maxima [73]. Consequently, it was determined to undertake the investigation of previously unexplored benzanthrone alkynes.

As of now, within the realm of palladium-catalyzed reactions, the only documented methods for synthesizing novel derivatives of benzanthrone are aryl cyanation and Buchwald–Hartwig amination reactions [19], [74]. The Sonogashira reaction is a cross-coupling reaction employed for synthesizing alkynes. It entails the reaction of a terminal alkyne with a palladium catalyst, a copper(I) co-catalyst, and an aryl (or vinyl) halide [75]. These conditions were utilized for synthesizing compounds **64**–**68** (Table 7) from 3-bromobenzanthrone (**53**) in *N*,*N*-dimethylacetamide, with triethylamine serving as a base (Scheme 6). The reaction progresses through a sequence of stages, commencing with the oxidative addition of the palladium catalyst to the aryl or vinyl halide, leading to the reductive elimination of the desired alkyne product. The copper(I) co-catalyst is crucial for facilitating the transmetalation step [76]. To determine the effect of the nature of the substituent R on the properties of the compounds, synthesis was carried out using terminal alkynes with electron-donating and electron-withdrawing groups of varying strength.

In the Sonogashira reaction, the products are formed through the creation of a new C-C bond between two covalent ligands as a result of reductive elimination. It is known that reductive elimination occurs slower in electron-rich complexes than in electron-deficient ones [77]. Consequently, higher reaction yields could be expected with alkynes containing electron-withdrawing groups; however, no correlation was found between the substrate structures and the reaction yields.

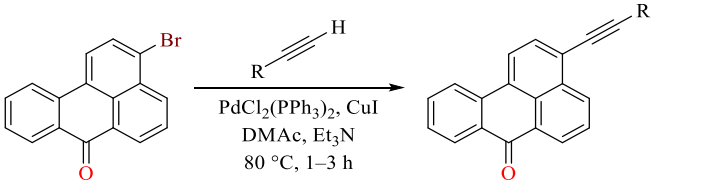

53 **64 - 69** Yield: 43–89 %

Scheme 6. Synthesis of benzanthrone alkynyl-derivatives **64**–**69**.

Table 7

Summary of the structures of the obtained compounds **64**–**69**

R	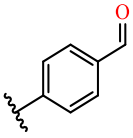	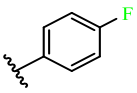	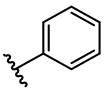	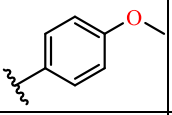	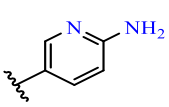	
Nr.	**64**	**65**	**66**	**67**	**68**	**69**

Table 8

Absorption maxima and logarithmic value of molar absorption coefficient of compounds **64**–**69** in organic solvents (concentration 10^{-5} M)

Solvent	Absorption λ_{abs}, nm; (lgε)				
	64	**65**	**67**	**68**	**69**
Benzene	416 (4.65)	423 (4.55)	427 (4.51)	432 (4.32)	423 (4.24)
EtOAc	412 (4.68)	416 (4.56)	425 (4.51)	437 (4.29)	419 (4.29)
$CHCl_3$	420 (4.72)	425 (4.52)	436 (4.46)	438 (4.49)	427 (4.22)
Acetone	414 (4.65)	419 (4.55)	432 (4.49)	445 (4.41)	419 (4.27)
DMF	419 (4.71)	423 (4.58)	437 (4.48)	455 (4.54)	422 (4.25)
DMSO	422 (4.68)	435 (4.50)	440 (4.42)	462 (4.55)	424 (4.26)
EtOH	430 (4.25)	429 (4.57)	442 (4.45)	446 (4.36)	419 (4.19)

Table 9

Fluorescence maxima and Stokes shifts of compounds **64**–**69** in organic solvents (concentration 10^{-5} M)

Solvent	Emission λ_{em}, nm, and Stokes shift, cm^{-1}				
	64	**65**	**67**	**68**	**69**
Benzene	463 (2440)	466 (2181)	502 (3499)	530 (4280)	482 (2894)
$CHCl_3$	462 (2627)	473 (2897)	510 (3922)	576 (5522)	479 (2990)
EtOAc	479 (2933)	498 (3449)	534 (4209)	574 (5409)	491 (3053)
Acetone	475 (3102)	492 (3541)	565 (5449)	641 (6871)	488 (3375)
DMF	481 (3076)	497 (3520)	553 (4800)	691 (7506)	495 (3495)
DMSO	489 (3247)	506 (3226)	570 (5183)	720 (7756)	494 (3342)
EtOH	515 (3838)	531 (4478)	598 (5902)	701 (8156)	495 (3664)

All investigated dyes exhibit fluorescence and demonstrate a significant solvatochromic effect (Tables 8 and 9). Figure 16 represents UV-Vis absorption and fluorescence emission spectra of compound **66** in various organic solvents. In solutions, benzanthrone alkynes exhibit two absorption bands around 310–330 nm and 420–450 nm, showing a bathochromic shift of 12–30 nm for the long wavelength absorption band between the maxima in benzene and DMSO. The impact of the polarity of solvents on fluorescence is more prominent than on absorbance. Synthesized compounds are fluorescent with emission from 462 nm (**64**, EtOAc) to 701 nm (**68**, EtOH). Obtained compounds display dual solvatochromism – not only emission

peak of each individual compound is influenced by solvent polarity, but a strong correlation between the electronic nature of substituents and photophysical parameters is evident as well; electron-withdrawing substituents shift emission hypsochromically and strong electron-donating substituents – bathochromically in the same solvent (Fig. 17). The electronic properties of the substituents significantly influence the emission efficiency of the studied substances. Derivatives with electron-withdrawing groups (**64** and **65**) have a higher luminescence quantum yield in ethanol (0.67 and 0.74, respectively) compared with less polar solvents (0.01–0.41). In contrast, derivatives with donor groups luminesce more intensely in chloroform than in ethanol. In turn, the presence of a trimethylsilyl group leads to a dramatic drop in emission efficiency. The alteration of photophysical parameters also has an impact on Stokes shifts. Specifically, the range of Stokes shifts varies from 2181 cm^{-1} for compound **65** in a less polar solvent (benzene) to 8156 cm^{-1} for compound **68** in a polar ethanol. Thus, the presence of an electron-donating substituent leads to a larger Stokes shift.

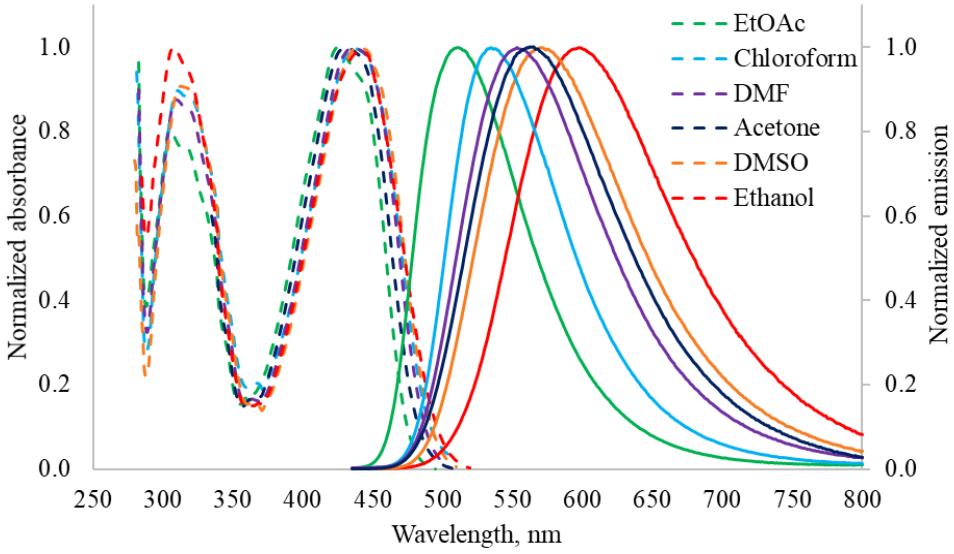

Fig. 16. Normalized UV-Vis absorption and fluorescence emission spectra of compound **66** in various organic solvents.

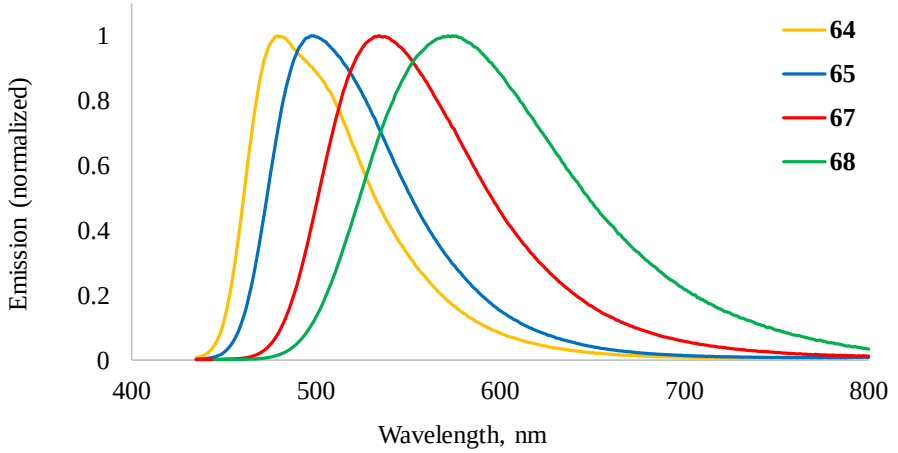

Fig. 17. Normalized fluorescence emission spectra of compounds **64**–**67** in chloroform.

To estimate the photostability of the dyes **64**–**69**, the photofading process of synthesized derivatives was conducted in ethanol (at a concentration of 10^{-4} M) and compared with the widely used test dye, fluorescein. The results are illustrated in Fig. 18. Following a 4-hour irradiation period, fluorescein exhibited an absorbance of 71 % of its initial level. Among the synthesized compounds, derivative **65** with a fluorine atom displayed the highest photostability, retaining 96 % of its initial absorption. Following closely is compound **64**, featuring a formyl group with a photostability of 82 %. Conversely, the derivative containing a methoxy group, compound **67**, demonstrated the lowest stability, losing more than half of its absorption (57 %) by the end of the experiment. These findings indicate that three of the synthesized substances – **64**, **65**, and **69** – exhibit greater photostability than fluorescein.

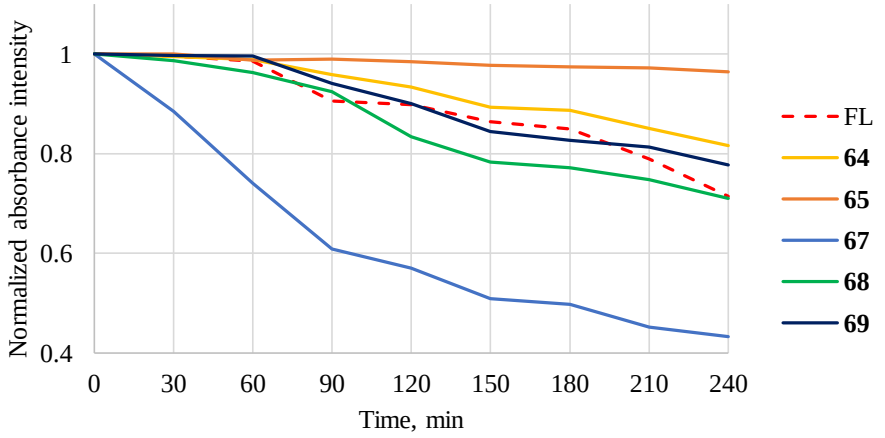

Fig. 18. Normalized absorbance intensities as a function of irradiation time upon 365 nm of fluoresceine (FL) and compounds **64**–**68**.

Given the established nonlinear optical properties of certain benzanthrones and the understanding that extending π-conjugation may enhance these properties, both these benzanthrone alkynes and compounds not covered in the Thesis, specifically, products obtained in reaction with 4-ethynyl-*N*,*N*-dimethylaniline, 1-ethynyl-4-(trifluoromethyl)benzene, 3-ethynylthiophene and methyl propiolate, are currently being investigated for their nonlinear optical characteristics.

As a result of the work, the collection of fluorescent compounds of benzanthrone and anthraquinone was expanded. The Stokes shift dependence on the absorption maximum in acetone for the compounds studied in the Thesis is shown in Fig. 19. Benzanthrone and anthraquinone amino derivatives exhibit longer wavelength absorption and emission, allowing them to be used in microscopy for staining biological objects, as this reduces sample autofluorescence and achieves increased image contrast. Thioalkyl and thiophenyl substituents have a weaker electron-donating effect, which increases the required energy for the benzanthrone's excited state. Although benzanthrone thio derivatives generally have larger Stokes shifts (from 4089 cm^{-1} to 6052 cm^{-1}) than α-aminophosphonates (from 3798 cm^{-1} to 4170 cm^{-1}), their emission wavelength is too short for effective application in confocal laser scanning microscopy. Additionally, for benzanthrone alkyne derivatives, the absorption and emission maxima increase with the enhancement of the substituent's electron-donating effect; however, in contrast to other compounds, as the absorption maximum increases, the Stokes shift also increases. For example, compound (**64**) with a strong electron-withdrawing substituent absorbs light with a maximum at 414 nm, and its Stokes shift is 3102 cm^{-1}. In contrast, compound (**68**) with a strong electron-donating substituent absorbs light with a maximum at 445 nm, and its Stokes shift is 6871 cm^{-1}. In order to reasonably establish the nature of these relationships, further research is needed.

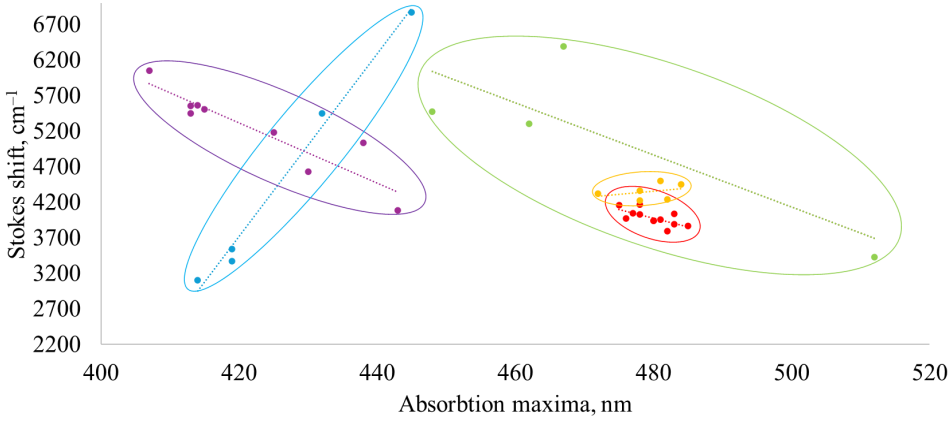

Fig. 19. The dependence of the Stokes shift of the compounds studied in this work on the absorption maximum in acetone. Green: benzanthrone 3-amino-9-nitro derivatives; red: benzanthrone α-aminophosphonates; orange: anthraquinone α-aminophosphonates; purple: benzanthrone thio derivatives; blue: benzanthrone alkynyl derivatives.

CONCLUSIONS

1. As a result of the research, new synthesis methods for benzanthrone and anthraquinone derivatives were successfully investigated. The range of fluorescent compounds was expanded with derivatives obtained through nucleophilic aromatic substitution, Kabachnik-Fields, and Sonogashira reactions. Spectral analysis was performed on the obtained compounds, and their photophysical properties were studied. Additionally, the practical application of the new compounds with enhanced properties in microscopy was demonstrated.

2. Aromatic substitution reaction of 3-bromo-9-nitrobenzanthrone provides substituted 3-amino-9-nitrobenzanthrones in 48–63 % yield with absorption from 447 nm to 531 nm and emit light from 570 nm to 650 nm. The reactivity of 3-bromo-9-nitrobenzanhtrone is enhanced compared to non-nitrated analogues, and higher molar absorption coefficients render them better candidates for non-linear optics.

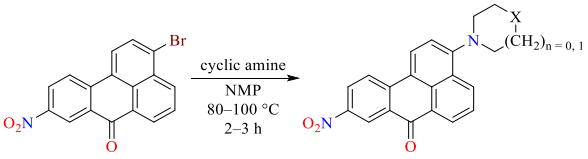

3. Kabachnik-Fields reaction of 3-aminobenzanthrone and 1-aminoanthraquinone provides fluorescent α-aminophosphonates in 55–89 % yield. The emission band shows a bathochromic shift from hexane to DMSO; for benzanthrone derivatives, it reaches 100 nm, while for anthraquinone, it is only 40 nm. Fluorescence quantum yields of benzanthrone α-aminophosphonates are up to 10 times higher, from 0.01 to 0.17 for anthraquinone derivatives and from 0.1 to 0.56 for benzanthrone derivatives.

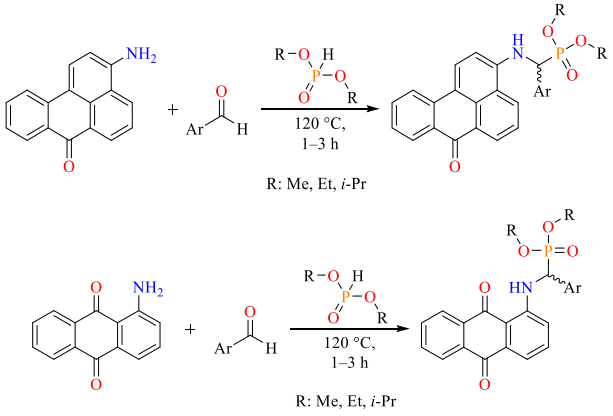

4. Both benzanthrone and anthraquinone α-aminophosphonates (compounds **12**, **15**, **35**, **38**, and **49**) are suitable for staining and studying biological samples, particularly parasitic trematodes, using confocal laser scanning microscopy.

5. Aromatic substitution reaction of 3-bromobenzanthrone with thiols provides alkyl and aryl substituted 3-thiobenzanthrone dyes in 59–86 % yield. Studied compounds exhibit fluorescence and solvatochromism with quantum yields of up to 52 %, absorption from 403 nm to 448 nm and emit light from 507 nm to 591 nm.

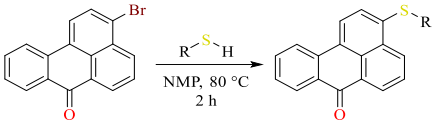

6. Sonogashira reaction of 3-bromobenzanthrone with terminal alkynes was studied. This reaction provides substituted 3-alkynylbenzanthrones in 43–89 % yield with 420–450 nm long-wave absorption and emits light from 462 nm to 701 nm. Electron-donating groups on aryl rings of alkynes shift absorption and emission maxima bathochromically, whereas electron-withdrawing groups – hypsochromically. High photostability and elongated π-conjugation make them possible candidates for applications in non-linear optical technologies.

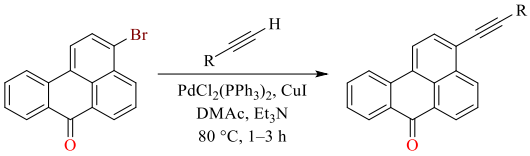

REFERENCES

1. Introduction to Fluorescence. In *Principles of Fluorescence Spectroscopy*; Springer US: Boston, MA, 2006; pp. 1–26.
2. Grabchev, I.; Bojinov, V.; Moneva, I. The Synthesis and Application of Fluorescent Dyes Based on 3-Amino Benzanthrone. *Dyes and Pigments* **2001**, *48*, 143–150, doi:10.1016/S0143-7208(00)00098-X.
3. Kirilova, E. M.; Meirovics, I.; Belyakov, S. V. Preparation and Properties of Nitrogen Derivatives of Benzanthrone with Heterocyclic Fragments. *Chem. Heterocycl. Compd. (N Y)* **2002**, *38*, 789–792, doi:10.1023/A:1020621418164.
4. Siddlingeshwar, B.; Hanagodimath, S. M.; Kirilova, E. M.; Kirilov, G. K. Photophysical Characteristics of Three Novel Benzanthrone Derivatives: Experimental and Theoretical Estimation of Dipole Moments. *J. Quant. Spectrosc. Radiat. Transf.* **2011**, *112*, 448–456, doi:10.1016/j.jqsrt.2010.09.001.
5. Thomas, A.; Kirilova, E. M.; Nagesh, B. V.; Manohara, S. R.; Siddlingeshwar, B.; Belyakov, S. V. Synthesis, Solvatochromism and DFT Study of Pyridine Substituted Benzanthrone with ICT Characteristics. *J. Mol. Struct.* **2022**, *1262*, 132971, doi:10.1016/j.molstruc.2022.132971.
6. Grabchev, I.; Moneva, I. Synthesis and Properties of Benzanthrone Derivatives as Luminophore Dyes for Liquid Crystals. *Dyes and Pigments.* **1998**, *37*, 155–164, doi:10.1016/S0143-7208(97)00050-8.
7. Grabtchev, I. K.; Bojinov, V. B.; Moneva, I. T. Functional Properties of Azomethine Substituted Benzanthrone Dyes for Use in Nematic Liquid Crystals. *J. Mol. Struct.* **1998**, *471*, 19–25, doi:10.1016/S0022-2860(98)00400-1.
8. Grabchev, I.; Mykowska, E.; Moneva, I.; Bauman, D. Molecular Orientation of Some Fluorescent Dichroic Dyes in Nematic Liquid Crystal. *Zeitschrift für Naturforschung A.* **2004**, *59*, 368–374, doi:10.1515/zna-2004-0610.
9. Almalki, A. S. A.; Alhadhrami, A.; Obaid, R. J.; Alsharif, M. A.; Adam, A. M. A.; Grabchev, I.; Refat, M. S. Preparation of Some Compounds and Study Their Thermal Stability for Use in Dye Sensitized Solar Cells. *J. Mol. Liq.* **2018**, *261*, 565–582, doi:10.1016/j.molliq.2018.04.057.
10. Orlova, N.; Nikolajeva, I.; Pučkins, A.; Belyakov, S.; Kirilova, E. Heterocyclic Schiff Bases of 3-Aminobenzanthrone and Their Reduced Analogues: Synthesis, Properties and Spectroscopy. *Molecules.* **2021**, *26*, 2570, doi:10.3390/molecules26092570.
11. Kirilova, A.; Pučkins, A.; Belyakov, S.; Kirilova, E. 3-[N-(4-Methoxybenzyl)Amino]Benzo[de]Anthracen-7-One. *Molbank.* **2021**, *2021*, M1287, doi:10.3390/M1287.
12. Staneva, D.; Betcheva, R. Synthesis and Functional Properties of New Optical PH Sensor Based on Benzo[de]Anthracen-7-One Immobilized on the Viscose. *Dyes and Pigments.* **2007**, *74*, 148–153, doi:10.1016/j.dyepig.2006.01.029.
13. Staneva, D.; Grabchev, I. Heterogeneous Sensors for Ammonia, Amines and Metal Ions Based on a Dendrimer Modified Fluorescent Viscose Fabric. *Dyes and Pigments.* **2018**, *155*, 164–170, doi:10.1016/j.dyepig.2018.03.044.
14. Staneva, D.; Vasileva-Tonkova, E.; Makki, M. S. I.; Sobahi, T. R.; Abdel-Rahman, R. M.; Asiri, A. M.; Grabchev, I. Synthesis, Photophysical and Antimicrobial Activity of New Water Soluble Ammonium Quaternary Benzanthrone in Solution and in

Polylactide Film. *J. Photochem. Photobiol. B.* **2015**, *143*, 44–51, doi:10.1016/j.jphotobiol.2014.12.024.
15. Gonta, S.; Utinans, M.; Kirilov, G.; Belyakov, S.; Ivanova, I.; Fleisher, M.; Savenkov, V.; Kirilova, E. Fluorescent Substituted Amidines of Benzanthrone: Synthesis, Spectroscopy and Quantum Chemical Calculations. *Spectrochim Acta A Mol. Biomol. Spectrosc.* **2013**, *101*, 325–334, doi:10.1016/j.saa.2012.09.104.
16. Kirilova, E.; Kecko, S.; Mežaraupe, L.; Gavarāne, I.; Pučkins, A.; Mickeviča, I.; Rubeniņa, I.; Osipovs, S.; Bulanovs, A.; Pupiņš, M.; et al. Novel Luminescent Dyes for Confocal Laser Scanning Microscopy Used in Trematoda Parasite Diagnostics. *Acta Biochim. Pol.* **2018**, *65*, 449–454, doi:10.18388/abp.2018_2574.
17. Rubenina, I.; Gavarane, I.; Kirilova, E.; Mezaraupe, L.; Kirjusina, M. Comparison of the Benzanthrone Luminophores: They Are Not Equal for Rapid Examination of Parafasciolopsis Fasciolaemorpha (Trematoda: Digenea). *Biomolecules.* **2021**, *11*, 598, doi:10.3390/biom11040598.
18. Grabchev, I.; Moneva, I.; Wolarz, E.; Bauman, D. Fluorescent 3-Oxy Benzanthrone Dyes in Liquid Crystalline Media. *Dyes and Pigments.* **2003**, *58*, 1–6, doi:10.1016/S0143-7208(03)00033-0.
19. Tsiko, U.; Bezvikonnyi, O.; Volyniuk, D.; Minaev, B. F.; Keruckas, J.; Cekaviciute, M.; Jatautiene, E.; Andruleviciene, V.; Dabuliene, A.; Grazulevicius, J.V. TADF Quenching Properties of Phenothiazine or Phenoxazine-Substituted Benzanthrones Emitting in Deep-Red/near-Infrared Region towards Oxygen Sensing. *Dyes and Pigments.* **2022**, *197*, 109952, doi:10.1016/j.dyepig.2021.109952.
20. Tsiko, U.; Sych, G.; Volyniuk, D.; Bezvikonnyi, O.; Keruckiene, R.; Lazauskas, A.; Grazulevicius, J. V. Self-Recovering Mechanochromic Luminescence of the Derivatives of Benzanthrone and Carbazole: Towards Damage-Resistive Information Recording and Security Probes. *Dyes and Pigments.* **2022**, *199*, 110082, doi:10.1016/j.dyepig.2022.110082.
21. Thomas, A.; Patil, P. S.; Siddlingeshwar, B.; Manohara, S. R.; Gummagol, N. B.; Krishna Chaitanya, G.; Kirilova, E. M. Nonlinear Optical Properties of Benzanthrone Derivatives with N'-Methylpiperazin-1-Yl and N'-Phenylpiperazin-1-Yl Substituents: Experimental and Quantum Chemical Study. *Opt. Laser Technol.* **2022**, *156*, 108616, doi:10.1016/j.optlastec.2022.108616.
22. Thomas, A.; Kirilova, E. M.; Nagesh, B. V.; Krishna Chaitanya, G.; Philip, R.; Manohara, S. R.; Sudeeksha, H. C.; Siddlingeshwar, B. Influence of Nitro Group on Solvatochromism, Nonlinear Optical Properties of 3-Morpholinobenzanthrone: Experimental and Theoretical Study. *J. Photochem. Photobiol. A. Chem.* **2023**, *437*, 114434, doi:10.1016/j.jphotochem.2022.114434.
23. Day, F. H. Nitration of the 13-Halogenobenzanthrones. *Journal of the Chemical Society (Resumed)* **1940**, 1474, doi:10.1039/jr9400001474.
24. Cerón-Carrasco, J. P.; Jacquemin, D.; Laurence, C.; Planchat, A.; Reichardt, C.; Sraïdi, K. Solvent Polarity Scales: Determination of New ET(30) Values for 84 Organic Solvents. *J. Phys. Org. Chem.* **2014**, *27*, 512–518, doi:10.1002/poc.3293.
25. Mucha, A.; Kafarski, P.; Berlicki, Ł. Remarkable Potential of the α-Aminophosphonate/Phosphinate Structural Motif in Medicinal Chemistry. *J. Med. Chem.* **2011**, *54*, 5955–5980, doi:10.1021/jm200587f.
26. Litim, B.; Djahoudi, A.; Meliani, S.; Boukhari, A. Synthesis and Potential Antimicrobial Activity of Novel α-Aminophosphonates Derivatives Bearing Substituted Quinoline or

Quinolone and Thiazole Moieties. *Medicinal Chemistry Research.* **2022**, *31*, 60–74, doi:10.1007/s00044-021-02815-5.
27. Rezaei, Z.; Khabnadideh, S.; Zomorodian, K.; Pakshir, K.; Nadali, S.; Mohtashami, N.; Faghih Mirzaei, E. Design, Synthesis, and Antifungal Activity of New α -Aminophosphonates. *Int. J. Med. Chem.* **2011**, *2011*, 1–11, doi:10.1155/2011/678101.
28. Varga, P. R.; Szabó, R. O.; Dormán, G.; Bősze, S.; Keglevich, G. Cytotoxic Activity of α-Aminophosphonic Derivatives Coming from the Tandem Kabachnik-Fields Reaction and Acylation. *Pharmaceuticals.* **2023**, *16*, 506, doi:10.3390/ph16040506.
29. Grzyś, E.; Bielecki, K.; Sarapuk, J. Aminophosphonate-Induced Changes of Betacyanine and Ionic Efflux. *Zeitschrift für Naturforschung C.* **2001**, *56*, 349–352, doi:10.1515/znc-2001-5-605.
30. Kafarski, P.; Lejczak, B. Biological Activity of Aminophosphonic Acids. *Phosphorus Sulfur Silicon Relat. Elem.* **1991**, *63*, 193–215, doi:10.1080/10426509108029443.
31. Reddy, N. B.; Sundar, C. S.; Krishna, B. S.; Santhisudha, S.; Sreelakshmi, P.; Nayak, S. K.; Reddy, C. S. Cellulose-SO3H Catalyzed Synthesis of Bis(α-Aminophosphonates) and Their Antioxidant Activity. *Organic Communications.* **2017**, *10*, 46–55, doi:10.25135/acg.oc.8.16.06.422.
32. Fouda, S. R.; El-Sayed, I. E.; Attia, N. F.; Abdeen, M. M.; Abdel Aleem, A. A. H.; Nassar, I. F.; Mira, H. I.; Gawad, E. A.; Kalam, A.; Al-Ghamdi, A. A.; et al. Mechanistic Study of Hg(II) Interaction with Three Different α-Aminophosphonate Adsorbents: Insights from Batch Experiments and Theoretical Calculations. *Chemosphere.* **2022**, *304*, 135253, doi:10.1016/j.chemosphere.2022.135253.
33. Imam, E. A.; Hashem, A. I.; Tolba, A. A.; Mahfouz, M. G.; El-Sayed, I. E.-T.; El-Tantawy, A. I.; Galhoum, A. A.; Guibal, E. Effect of Mono- vs. Bi-Functionality of Aminophosphonate Derivatives on the Enhancement of U(VI) Sorption: Physicochemical Properties and Sorption Performance. *J. Environ. Chem. Eng.* **2023**, *11*, 109951, doi:10.1016/j.jece.2023.109951.
34. Moumeni, O.; Mehri, M.; Kerkour, R.; Boublia, A.; Mihoub, F.; Rebai, K.; Khan, A. A.; Erto, A.; Darwish, A. S.; Lemaoui, T.; et al. Experimental and Detailed DFT/MD Simulation of α-Aminophosphonates as Promising Corrosion Inhibitor for XC48 Carbon Steel in HCl Environment. *J. Taiwan Inst. Chem. Eng.* **2023**, *147*, 104918, doi:10.1016/j.jtice.2023.104918.
35. Li, S.; Liu, R.; Han, X.; Ge, C.; Zhang, X. Diethyl α-Aminophosphonate Containing Lubricating Additives Synthesized from (3-Aminophenyl)Boronic Acid Pinacol Ester. *Inorg. Chem. Commun.* **2022**, *140*, 109477, doi:10.1016/j.inoche.2022.109477.
36. Górny vel Górniak, M.; Kafarski, P. Preparation of the Library of Fluorescent Aromatic Aminophosphonate Phenyl and Benzyl Esters. *Phosphorus Sulfur Silicon Relat. Elem.* **2016**, *191*, 511–519, doi:10.1080/10426507.2015.1094658.
37. Kuśnierz, A.; Chmielewska, E. Synthesis of Fluorescent Aminophosphonates by Green Chemistry Procedures. *Phosphorus Sulfur Silicon Relat. Elem.* **2017**, *192*, 700–705, doi:10.1080/10426507.2017.1308934.
38. Wang, Q.-M.; Gao, W.; Song, J.-L.; Liu, Y.; Qi, H.; Tang, X.-H. Synthesis, X-Ray Crystallographic Analysis and BSA Interaction of a New α-Aminophosphonate. *J. Appl. Spectrosc.* **2016**, *83*, 703–709, doi:10.1007/s10812-016-0351-9.
39. Lewkowski, J.; Rodriguez Moya, M.; Wrona-Piotrowicz, A.; Zakrzewski, J.; Kontek, R.; Gajek, G. Synthesis, Fluorescence Properties and the Promising

Cytotoxicity of Pyrene–Derived Aminophosphonates. *Beilstein Journal of Organic Chemistry.* **2016**, *12*, 1229–1235, doi:10.3762/bjoc.12.117.
40. Kraicheva, I.; Vodenicharova, E.; Tashev, E.; Tosheva, T.; Tsacheva, I.; Troev, K. Synthesis and NMR Characterization of Two Novel Anthracene-Derived BIS-Aminophosphonates. Basic Hydrolysis of Some Aminophosphonate Derivatives. *Phosphorus Sulfur Silicon Relat. Elem* **2012**, *187*, 660–667, doi:10.1080/10426507.2011.638349.
41. Varga, P. R.; Keglevich, G. Synthesis of α-Aminophosphonates and Related Derivatives; The Last Decade of the Kabachnik-Fields Reaction. *Molecules.* **2021**, *26*, 2511, doi:10.3390/molecules26092511.
42. Lüttringhaus, A.; Neresheimer, H. Zur Kenntnis Des Benzanthrons. *Justus Liebigs Ann. Chem.* **1929**, *473*, 259–289, doi:10.1002/jlac.19294730115.
43. Keglevich, G.; Bálint, E. The Kabachnik-Fields Reaction: Mechanism and Synthetic Use. *Molecules.* **2012**, *17*, 12821–12835, doi:10.3390/molecules171112821.
44. Kirilova, E. M.; Puckins, A. I.; Romanovska, E.; Fleisher, M.; Belyakov, S. V. Novel Amidine Derivatives of Benzanthrone: Effect of Bromine Atom on the Spectral Parameters. *Spectrochim. Acta A Mol. Biomol. Spectrosc.* **2018**, *202*, 41–49, doi:10.1016/j.saa.2018.05.029.
45. Armignacco, O.; Caterini, L.; Marucci, G.; Ferri, F.; Bernardini, G.; Raponi, G. N.; Ludovisi, A.; Bossù, T.; Morales, M. A. G.; Pozio, E. Human Illnesses Caused by Opisthorchis Felineus Flukes, Italy. *Emerg. Infect. Dis.* **2008**, *14*, 1902–1905, doi:10.3201/eid1412.080782.
46. Kaur, N.; Gauri Anthraquinone Appended Chemosensors for Fluorescence Monitoring of Anions and/or Metal Ions. *Inorganica Chim. Acta.* **2022**, *536*, 120917, doi:10.1016/j.ica.2022.120917.
47. Bin Huang; Ji, Y.; Li, Z.; Zhou, N.; Jiang, W.; Feng, Y.; Lin, B.; Sun, Y. Simple Aggregation-Induced Delayed Fluorescence Materials Based on Anthraquinone Derivatives for Highly Efficient Solution-Processed Red OLEDs. *J. Lumin.* **2017**, *187*, 414–420, doi:10.1016/j.jlumin.2017.03.038.
48. Yang, L.; Fu, Z.; Niu, X.; Zhang, G.; Cui, F.; Zhou, C. Probing the Interaction of Anthraquinone with DNA by Spectroscopy, Molecular Modeling and Cancer Cell Imaging Technique. *Chem. Biol. Interact.* **2015**, *233*, 65–70, doi:10.1016/j.cbi.2015.03.026.
49. Malik, M. S.; Alsantali, R. I.; Jassas, R. S.; Alsimaree, A. A.; Syed, R.; Alsharif, M. A.; Kalpana, K.; Morad, M.; Althagafi, I. I.; Ahmed, S. A. Journey of Anthraquinones as Anticancer Agents – a Systematic Review of Recent Literature. *RSC Adv.* **2021**, *11*, 35806–35827, doi:10.1039/D1RA05686G.
50. Zhao, L.; Zheng, L. A Review on Bioactive Anthraquinone and Derivatives as the Regulators for ROS. *Molecules.* **2023**, *28*, 8139, doi:10.3390/molecules28248139.
51. Bespalaya, Y. V.; Kondakov, A. V.; Travina, O. V.; Khrebtova, I. S.; Kropotin, A. V.; Aksenova, O. V.; Gofarov, M. Yu.; Lyubas, A. A.; Tomilova, A. A.; Vikhrev, I. V. First Record of Metacercariae Trematodes Opisthioglyphe Ranae (Digenea: Telorchiidae) and Echinostoma Bolschewense (Digenea: Echinostomatidae) in Dreissena Polymorpha (Bivalvia: Dreissenidae) from the Don and Volga River Basins, Russia. *Ecol Montenegrina.* **2022**, *54*, 57–76, doi:10.37828/em.2022.54.8.
52. Monçalves, M.; Zanotto, G. M.; Toldo, J. M.; Rampon, D. S.; Schneider, P. H.; Gonçalves, P. F. B.; Rodembusch, F. S.; Silveira, C. C. Dipolar Vinyl Sulfur Fluorescent

Dyes. Synthesis and Photophysics of Sulfide, Sulfoxide and Sulfone Based D–π–A Compounds. *RSC Adv.* **2017**, *7*, 8832–8842, doi:10.1039/C6RA27989A.
53. Rachi, Y.; Yamakado, R.; Okada, S. Synthesis of Dyes with a Sulfur-Containing Heterocyclic Donor and a Pyrroline-Type Acceptor. *Dyes and Pigments.* **2018**, *159*, 345–351, doi:10.1016/j.dyepig.2018.06.032.
54. Sims, M. T.; Abbott, L. C.; Cowling, S. J.; Goodby, J. W.; Moore, J. N. Molecular Design Parameters of Anthraquinone Dyes for Guest-Host Liquid-Crystal Applications: Experimental and Computational Studies of Spectroscopy, Structure, and Stability. *The Journal of Physical Chemistry C.* **2016**, *120*, 11151–11162, doi:10.1021/acs.jpcc.6b03607.
55. Cowling, S. J.; Ellis, C.; Goodby, J. W. Anthraquinone Liquid Crystal Dichroic Dyes – a New Form of Chromonic Dye? *Liq. Cryst.* **2011**, *38*, 1683–1698, doi:10.1080/02678292.2011.620181.
56. Ye, J.; Gao, Y.; He, L.; Tan, T.; Chen, W.; Liu, Y.; Wang, Y.; Ning, G. Efficient Blue-Emitting Molecules by Incorporating Sulfur-Containing Moieties into Triarylcyclopentadiene: Synthesis, Crystal Structures and Photophysical Properties. *Dyes and Pigments.* **2016**, *124*, 145–155, doi:10.1016/j.dyepig.2015.09.018.
57. Liu, Y.; Yu, Y.; Zhao, Q.; Tang, C.; Zhang, H.; Qin, Y.; Feng, X.; Zhang, J. Fluorescent Probes Based on Nucleophilic Aromatic Substitution Reactions for Reactive Sulfur and Selenium Species: Recent Progress, Applications, and Design Strategies. *Coord. Chem. Rev.* **2021**, *427*, 213601, doi:10.1016/j.ccr.2020.213601.
58. Vaidyanathan, T.; Seshadri, S. Nucleophilic Substitution Reactions on 3-Bromo- and 3-Nitrobenzanthrones. *Dyes and Pigments.* **1984**, *5*, 431–436, doi:10.1016/0143-7208(84)80035-2.
59. Melville, O. A.; Grant, T. M.; Rice, N. A.; Wang, B.; Josse, P.; Lessard, B. H. Functionalization of Commercial Pigment Hostasol Red GG for Incorporation into Organic Thin-Film Transistors. *New Journal of Chemistry.* **2020**, *44*, 845–851, doi:10.1039/C9NJ04851K.
60. Montanari, S.; Paradisi, C.; Scorrano, G. Thiol Anions in Nucleophilic Aromatic Substitution Reactions with Activated Aryl Halides. Attack on Carbon vs Attack on Halogen. *J. Org. Chem.* **1993**, *58*, 5628–5631, doi:10.1021/jo00073a020.
61. Campodónico, P. R.; Alarcón-Espósito, J.; Olivares, B. Kinetics and Reaction Mechanism of Biothiols Involved in SNAr Reactions: An Experimental Study. *Front. Chem.* **2022**, *10*, doi:10.3389/fchem.2022.854918.
62. Rohrbach, S.; Smith, A. J.; Pang, J. H.; Poole, D. L.; Tuttle, T.; Chiba, S.; Murphy, J. A. Concerted Nucleophilic Aromatic Substitution Reactions. *Angewandte Chemie International Edition.* **2019**, *58*, 16368–16388, doi:10.1002/anie.201902216.
63. Kunda, G.; Akhmadullin, R. M.; Zakirov, R. K.; Akhmadullina, F. Y.; Gizyatullov, R. N.; Madaminov, N. V.; Musin, L. I. Thiol Synthesis Methods: A Review. *Journal of Sulfur Chemistry.* **2024**, 1–34, doi:10.1080/17415993.2024.2428607.
64. Hansch, C.; Leo, A.; Taft, R. W. A Survey of Hammett Substituent Constants and Resonance and Field Parameters. *Chem. Rev.* **1991**, *91*, 165–195, doi:10.1021/cr00002a004.
65. Maeda, H.; Maeda, T.; Mizuno, K.; Fujimoto, K.; Shimizu, H.; Inouye, M. Alkynylpyrenes as Improved Pyrene-Based Biomolecular Probes with the Advantages of High Fluorescence Quantum Yields and Long Absorption/Emission Wavelengths. *Chemistry – A European Journal.* **2006**, *12*, 824–831, doi:10.1002/chem.200500638.

66. Chen, M.; Wei, J.; Zhang, Y.; Wu, L.; Tan, L.; Shi, S.; Shi, J.; Ji, L. 2,7-Carbazole Derived Organoboron Compounds: Synthesis and Molecular Fluorescence. *Front. Chem.* **2021**, *9*, doi:10.3389/fchem.2021.754298.
67. Yang, J.; Dass, A.; Rawashdeh, A.-M. M.; Sotiriou-Leventis, C.; Panzner, M. J.; Tyson, D. S.; Kinder, J. D.; Leventis, N. Arylethynyl Substituted 9,10-Anthraquinones: Tunable Stokes Shifts by Substitution and Solvent Polarity. *Chemistry of Materials.* **2004**, *16*, 3457–3468, doi:10.1021/cm049590g.
68. Yang, J.-X.; Wang, X.-L.; Wang, X.-M.; Xu, L.-H. The Synthesis and Spectral Properties of Novel 4-Phenylacetylene-1,8-Naphthalimide Derivatives. *Dyes and Pigments.* **2005**, *66*, 83–87, doi:10.1016/j.dyepig.2004.07.015.
69. Bai, J.-Y.; Xie, Y.-Z.; Wang, C.-J.; Fang, S.-Q.; Cao, L.-N.; Wang, L.-L.; Jin, J.-Y. A Quninolylthiazole Derivatives as an ICT-Based Fluorescent Probe of Hg(II) and Its Application in Ratiometric Imaging in Live HeLa Cells. *J. Fluoresc.* **2018**, *28*, 795–800, doi:10.1007/s10895-018-2241-4.
70. Altınok, E.; Smith, Z. C.; Thomas, S. W. Two-Dimensional, Acene-Containing Conjugated Polymers That Show Ratiometric Fluorescent Response to Singlet Oxygen. *Macromolecules.* **2015**, *48*, 6825–6831, doi:10.1021/acs.macromol.5b01076.
71. Tlach, B. C.; Tomlinson, A. L.; Bhuwalka, A.; Jeffries-EL, M. Tuning the Optical and Electronic Properties of 4,8-Disubstituted Benzobisoxazoles via Alkyne Substitution. *J. Org. Chem.* **2011**, *76*, 8670–8681, doi:10.1021/jo201078w.
72. Saeed, M. A.; Le, H. T. M.; Miljanić, O. Š. Benzobisoxazole Cruciforms as Fluorescent Sensors. *Acc. Chem. Res.* **2014**, *47*, 2074–2083, doi:10.1021/ar500099z.
73. Yamaguchi, Y.; Matsubara, Y.; Ochi, T.; Wakamiya, T.; Yoshida, Z. How the π Conjugation Length Affects the Fluorescence Emission Efficiency. *J. Am. Chem. Soc.* **2008**, *130*, 13867–13869, doi:10.1021/ja8040493.
74. Maļeckis, A.; Avotiņa, L.; Ķizāne, G.; Pučkins, A.; Osipovs, S.; Kirilova, E. New Fluorescent Heterocyclic Compounds Derived From 3-Cyanobenzanthrone. *Polycycl. Aromat. Compd.* **2022**, *42*, 5508–5520, doi:10.1080/10406638.2021.1939068.
75. Sonogashira, K.; Tohda, Y.; Hagihara, N. A Convenient Synthesis of Acetylenes: Catalytic Substitutions of Acetylenic Hydrogen with Bromoalkenes, Iodoarenes and Bromopyridines. *Tetrahedron Lett.* **1975**, *16*, 4467–4470, doi:10.1016/S0040-4039(00)91094-3.
76. Kanwal, I.; Mujahid, A.; Rasool, N.; Rizwan, K.; Malik, A.; Ahmad, G.; Shah, S. A. A.; Rashid, U.; Nasir, N. M. Palladium and Copper-Catalyzed Sonogashira Cross-Coupling an Excellent Methodology for C-C Bond Formation over 17 Years: A Review. *Catalyst.s* **2020**, *10*, 443, doi:10.3390/catal10040443.
77. Hartwig, J. F. Electronic Effects on Reductive Elimination To Form Carbon−Carbon and Carbon−Heteroatom Bonds from Palladium(II) Complexes. *Inorg. Chem.* **2007**, *46*, 1936–1947, doi:10.1021/ic061926w.

PIELIKUMI / APPENDICES

1. pielikums
Appendix I

Maļeckis, A.; Griškjāns, E.; Cvetinska, M.; Savicka, M.; Belyakov, S.; Kirilova, E.

Synthesis, Characterization, Spectroscopic Studies and Evaluation of Toxicological Effect on Growth of Wheat Sprouts (*Triticum Aestivum*) of New Benzanthrone α-Aryl-α-Aminophosphonates

J. Mol. Struct. 2023, 1277, 134838.

https://doi.org/10.1016/j.molstruc.2022.134838

Journal of Molecular Structure 1277 (2023) 134838

Contents lists available at ScienceDirect

Journal of Molecular Structure

journal homepage: www.elsevier.com/locate/molstr

Synthesis, characterization, spectroscopic studies and evaluation of toxicological effect on growth of wheat sprouts (*Triticum aestivum*) of new benzanthrone α-aryl-α-aminophosphonates

Armands Maļeckis[a,*], Evans Griškjāns[a], Marija Cvetinska[a], Marina Savicka[b], Sergey Belyakov[c], Elena Kirilova[d]

[a] Institute of Technology of Organic Chemistry, Faculty of Materials Science and Applied Chemistry, Riga Technical University, P. Valdena Str. 3, Riga LV-1048, Latvia
[b] Department of Ecology, Institute of Life Sciences and Technology, Daugavpils University, Parades Str. 1A, Daugavpils LV-5401, Latvia
[c] Latvian Institute of Organic Synthesis, Aizkraukles Str. 21, Riga LV-1006, Latvia
[d] Department of Applied Chemistry, Institute of Life Sciences and Technology, Daugavpils University, Parades Str. 1A, Daugavpils LV-5401, Latvia

ARTICLE INFO

Article history:
Received 7 November 2022
Revised 18 December 2022
Accepted 19 December 2022
Available online 21 December 2022

Keywords:
Benzanthrone
Fluorescence
α-aminophosphonates
Kabachnik-Fields reaction
Toxicology

ABSTRACT

A small library of new benzanthrone α-aryl-α-aminophosphonates has been synthesized by solvent-free one-pot reaction of 3-aminobenzanthrone, different aromatic aldehydes and dialkylphosphonates under Kabachnik-Fields reaction conditions. FTIR, ^{1}H-, ^{13}C-, ^{31}P-NMR spectroscopy, mass spectrometry and X-ray diffraction crystallographic analysis has confirmed structures of novel dyes. Photophysical properties of studied α-aminophosphonates have been investigated by means of UV-Vis and fluorescence spectroscopy in various organic solvents. Thermogravimetric analysis (DTA and TG) has been used to outline thermal stability of obtained derivatives. Morphology, electrolyte leakage, MDA and pigment quantification experiments were carried out to determine toxic effect on growth of wheat sprouts.

1. Introduction

Fluorescent compounds have now become of great importance in industrial and scientific applications. Amidst historically important anthraquinone dye family with electron-donor and acceptor units with underlying internal charge transfer (ICT) fluorescence mechanism, benzanthrone (7*H*-benzo[*de*]anthracen-7-one) derivatives have attained increasing acknowledgment due to palpable solvatochromic properties: many of these compounds exhibit fluorescence emission from green to red (depending on substituents and environment), as well as substantial Stokes shifts and photostability [1,2]. Recent studies that have been devoted to research of *N*-substituted 3-aminobenzanthrone derivatives demonstrated that these fluorophores can be used in many areas, which include, but are not limited to, confocal laser scanning microscopy imaging of various plant species' callus embryos [3]; parasitic nematodes and trematodes [4,5]; selective detection of amyloid fibrils of the lysozyme enzyme [6]; probes for the pH of solutions and metal cations [7,8]; liquid crystal displays [9,10]; organic thin films and fluorescent polymers [11,12].

α-Aminophosphonates (analogues of amino acids (N-C-CO_2H and N-C-PO_3H_2 structural frames) with the carboxylic group changed by a phosphonic acid or a homologous group) are widely studied compounds as these substances poses broad biological activity [13]. The frame similarity of α-aminophosphonic acids and amino acids allows for previous to inhibit several enzymes, as a rule – those that are involved in the metabolism of amino acids, that is, acting as antagonists. Moreover, α-aminophosphonates are an important class of compounds for synthesis of novel potential antibiotics, herbicides and neuromodulators [14].

Some research has been committed to the study of fluorescent properties of some α-aminophosphonates as well. Synthesis and fluorescent properties of α-aminophosphonates obtained from aromatic amines derived from benzene, naphthalene, anthracene and phenanthrene, as well as bis-aminophosphonates bearing anthracene rings, have been recently reported [15–19]. Pyrene–derived aminophosphonates were found both to be fluorescent and cytotoxic for two colon cancer cell lines, while showing nearly no toxicity towards lymphocytes [20].

* Corresponding author.
E-mail address: armands5maleckis@inbox.lv (A. Maļeckis).

https://doi.org/10.1016/j.molstruc.2022.134838
0022-2860/

Bearing aforementioned in mind, we have come to a decision to synthesize and investigate properties of new α-aryl-α-aminophosphonate derivatives of 3-aminobenzanthrone.

2. Experimental

2.1. Materials and general measurements

3-Aminobenzanthrone was synthesized according to previously reported procedure via nitration of benzanthrone and subsequent reduction with sodium sulfide. The rest of the reagents and solvents were obtained commercially and used without any additional purification [21].

The assessment of the progress of reactions and purity of the synthesized compounds was performed by TLC on MERCK Silica gel 60 F_{254} plates in benzene/acetonitrile (3:1) as an eluent and visualized under UV light. Melting points were determined on METTLER TOLEDO™ Melting Point System MP70 apparatus. The identification of the chemical bonds was performed by means of Fourier-transform infrared (FTIR) spectrometry. A Bruker Vertex 70v vacuum spectrometer equipped with an attenuated total reflection (ATR) accessory was used in this study. At least three spectra per sample were measured with a recording range 400 – 4000 cm^{-1}, spectral resolution ± 2 cm^{-1}, in vacuum (2.95 hPa), and the average spectrum was calculated from the measured spectra. ^{1}H-, ^{13}C- and ^{31}P-NMR spectra were recorded on a Bruker Avance 500 MHz (Bruker Corporation, Billerica, MA, USA) in DMSO-d_6 at ambient temperature, using solvent peaks as the internal reference. Chemical shift (δ) values are reported in ppm. LC–MS were recorded with a Waters Acquity UPLC system equipped with Acquity UPLC BEH C18 column (1.7 μm, 2.1 $\times$ 50 mm).

The fluorescence emission spectra were recorded on a FLSP920 (Edinburgh Instruments Ltd, UK) spectrofluorometer in the visible range 450–800 nm and the absorption spectra were obtained using the UV–visible spectrophotometer SPECORD® 80 (Analytik Jena AG, Germany). The spectral properties of the investigated compound were measured at an ambient temperature in 10 mm quartz cuvettes in hexane, benzene, chloroform, ethyl acetate (EtOAc), acetone, ethanol (EtOH), dimethyl sulfoxide (DMSO) and dimethylformamide (DMF) with concentrations 10^{-5} M. All solvents were of p.a. or analytical grade. Simultaneous TG-DTA curves were collected using a Exstar6000 TG/DTA (Seiko Instruments Inc., Tokyo, Japan) 6300 thermal analyzer with a heating rate of 10 K min^{-1} in temperature interval 30–1000°C with sample mass of 5.108 mg. Ceramic crucibles were used for analysis.

Single crystals of **3a** were investigated on a Rigaku, XtaLAB Synergy, Dualflex, HyPix diffractometer. The crystal was kept at 150.0(1) K during data collection. Using Olex2 [22], the structure was solved with the Superflip [23] structure solution program using Charge Flipping and refined with the olex2.refine [24] refinement package using Gauss-Newton minimization. Diffraction data of **3g** were collected at 173 K on a Bruker-Nonius KappaCCD diffractometer using MoK_α radiation (λ = 0.71073 Å). The crystal structure was solved by direct methods and refined by full-matrix least squares with the help of software package [25]. Diffraction data of **4a** were collected at 140 K on a Rigaku, XtaLAB Synergy, Dualflex, HyPix diffractometer using CuK_α radiation (λ = 1.54184 Å). The crystal structure was solved by direct methods and refined by full-matrix least squares with the help of software package [22]. For further details, see crystallographic data deposited at the Cambridge Crystallographic Data Centre as Supplementary Publication Number CCDC 2218839 (compound **3a**), CCDC 2213262 (compound **3g**) and CCDC 2213261 (compound **4a**). Copies of the data can be obtained, free of charge, on application to CCDC, 12 Union Road, Cambridge CB2 1EZ, UK.

2.2. Synthesis of compounds 2a – 4g

Target compounds were synthesized according to Scheme 1 and structures of obtained compounds are summarized in Table 1.

2.2.1. General methodology

A 10 mL round-bottom flask with a magnetic stirrer bar is charged with 490 mg (2 mmol) of 3-aminobenzanthrone, 6 mmol of an aldehyde and 5 mL of a dialkylphosphonate. Obtained mixture is stirred on an oil bath at 120°C for 1 – 3 hours (progress assessed with TLC). After completion of the reaction, the mixture is poured into 100 mL of concentrated sodium bicarbonate ($NaHCO_3$) solution and stirred until solid product is formed. The precipitate then is filtered, thoroughly washed with water and dried. Purified by means of multi-solvent recrystallization from xylenes and hexane.

2.2.2. Dimethyl (((7-oxo-7H-benzo[de]anthracen-3-yl)amino)(phenyl)methyl)phosphonate (2a)

Red solid. Yield: 74 %. Melting point: 199°C. R_f = 0.26 (Benzene/Acetonitrile) (3:1). IR, λ_{max} (KBr) cm^{-1}: 472, 548, 618, 699, 774, 958, 1019, 1121, 1221, 1269, 1311, 1384, 1461, 1572, 1642 (C=O), 2978 (CH), 3316 (NH). ^{1}H NMR (500 MHz, DMSO-d_6) δ 9.02 (d, J = 8.3 Hz, 1H), 8.70 (d, J = 7.3 Hz, 1H), 8.47 (d, J = 8.4 Hz, 1H), 8.40 (d, J = 8.2 Hz, 1H), 8.28 (d, J = 7.9 Hz, 1H), 7.88 (t, J = 7.6 Hz, 1H), 7.77 – 7.70 (m, 3H), 7.46 (t, J = 7.7 Hz, 1H), 7.38 (t, J = 7.7 Hz, 2H), 7.30 (t, J = 7.9 Hz, 2H), 6.94 (d, J = 8.4 Hz, 1H), 5.57 (dd, J = 24.9, 9.2 Hz, 1H), 3.74 (d, J = 10.5 Hz, 3H), 3.58 (d, J = 10.4 Hz, 3H). ^{13}C NMR (126 MHz, DMSO-d_6) δ 183.08 (C=O), 146.35 (d, J = 12.9 Hz, C), 137.17 (C), 136.42 (C), 133.93 (CH), 130.52 (CH), 130.07 (CH), 129.06 (C), 128.79 (CH), 128.77 (CH), 128.40 (C), 128.26 (d, J = 2.8 Hz, CH), 128.20 (C), 128.14 (CH), 127.47 (CH), 126.77 (CH), 125.31 (CH), 123.69 (C), 123.23 (CH), 115.27 (C), 107.32 (CH), 54.45 (d, J = 149.9 Hz, CHP), 54.08 (d, J = 6.8 Hz, CH_3), 53.83 (d, J = 4.9 Hz, CH_3). ^{31}P NMR (202 MHz, DMSO-d_6) δ 23.89. MS (ES+): m/z calculated for $C_{26}H_{22}NO_4P$ ($[M+H]^+$) 444.14, found 444.76.

2.2.3. Dimethyl (((7-oxo-7H-benzo[de]anthracen-3-yl)amino)(p-tolyl)methyl)phosphonate (2b)

Red solid. Yield: 79 %. Melting point: 160°C. R_f = 0.32 (Benzene/Acetonitrile) (3:1). IR, λ_{max} (KBr) cm^{-1}: 474, 540, 701, 771, 837, 955, 1052, 1182, 1234, 1308, 1385, 1463, 1573, 1642 (C=O), 2956 (CH), 3287 (NH). ^{1}H NMR (500 MHz, DMSO-d_6) δ 9.00 (dd, J = 8.5, 1.3 Hz, 1H), 8.69 (dd, J = 7.4, 1.2 Hz, 1H), 8.47 (d, J = 8.5 Hz, 1H), 8.41 (d, J = 8.2 Hz, 1H), 8.28 (dd, J = 7.9, 1.5 Hz, 1H), 7.88 (t, J = 7.8 Hz, 1H), 7.77 – 7.70 (m, 1H), 7.61 (dd, J = 8.2, 2.1 Hz, 2H), 7.46 (t, J = 7.5 Hz, 1H), 7.25 (dd, J = 9.3, 6.1 Hz, 1H), 7.18 (d, J = 7.8 Hz, 2H), 6.92 (d, J = 8.5 Hz, 1H), 5.50 (dd, J = 24.6, 9.2 Hz, 1H), 3.74 (d, J = 10.6 Hz, 3H), 3.58 (d, J = 10.6 Hz, 3H), 2.28 (s, 3H). ^{13}C NMR (126 MHz, DMSO-d_6) δ 183.08 (C=O), 146.37 (d, J = 13.0 Hz, C), 137.50 (d, J = 3.1 Hz, C), 137.19 (C), 133.93 (CH), 133.29 (C), 130.48 (CH), 130.05 (CH), 129.38 (d, J = 2.1 Hz, CH), 129.06 (C), 128.67 (d, J = 5.4 Hz, CH), 128.39 (C), 128.20 (C), 128.15 (CH), 127.47 (CH), 126.75 (CH), 125.30 (CH), 123.69 (C), 123.22 (CH), 115.20 (C), 107.36 (CH), 54.19 (d, J = 152.3 Hz, CHP), 54.04 (d, J = 6.9 Hz, CH_3), 53.81 (d, J = 7.0 Hz, CH_3), 21.18 ($C_{Ar}\underline{C}H_3$). ^{31}P NMR (202 MHz, DMSO-d_6) δ 24.04. MS (ES+): m/z calculated for $C_{27}H_{24}NO_4P$ ($[M+H]^+$) 458.15, found 458.17.

2.2.4. Dimethyl ((4-fluorophenyl)((7-oxo-7H-benzo[de]anthracen-3-yl)amino)methyl)phosphonate (2c)

Orange solid. Yield: 77 %. Melting point: 203°C. R_f = 0.30 (Benzene/Acetonitrile) (3:1). IR, λ_{max} (KBr) cm^{-1}: 457, 541, 617, 657,

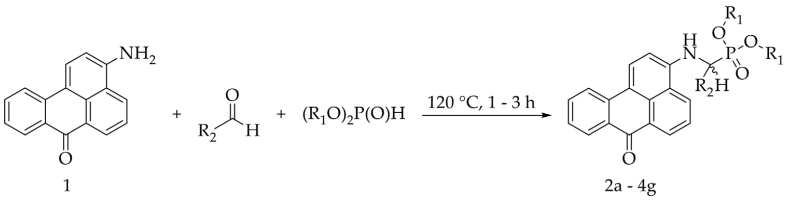

Scheme 1. Synthesis of benzanthrone α-aminophosphonates.

Table 1
Summary of structures of obtained compounds.

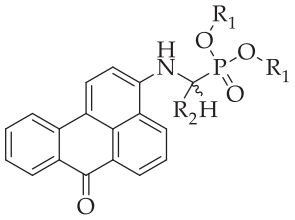

R2/R1							
Me	*2a*	*2b*	*2c*	*2d*	*2e*	*2f*	*2g*
Et	*3a*	*3b*	*3c*	*dI*	*3e*	*3f*	*3g*
i-Pr	*4a*	*4b*	*4c*	*4d*	*4e*	–	*4g*

703, 770, 835, 958, 1036, 1122, 1226, 1310, 1385, 1462, 1509,1575, 1646 (C=O), 2953 (CH), 3310 (NH). ^{1}H NMR (500 MHz, DMSO-d_6) δ 9.01 (dd, J = 8.4, 1.3 Hz, 1H), 8.70 (dd, J = 7.3, 1.2 Hz, 1H), 8.48 (d, J = 8.5 Hz, 1H), 8.42 (d, J = 8.2 Hz, 1H), 8.28 (dd, J = 7.9, 1.5 Hz, 1H), 7.89 (t, J = 8.1 Hz, 1H), 7.84 – 7.77 (m, 2H), 7.77 – 7.71 (m, 1H), 7.47 (td, J = 7.4, 6.9, 1.0 Hz, 1H), 7.31 (dd, J = 9.4, 5.9 Hz, 1H), 7.23 (t, J = 8.9 Hz, 2H), 6.95 (d, J = 8.5 Hz, 1H), 5.62 (dd, J = 24.8, 9.3 Hz, 1H), 3.75 (d, J = 10.5 Hz, 3H), 3.60 (d, J = 10.6 Hz, 3H). ^{13}C NMR (126 MHz, DMSO-d_6) δ 183.09 (C=O), 162.23 (dd, J = 243.7, 3.2 Hz, C), 146.24 (d, J = 12.8 Hz, C), 137.16 (C), 133.95 (CH), 132.64 (d, J = 2.7 Hz, C), 130.84 (dd, J = 8.1, 5.6 Hz, CH), 130.57 (CH), 130.08 (CH), 129.08 (C), 128.41 (C), 128.20 (C), 128.11 (CH), 127.48 (CH), 126.81 (CH), 125.31 (CH), 123.70 (C), 123.25 (CH), 115.63 (dd, J = 21.5, 1.8 Hz, CH), 115.37 (C), 53.64 (d, J = 153.0 Hz, CHP), 54.13 (d, J = 6.9 Hz, CH_3), 53.85 (d, J = 7.0 Hz, CH_3). ^{31}P NMR (202 MHz, DMSO-d_6) δ 23.72 (d, J = 4.6 Hz). MS (ES+): *m/z* calculated for $C_{26}H_{21}FNO_4P$ ([M+H]$^+$) 462.13, found 462.05.

2.2.5. Dimethyl ((4-methoxyphenyl)((7-oxo-7H-benzo[de]anthracen-3-yl)amino)methyl)phosphonate (2d)

Orange solid. Yield: 71 %. Melting point: 166°C. R_f = 0.23 (Benzene/Acetonitrile) (3:1). IR, λ_{max} (KBr) cm^{-1}: 478, 548, 617, 657, 701, 770, 843, 956, 1028, 1124, 1177, 1232, 1306, 1386, 1463, 1510, 1575, 1645 (C=O), 2956 (CH), 3305 (NH). ^{1}H NMR (500 MHz, DMSO-d_6) δ 9.00 (dd, J = 8.4, 1.3 Hz, 1H), 8.69 (dd, J = 7.4, 1.2 Hz, 1H), 8.47 (d, J = 8.5 Hz, 1H), 8.41 (d, J = 8.2 Hz, 1H), 8.28 (dd, J = 7.9, 1.5 Hz, 1H), 7.87 (t, J = 7.8 Hz, 1H), 7.77 – 7.70 (m, 1H), 7.70 – 7.63 (m, 2H), 7.46 (t, J = 7.5 Hz, 1H), 7.24 (dd, J = 9.4, 6.0 Hz, 1H), 7.00 – 6.92 (m, 3H), 5.49 (dd, J = 24.4, 9.2 Hz, 1H), 3.74 (t, J = 5.3 Hz, 6H), 3.57 (d, J = 10.6 Hz, 3H). ^{13}C NMR (126 MHz, DMSO-d_6) δ 183.08 (C=O), 159.36 (C), 146.39 (d, J = 13.1 Hz, C), 137.20 (C), 133.93 (CH), 130.49 (CH), 130.04 (CH), 129.99 (CH), 129.05 (C), 128.39 (C), 128.20 (C), 128.15 (CH), 128.03 (C), 127.47 (CH), 126.73 (CH), 125.27 (CH), 123.69 (C), 123.21 (CH), 115.16 (C), 114.23 (d, J = 1.7 Hz, CH), 107.33 (CH), 55.53 ($C_{Ar}O\underline{C}H_3$), 53.78 (d, J = 153.6 Hz, CHP), 53.99 (d, J = 6.9 Hz, CH_3), 53.79 (d, J = 7.0 Hz, CH_3). ^{31}P NMR (202 MHz, DMSO-d_6) δ 24.18. MS (ES+): *m/z* calculated for $C_{27}H_{24}NO_5P$ ([M+H]$^+$) 474.15, found 474.67.

2.2.6. Dimethyl ((2-methoxyphenyl)((7-oxo-7H-benzo[de]anthracen-3-yl)amino)methyl)phosphonate (2e)

Red solid. Yield: 77 %. Melting point: 219°C. R_f = 0.23 (Benzene/Acetonitrile) (3:1). IR, λ_{max} (KBr) cm^{-1}: 464, 509, 569, 617, 702, 768, 832, 956, 1042, 1169, 1239, 1305, 1385, 1460, 1571, 1640 (C=O), 2954 (CH), 3325 (NH). ^{1}H NMR (500 MHz, DMSO-d_6) δ 8.95 (dd, J = 8.4, 1.3 Hz, 1H), 8.69 (dd, J = 7.3, 1.2 Hz, 1H), 8.52 (d, J = 8.5 Hz, 1H), 8.40 (d, J = 8.2 Hz, 1H), 8.27 (dd, J = 7.9, 1.5 Hz, 1H), 7.88 (t, J = 7.8 Hz, 1H), 7.81 – 7.70 (m, 2H), 7.50 – 7.43 (m, 1H), 7.35 – 7.27 (m, 2H), 7.13 (d, J = 8.3 Hz, 1H), 6.96 (t, J = 7.4 Hz, 1H), 6.75 (d, J = 8.5 Hz, 1H), 5.64 (dd, J = 24.4, 9.3 Hz, 1H), 4.01 (s, 3H), 3.76 (d, J = 10.6 Hz, 3H), 3.53 (d, J = 10.6 Hz, 3H). ^{13}C NMR (126 MHz, DMSO-d_6) δ 183.07 (C=O), 157.25 (d, J = 6.3 Hz, C), 146.35 (d, J = 13.0 Hz, C), 137.17 (C), 133.95 (CH), 130.40 (CH), 130.09 (CH), 129.85 (d, J = 2.5 Hz, CH), 129.38 (d, J = 4.2 Hz, CH), 129.06 (C), 128.42 (C), 128.38 (CH), 128.20 (C), 127.47 (CH), 126.79 (CH), 125.37 (CH), 124.15 (C), 123.64 (C), 123.21 (CH), 121.13 (d, J = 2.3 Hz, CH), 115.38 (C), 111.62 (CH), 106.28 (CH), 56.56 ($C_{Ar}O\underline{C}H_3$), 54.00 (d, J = 6.9 Hz, CH_3), 53.91 (d, J = 7.0 Hz, CH_3), 47.92 (d, J = 156.4 Hz, CHP). ^{31}P NMR (202 MHz, DMSO-d_6) δ 23.85. MS (ES+): *m/z* calculated for $C_{27}H_{24}NO_5P$ ([M+H]$^+$) 474.15, found 474.78.

2.2.7. Dimethyl ((4-chlorophenyl)((7-oxo-7H-benzo[de]anthracen-3-yl)amino)methyl)phosphonate (2f)

Orange solid. Yield: 74 %. Melting point: 164°C. R_f = 0.30 (Benzene/Acetonitrile) (3:1). IR, λ_{max} (KBr) cm^{-1}: 457, 560, 618, 704, 770, 826, 956, 1033, 1173, 1219, 1270, 1306, 1385, 1461, 1573, 1643 (C=O), 2956 (CH), 3318 (NH). ^{1}H NMR (500 MHz, DMSO-d_6) δ 9.01 (dd, J = 8.5, 1.3 Hz, 1H), 8.70 (dd, J = 7.4, 1.2 Hz, 1H), 8.47 (d, J = 8.5 Hz, 1H), 8.41 (d, J = 8.2 Hz, 1H), 8.28 (dd, J = 7.9, 1.5 Hz, 1H), 7.92 – 7.85 (m, 1H), 7.78 (dd, J = 8.7, 2.2 Hz, 2H), 7.77 – 7.70 (m, 1H), 7.47 (t, J = 7.9 Hz, 3H), 7.33 (dd, J = 9.4, 6.0 Hz, 1H), 6.92 (d, J = 8.5 Hz, 1H), 5.64 (dd, J = 25.1, 9.3 Hz, 1H), 3.76 (d, J = 10.6 Hz, 3H), 3.62 (d, J = 10.6 Hz, 3H). ^{13}C NMR (126 MHz, DMSO-d_6) δ 183.09 (C=O), 146.18 (d, J = 12.9 Hz, C), 137.14 (C), 135.62 (C), 133.94 (CH), 132.96 (d, J = 3.5 Hz, C), 130.63 (d, J = 5.4 Hz, CH), 130.59 (CH), 130.08 (CH), 129.09 (C), 128.79 (d, J = 2.0 Hz, CH), 128.41 (C), 128.20 (C), 128.07 (CH), 127.48 (CH), 126.83 (CH), 125.33 (CH), 123.72 (C), 123.25 (CH), 115.46 (C), 107.39 (CH), 54.21 (d, J = 6.9 Hz, CH_3), 53.89 (d, J = 7.0 Hz, CH_3), 53.78 (d, J = 152.2 Hz, CHP). ^{31}P NMR (202 MHz, DMSO-d_6) δ 23.43. MS (ES+): m/z calculated for $C_{26}H_{21}ClNO_4P$ ($[M+H]^+$) 478.10, found 478.16.

2.2.8. Dimethyl (((7-oxo-7H-benzo[de]anthracen-3-yl)amino)(thiophen-2-yl)methyl)phosphonate (2g)

Red solid. Yield: 67 %. Melting point: 189°C. R_f = 0.28 (Benzene/Acetonitrile) (3:1). IR, λ_{max} (KBr) cm^{-1}: 469, 549, 614, 699, 768, 832, 954, 1027, 1165, 1239, 1302, 1385, 1459, 1572, 1643 (C=O), 2956 (CH), 3302 (NH). ^{1}H NMR (500 MHz, DMSO-d_6) δ 8.98 (d, J = 8.1 Hz, 1H), 8.69 (dd, J = 7.5, 2.8 Hz, 1H), 8.52 (dd, J = 8.6, 2.9 Hz, 1H), 8.44 (d, J = 8.2 Hz, 1H), 8.29 (d, J = 7.9 Hz, 1H), 7.86 (td, J = 8.0, 2.9 Hz, 1H), 7.75 (t, J = 7.6 Hz, 1H), 7.51 – 7.41 (m, 3H), 7.29 – 7.22 (m, 1H), 7.14 (dd, J = 8.5, 3.0 Hz, 1H), 7.07 – 7.03 (m, 1H), 5.98 – 5.88 (m, 1H), 3.76 (dd, J = 10.7, 2.9 Hz, 3H), 3.68 (dd, J = 10.5, 3.0 Hz, 3H). ^{13}C NMR (126 MHz, DMSO-d_6) δ 183.10 (C=O), 146.11 (d, J = 10.9 Hz, C), 139.14 (C), 137.16 (C), 133.96 (CH), 130.45 (CH), 130.06 (CH), 129.10 (C), 128.41 (C), 128.23 (C), 128.12 (CH), 127.81 (d, J = 6.7 Hz, CH), 127.49 (CH), 127.38 (d, J = 2.1 Hz, CH), 126.83 (CH), 126.59 (d, J = 2.9 Hz, CH), 125.36 (CH), 123.68 (C), 123.28 (CH), 115.53 (C), 107.46 (CH), 54.24 (d, J = 6.9 Hz, CH_3), 53.99 (d, J = 7.0 Hz, CH_3), 50.42 (d, J = 158.7 Hz, CHP). ^{31}P NMR (202 MHz, DMSO-d_6) δ 22.40. MS (ES+): m/z calculated for $C_{24}H_{20}NO_4PS$ ($[M+H]^+$) 450.09, found 450.04.

2.2.9. Diethyl (((7-oxo-7H-benzo[de]anthracen-3-yl)amino)(phenyl)methyl)phosphonate (*3a*)

Orange solid. Yield: 81 %. Melting point: 201°C. R_f = 0.33 (Benzene/Acetonitrile) (3:1). IR, λ_{max} (KBr) cm^{-1}: 472, 548, 518, 698, 772, 958, 1020, 1121, 1221, 1269, 1310, 1384, 1461, 1572, 1643 (C=O), 2978 (CH), 3312 (NH). ^{1}H NMR (500 MHz, DMSO-d_6) δ 8.99 (dd, J = 8.4, 1.3 Hz, 1H), 8.69 (dd, J = 7.3, 1.2 Hz, 1H), 8.47 (d, J = 8.6 Hz, 1H), 8.40 (d, J = 8.2 Hz, 1H), 8.28 (dd, J = 7.9, 1.5 Hz, 1H), 7.89 (t, J = 7.8 Hz, 1H), 7.77 – 7.70 (m, 3H), 7.46 (t, J = 7.5 Hz, 1H), 7.38 (t, J = 7.5 Hz, 2H), 7.34 – 7.27 (m, 1H), 7.24 (dd, J = 9.3, 6.3 Hz, 1H), 6.94 (d, J = 8.5 Hz, 1H), 5.48 (dd, J = 24.6, 9.2 Hz, 1H), 4.17 – 4.07 (m, 2H), 4.04 – 3.92 (m, 1H), 3.89 – 3.77 (m, 1H), 1.20 (t, J = 7.1 Hz, 3H), 1.10 (t, J = 7.1 Hz, 3H). ^{13}C NMR (126 MHz, DMSO-d_6) δ 183.08 (C=O), 146.42 (d, J = 12.8 Hz, C), 137.18 (C), 136.53 (C), 133.93 (CH), 130.37 (CH), 130.06 (CH), 129.05 (C), 128.84 (d, J = 5.4 Hz, CH), 128.68 (d, J = 1.9 Hz, CH), 128.39 (C), 128.22 (C), 128.20 (CH), 128.16 (CH), 127.47 (CH), 126.75 (CH), 125.33 (CH), 123.66 (C), 123.22 (CH), 115.19 (C), 107.34 (CH), 63.22 (d, J = 6.9 Hz, CH_2), 63.03 (d, J = 6.9 Hz, CH_2), 54.98 (d, J = 151.7 Hz, CHP), 16.81 (d, J = 5.2 Hz, CH_3), 16.57 (d, J = 5.5 Hz, CH_3). ^{31}P NMR (202 MHz, DMSO-d_6) δ 21.69. MS (ES+): m/z calculated for $C_{28}H_{26}NO_4P$ ($[M+H]^+$) 472.17, found 472.08.

2.2.10. Diethyl (((7-oxo-7H-benzo[de]anthracen-3-yl)amino)(p-tolyl)methyl)phosphonate (3b)

Red solid. Yield: 78 %. Melting point: 173°C. R_f = 0.27 (Benzene/Acetonitrile) (3:1). IR, λ_{max} (KBr) cm^{-1}: 458, 538, 616, 705, 774, 817, 956, 1021, 1117, 1241, 1311, 1385, 1461, 1572, 1642 (C=O), 2979 (CH), 3304 (NH). ^{1}H NMR (500 MHz, DMSO-d_6) δ 8.98 (dd, J = 8.4, 1.3 Hz, 1H), 8.69 (dd, J = 7.3, 1.1 Hz, 1H), 8.46 (d, J = 8.5 Hz, 1H), 8.40 (d, J = 8.1 Hz, 1H), 8.28 (dd, J = 7.9, 1.5 Hz, 1H), 7.88 (t, J = 7.9 Hz, 1H), 7.73 (td, J = 7.6, 6.8, 1.6 Hz, 1H), 7.61 (dd, J = 8.2, 2.1 Hz, 2H), 7.46 (t, J = 7.5 Hz, 1H), 7.23 – 7.15 (m, 3H), 6.91 (d, J = 8.4 Hz, 1H), 5.41 (dd, J = 24.4, 9.1 Hz, 1H), 4.17 – 4.04 (m, 2H), 4.04 – 3.93 (m, 1H), 3.90 – 3.78 (m, 1H), 2.28 (s, 3H), 1.20 (t, J = 7.0 Hz, 3H), 1.12 (t, J = 7.0 Hz, 3H). ^{13}C NMR (126 MHz, DMSO-d_6) δ 183.07 (C=O), 146.45 (d, J = 12.9 Hz, C), 137.41 (d, J = 3.0 Hz, C), 137.20 (C), 133.93 (CH), 133.41 (C), 130.34 (CH), 130.04 (CH), 129.29 (CH), 129.04 (C), 128.73 (d, J = 5.4 Hz, CH), 128.38 (C), 128.22 (C), 128.16 (CH), 127.47 (CH), 126.73 (CH), 125.31 (CH), 123.66 (C), 123.20 (CH), 115.13 (C), 107.36 (CH), 63.17 (d, J = 6.9 Hz, CH_2), 62.99 (d, J = 6.9 Hz, CH_2), 54.72 (d, J = 152.4 Hz, CHP), 21.19 ($C_{Ar}\underline{C}H_3$), 16.82 (d, J = 5.1 Hz, CH_3), 16.62 (d, J = 5.5 Hz, CH_3). ^{31}P NMR (202 MHz, DMSO-d_6) δ 21.82. MS (ES+): m/z calculated for $C_{29}H_{28}NO_4P$ ($[M+H]^+$) 486.18, found 486.79.

2.2.11. Diethyl ((4-fluorophenyl)((7-oxo-7H-benzo[de]anthracen-3-yl)amino)methyl)phosphonate (3c)

Orange solid. Yield: 74 %. Melting point: 185°C. R_f = 0.31 (Benzene/Acetonitrile) (3:1). IR, λ_{max} (KBr) cm^{-1}: 459, 542, 619, 707, 776, 956, 1023, 1120, 1160, 1239, 1309, 1384, 1509, 1572, 1640 (C=O), 2983 (CH), 3321 (NH). ^{1}H NMR (500 MHz, DMSO-d_6) δ 8.99 (dd, J = 8.4, 1.3 Hz, 1H), 8.69 (dd, J = 7.3, 1.2 Hz, 1H), 8.47 (d, J = 8.5 Hz, 1H), 8.40 (d, J = 8.2 Hz, 1H), 8.28 (dd, J = 7.9, 1.6 Hz, 1H), 7.88 (dd, J = 40.5, 8.1 Hz, 1H), 7.84 – 7.77 (m, 2H), 7.76 – 7.69 (m, 1H), 7.49 – 7.43 (m, 1H), 7.29 – 7.18 (m, 3H), 6.95 (d, J = 8.8 Hz, 1H), 5.53 (dd, J = 24.5, 9.3 Hz, 1H), 4.17 – 4.08 (m, 2H), 4.05 – 3.94 (m, 1H), 3.92 – 3.81 (m, 1H), 1.19 (t, J = 7.0 Hz, 3H), 1.11 (t, J = 7.0 Hz, 3H). ^{13}C NMR (126 MHz, DMSO-d_6) δ 183.08 (C=O), 162.22 (dd, J = 243.8, 3.0 Hz, C), 146.32 (d, J = 12.7 Hz, C), 137.16 (C), 133.92 (CH), 132.77 (d, J = 2.7 Hz, C), 130.90 (dd, J = 8.1, 5.5 Hz, CH), 130.43 (CH), 130.06 (CH), 129.07 (C), 128.41 (C), 128.21 (C), 128.11 (CH), 127.47 (CH), 126.77 (CH), 125.31 (CH), 123.68 (C), 123.22 (CH), 115.52 (dd, J = 21.4, 1.6 Hz, CH), 115.30 (C), 107.34 (CH), 63.27 (d, J = 6.9 Hz, CH_2), 63.04 (d, J = 7.0 Hz, CH_2), 54.18 (d, J = 152.8 Hz, CHP), 16.80 (d, J = 5.2 Hz, CH_3), 16.60 (d, J = 5.4 Hz, CH_3). ^{31}P NMR (202 MHz, DMSO-d_6) δ 21.52 (d, J = 4.5 Hz). MS (ES+): m/z calculated for $C_{28}H_{25}FNO_4P$ ($[M+H]^+$) 490.16, found 490.28.

2.2.12. Diethyl ((2-methoxyphenyl)((7-oxo-7H-benzo[de]anthracen-3-yl)amino)methyl)phosphonate (3e)

Red solid. Yield: 72 %. Melting point: 202°C. R_f = 0.29 (Benzene/Acetonitrile) (3:1). IR, λ_{max} (KBr) cm^{-1}: 482, 570, 618, 656, 702, 775, 837, 947, 1020, 1160, 1217, 1307, 1385, 1463, 1572, 1647 (C=O), 2983 (CH), 3291 (NH). ^{1}H NMR (500 MHz, DMSO-d_6) δ 8.93 (dd, J = 8.5, 1.3 Hz, 1H), 8.69 (dd, J = 7.3, 1.2 Hz, 1H), 8.53 (d, J = 8.5 Hz, 1H), 8.40 (d, J = 8.2 Hz, 1H), 8.27 (dd, J = 8.0, 1.5 Hz, 1H), 7.89 (t, J = 7.8 Hz, 1H), 7.79 – 7.72 (m, 2H), 7.47 (t, J = 7.5 Hz, 1H), 7.35 – 7.26 (m, 1H), 7.25 (dd, J = 9.5, 5.8 Hz, 1H), 7.12 (d, J = 8.3 Hz, 1H), 6.95 (t, J = 7.6 Hz, 1H), 6.75 (d, J = 8.6 Hz, 1H), 5.58 (dd, J = 24.4, 9.3 Hz, 1H), 4.19 – 4.08 (m, 2H), 4.00 (s, 3H), 3.97 – 3.87 (m, 1H), 3.82 – 3.70 (m, 1H), 1.21 (t, J = 7.1 Hz, 3H), 1.05 (t, J = 7.1 Hz, 3H). ^{13}C NMR (126 MHz, DMSO-d_6) δ 183.07 (C=O), 157.31 (d, J = 6.4 Hz, C), 146.45 (d, J = 12.9 Hz, C), 137.19, (C) 133.96 (CH), 130.29 (CH), 130.09 (CH), 129.77 (d, J = 2.4 Hz, CH), 129.32 (d, J = 4.3 Hz, CH), 129.05 (C), 128.42 (C), 128.41 (CH), 128.21 (C), 127.48 (CH), 126.78 (CH), 125.38 (CH), 124.29 (C),

123.61 (C), 123.21 (CH), 121.04 (d, J = 2.5 Hz, CH), 115.31 (C), 111.47 (CH), 106.29 (CH), 63.11 (dd, J = 6.9, 3.8 Hz, CH_2), 56.47 ($C_{Ar}O\underline{C}H_3$), 48.36 (d, J = 156.3 Hz, CHP), 16.82 (d, J = 5.2 Hz, CH_3), 16.49 (d, J = 5.6 Hz, CH_3). ^{31}P NMR (202 MHz, DMSO-d_6) δ 21.69. MS (ES+): m/z calculated for $C_{29}H_{28}NO_5P$ ($[M+H]^+$) 502.18, found 502.86.

2.2.13. Diethyl ((4-chlorophenyl)((7-oxo-7H-benzo[de]anthracen-3-yl) amino)methyl)phosphonate (3f)

Orange solid. Yield: 77 %. Melting point: 183°C. R_f = 0.34 (Benzene/Acetonitrile) (3:1). IR, λ_{max} (KBr) cm^{-1}: 457, 565, 617, 705, 775, 818, 956, 1014, 1092, 1239, 1310, 1384, 1476, 1571, 1642 (C=O), 2980 (CH), 3314 (NH). ^{1}H NMR (500 MHz, DMSO-d_6) δ 8.98 (dd, J = 8.5, 1.3 Hz, 1H), 8.70 (dd, J = 7.3, 1.2 Hz, 1H), 8.46 (d, J = 8.5 Hz, 1H), 8.40 (d, J = 8.2 Hz, 1H), 8.28 (dd, J = 7.9, 1.5 Hz, 1H), 7.88 (t, J = 7.8 Hz, 1H), 7.78 (dd, J = 8.7, 2.2 Hz, 2H), 7.75 – 7.71 (m, 1H), 7.49 – 7.43 (m, 3H), 7.27 (dd, J = 9.4, 6.2 Hz, 1H), 6.92 (d, J = 8.8 Hz, 1H), 5.54 (dd, J = 24.8, 9.2 Hz, 1H), 4.19 – 4.07 (m, 2H), 4.07 – 3.96 (m, 1H), 3.95 – 3.84 (m, 1H), 1.20 (t, J = 7.0 Hz, 3H), 1.13 (t, J = 7.0 Hz, 3H). ^{13}C NMR (126 MHz, DMSO-d_6) δ 183.08 (C=O), 146.26 (d, J = 12.8 Hz, C), 137.14 (C), 135.75 (C), 133.93 (CH), 132.89 (d, J = 3.5 Hz, C), 130.70 (d, J = 5.3 Hz, CH), 130.44 (CH), 130.07 (CH), 129.08 (C), 128.68 (d, J = 1.9 Hz, CH), 128.41 (C), 128.22 (C), 128.07 (CH), 127.48 (CH), 126.79 (CH), 125.33 (CH), 123.70 (C), 123.23 (CH), 115.39 (C), 107.40 (CH), 63.37 (d, J = 6.9 Hz, CH_2), 63.09 (d, J = 7.0 Hz, CH_2), 54.31 (d, J = 152.0 Hz, CHP), 16.80 (d, J = 5.1 Hz, CH_3), 16.61 (d, J = 5.4 Hz, CH_3). ^{31}P NMR (202 MHz, DMSO-d_6) δ 21.19. MS (ES+): m/z calculated for $C_{28}H_{25}ClNO_4P$ ($[M+H]^+$) 506.13, found 506.13.

2.2.14. Diethyl (((7-oxo-7H-benzo[de]anthracen-3-yl)amino) (thiophen-2-yl)methyl)phosphonate (3g)

Red solid. Yield: 67 %. Melting point: 148°C. R_f = 0.34 (Benzene/Acetonitrile) (3:1). IR, λ_{max} (KBr) cm^{-1}: 449, 549, 709, 777, 853, 955, 1023, 1119, 1172, 1234, 1310, 1385, 1460, 1574, 1636 (C=O), 2990 (CH), 3281 (NH). ^{1}H NMR (500 MHz, DMSO-d_6) δ 8.95 (dd, J = 8.4, 1.2 Hz, 1H), 8.69 (dd, J = 7.4, 1.1 Hz, 1H), 8.52 (d, J = 8.2 Hz, 1H), 8.44 (d, J = 8.1 Hz, 1H), 8.29 (dd, J = 7.9, 1.5 Hz, 1H), 7.87 (t, J = 7.8 Hz, 1H), 7.75 (t, J = 7.6 Hz, 1H), 7.50 – 7.42 (m, 3H), 7.19 (dd, J = 9.3, 5.1 Hz, 1H), 7.13 (d, J = 8.6 Hz, 1H), 7.05 (t, J = 4.3 Hz, 1H), 5.83 (dd, J = 24.0, 9.1 Hz, 1H), 4.21 – 4.03 (m, 3H), 4.03 – 3.92 (m, 1H), 1.18 (q, J = 7.3 Hz, 6H). ^{13}C NMR (126 MHz, DMSO-d_6) δ 183.09 (C=O), 146.18 (d, J = 10.8 Hz, C), 139.27 (C), 137.17 (C), 133.96 (CH), 130.31 (CH), 130.05 (CH), 129.09 (C), 128.39 (C), 128.24 (C), 128.13 (CH), 127.78 (d, J = 6.7 Hz, CH), 127.49 (CH), 127.32 (d, J = 2.3 Hz, CH), 126.81 (CH), 126.50 (d, J = 3.0 Hz, CH), 125.38 (CH), 123.66 (C), 123.27 (CH), 115.46 (C), 107.51 (CH), 63.44 (d, J = 6.9 Hz, CH_2), 63.23 (d, J = 7.0 Hz, CH_2), 50.93 (d, J = 158.4 Hz, CHP), 16.81 (d, J = 5.2 Hz, CH_3), 16.66 (d, J = 5.5 Hz, CH_3). ^{31}P NMR (202 MHz, DMSO-d_6) δ 20.18. MS (ES+): m/z calculated for $C_{26}H_{24}NO_4PS$ ($[M+H]^+$) 478.12, found 478.01.

2.2.15. Diisopropyl (((7-oxo-7H-benzo[de]anthracen-3-yl)amino) (phenyl)methyl)phosphonate (4a)

Red solid. Yield: 81 %. Melting point: 197°C. R_f = 0.40 (Benzene/Acetonitrile) (3:1). IR, λ_{max} (KBr) cm^{-1}: 455, 552, 657, 702, 775, 822, 891, 990, 1105, 1162, 1225, 1307, 1382, 1462, 1518, 1574, 1644 (C=O), 2978 (CH), 3287 (NH). ^{1}H NMR (500 MHz, DMSO-d_6) δ 8.96 (dd, J = 8.4, 1.2 Hz, 1H), 8.69 (dd, J = 7.3, 1.1 Hz, 1H), 8.47 (d, J = 8.5 Hz, 1H), 8.41 (d, J = 8.3 Hz, 1H), 8.27 (dd, J = 8.0, 1.5 Hz, 1H), 7.89 (t, J = 7.8 Hz, 1H), 7.77 – 7.70 (m, 3H), 7.46 (t, J = 7.5 Hz, 1H), 7.37 (t, J = 7.5 Hz, 2H), 7.29 (td, J = 7.2, 1.6 Hz, 1H), 7.19 (dd, J = 9.4, 6.3 Hz, 1H), 6.95 (d, J = 8.5 Hz, 1H), 5.36 (dd, J = 24.8, 9.3 Hz, 1H), 4.80 – 4.70 (m, 1H), 4.45 (dq, J = 12.6, 6.3 Hz, 1H), 1.27 (d, J = 6.2 Hz, 3H), 1.22 (d, J = 6.2 Hz, 3H), 1.13 (d, J = 6.2 Hz, 3H), 0.94 (d, J = 6.2 Hz, 3H). ^{13}C NMR (126 MHz, DMSO-d_6) δ 183.07 (C=O), 146.51 (d, J = 13.0 Hz, C), 137.19 (C), 136.66 (C), 133.94 (CH), 130.20 (CH), 130.05 (CH), 129.04 (d, J = 5.7 Hz, CH), 129.03 (C), 128.55 (d, J = 1.7 Hz, CH), 128.39 (C), 128.23 (C), 128.21 (CH), 128.16 (d, J = 2.5 Hz, CH), 127.47 (CH), 126.73 (CH), 125.34 (CH), 123.61 (C), 123.21 (CH), 115.11 (C), 107.28 (CH), 71.66 (dd, J = 12.4, 7.2 Hz, O$\underline{C}$H$(CH_3)_2$), 55.46 (d, J = 153.7 Hz, CHP), 24.41 (dd, J = 7.5, 3.2 Hz, CH_3), 23.95 (d, J = 5.1 Hz, CH_3), 23.53 (d, J = 5.5 Hz, CH_3). ^{31}P NMR (202 MHz, DMSO-d_6) δ 20.12. MS (ES+): m/z calculated for $C_{30}H_{30}NO_4P$ ($[M+H]^+$) 500.20, found 500.89.

2.2.16. Diisopropyl (((7-oxo-7H-benzo[de]anthracen-3-yl)amino)(p-tolyl)methyl)phosphonate (4b)

Red solid. Yield: 79 %. Melting point: 188°C. R_f = 0.36 (Benzene/Acetonitrile) (3:1). IR, λ_{max} (KBr) cm^{-1}: 453, 539, 655, 703, 774, 835, 889, 987, 1103, 1222, 1306, 1383, 1461, 1526, 1572, 1644 (C=O), 2974 (CH), 3299 (NH). ^{1}H NMR (500 MHz, DMSO-d_6) δ 8.94 (dd, J = 8.4, 1.2 Hz, 1H), 8.69 (dd, J = 7.3, 1.1 Hz, 1H), 8.46 (d, J = 8.5 Hz, 1H), 8.40 (d, J = 8.2 Hz, 1H), 8.27 (dd, J = 8.0, 1.5 Hz, 1H), 7.88 (t, J = 7.8 Hz, 1H), 7.77 – 7.70 (m, 1H), 7.61 (dd, J = 8.2, 2.1 Hz, 2H), 7.46 (t, J = 7.5 Hz, 1H), 7.17 (d, J = 8.0 Hz, 2H), 7.14 (dd, J = 9.2, 6.2 Hz, 1H), 6.92 (d, J = 8.6 Hz, 1H), 5.29 (dd, J = 24.7, 9.2 Hz, 1H), 4.75 (dq, J = 12.4, 6.2 Hz, 1H), 4.46 (dq, J = 12.7, 6.3 Hz, 1H), 2.27 (s, 3H), 1.27 (d, J = 6.1 Hz, 3H), 1.23 (d, J = 6.2 Hz, 3H), 1.14 (d, J = 6.1 Hz, 3H), 0.97 (d, J = 6.1 Hz, 3H). ^{13}C NMR (126 MHz, DMSO-d_6) δ 183.06 (C=O), 146.52 (d, J = 13.1 Hz, C), 137.32 (d, J = 2.9 Hz, C), 137.20 (C), 133.92 (CH), 133.54 (C), 130.16 (CH), 130.03 (CH), 129.14 (d, J = 1.7 Hz, CH), 129.02 (C), 128.92 (d, J = 5.5 Hz, CH), 128.38 (C), 128.23 (C), 128.20 (CH), 127.47 (CH), 126.70 (CH), 125.31 (CH), 123.61 (C), 123.18 (CH), 115.04 (C), 107.29 (CH), 71.59 (dd, J = 13.0, 7.1 Hz, O$\underline{C}$H$(CH_3)_2$), 55.21 (d, J = 154.2 Hz, CHP), 24.42 (dd, J = 6.5, 3.1 Hz, CH_3), 23.97 (d, J = 5.2 Hz, CH_3), 23.61 (d, J = 5.5 Hz, CH_3), 21.19 ($C_{Ar}\underline{C}H_3$). ^{31}P NMR (202 MHz, DMSO-d_6) δ 20.22. MS (ES+): m/z calculated for $C_{31}H_{32}NO_4P$ ($[M+H]^+$) 514.21, found 514.22.

2.2.17. Diisopropyl ((4-fluorophenyl)((7-oxo-7H-benzo[de]anthracen-3-yl)amino)methyl)phosphonate (4c)

Red solid. Yield: 74 %. Melting point: 191°C. R_f = 0.34 (Benzene/Acetonitrile) (3:1). IR, λ_{max} (KBr) cm^{-1}: 454, 541, 657, 702, 773, 844, 891, 989, 1103, 1161, 1222, 1268, 1308, 1383, 1462, 1509, 1575, 1645 (C=O), 2981 (CH), 3304 (NH). ^{1}H NMR (500 MHz, DMSO-d_6) δ 8.96 (dd, J = 8.6, 1.2 Hz, 1H), 8.69 (dd, J = 7.4, 1.1 Hz, 1H), 8.48 (d, J = 8.5 Hz, 1H), 8.41 (d, J = 8.3 Hz, 1H), 8.28 (dd, J = 7.9, 1.5 Hz, 1H), 7.88 (t, J = 7.8 Hz, 1H), 7.84 – 7.77 (m, 2H), 7.77 – 7.70 (m, 1H), 7.46 (t, J = 7.5 Hz, 1H), 7.21 (t, J = 8.8 Hz, 3H), 6.96 (d, J = 8.6 Hz, 1H), 5.42 (dd, J = 24.8, 9.4 Hz, 1H), 4.75 (dq, J = 12.5, 6.2 Hz, 1H), 4.47 (dq, J = 12.6, 6.3 Hz, 1H), 1.27 (d, J = 6.1 Hz, 3H), 1.23 (d, J = 6.1 Hz, 3H), 1.12 (d, J = 6.2 Hz, 3H), 0.97 (d, J = 6.1 Hz, 3H). ^{13}C NMR (126 MHz, DMSO-d_6) δ 183.07 (C=O), 162.20 (dd, J = 243.8, 3.0 Hz, C), 146.42 (d, J = 12.8 Hz, C), 137.17 (C), 133.94 (CH), 132.93 (d, J = 2.7 Hz, C), 131.09 (dd, J = 7.9, 5.7 Hz, CH), 130.29 (CH), 130.05 (CH), 129.05 (C), 128.41 (C), 128.22 (C), 128.17 (CH), 127.47 (CH), 126.75 (CH), 125.31 (CH), 123.64 (C), 123.22 (CH), 115.36 (dd, J = 21.8, 1.3 Hz, CH), 115.21 (C), 107.29 (CH), 71.68 (dd, J = 24.0, 7.1 Hz, O$\underline{C}$H$(CH_3)_2$), 54.62 (d, J = 154.7 Hz, CHP), 24.39 (dd, J = 9.5, 3.2 Hz, CH_3), 23.93 (d, J = 5.1 Hz, CH_3), 23.60 (d, J = 5.3 Hz, CH_3). ^{31}P NMR (202 MHz, DMSO-d_6) δ 19.90 (d, J = 4.2 Hz). MS (ES+): m/z calculated for $C_{30}H_{29}FNO_4P$ ($[M+H]^+$) 518.19, found 518.02.

2.2.18. Diisopropyl ((4-methoxyphenyl)((7-oxo-7H-benzo[de] anthracen-3-yl)amino)methyl)phosphonate (4d)

Red solid. Yield: 68 %. Melting point: 152°C. R_f = 0.31 (Benzene/Acetonitrile) (3:1). IR, λ_{max} (KBr) cm^{-1}: 452, 546, 655, 703,

773, 837, 890, 985, 1103, 1175, 1222, 1305, 1383, 1461, 1512, 1572, 1641 (C=O), 2976 (CH), 3296 (NH). ^{1}H NMR (500 MHz, DMSO-d_6) δ 8.95 (dd, J = 8.5, 1.3 Hz, 1H), 8.69 (dd, J = 7.3, 1.2 Hz, 1H), 8.47 (d, J = 8.5 Hz, 1H), 8.41 (d, J = 8.3 Hz, 1H), 8.27 (dd, J = 7.9, 1.5 Hz, 1H), 7.87 (t, J = 7.8 Hz, 1H), 7.77 – 7.70 (m, 1H), 7.66 (dd, J = 8.9, 1.8 Hz, 2H), 7.46 (t, J = 7.3 Hz, 1H), 7.13 (dd, J = 9.4, 6.2 Hz, 1H), 6.98 – 6.90 (m, 3H), 5.29 (dd, J = 24.4, 9.3 Hz, 1H), 4.74 (dq, J = 12.5, 6.3 Hz, 1H), 4.45 (dq, J = 12.6, 6.2 Hz, 1H), 3.73 (s, 3H), 1.27 (d, J = 6.2 Hz, 3H), 1.23 (d, J = 6.2 Hz, 3H), 1.13 (d, J = 6.2 Hz, 3H), 0.97 (d, J = 6.2 Hz, 3H). ^{13}C NMR (126 MHz, DMSO-d_6) δ 183.06 (C=O), 159.29 (d, J = 2.7 Hz, C), 146.56 (d, J = 13.1 Hz, C), 137.22 (C), 133.92 (CH), 130.26 (d, J = 5.6 Hz, CH), 130.18 (CH), 130.02 (CH), 129.02 (C), 128.38 (C), 128.34 (C), 128.22 (C), 128.21 (CH), 127.47 (CH), 126.69 (CH), 125.29 (CH), 123.61 (C), 123.18 (CH), 114.98 (C), 113.98 (d, J = 1.4 Hz, CH), 107.28 (CH), 71.54 (t, J = 7.1 Hz, O$\underline{C}$H(CH$_3$)$_2$), 55.53 ($C_{Ar}O\underline{C}H_3$), 54.77 (d, J = 155.4 Hz, CHP), 24.43 (t, J = 3.5 Hz, CH$_3$), 23.98 (d, J = 5.1 Hz, CH$_3$), 23.63 (d, J = 5.4 Hz, CH$_3$). ^{31}P NMR (202 MHz, DMSO-d_6) δ 20.40. MS (ES+): m/z calculated for $C_{31}H_{32}NO_5P$ ([M+H]$^+$) 530.21, found 530.26.

2.2.19. Diisopropyl ((2-methoxyphenyl)((7-oxo-7H-benzo[de] anthracen-3-yl)amino)methyl)phosphonate (4e)

Red solid. Yield: 72 %. Melting point: 201°C. R_f = 0.33 (Benzene/Acetonitrile) (3:1). IR, λ_{max} (KBr) cm^{-1}: 557, 621, 706, 780, 990, 1106, 1174, 1235, 1310, 1388, 1463, 1538, 1574, 1648 (C=O), 2977 (CH), 3325 (NH). ^{1}H NMR (500 MHz, DMSO-d_6) δ 9.00 (d, J = 8.3 Hz, 1H), 8.78 (d, J = 7.3 Hz, 1H), 8.62 (d, J = 8.5 Hz, 1H), 8.49 (d, J = 8.2 Hz, 1H), 8.37 (dd, J = 8.0, 1.5 Hz, 1H), 7.98 (t, J = 7.8 Hz, 1H), 7.88 (dt, J = 7.8, 2.1 Hz, 1H), 7.86 – 7.79 (m, 1H), 7.55 (t, J = 7.5 Hz, 1H), 7.40 (t, J = 7.8 Hz, 1H), 7.30 (dd, J = 9.6, 5.9 Hz, 1H), 7.20 (d, J = 8.3 Hz, 1H), 7.04 (t, J = 7.5 Hz, 1H), 6.86 (d, J = 8.5 Hz, 1H), 5.60 (dd, J = 24.7, 9.5 Hz, 1H), 4.91 – 4.80 (m, 1H), 4.51 – 4.39 (m, 1H), 4.09 (s, 3H), 1.37 (d, J = 6.2 Hz, 3H), 1.28 (d, J = 6.2 Hz, 3H), 1.25 (d, J = 6.2 Hz, 3H), 0.92 (d, J = 6.1 Hz, 3H). ^{13}C NMR (126 MHz, DMSO-d_6) δ 183.06 (C=O), 157.36 (d, J = 6.4 Hz, C), 146.58 (d, J = 13.1 Hz, C), 137.20 (CH), 133.93 (C), 130.15 (CH), 130.07 (CH), 129.67 (d, J = 1.6 Hz, CH), 129.35 (d, J = 4.0 Hz, CH), 129.03 (C), 128.44 (CH), 128.43 (C), 128.22 (C), 127.47 (CH), 126.74 (CH), 125.36 (CH), 124.49 (C), 123.57 (C), 123.18 (CH), 120.97 (d, J = 2.5 Hz, CH), 115.22 (C), 111.36 (CH), 106.23 (CH), 71.61 (dd, J = 8.8, 7.4 Hz, O$\underline{C}$H(CH$_3$)$_2$), 56.38 ($C_{Ar}O\underline{C}H_3$), 48.60 (d, J = 158.6 Hz, CHP), 24.40 (dd, J = 4.9, 3.3 Hz, CH$_3$), 24.00 (d, J = 4.9 Hz, CH$_3$), 23.25 (d, J = 5.6 Hz, CH$_3$). ^{31}P NMR (202 MHz, DMSO-d_6) δ 20.35. MS (ES+): m/z calculated for $C_{31}H_{32}NO_5P$ ([M+H]$^+$) 530.21, found 530.18.

2.2.20. Diisopropyl (((7-oxo-7H-benzo[de]anthracen-3-yl)amino) (thiophen-2-yl)methyl)phosphonate (4g)

Red solid. Yield: 66 %. Melting point: 141°C. R_f = 0.37 (Benzene/Acetonitrile) (3:1). IR, λ_{max} (KBr) cm^{-1}: 474, 557, 656, 703, 774, 837, 892, 998, 1102, 1171, 1232, 1310, 1385, 1462, 1525, 1575, 1644 (C=O), 2978 (CH), 3288 (NH). ^{1}H NMR (500 MHz, DMSO-d_6) δ 8.91 (dd, J = 8.3, 1.3 Hz, 1H), 8.69 (dd, J = 7.3, 1.1 Hz, 1H), 8.53 (d, J = 8.4 Hz, 1H), 8.44 (d, J = 8.1 Hz, 1H), 8.28 (dd, J = 8.0, 1.5 Hz, 1H), 7.87 (t, J = 7.8 Hz, 1H), 7.79 – 7.72 (m, 1H), 7.50 – 7.42 (m, 3H), 7.15 (d, J = 8.6 Hz, 1H), 7.11 (dd, J = 9.3, 5.4 Hz, 1H), 7.04 (d, J = 3.9 Hz, 1H), 5.71 (dd, J = 24.4, 9.2 Hz, 1H), 4.81 – 4.70 (m, 1H), 4.59 (dq, J = 12.6, 6.3 Hz, 1H), 1.27 (t, J = 5.8 Hz, 6H), 1.09 (dd, J = 17.1, 6.2 Hz, 6H). ^{13}C NMR (126 MHz, DMSO-d_6) δ 183.09 (C=O), 146.22 (d, J = 11.1 Hz, C), 139.31 (C), 137.18 (C), 133.97 (CH), 130.08 (d, J = 9.4 Hz, CH), 129.24 (CH), 129.07 (C), 128.39 (C), 128.26 (C), 128.17 (CH), 127.94 (d, J = 6.9 Hz, CH), 127.49 (CH), 127.21 (d, J = 2.1 Hz, CH), 126.80 (CH), 126.41 (d, J = 1.8 Hz, CH), 125.41 (CH), 123.60 (C), 123.27 (CH), 115.38 (C), 107.48 (CH), 72.04 (d, J = 7.1 Hz, O$\underline{C}$H(CH$_3$)$_2$), 71.87 (d, J = 7.3 Hz, O$\underline{C}$H(CH$_3$)$_2$), 51.33 (d, J = 160.5 Hz, CHP), 24.43 (dd, J = 8.4, 3.1 Hz, CH$_3$), 23.89 (d, J = 5.2 Hz, CH$_3$), 23.71 (d, J = 5.4 Hz, CH$_3$). ^{31}P NMR (202 MHz, DMSO-d_6) δ 18.63. MS (ES+): m/z calculated for $C_{28}H_{28}NO_4PS$ ([M+H]$^+$) 506.15, found 506.17.

3. Results and discussion

3.1. Synthesis

Target compounds were synthesized under Kabachnik-Fields reaction conditions (Scheme 2). Several reviews have described mechanism and summarized varying methods for this three-component reaction, including catalyzed and catalyst-free variations, as well as synthesis with the employment of microwave irradiation, ionic liquids and dehydrating agents [27–29]. In the case of benzanthrone derivatives, we have plumped for the most advantageous approach: reaction of the 3-aminobenzanthrone with appropriate aromatic aldehydes in excess and a dialkylphosphonate as both – reactants and solvents (see Section 2.2.1.). This method is conditioned by the ease of the subsequent extraction and purification of α-aminophosphonates, where excess of an aldehyde and a dialkylphosphonate is hydrolyzed under moderately basic conditions and a pure compound is obtained through recrystallization. Consequently, acquiring new benzanthrone α-aminophosphonates in good yields.

3.2. Structural and spectral characterization

FTIR, ^{1}H-, ^{13}C- and ^{31}P-NMR spectra and mass spectrometric analysis confirms chemical structures of newly prepared compounds **2a** – **4g**.

Obtained infrared spectra show peaks of benzanthrone carbonyl group (C=O) vibration band around 1636 – 1647 cm^{-1}, a broad aliphatic carbon–hydrogen (C–H) vibration band around 2953 – 2990 cm^{-1} and broad amino group (NH) band around 3281 – 3321 nm.

Structures of obtained compounds are confirmed by ^{1}H-NMR spectroscopy, with the corresponding signals of aromatic protons characteristic for phenyl and thienyl groups and benzanthrone residue. Signal of the α-carbon hydrogen shows as doublet of doublets on the account of coupling with phosphorus. Hydrogens of alkyl groups of the phosphonate moiety appear as separate multiplets due to their magnetic non-equivalence. In APT NMR spectra, appropriate peaks of the benzanthrone carbonyl group carbon at 183 ppm is found. In addition, on account of carbon-phosphorous coupling and magnetic non-equivalence of carbon atoms of the phosphonate moiety, appearance of separate doublets is observed in APT spectra. In ^{31}P-NMR spectra phosphorous peaks appears at around 24 – 19 ppm as singlets (decoupled mode) or as doublets for fluorine containing compounds **2c, 3c** and **4c**. The obtained data is in good correlation with the previously reported NMR results of other α-amino phosphonates and benzanthrone derivatives [30–35].

Analysis of mass spectra revealed presence of quasimolecular ions ([M+H]$^+$) for all of the obtained compounds, as well as presence of the 1-phenylnaphthalene (M = 201) ion peaks, which is usual for benzanthrone derivatives losing C=O and groups attached to aromatic system. Peaks of molecular ions of unsubstituted benzanthrone (M = 230), 3-aminobenzanthrone (M = 245) and [BA–N=C]$^+$ (M = 256), characteristic to other nitrogen containing derivatives of benzanthrone, are also present [7].

3.3. Crystal structure analysis

Figs. 1 and 2 give a perspective view of molecules **3g** and **4a** respectively with thermal ellipsoids and the atom-numbering

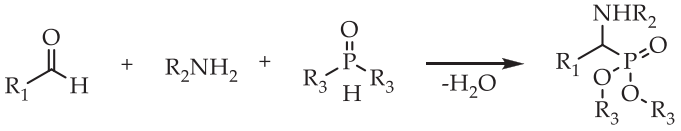

Scheme 2. Kabachnik-Fields reaction.

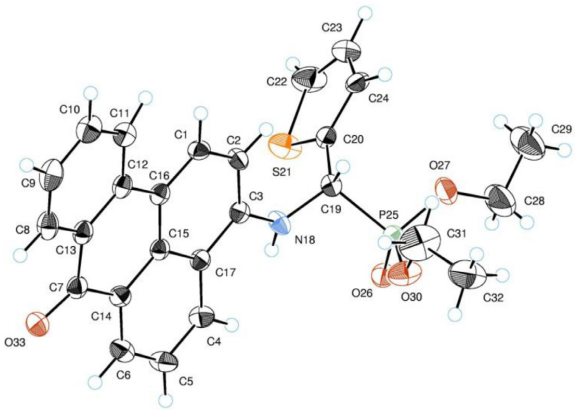

Fig. 1. ORTEP diagram for molecule **3g**.

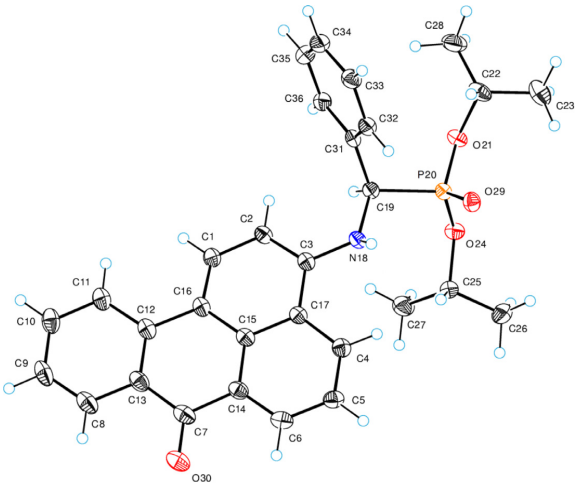

Fig. 2. ORTEP diagram for molecule **4a**.

scheme followed in the text. Both molecular structures contain an asymmetric carbon atom (atom C19), however the crystal structures are achiral (space groups are *P*1 and $P2_1/c$), therefore, these compounds represent racemates (Table 2). In the crystal structures there are quite strong intermolecular hydrogen bonds of NH···O type with lengths of 3.046(2) (for **4a**) and 2.911(3) Å (for **3g**). By means of these bonds centrosymmetric molecular dimers are formed in the crystals. Fig. 3 shows the molecular dimer for **3g**. It is possible that in the thienyl substituent there has occurred a static disorder, which is so characteristic of 2-thienyl derivatives [36]. Therefore, this structure is characterized by higher value of *R*-factor and the estimated standard deviations. Fig. 5 gives a perspective view of molecule **3a**.

In the crystal structure of **4a** there are π-π stacking interactions between benzanthrone systems. Fig. 4 illustrates these interactions. The shortest interatomic contact in these interactions is C11···C16 (Fig. 4) with length of 3.326(2) Å. In the **3g** structure, such π-π interactions are not observed.

3.4. Photophysical properties

For the examination of photophysical properties of newly synthesized compounds, **2a** – **2g, 3a** and **4a**, absorbance and emission spectra were acquired in solvents of varying polarity, specifically, in hexane, chloroform, benzene, ethyl acetate, acetone, DMF

Table 2
Crystal data of the compounds **3a, 3g** and **4a**.

	3a	3g	4a
Empirical formula	$C_{28}H_{26}NO_4P$	$C_{26}H_{24}NO_4PS$	$C_{30}H_{30}NO_4P$
Formula weight	471.50	477.16	499.19
Crystal system	orthorhombic	monoclinic	triclinic
a (Å)	15.8586(2)	11.8473(3)	10.7140(4)
b (Å)	12.0930(1)	15.5786(5)	11.3082(4)
c (Å)	24.0436(3)	12.5066(3)	11.9985(4)
α (°)	90	-	113.362(4)
β (°)	90	94.648(2)	105.631(3)
γ (°)	90	-	97.466(3)
V (Å^3)	4611.03(9)	2300.7(1)	1238.2(1)
Z	8	4	2
μ (mm^{-1})	1.354	0.244	1.290
Density (calculated) (g/cm^3)	1.3583	1.379	1.340
Space group	*Pbca*	*P* 2$_1$/*c*	*P*1
$R[F^2>2\sigma(F^2)]$	0.0402	0.0623	0.0448
CCDC deposition number	CCDC 2218839	CCDC 2213262	CCDC 2213261

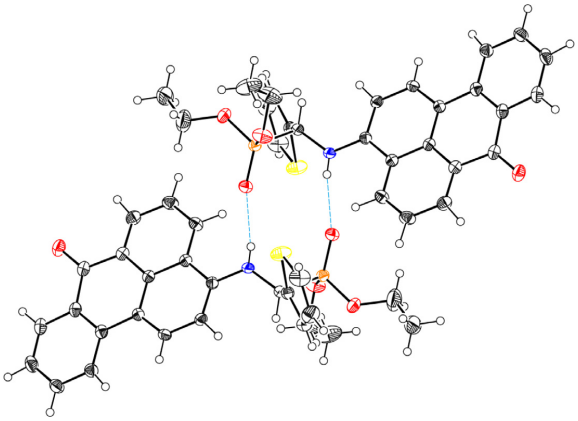

Fig. 3. ORTEP diagram of molecular dimer of **3g**.

Table 3
Absorption maxima of prepared dyes in organic solvents (concentration 10^{-5} M).

	Absorption λ_{abs} (lgε) (nm)								
	2a	***2b***	***2c***	***2d***	***2e***	***2f***	***2g***	***3a***	***4a***
Hexane	458 (3.86)	-	-	-	-	-	449 (4.12)	458 (3.23)	-
Benzene	470 (4.10)	470 (4.43)	466 (4.05)	470 (4.27)	473 (4.21)	466 (4.02)	464 (4.18)	470 (4.05)	473 (4.60)
CH_3Cl	478 (4.14)	481 (4.40)	480 (4.02)	481 (4.23)	485 (4.13)	477 (4.08)	473 (4.22)	482 (4.12)	485 (4.61)
EtOAc	473 (4.10)	475 (4.37)	472 (4.03)	475 (4.29)	477 (3.97)	471 (4.12)	468 (4.22)	474 (4.01)	476 (4.64)
Acetone	482 (4.10)	481 (4.42)	480 (4.06)	483 (4.28)	483 (4.13)	478 (4.10)	475 (4.48)	480 (4.09)	485 (4.61)
EtOH	491 (4.04)	493 (4.42)	491 (4.07)	493 (4.22)	496 (4.05)	491 (4.05)	484 (4.14)	491 (4.03)	495 (4.64)
DMF	492 (4.10)	494 (4.43)	491 (4.10)	495 (4.30)	491 (4.24)	491 (4.08)	489 (4.22)	494 (4.09)	495 (4.61)
DMSO	501 (4.08)	501 (4.46)	497 (4.09)	501 (4.26)	497 (4.12)	500 (4.10)	497 (4.16)	500 (4.03)	502 (4.65)

(N,N-dimethylformamide), DMSO (dimethyl sulfoxide) and EtOH (ethanol).

All of the studied dyes were found to be fluorescent and showing substantial solvatochromic response, emitting light from green in hexane to red in ethanol. Observed solvatochromic properties of these benzanthrone derivatives evinces that underlying mechanism responsible for fluorescence thus is internal charge transfer (ICT) during excitation from the electron donating amino group to the electron withdrawing carbonyl group.

Data representing absorption maxima and molar attenuation coefficients, fluorescence maxima and Stokes shifts are summarized in Tables 3–5. No significant influence of substituents on

Table 4
Fluorescence maxima of prepared dyes in organic solvents (concentration 10^{-5} M).

	Fluorescence λ_{abs} (nm)								
	2a	***2b***	***2c***	***2d***	***2e***	***2f***	***2g***	***3a***	***4a***
Hexane	520	-	-	-	-	-	525	534	-
Benzene	554	559	554	560	572	554	574	555	561
CH_3Cl	586	593	590	594	604	590	590	588	597
EtOAc	571	574	571	575	579	571	571	571	578
Acetone	590	594	592	595	600	592	592	592	597
EtOH	635	638	635	639	640	635	637	636	640
DMF	604	606	605	608	612	603	605	606	607
DMSO	614	618	616	617	622	616	617	616	617

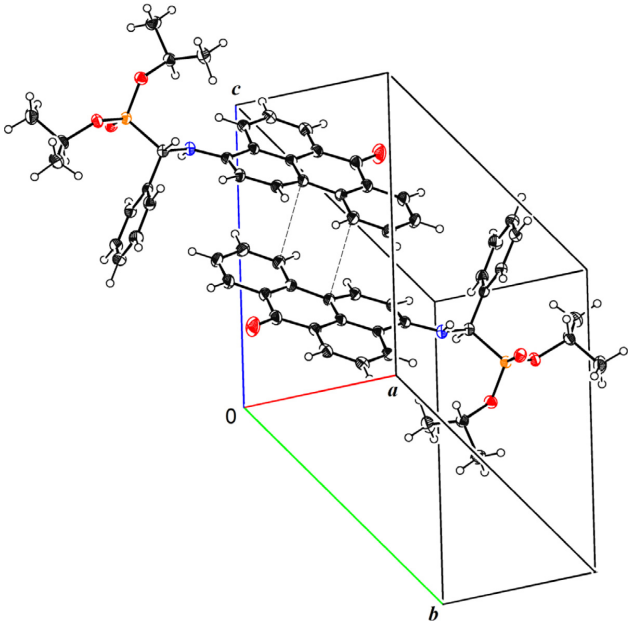

Fig. 4. Part of the crystal structure of **4a**, showing the π-π stacking interactions.

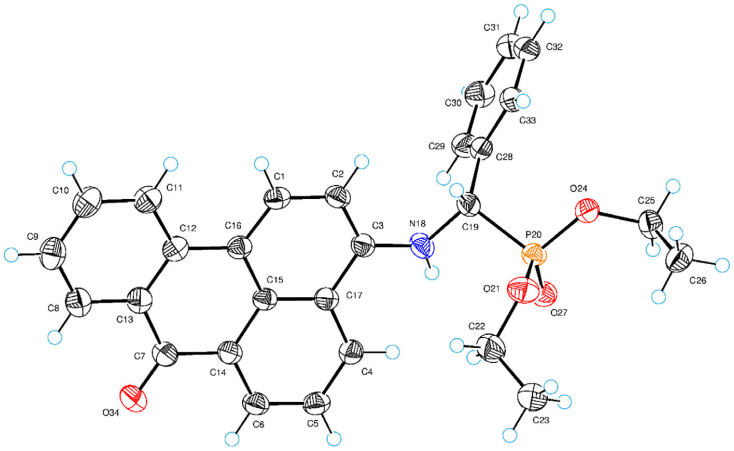

Fig. 5. ORTEP diagram for molecule **3a**.

Table 5
Stokes shift of prepared dyes in organic solvents (concentration 10^{-5} M).

	Stokes shift (cm^{-1})								
	2a	***2b***	***2c***	***2d***	***2e***	***2f***	***2g***	***3a***	***4a***
Hexane	2603	-	-	-	-	-	3224	3107	-
Benzene	3226	3388	3409	3419	3659	3409	4130	3259	3316
CH_3Cl	3856	3927	3884	3955	4062	4015	4192	3740	3868
EtOAc	3629	3631	3673	3661	3693	3718	3854	3584	3707
Acetone	3798	3955	3941	3897	4037	4029	4161	3941	3868
EtOH	4619	4610	4619	4635	4536	4619	4963	4643	4577
DMF	3769	3741	3838	3755	4027	3783	3921	3741	3728
DMSO	3673	3779	3887	3753	4044	3766	3913	3766	3713

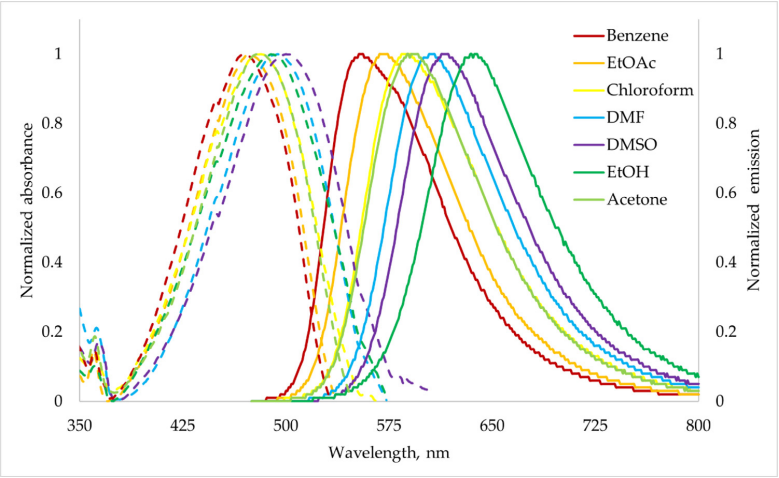

Fig. 6. The UV-Vis absorption and fluorescence emission spectra of compound **3a** in various organic solvents.

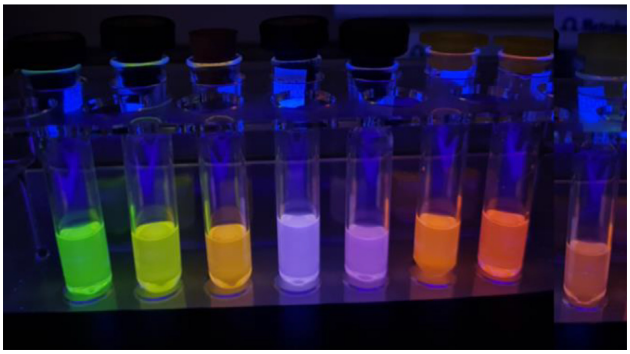

Fig. 7. Solutions of compound **2g** in ultraviolet light in different organic solvents (from left to right: in hexane, chloroform, benzene, ethyl acetate, acetone, DMF, DMSO and ethanol).

phenyl group or nature of aromatic substituent on α-carbon (phenyl or thienyl), or phosphonate alkyl groups (methyl, ethyl or isopropyl) on photophysical properties of the obtained chromophores was found, with the exception of slightly higher molar attenuation coefficients of compound **4a**, bearing bulkier isopropyl groups, compared to compounds **2a** and **3a**, thus demonstrating more intense absorbance of electromagnetic radiation.

On the example of compound **3a** (Fig. 6) it is observed that in solutions benzanthrone α-aminophosphonates exhibit broad band absorbance around 458 – 500 nm and are fluorescence from 534 nm (hexane) to 636 nm (ethanol) thus attaining bathochromic shifts of 42 and 102 nm respectively, hence polarity effect of the medium on fluorescence is more pronounced than on the absorption. Among studied dyes highest Stokes shift of 4963 cm^{-1} was observed for the compound **2g** (Fig. 7) in ethanol.

Absorption spectra of previously studied benzanthrone amidines lie between 410 and 495 nm, that is, in the shorter wave range, while 3-substituted benzanthrone amino derivatives exhibit absorption in the range of 430 – 520 nm, that is, in the longer wave range [37,38]. It may be concluded that benzanthrone amino group attached to a phosphoryl group manifests stronger donating effect than amidino group, but to a slightly lesser degree than alkyl amino group.

3.5. Toxicology: methods and evaluation of compounds 2a and 2g

For the evaluation of toxicity of compounds **2a** and **2g**, 6×10^{-5} M and 3×10^{-6} M solutions were prepared (concentrations were chosen based on previously reported studies on toxicity of dyes) [39–41]. On account of compound **2g** 6×10^{-5} M solution being too toxic for the analyzed plants to measure pigment concentrations, malondialdehyde (MDA) amounts and electrolyte leakage, solutions were diluted to concentrations of 1×10^{-6} M and 1×10^{-7} M.

It is characteristic of grain crops to grow and develop synchronously throughout orthogenesis and thus wheat sprouts are used for morphology, physiology and molecular biology research. Experiments were caried out on organs of etiolated '*Brencis*' wheat species' sprouts – cotyledon and coleoptile. These were measured in comparison due to cotyledon being the developing and coleoptile being the senescent organs of a sprout. All of the results were obtained from three independent measurements. For all of these results standard deviation was calculated.

3.5.1. Cultivation and morphology of wheat sprouts

Etiolated seeds of '*Brencis*' wheat species were germinated in a climate camera (*Sanyo*) at 26°C on a moist filter paper in the

Table 6
Influence of compound **2a** and **2g** with different concentrations on wheat morphology.

		Cotyledon length (mm)	Coleoptile length (mm)	Phytotoxicity in cotyledon, %	Phytotoxicity in coleoptile, %
***Concentration of compound 2a* (M)**	0	85,80 ± 4,42	39,90 ± 1,21	-	-
	3×10^{-6}	67,05 ± 3,90	42,45 ± 2,04	22	-
	6×10^{-5}	54,00 ± 2,87	43,25 ± 2,27	37	-
***Concentration of compound 2g* (M)**	0	91,27 ± 5,48	44,27 ± 1,75	-	-
	1×10^{-7}	86,05 ± 4,83	36,81 ± 1,29	6	17
	1×10^{-6}	86,80 ± 4,40	35,70 ± 2,56	5	19
	3×10^{-6}	30,00 ± 2,42	11,40 ± 0,91	67	74
	6×10^{-5}	15,00 ± 0,93	7,47 ± 0,52	84	83

Table 7
Influence of compound **2a** and **2g** with different concentrations on electrolyte leakage and MDA amount in wheat sprouts.

		Electrolyte leakage (%)		MDA amount (nmol/g×FW)	
		Cotyledon	Coleoptile	Cotyledon	Coleoptile
Concentration of compound 2a (M)	0	25 ±5,9	16 ± 1,0	19,6 ± 0,6	35,8 ± 1,4
	3×10^{-6}	21 ±1,0	19 ± 2,4	34,6 ± 5,9	39,2 ± 1,7
	6×10^{-5}	41 ± 6,6	34 ± 0,8	59,9 ± 0,9	47,4 ±1,4
Concentration of compound 2g (M)	0	27 ± 1,5	12 ± 0,6	60,6 ± 5,6	39,9 ± 5,8
	1×10^{-7}	24 ± 0,7	14 ± 4,2	63,6 ± 0,5	36,3 ± 2,7
	1×10^{-6}	21 ± 0,4	14 ± 1,2	62,4 ± 4,7	42,7 ± 2,6
	3×10^{-6}	10 ± 1,0	14 ± 0,5	79,3 ± 5,8	40,7 ± 0,9

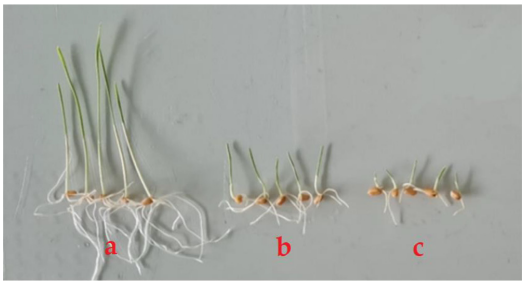

Fig. 8. Wheat sprouts cultivated in the presence of compound **2g** with different concentrations: a (0 M), b (6×10^{-5} M), c (3×10^{-6} M).

course of 24 hours in the absence of light. In 24 hours equally sprouted seeds were transported to new cuvettes and were cultivated in the absence of light in the climate camera (26°C, 75 % moisture) as control samples, in the presence of compound **2a** (6×10^{-5} M, 3×10^{-6} M) or **2g** (6×10^{-5} M, 3×10^{-6} M, 1×10^{-6} M, 1×10^{-7} M) solutions. For all of the measurements 5 days old sprouts were used. From each cuvette of differing compound **2a** and compound **2g** concentrations, 25 average height wheat sprouts were taken; coleoptiles were separated from cotyledons and lengths were measured.

3.5.2. Quantification of malondialdehyde

Malondialdehyde amount was determined based on the reaction with thiobarbituric acid. Wheat cotyledons and coleoptiles were homogenized in 0.1 % trichloroacetic acid solution (1/10) and centrifuged for 15 minutes (14 000 rpm). Following centrifugation, to 1 mL of the upper fraction, 2.5 mL of 0.5 % thiobarbituric acid (dissolved in 20 % trichloroacetic acid) were added and obtained solution was incubated in hot water (95°C) for 30 minutes. Solution was then quickly cooled to stop the reaction and centrifuged for 30 minutes (14 000 rpm).

Optical density of solutions was determined at wavelengths of 532 nm and 600 nm using Cary 50 UV/VIS (Varian) spectrophotometer. MDA concentrations were calculated using non-specific adsorption (600 nm) reduction from adsorption wavelength of 532 nm (ε = 155 $mM^{-1}\times cm^{-1}$).

3.5.3. Electrolyte leakage measurement

Four cotyledons and coleoptiles per experiment were submerged in 15 mL of deionized water for 24 hours at room temperature, after which initial conductivity was measured (ALL-CHEM-MISST, AK Kappenberg). Test tubes with samples were then heated in boiling water for 15 minutes and after cooling to room temperature second measurement of conductivity was performed. Electrolyte leakage (EL) thus calculated as ratio of conductivity before and after heating (1):

$$EL = \frac{V_{before\ heating} - V_{H_2O}}{V_{after\ heating} - V_{H_2O}} \times 100\ \%,$$

where EL – electrolyte leakage, %; V – conductivity, $\mu S\times cm^{-1}$ [42].

3.5.4. Determination of concentrations of chlorophyll a, chlorophyll b and carotenoids

For the extraction of pigments 80 % aqueous acetone was used. Magnesium carbonate ($MgCO_3$) was used for acid neutralization and prevention of phaeophytization. 0.2 g plant material was grinded using scissors, placed in a small pestle with a small amount of $MgCO_3$, 1 mL of 80 % acetone and was thoroughly grinded. Obtained homogenate was then transferred to a test tube, 3 mL of the acetone were added, and the resultant mixture was left overnight.

Test tubes were centrifuged several times for 10 minutes each time (7000 rpm). Clear solution was transferred to another test tube and to the residue 3 mL of the acetone were added. Procedure was repeated 2 – 3 times, until precipitates became colorless.

Optical densities of solutions were determined at wavelengths of 470 nm, 646 nm and 663 nm using Cary 50 UV/VIS (Varian) spectrophotometer.

3.5.5. Evaluation

Data representing influence of compound **2a** and compound **2g** with different concentrations on length of cotyledons and coleoptiles is summarized in Table 6. It is evident that with increase in concentration of both of these compounds there is substantial delay in growth of cotyledons. At concentration of 6×10^{-5} M

Table 8
Influence of compound **2a** with different concentrations on concentration of pigments: chlorophyll *a*, chlorophyll *b* and carotenoids.

Concentration of compound 2a (M)	Concentration of chlorophyll *a* (mg/L)		Concentration of chlorophyll *b* (mg/L)		Concentration of carotenoids (mg/L)	
	Cotyledon	Coleoptile	Cotyledon	Coleoptile	Cotyledon	Coleoptile
0	22,7 ± 0,46	4,9 ± 0,64	5,1 ±0,07	1,6 ± 0,01	5,7 ± 0,03	0,9 ± 0,03
3×10^{-6}	25,4 ± 0,78	4,8 ± 0,41	6,7 ± 0,28	2,1 ± 0,41	6,3 ± 0,03	0,7 ± 0,01
6×10^{-5}	26,4 ± 0,54	4,6 ± 0,23	7,8 ± 0,22	2,5 ± 0,12	6,5 ± 0,06	0,8 ± 0,01

Table 9
Influence of compound **2g** with different concentrations on concentration of pigments: chlorophyll *a*, chlorophyll *b* and carotenoids.

Concentration of compound 2g (M)	Concentration of chlorophyll *a* (mg/L)		Concentration of chlorophyll *b* (mg/L)		Concentration of carotenoids (mg/L)	
	Cotyledon	Coleoptile	Cotyledon	Coleoptile	Cotyledon	Coleoptile
0	14,9 ± 1,79	1,8 ± 0,21	3,3 ± 0,57	0,9 ± 0,09	3,4 ± 0,37	0,3 ± 0,02
1×10^{-7}	14,2 ± 0,66	2,1 ± 0,16	3,0 ± 0,10	1,0 ± 0,15	3,2 ±0,18	0,2 ± 0,04
1×10^{-6}	13,6 ± 0,47	2,2 ± 0,08	2,5 ± 0,14	0,7 ± 0,22	3,0 ±0,13	0,3 ± 0,01
3×10^{-6}	12,3 ± 0,31	0,9 ± 0,01	2,5 ± 0,12	0,5 ± 0,01	3,5 ±0,04	0,1 ± 0,01

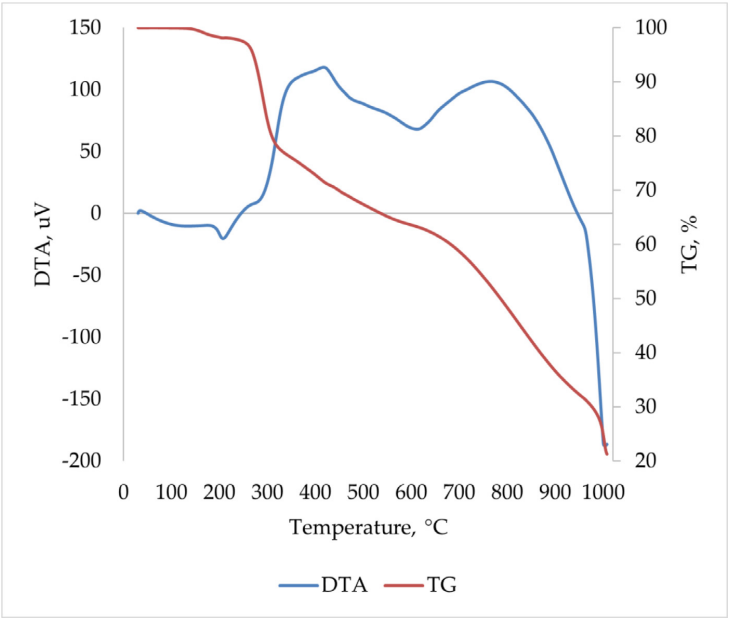

Fig. 9. DTA and TG curves of compound **3a**.

phytotoxicity reaches 37 % for compound **2a** and 83 % for compound **2g**. Results indicate that compound **2a** (both 3×10^{-6} M and 6×10^{-5} M) insignificantly stimulates coleoptile growth, hence toxic effect is not observed, whilst compound **2g** does exhibit phytotoxic effect on coleoptile development, which increases along with concentration of **2g** (Fig. 8).

Influence of compounds **2a** and **2g** on lipid peroxidation product MDA amount changes was studied as it is known that MDA concentration increase is one of indictors of plant cell membrane damage during oxidative stress. Organs of wheat sprouts responded to stress effects caused both by compound **2a** and **2g**, loosing regenerative abilities with increase in concentrations of studied dyes. Compound **2a** (3×10^{-6} M and 6×10^{-5} M) caused considerable damage to cotyledons and coleoptiles as stipulated by MDA levels when compared to control samples (Table 7). Membrane stability has decreased as a result of membrane lipid peroxidation, which is designated by amplification of passive transport (electrolyte leakage). When compared with control samples, electrolyte leakage in cotyledons and coleoptiles doubles by influence of the compound **2a** (6×10^{-5} M). While for compound **2g** lower concentrations were used, electrolyte leakage was not significantly impacted in coleoptiles and negligibly subsided in cotyledons. Cotyledons are able to develop in the presence of compound **2g** (1×10^{-7} M – 3×10^{-6} M), despite the fact that MDA amounts increase both in cotyledons and coleoptiles, which suggests passing oxidative stress. Perhaps, it is due to activity of antioxidant system, which is capable to neutralize accumulated MDA, preventing changes in membrane stability.

Data representing change in concentrations of pigments in wheat sprouts impacted by studied dyes is summarized in Table 8 (for **2a**) and Table 9 (for **2g**). Chlorophyll *a* and *b* concentrations slightly increase in cotyledons with increasing concentrations (3×10^{-6} - 6×10^{-5}) of compound **2a**, when compared with control sample. In coleoptiles chlorophyll *a* concentrations do not change significantly, but concentration of chlorophyll *b* moderately increases. Compound **2g** has somewhat greater impact on decrease of amounts of chlorophyll *a* and *b* in both – cotyledons and coleoptiles.

Wheat produces several compounds that exhibit antioxidant activities, among these – carotenoids, which repair damage from the effects of reactive oxygen substances. Concentration of carotenoids insignificantly increases in cotyledons along with concentration of compound **2a**. With higher concentrations of compound **2g**, concentration of carotenoids slightly decreases in coleoptiles and cotyledons, but somewhat increases at concentration of 3×10^{-6} M.

When comparing toxicity effects of compounds **2a** and **2g** at equal concentrations, it may be concluded that compound **2g** exhibits greater phytotoxicity and cytotoxicity, which is expressed in increase of products of oxidative processes and delay in growth of wheat sprouts. Juxtaposing chemical structures of studied compounds **2a** and **2g**, one bearing phenyl ring and second – thienyl ring, it suggests that toxic properties are increased due to presence of thienyl group.

To determine effect of studied compounds on pigment amount in sprouts, concentrations of chlorophyll *a*, chlorophyll *b* and carotenoids are calculated according to formulas (1 – 3):

$$C_a = 12.21 \times D_{663} - 2.81 \times D_{646} \quad (1)$$

$$C_b = 20.13 \times D_{646} - 5.03 \times D_{663} \quad (2)$$

$$C_{car} = \frac{1000 \times D_{470} - 3.27 \times C_a - 1000 \times C_b}{229}, \quad (3)$$

where C_a, C_b, C_{car} – concentrations of chlorophyll a, chlorophyll b and carotenoids (mg/L); D_{663}, D_{646}, D_{470} – optical densities at 663, 646 and 470 nm respectively.

3.5.6. Thermogravimetric analysis of compound 3a

Thermal stability of obtained benzanthrone α-aminophosphonates was examined on the example of compound **3a**, using DTA and TG techniques (Fig. 9). Based on the TG curve, it is observed that thermal degradation proceeds in two main steps: at 270 – 330°C (approximately 20 wt. % are lost) and at 630 – 950°C (approximately 30 wt. % are lost), both processes being exothermic as indicated by DTA curve. Endothermic process with a peak at 203°C corresponds to melting temperature of the compound **3a**. Generally, the analyzed compound is thermally stable up to about 270°C, at which point 5 % of initial mass is lost, and is of comparable stability with previously studied benzanthrone amino derivatives [43].

Conclusions

As a result, a small library of new benzanthrone α-aryl-α-amino phosphonates was obtained. Synthesized compounds were found to be fluorescent in solutions with maxima from 520 nm (hexane) to 640 nm (ethanol), exhibiting solvatochromic properties with emission of light upon excitation from green to red, attaining bathochromic shift of more than 100 nm and Stokes shift of more than 4900 cm^{-1}. Structures of newly prepared dyes were confirmed and characterized by means of FTIR, ^{1}H-, ^{13}C-, ^{31}P-NMR spectroscopy, mass spectrometry and X-ray diffraction crystallographic analysis. Experiments – morphology, electrolyte leakage, MDA and pigment quantification – revealed benzanthrone α-amino phosphonates to exhibit toxic effect on growth of wheat sprouts to a varying degree with dependance on concentration and substituent on α-carbon. Thermogravimetric analysis showed analyzed compound **3a** to be thermally stable up to 270°C.

Credit Author Statement

Armands Maļeckis: Methodology, Validation, Formal analysis, Investigation, Writing - original draft, Project administration, Funding acquisition

Evans Griškjāns: Methodology, Validation, Investigation

Marija Cvetinska: Methodology, Validation, Investigation

Marina Savicka: Conceptualization, Methodology, Formal analysis, Investigation

Sergey Belyakov: Investigation, Formal analysis, Data Curation

Elena Kirilova: Conceptualization, Methodology, Resources, Writing - review & editing, Supervision.

Declaration of Competing Interest

The authors declare that they have no known competing financial interests or personal relationships that could have appeared to influence the work reported in this paper.

Data Availability

Data will be made available on request.

Acknowledgments

This work has been supported by the European Social Fund within the Project No 8.2.2.0/20/I/008 «Strengthening of PhD students and academic personnel of Riga Technical University and BA School of Business and Finance in the strategic fields of specialization» of the Specific Objective 8.2.2 «To Strengthen Academic Staff of Higher Education Institutions in Strategic Specialization Areas» of the Operational Programme «Growth and Employment».

Supplementary materials

Supplementary material associated with this article can be found, in the online version, at doi:10.1016/j.molstruc.2022.134838.

References

[1] A. Thomas, E.M. Kirilova, B.V. Nagesh, S.R. Manohara, B. Siddlingeshwar, S. v Belyakov, Synthesis, solvatochromism and DFT study of pyridine substituted benzanthrone with ICT characteristics, J. Mol. Struct. 1262 (2022) 132971, doi:10.1016/j.molstruc.2022.132971.

[2] D. Staneva, E. Vasileva-Tonkova, R. Kukeva, R. Stoyanova, I. Grabchev, Synthesis, spectral characteristics and microbiological activity of benzanthrone derivatives and their Cu(II) complexes, J. Mol. Struct. 1197 (2019) 576–582, doi:10.1016/j.molstruc.2019.07.087.

[3] E. Kirilova, I. Mickevica, L. Mezaraupe, A. Puckins, I. Rubenina, S. Osipovs, I. Kokina, A. Bulanovs, M. Kirjusina, I. Gavarane, Novel dye for detection of callus embryo by confocal laser scanning fluorescence microscopy, Luminescence 34 (2019) 353–359, doi:10.1002/bio.3616.

[4] I. Rubenina, I. Gavarane, E. Kirilova, L. Mezaraupe, M. Kirjusina, Comparison of the benzanthrone luminophores: they are not equal for rapid examination of parafasciolopsis fasciolaemorpha (Trematoda: Digenea), Biomolecules 11 (2021) 598, doi:10.3390/biom11040598.

[5] I. Gavarane, E. Kirilova, I. Rubeniņa, L. Mežaraupe, S. Osipovs, G. Deksne, A. Pučkins, I. Kokina, A. Bulanovs, M. Kirjušina, A simple and rapid staining technique for sex determination of trichinella larvae parasites by confocal laser scanning microscopy, Microsc. Microanal. 25 (2019) 1491–1497, doi:10.1017/S1431927619015046.

[6] K. Vus, V. Trusova, G. Gorbenko, E. Kirilova, G. Kirilov, I. Kalnina, P. Kinnunen, Novel aminobenzanthrone dyes for amyloid fibril detection, Chem. Phys. Lett. 532 (2012) 110–115, doi:10.1016/j.cplett.2012.02.061.

[7] A. Maļeckis, L. Avotiņa, G. Ķizāne, A. Pučkins, S. Osipovs, E. Kirilova, New fluorescent heterocyclic compounds derived from 3-cyanobenzanthrone, Polycycl. Aromat. Compd. 42 (2022) 5508–5520, doi:10.1080/10406638.2021.1939068.

[8] E. Kirilova, A. Bulanovs, A. Puckins, E. Romanovska, G. Kirilov, Spectral and structural characterization of chromium(III) complexes bearing 7-oxo-7H-benzo[de]anthracen-3-yl-amidines ligand, Polyhedron 157 (2019) 107–115, doi:10.1016/j.poly.2018.09.072.

[9] I. Grabchev, I. Moneva, E. Wolarz, D. Bauman, Fluorescent 3-oxy benzanthrone dyes in liquid crystalline media, Dyes Pigm. 58 (2003) 1–6, doi:10.1016/S0143-7208(03)00033-0.

[10] I. Grabchev, I. Moneva, Synthesis and properties of benzanthrone derivatives as luminophore dyes for liquid crystals, Dyes Pigm. 37 (1998) 155–164, doi:10.1016/S0143-7208(97)00050-8.
[11] A. Bulanovs, G. Kirilov, M. Fleisher, E. Kirilova, I. Mihailova, Luminescence and structural properties of thermally evaporated benzanthrone dyes thin films, OptoElectron. Rev. 21 (2013), doi:10.2478/s11772-013-0087-5.
[12] T.N. Konstantinova, The synthesis of some benzanthrone derivatives for use as dyes for polymeric materials, Dyes Pigm. 10 (1989) 63–67, doi:10.1016/0143-7208(89)85040-5.
[13] A. Mucha, P. Kafarski, Ł. Berlicki, Remarkable potential of the α-aminophosphonate/phosphinate structural motif in medicinal chemistry, J. Med. Chem. 54 (2011) 5955–5980, doi:10.1021/jm200587f.
[14] P. Kafarski, B. Lejczak, Biological activity of aminophosphonic acids, Phosphorus Sulfur Silicon Relat. Elem. 63 (1991) 193–215, doi:10.1080/10426509108029443.
[15] I. Kraicheva, E. Vodenicharova, E. Tashev, T. Tosheva, I. Tsacheva, K. Troev, Synthesis and NMR characterization of two novel anthracene-derived bis-aminophosphonates. basic hydrolysis of some aminophosphonate derivatives, Phosphorus Sulfur Silicon Relat. Elem. 187 (2012) 660–667, doi:10.1080/10426507.2011.638349.
[16] M. Górny vel Górniak, P. Kafarski, Preparation of the library of fluorescent aromatic aminophosphonate phenyl and benzyl esters, Phosphorus Sulfur Silicon Relat. Elem. 191 (2016) 511–519, doi:10.1080/10426507.2015.1094658.
[17] A. Kuśnierz, E. Chmielewska, Synthesis of fluorescent aminophosphonates by green chemistry procedures, Phosphorus Sulfur Silicon Relat. Elem. 192 (2017) 700–705, doi:10.1080/10426507.2017.1308934.
[18] Q.-M. Wang, W. Gao, J.-L. Song, Y. Liu, H. Qi, X.-H. Tang, Synthesis, x-ray crystallographic analysis and BSA interaction of a new α-aminophosphonate, J. Appl. Spectrosc. 83 (2016) 703–709, doi:10.1007/s10812-016-0351-9.
[19] M.G. vel Górniak, A. Czernicka, P. Młynarz, W. Balcerzak, P. Kafarski, Synthesis of fluorescent (benzyloxycarbonylamino)(aryl)methylphosphonates, Beilstein J. Org. Chem. 10 (2014) 741–745, doi:10.3762/bjoc.10.68.
[20] J. Lewkowski, M. Rodriguez Moya, A. Wrona-Piotrowicz, J. Zakrzewski, R. Kontek, G. Gajek, Synthesis, fluorescence properties and the promising cytotoxicity of pyrene–derived aminophosphonates, Beilstein J. Org. Chem. 12 (2016) 1229–1235, doi:10.3762/bjoc.12.117.
[21] A. Lüttringhaus, H. Neresheimer, Zur Kenntnis des Benzanthrons, Justus Liebigs Ann. Chem. 473 (1929) 259–289, doi:10.1002/jlac.19294730115.
[22] O.V. Dolomanov, L.J. Bourhis, R.J. Gildea, J.A.K. Howard, H. Puschmann, OLEX2: a complete structure solution, refinement and analysis program, J. Appl. Crystallogr. 42 (2009) 339–341, doi:10.1107/S0021889808042726.
[23] L. Palatinus, G. Chapuis, SUPERFLIP – a computer program for the solution of crystal structures by charge flipping in arbitrary dimensions, J. Appl. Crystallogr. 40 (2007) 786–790, doi:10.1107/S0021889807029238.
[24] L.J. Bourhis, O.v. Dolomanov, R.J. Gildea, J.A.K. Howard, H. Puschmann, The anatomy of a comprehensive constrained, restrained refinement program for the modern computing environment – *Olex2* dissected, Acta Crystallogr A Found Adv. 71 (2015) 59–75, doi:10.1107/S2053273314022207.
[25] G.M. Sheldrick, A short history of SHELX, Acta Crystallogr. A 64 (2008) 112–122, doi:10.1107/S0108767307043930.
[26] G. Sravya, A. Balakrishna, G.v. Zyryanov, G. Mohan, C.S. Reddy, N.Bakthavatchala Reddy, Synthesis of α-aminophosphonates by the Kabachnik-Fields reaction, Phosphorus Sulfur Silicon Relat. Elem. 196 (2021) 353–381, doi:10.1080/10426507.2020.1854258.
[27] P.R. Varga, G. Keglevich, Synthesis of α-aminophosphonates and related derivatives; the last decade of the kabachnik–fields reaction, Molecules 26 (2021) 2511, doi:10.3390/molecules26092511.
[28] A. Amira, Z. Aouf, H. K'tir, Y. Chemam, R. Ghodbane, R. Zerrouki, N. Aouf, Recent advances in the synthesis of α-aminophosphonates: a review, ChemistrySelect 6 (2021) 6137–6149, doi:10.1002/slct.202101360.
[29] F. Serigne Abdou Khadir, S. Boukhssas, S. Achamlale, Y. Aouine, A. Nakkabi, H. Faraj, A. Alami, Synthesis and characterization of the structure of diethyl [(4-{(1h-benzo[d]imidazol-1-yl)methyl}-1h-1,2,3-triazol-1-yl)(benzamido)methyl]phosphonate using 1d and 2d nmr experiments, European J. Adv. Chem. Res. 2 (2021) 1–7, doi:10.24018/ejchem.2021.2.1.42.
[30] S. Khabnadideh, M. Fadaei, Z. Rezaei, Y. Ghasemi, Z. Karimi, Design and one-pot synthesis of new α-aminophosphonates and antimicrobial activity, J. Pharm. Negat. Results 2 (2011) 78, doi:10.4103/0976-9234.90219.
[31] A. Balakrishna, C. Suresh Reddy, S.K. Naik, M. Manjunath, C. Naga Raju, Synthesis, characterization and bio-activity of some new aminophosphonates, Bull. Chem. Soc. Ethiop. 23 (2009), doi:10.4314/bcse.v23i1.21300.
[32] M. Takekawa, J. Aoki, S. Iwashima, T. Ueda, Complete assignment of 1H and 13C NMR spectra of chlorobenzanthrones, Magnetic Resonance in Chemistry 32 (1994) 87–92, doi:10.1002/mrc.1260320205.
[33] A. Vaidyanathan, The carbon-13 NMR spectra of benzanthrone and its derivatives, Dyes Pigm. 3 (1982) 243–248, doi:10.1016/0143-7208(82)80026-0.
[34] A.V.R. Rao, A. Vaidyanathan, The 1H NMR spectrum of benzanthrone, Spectrochim Acta A 37 (1981) 145–146, doi:10.1016/0584-8539(81)80102-X.
[35] E. Lukevics, L. Ignatovich, S. Belyakov, Disordering in the crystal structures of thienylgermatranes, Chem. Heterocycl. Compd. (N Y) 43 (2007) 243–249, doi:10.1007/s10593-007-0038-5.
[36] S. Gonta, M. Utinans, G. Kirilov, S. Belyakov, I. Ivanova, M. Fleisher, V. Savenkov, E. Kirilova, Fluorescent substituted amidines of benzanthrone: Synthesis, spectroscopy and quantum chemical calculations, Spectrochim. Acta A Mol. Biomol. Spectrosc. 101 (2013) 325–334, doi:10.1016/j.saa.2012.09.104.
[37] E.M. Kirilova, I. Kalnina, G.K. Kirilov, I. Meirovics, Spectroscopic study of benzanthrone 3-n-derivatives as new hydrophobic fluorescent probes for biomolecules, J. Fluoresc. 18 (2008) 645–648, doi:10.1007/s10895-008-0340-3.
[38] X.-H. Zhang, X.-Z. Yu, D.-M. Yue, Phytotoxicity of dimethyl sulfoxide (DMSO) to rice seedlings, Int. J. Environ. Sci. Technol. 13 (2016) 607–614, doi:10.1007/s13762-015-0899-6.
[39] X.-Z. Yu, X.-H. Zhang, D.-M. Yue, Alternation of antioxidative enzyme gene expression in rice seedlings exposed to methylene blue, Environ. Sci. Pollution Res. 21 (2014) 14014–14022, doi:10.1007/s11356-014-3306-9.
[40] G. Athinarayanan, R. Mariselvam, A.J.A. Ranjitsingh, A. Usha Raja Nanthini, Phytotoxicity of selected different natural plant dyes study on phaseolus aureus(Green Gram), Int. J. Sci. Res. 4 (2015) 2061–2067.
[41] Z. Guo, W. Ou, S. Lu, Q. Zhong, Differential responses of antioxidative system to chilling and drought in four rice cultivars differing in sensitivity, Plant Physiol. Biochem. 44 (2006) 828–836, doi:10.1016/j.plaphy.2006.10.024.
[42] N. Orlova, I. Nikolajeva, A. Pučkins, S. Belyakov, E. Kirilova, Heterocyclic Schiff bases of 3-aminobenzanthrone and their reduced analogues: synthesis, properties and spectroscopy, Molecules 26 (2021) 2570, doi:10.3390/molecules26092570.

2. pielikums
Appendix II

Maļeckis, A.; Cvetinska, M.; Griškjāns, E.; Mežaraupe, L.; Kirjušina, M.; Pavlova, V.; Kirilova, E.

Novel Anthraquinone α-Aryl-α-Aminophosphonates: Synthesis, Spectroscopy and Imaging by Confocal Laser Scanning Microscopy of Trematode *Opisthioglyphe Ranae*

J. Photochem. Photobiol. A Chem. **2023**, *444*, 114918.

https://doi.org/10.1016/j.jphotochem.2023.114918

Journal of Photochemistry & Photobiology, A: Chemistry 444 (2023) 114918

Contents lists available at ScienceDirect

Journal of Photochemistry & Photobiology, A: Chemistry

journal homepage: www.elsevier.com/locate/jphotochem

Novel anthraquinone α-aryl-α-aminophosphonates: Synthesis, spectroscopy and imaging by confocal laser scanning microscopy of trematode *Opisthioglyphe ranae*

Armands Maļeckis [a,*], Marija Cvetinska [a], Evans Griškjāns [a], Ligita Mežaraupe [b], Muza Kirjušina [b], Veronika Pavlova [b], Elena Kirilova [c]

[a] Institute of Technology of Organic Chemistry, Faculty of Materials Science and Applied Chemistry, Riga Technical University, P. Valdena Str. 3, LV-1048 Riga, Latvia
[b] Department of Ecology, Institute of Life Sciences and Technology, Daugavpils University, Parades Str. 1A, LV-5401 Daugavpils, Latvia
[c] Department of Applied Chemistry, Institute of Life Sciences and Technology, Daugavpils University, Parades Str. 1A, LV-5401 Daugavpils, Latvia

ARTICLE INFO

Keywords:
Anthraquinone
α-aminophosphonates
Kabachnik-Fields reaction
Fluorescence
Confocal microscopy

ABSTRACT

A small library of new anthraquinone α-aryl-α-aminophosphonates with N-C-P molecular fragment was synthesized under Kabachnik-Fields one-pot solvent-free reaction conditions from 1-aminoanthraquinone. ^{1}H-, ^{13}C-, ^{31}P NMR and FTIR spectroscopy and high-resolution accurate mass measurement was employed to confirm structures of new dyes. The photophysical parameters of the studied α-aminophosphonates have been investigated by means of UV–Vis and fluorescence spectroscopy in organic solvents of varying polarity. Obtained compounds were found to emit light from 586 nm (EtOAc) to 620 nm (DMSO) with fluorescence bathochromic shifts reaching up to 30 nm, Stokes shift of 4573 cm^{-1} and photostability of up to 60 % of initial intensity upon photofading for 4 h. α-Aryl-α-aminophosphonate was used for the first time as a dye for rapid bioimaging of trematode *Opisthioglyphe ranae* in confocal laser scanning microscopy.

1. Introduction

Organic luminescent materials are of particular interest nowadays due to their capabilities in various functional applications: sensing, displays, solar cells, lasers, photocatalysis, photodynamic therapy, bioimaging and numerous other practices [1–7]. Long emission wavelengths, substantial Stokes shifts and high fluorescence quantum yields are particularly advantageous attributes for fluorescent dyes: the properties distinctive of donor–π-acceptor (D–π-A) fluorophores, consisting of a donor unit, a π linker and an acceptor moiety, have attracted considerable attention over the past decades [8,9].

Amongst such compounds, anthraquinone derivatives have historically played a significant role in the development of the dye industry because of their high stability and durability [10]. Although commonly anthraquinone compounds are used in vat dyeing processes, a good deal of other utilizations has also emerged, just some of which include: emitters for organic light-emitting diodes (OLEDs), chemosensory of ionic species, cellular imaging and medical sphere (fungicidal, antibacterial, insecticidal, antiparasitic, antiviral and anticancer agents) [11–16].

α-Aminophosphonates, being natural amino acid analogues, are able to inhibit several enzymes, typically involved in the metabolism of amino acids, that is, acting as antagonists, exhibit a broad range of biological activity (antifungal, antimicrobial, antiviral, anticancer, herbicidal and neuromodulatory) [17,18]. Moreover, synthetic α-aminophosphonates have demonstrated promising potential for utilization as lubricating additives [19], antioxidants [20], sorbents [21–23], corrosion inhibitors [24], and, therefore, are exhaustively studied compounds.

A certain amount of research has been devoted to the study of fluorescent properties of some α-aminophosphonates as well. While synthesis and fluorescent properties of α-aminophosphonates obtained from aromatic amines derived from benzene, naphthalene, anthracene, pyrene, phenanthrene and benzanthrone, as well as bis-aminophosphonates bearing anthracene rings, have been reported not long ago, to our knowledge, there is little to no research on employment of α-aminophosphonates as dyes for bioimaging [25–31].

With all of the above mentioned in mind, we have come to a decision to provide our knowledge on new α-aryl-α-aminophosphonate derivatives of 1-aminoanthraquinone: synthesis, photophysical properties

* Corresponding author.
E-mail address: armands5maleckis@inbox.lv (A. Maļeckis).

https://doi.org/10.1016/j.jphotochem.2023.114918
Received 13 February 2023; Received in revised form 25 May 2023; Accepted 5 June 2023
Available online 9 June 2023

Table 1

Summary of structures of obtained compounds.

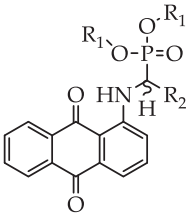

R_1	R_2						
		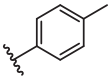	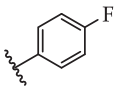	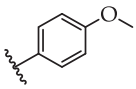	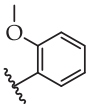	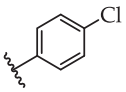	
Me	***2a***	***2b***	***2c***	***2d***	***2e***	***2f***	***2g***
Et	***3a***	***3b***	***3c***	***3d***	***3e***	***3f***	–
i-Pr	***4a***	***4b***	***4c***	***4d***	***4e***	***4f***	***4g***

and rapid staining protocol for confocal laser scanning microscopy (CLSM) of *Opisthioglyphe ranae* trematodes. The main novelty of our work lies in the utilization of these α-aminophosphonates as dyes for bioimaging, which contributes to the advancement of fluorescent dyes with enhanced capabilities for staining protocols for CLSM.

2. Experimental

2.1. Materials and methods

All of the reagents and solvents were obtained commercially and used without any additional purification.

The assessment of the progress of reactions and purity of the synthesized compounds was performed by TLC on MERCK Silica gel 60 F_{254} plates in benzene/acetonitrile (3:1) as an eluent and visualized under UV light. Melting points were determined on METTLER TOLEDO™ Melting Point System MP70 apparatus. The IR spectrum was recorded on a Thermo Scientific Nicolet iS50 Spectrometer (ATR accessory; no. of scans: 64; resolution: 4; data spacing: 0.482 cm^{-1}). ^{1}H-, ^{13}C- and ^{31}P NMR spectra were recorded on a Bruker Avance 500 MHz (Bruker Corporation, Billerica, MA, USA) in DMSO-d_6 at ambient temperature, using solvent peaks as the internal reference. Chemical shift (δ) values are reported in ppm. High-resolution accurate mass measurements were performed employing Orbitrap Exploris 120 (Thermo Fischer Scientific) operating at Full Scan mode at 120,000 resolution.

The fluorescence emission spectra were recorded on a FLSP920 (Edinburgh Instruments Ltd, UK) spectrofluorometer in the visible range 450–800 nm and the absorption spectra were obtained using the UV–visible spectrophotometer SPECORD® 80 (Analytik Jena AG, Germany). The spectral properties of the investigated compound were measured at an ambient temperature in quartz cuvettes of 10 mm in hexane, benzene, chloroform, ethyl acetate (EtOAc), acetone, ethanol (EtOH), dimethyl sulfoxide (DMSO) and dimethylformamide (DMF) with concentration of 10^{-5}M. The photofading were carried out in quartz cells where sample solution (with concentration 10^{-4} M) in ethanol was irradiated with a UV-lamp (365 nm, maximum power 15 W) at room temperature. The distance between the cells and the lamp was 10 cm. The bleaching of the dyes at the absorption maximum was monitored as a function of time every 30 min. All solvents were of p.a. or analytical grade.

2.1.1. Imaging

Opisthioglyphe ranae was fixed in 70 % ethanol and stored at 4 °C until use. Ethanol solution of the luminophore ***4f*** with a molar concentration 10^{-5} M was used. The parasite sample was placed in the luminophore ***4f*** solution for 10 min. Then, the dye was washed out three times with 70 % ethanol. Further, the sample was placed in ethanol–xylene solution (1:1) for 10 min. Finally, the specimens were mounted on Canada balsam and covered with a coverslip (24 × 24 mm).

CLSM Eclipse Ti-E microscope equipped with digital sight DS-U3 camera; configured with a high speed multiphoton A1R MP confocal system and motorized stage (Nikon, Japan) was used. CLSM images were processed by NIS Elements Advanced Research 3.2 64-bit software (Nikon, Japan). Two lasers 488 nm laser with FITC (500–550 nm) filter and 638 nm laser with a Cy5 filter (662–737 nm) were used to visualize the parasite. The registration of the fluorescence signal was done by internal spectral detector. The start wavelength for registration was chosen at 20 nm higher than excitation wavelength till the edge of red visible spectra. No passive cutoff filters were used in the optical path. Images were acquired as Z stacks with a 2.0 μm Z step size.

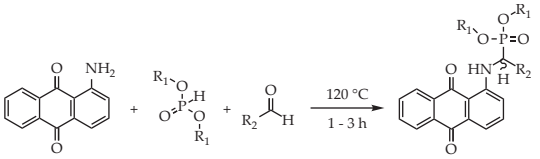

Scheme 1. Synthesis of anthraquinone α-aryl-α-aminophosphonates.

2.2. Synthesis of compounds ***2a–4g***

Structures of target compounds are summarized in Table 1 and were synthesized according to Scheme 1.

2.2.1. General methodology

A 10 mL round-bottom flask with a magnetic stirrer bar was charged with 446 mg (2 mmol) of 1-aminoanthraquinone, 6 mmol of an aldehyde and 5 mL of a dialkylphosphonate. Obtained mixture was stirred in an oil bath at 120 °C for 1–3 h (progress assessed with TLC). After completion of the reaction, the mixture was poured into 100 mL of concentrated sodium bicarbonate ($NaHCO_3$) solution and left stirring overnight, until solid product was formed. The precipitate then was filtered, thoroughly washed with water, dried and then purified by means of multi-solvent recrystallization from xylenes and hexane.

*2.2.2. Dimethyl (((9,10-dioxo-9,10-dihydroanthracen-1-yl)amino)(phenyl)methyl)phosphonate **(2a)***

Red solid. Yield: 84 %. Melting point: 210 °C. R_f = 0.45 (Benzene/Acetonitrile) (3:1). FTIR (neat):

3241, 3080, 2951, 2849, 1666, 1632, 1590, 1500, 1453, 1404, 1360, 1311, 1254, 1165, 1053, 1026, 930, 896, 871, 837, 780, 730, 702, 667, 606, 542, 468. ^{1}H NMR (500 MHz, DMSO-d_6) δ 10.62 (t, J = 8.8 Hz, 1H), 8.30 (d, J = 7.7 Hz, 1H), 8.14 (d, J = 7.6 Hz, 1H), 7.94 (t, J = 7.6 Hz, 1H), 7.87 (t, J = 7.6 Hz, 1H), 7.59 (t, J = 8.1 Hz, 1H), 7.55–7.47 (m, 3H), 7.39 (t, J = 7.7 Hz, 2H), 7.32 (d, J = 8.2 Hz, 2H), 5.68 (dd, J = 23.8, 8.6 Hz, 1H), 3.73 (d, J = 10.6 Hz, 3H), 3.57 (d, J = 10.5 Hz, 3H). ^{13}C NMR (126 MHz, DMSO-d_6) δ 185.4 (C═O), 183.1 (C═O), 150.5 (C), 150.4 (C), 136.0 (CH), 136.0 (d, J = 2.9 Hz, C), 135.1 (CH), 134.6 (d, J = 5.6 Hz, C), 134.3 (CH), 132.9 (C), 129.0 (d, J = 2.0 Hz, CH), 128.5 (d, J = 2.7 Hz, CH), 128.3 (d, J = 5.3 Hz, CH), 127.2 (CH), 126.8 (CH), 119.8 (CH), 116.8 (CH), 114.1 (C), 54.1 (dd, J = 6.9, 2.4 Hz, NCH), 53.6 (CH_3), 52.4 (CH_3). ^{31}P NMR (202 MHz, DMSO-d_6) δ 23.93. HRMS-ESI *m/z* found: 422.1150, calculated for [$C_{23}H_{20}NO_5P$ + H^+]: 422.1152.

*2.2.3. Dimethyl (((9,10-dioxo-9,10-dihydroanthracen-1-yl)amino)(p-tolyl)methyl)phosphonate **(2b)***

Red solid. Yield: 79 %. Melting point: 174 °C. R_f = 0.45 (Benzene/Acetonitrile) (3:1). FTIR (neat): 3237, 3056, 3019, 2949, 2920, 2848, 1666, 1631, 1577, 1502, 1455, 1405, 1361, 1319, 1256, 1166, 1027, 899, 871, 843, 809, 758, 730, 702, 667, 607, 539, 469, 418. ^{1}H NMR (500 MHz, DMSO-d_6) δ 10.59 (t, J = 8.9 Hz, 1H), 8.30 (d, J = 7.7 Hz, 1H), 8.14 (d, J = 6.9 Hz, 1H), 7.93 (t, J = 7.6 Hz, 1H), 7.87 (t, J = 7.5 Hz, 1H), 7.59 (t, J = 7.9 Hz, 1H), 7.48 (dd, J = 7.3, 2.1 Hz, 1H), 7.40 (d, J = 7.7 Hz, 2H), 7.30 (d, J = 8.6 Hz, 1H), 7.19 (d, J = 7.7 Hz, 2H), 5.61 (dd, J = 23.6, 8.5 Hz, 1H), 3.72 (d, J = 10.6 Hz, 3H), 3.57 (d, J = 10.6 Hz, 3H), 2.27 (s, 3H). ^{13}C NMR (126 MHz, DMSO-d_6) δ 185.4 (C═O), 183.1 (C═O), 150.5 (C), 150.4 (C), 137.8 (d, J = 3.0 Hz, C), 136.0 (CH), 135.1 (CH), 134.6 (d, J = 9.7 Hz, C), 134.3 (CH), 132.9 (d, J = 3.0 Hz, C), 132.9 (C), 129.6 (d, J = 2.2 Hz, CH), 128.2 (d, J = 5.3 Hz, CH), 127.2 (CH), 126.8 (CH), 119.9 (CH), 116.7 (CH), 114.0 (C), 54.1 (dd, J = 6.9, 3.1 Hz, NCH), 53.4 (CH_3), 52.2 (CH_3), 21.2 (CH_3). ^{31}P NMR (202 MHz, DMSO-d_6) δ 24.08. HRMS-ESI *m/z* found: 436.1310, calculated for [$C_{24}H_{22}NO_5P$ + H^+]: 436.1308.

*2.2.4. Dimethyl (((9,10-dioxo-9,10-dihydroanthracen-1-yl)amino)(4-fluorophenyl)methyl)phosphonate **(2c)***

Red solid. Yield: 82 %. Melting point: 156 °C. R_f = 0.44 (Benzene/Acetonitrile) (3:1). FTIR (neat): 3221, 3193, 2958, 2904, 2854, 1667, 1631, 1589, 1500, 1402, 1359, 1310, 1276, 1251, 1216, 1168, 1019, 876, 828, 754, 730, 701, 661, 605, 582, 557, 513, 468, 410. ^{1}H NMR (500 MHz, DMSO-d_6) δ 10.59 (t, J = 8.8 Hz, 1H), 8.28 (dd, J = 7.7, 1.3 Hz, 1H), 8.13 (dd, J = 7.7, 1.5 Hz, 1H), 7.92 (td, J = 7.5, 1.4 Hz, 1H), 7.86 (td, J = 7.5, 1.4 Hz, 1H), 7.62–7.54 (m, 3H), 7.49 (dd, J = 7.3, 1.1 Hz, 1H), 7.30 (d, J = 8.6 Hz, 1H), 7.23 (t, J = 8.8 Hz, 2H), 5.72 (dd, J = 23.8, 8.6 Hz, 1H), 3.74 (d, J = 10.6 Hz, 3H), 3.60 (d, J = 10.6 Hz, 3H). ^{13}C NMR (126 MHz, DMSO-d_6) δ 185.5 (C═O), 183.0 (C═O), 162.3 (dd, J = 244.3, 3.2 Hz, C), 150.4 (C), 150.2 (C), 136.1 (CH), 135.0 (CH), 134.6 (C), 134.3 (CH), 132.8 (C), 132.2 (t, J = 2.9 Hz, C), 130.3 (dd, J = 8.3, 5.4 Hz, CH), 127.2 (CH), 126.8 (CH), 119.7 (CH), 116.8 (CH), 115.97 (dd, J = 21.6, 2.0 Hz, CH), 114.2 (C), 54.2 (d, J = 6.9 Hz, NCH), 52.8 (CH_3), 51.6 (CH_3). ^{31}P NMR (202 MHz, DMSO-d_6) δ 23.76 (d, J = 4.7 Hz). HRMS-ESI *m/z* found: 440.1056, calculated for [$C_{23}H_{19}FNO_5P$ + H^+]: 440.1058.

*2.2.5. Dimethyl (((9,10-dioxo-9,10-dihydroanthracen-1-yl)amino)(4-methoxyphenyl)methyl)phosphonate **(2d)***

Red solid. Yield: 74 %. Melting point: 157 °C. R_f = 0.36 (Benzene/Acetonitrile) (3:1). FTIR (neat): 3232, 3072, 3014, 2957, 2899, 2851, 1667, 1633, 1586, 1503, 1460, 1401, 1358, 1305, 1250, 1165, 1117, 1052, 1017, 871, 827, 767, 707, 662, 589, 560, 481. ^{1}H NMR (500 MHz, DMSO-d_6) δ 10.57 (t, J = 8.7 Hz, 1H), 8.30 (dd, J = 7.8, 1.3 Hz, 1H), 8.14 (dd, J = 7.6, 1.4 Hz, 1H), 7.94 (td, J = 7.5, 1.5 Hz, 1H), 7.87 (td, J = 7.5, 1.4 Hz, 1H), 7.63–7.57 (m, 1H), 7.49 (dd, J = 7.3, 1.0 Hz, 1H), 7.44 (dd, J = 8.8, 2.3 Hz, 2H), 7.32 (d, J = 8.5 Hz, 1H), 6.95 (d, J = 8.7 Hz, 2H), 5.59 (dd, J = 23.3, 8.6 Hz, 1H), 3.56 (d, J = 10.6 Hz, 3H), 3.34 (s, 6H). ^{13}C NMR (126 MHz, DMSO-d_6) δ 185.4 (C═O), 183.1 (C═O), 159.4 (d, J = 2.7 Hz, C), 150.5 (C), 150.4 (C), 136.0 (CH), 135.1 (CH), 134.6 (d, J = 10.0 Hz, C), 134.3 (CH), 132.9 (C), 129.5 (d, J = 5.4 Hz, CH), 127.6 (d, J = 3.0 Hz, C), 127.2 (CH), 126.8 (CH), 119.9 (CH), 116.7 (CH), 114.5 (d, J = 1.8 Hz, CH), 114.0 (C), 55.5 ($C_{Ar}O\underline{C}H_3$), 54.0 (t, J = 7.0 Hz, NCH), 53.0 (CH_3), 51.8 (CH_3). ^{31}P NMR (202 MHz, DMSO-d_6) δ 24.22. HRMS-ESI *m/z* found: 452.1259, calculated for [$C_{24}H_{22}NO_6P$ + H^+]: 452.1258.

*2.2.6. Dimethyl (((9,10-dioxo-9,10-dihydroanthracen-1-yl)amino)(2-methoxyphenyl)methyl)phosphonate **(2e)***

Red solid. Yield: 76 %. Melting point: 192 °C. R_f = 0.40 (Benzene/Acetonitrile) (3:1). FTIR (neat): 3239, 3073, 3009, 2951, 2847, 1668, 1630, 1589, 1490, 1458, 1405, 1361, 1243, 1166, 1020, 900, 874, 831, 757, 731, 702, 665, 600, 566, 530, 477, 419. ^{1}H NMR (500 MHz, DMSO-d_6) δ 10.62 (t, J = 8.6 Hz, 1H), 8.29 (d, J = 7.7 Hz, 1H), 8.13 (d, J = 7.6 Hz, 1H), 7.93 (t, J = 7.6 Hz, 1H), 7.87 (t, J = 7.6 Hz, 1H), 7.62 (t, J = 8.0 Hz, 1H), 7.48 (dd, J = 7.4, 2.2 Hz, 1H), 7.38 (d, J = 7.8 Hz, 1H), 7.32 (t, J = 8.0 Hz, 1H), 7.12 (d, J = 8.3 Hz, 1H), 7.05 (d, J = 8.6 Hz, 1H), 6.96 (t, J = 7.7 Hz, 1H), 5.62 (dd, J = 23.2, 8.5 Hz, 1H), 3.97 (s, 3H), 3.75 (dd, J = 10.7, 2.5 Hz, 3H), 3.53 (dd, J = 10.6, 2.5 Hz, 3H). ^{13}C NMR (126 MHz, DMSO-d_6) δ 185.3 (C═O), 183.1 (C═O), 157.3 (d, J = 5.9 Hz, C), 150.2 (C), 150.1 (C), 136.3 (CH), 135.1 (CH), 134.6 (d, J = 4.8 Hz, C), 134.3 (CH), 132.8 (C), 130.0 (d, J = 2.4 Hz, CH), 128.5 (d, J = 4.6 Hz, CH), 127.2 (CH), 126.8 (CH), 123.7 (d, J = 2.3 Hz, C), 121.3 (d, J = 2.3 Hz, CH), 118.9 (CH), 116.6 (CH), 114.1 (C), 111.9 (d, J = 1.3 Hz, CH), 56.5 ($C_{Ar}O\underline{C}H_3$), 54.1 (dd, J = 13.6, 6.9 Hz, NCH), 47.8 (CH_3), 46.6 (CH_3). ^{31}P NMR (202 MHz, DMSO-d_6) δ 23.80. HRMS-ESI *m/z* found: 452.1257, calculated for [$C_{24}H_{22}NO_6P$ + H^+]: 452.1258.

*2.2.7. Dimethyl ((4-chlorophenyl)((9,10-dioxo-9,10-dihydroanthracen-1-yl)amino)methyl)phosphonate **(2f)***

Red solid. Yield: 77 %. Melting point: 160 °C. R_f = 0.49 (Benzene/Acetonitrile) (3:1). FTIR (neat): 3222, 2953, 2905, 2853, 1667, 1631, 1590, 1486, 1403, 1360, 1276, 1251, 1168, 1063, 1027, 876, 837, 764, 730, 701, 661, 599, 546, 484, 444, 418. ^{1}H NMR (500 MHz, DMSO-d_6) δ 10.58 (t, J = 8.9 Hz, 1H), 8.30 (dd, J = 7.8, 1.4 Hz, 1H), 8.15 (dd, J = 7.6, 1.4 Hz, 1H), 7.94 (td, J = 7.6, 1.5 Hz, 1H), 7.88 (td, J = 7.5, 1.4 Hz, 1H), 7.61 (t, J = 8.2 Hz, 1H), 7.56–7.48 (m, 3H), 7.46 (d, J = 8.5 Hz, 2H), 7.28 (d, J = 8.5 Hz, 1H), 5.74 (dd, J = 24.1, 8.5 Hz, 1H), 3.74 (d, J = 10.6 Hz, 3H), 3.62 (d, J = 10.6 Hz, 3H). ^{13}C NMR (126 MHz, DMSO-d_6) δ 185.5 (C═O), 183.0 (C═O), 150.3 (C), 150.2 (C), 136.1 (CH), 135.2 (d, J = 3.1 Hz, C), 135.1 (CH), 134.6 (d, J = 2.7 Hz, C), 134.4 (CH), 133.1 (d, J = 3.7 Hz, C), 132.9 (C), 130.1 (d, J = 5.2 Hz, CH), 129.1 (d, J = 2.2 Hz, CH), 127.2 (CH), 126.8 (CH), 119.7 (CH), 116.9 (CH), 114.2 (C), 54.2 (dd, J = 6.9, 4.4 Hz, NCH), 52.9 (CH_3), 51.7 (CH_3). ^{31}P NMR (202 MHz, DMSO-d_6) δ 23.47. HRMS-ESI *m/z* found: 456.0763, calculated for [$C_{23}H_{19}ClNO_5P$ + H^+]: 456.0762.

*2.2.8. Dimethyl (((9,10-dioxo-9,10-dihydroanthracen-1-yl)amino)(thiophen-2-yl)methyl)phosphonate **(2g)***

Red solid. Yield: 71 %. Melting point: 181 °C. R_f = 0.40 (Benzene/Acetonitrile) (3:1). FTIR (neat): 3239, 3079, 2952, 2850, 1668, 1632, 1591, 1499, 1404, 1358, 1314, 1258, 1164, 1026, 895, 828, 730, 702, 662, 606, 540, 467, 417. ^{1}H NMR (500 MHz, DMSO-d_6) δ 10.47 (t, J = 8.2 Hz, 1H), 8.27 (dd, J = 7.8, 1.4 Hz, 1H), 8.13 (dd, J = 7.6, 1.4 Hz, 1H), 7.92 (td, J = 7.5, 1.4 Hz, 1H), 7.86 (td, J = 7.5, 1.4 Hz, 1H), 7.65 (dd, J = 8.6, 7.4 Hz, 1H), 7.52 (dd, J = 7.4, 1.1 Hz, 1H), 7.52–7.46 (m, 2H), 7.29–7.24 (m, 1H), 7.04 (dd, J = 5.0, 3.6 Hz, 1H), 6.06 (dd, J = 23.4, 8.8 Hz, 1H), 3.75 (d, J = 10.6 Hz, 3H), 3.66 (d, J = 10.7 Hz, 3H). ^{13}C NMR (126 MHz, DMSO-d_6) δ 185.5 (C═O), 183.0 (C═O), 150.3 (C), 150.2 (C), 139.3 (d, J = 2.8 Hz, C), 136.1 (CH), 135.1 (CH), 134.5 (d, J

= 2.4 Hz, C), 134.4 (CH), 132.9 (C), 127.6 (d, J = 7.5 Hz, CH), 127.5 (d, J = 2.6 Hz, CH), 127.2 (CH), 126.9 (CH), 126.8 (CH), 119.8 (CH), 117.0 (CH), 114.1 (C), 54.3 (dd, J = 6.9, 4.4 Hz, NCH), 49.8 (CH_3), 48.6 (CH_3). ^{31}P NMR (202 MHz, DMSO-d_6) δ 22.42. HRMS-ESI m/z found: 428.0714, calculated for [$C_{21}H_{18}NO_5PS + H^+$]: 428.0716.

2.2.9. Diethyl (((9,10-dioxo-9,10-dihydroanthracen-1-yl)amino)(phenyl)methyl)phosphonate (3a)

Red solid. Yield: 85 %. Melting point: 107 °C. R_f = 0.45 (Benzene/Acetonitirle) (3:1). FTIR (neat): 3261, 3075, 2988, 2906, 2864, 1668, 1632, 1589, 1500, 1453, 1404, 1359, 1313, 1249, 1162, 1016, 961, 869, 799, 773, 731, 702, 661, 605, 560, 481, 417. ^{1}H NMR (500 MHz, DMSO-d_6) δ 10.67 (t, J = 8.8 Hz, 1H), 8.34 (dd, J = 7.8, 1.4 Hz, 1H), 8.18 (dd, J = 7.6, 1.5 Hz, 1H), 7.98 (td, J = 7.5, 1.5 Hz, 1H), 7.91 (td, J = 7.5, 1.5 Hz, 1H), 7.63 (t, J = 8.0 Hz, 1H), 7.57 (dd, J = 7.8, 2.1 Hz, 2H), 7.52 (dd, J = 7.4, 1.1 Hz, 1H), 7.42 (t, J = 7.6 Hz, 2H), 7.39–7.30 (m, 2H), 5.63 (dd, J = 23.6, 8.6 Hz, 1H), 4.21–4.06 (m, 2H), 4.09–3.98 (m, 1H), 3.95–3.83 (m, 1H), 1.27 (t, J = 7.0 Hz, 3H), 1.16 (t, J = 7.1 Hz, 3H). ^{13}C NMR (126 MHz, DMSO-d_6) δ 185.3 (C═O), 183.1 (C═O), 150.6 (C), 150.5 (C), 136.2 (d, J = 2.9 Hz, C), 136.0 (CH), 135.1 (CH), 134.6 (d, J = 8.1 Hz, C), 134.3 (CH), 132.9 (C), 129.2 (CH), 128.9 (d, J = 2.2 Hz, CH), 128.4 (d, J = 5.2 Hz, CH), 127.2 (CH), 126.8 (CH), 119.9 (CH), 116.7 (CH), 114.0 (C), 63.3 (t, J = 6.8 Hz, CH_2), 54.2 (NCH), 53.0 (NCH), 16.7 (d, J = 5.4 Hz, CH_3), 16.6 (d, J = 5.5 Hz, CH_3). ^{31}P NMR (202 MHz, DMSO-d_6) δ 21.54. HRMS-ESI m/z found: 450.1465, calculated for [$C_{25}H_{24}NO_5P + H^+$]: 450.1465.

2.2.10. Diethyl (((9,10-dioxo-9,10-dihydroanthracen-1-yl)amino)(p-tolyl)methyl)phosphonate (3b)

Red solid. Yield: 89 %. Melting point: 144 °C. R_f = 0.51 (Benzene/Acetonitirle) (3:1). FTIR (neat): 3247, 2983, 2907, 2859, 1661, 1629, 1574, 1506, 1404, 1364, 1318, 1254, 1209, 1161, 1099, 1011, 953, 872, 802, 732, 708, 662, 609, 559, 512, 414. ^{1}H NMR (500 MHz, DMSO-d_6) δ 10.59 (t, J = 8.8 Hz, 1H), 8.30 (d, J = 7.7 Hz, 1H), 8.14 (d, J = 7.6 Hz, 1H), 7.94 (t, J = 7.5 Hz, 1H), 7.87 (t, J = 7.5 Hz, 1H), 7.58 (t, J = 7.9 Hz, 1H), 7.48 (d, J = 7.3 Hz, 1H), 7.40 (d, J = 7.7 Hz, 2H), 7.30 (d, J = 8.7 Hz, 1H), 7.18 (d, J = 7.7 Hz, 2H), 5.52 (dd, J = 23.4, 8.5 Hz, 1H), 4.08 (h, J = 10.0, 9.4 Hz, 2H), 3.99 (q, J = 7.9 Hz, 1H), 3.85 (q, J = 8.2 Hz, 1H), 2.27 (s, 3H), 1.22 (t, J = 6.8 Hz, 3H), 1.13 (t, J = 6.9 Hz, 3H). ^{13}C NMR (126 MHz, DMSO-d_6) δ 185.3 (C═O), 183.1 (C═O), 150.6 (C), 150.5 (C), 137.6 (d, J = 3.0 Hz, C), 136.0 (CH), 135.1 (CH), 134.6 (d, J = 12.1 Hz, C), 134.3 (CH), 133.1 (d, J = 3.0 Hz, C), 132.9 (C), 129.5 (d, J = 1.8 Hz, CH), 128.3 (d, J = 5.3 Hz, CH), 127.2 (CH), 126.8 (CH), 120.0 (CH), 116.6 (CH), 114.0 (C), 63.2 (t, J = 6.5 Hz, CH_2), 54.0 (NCH), 52.8 (NCH), 21.2 ($C_{Ar}\underline{C}H_3$), 16.8 (d, J = 5.3 Hz, CH_3), 16.6 (d, J = 5.4 Hz, CH_3). ^{31}P NMR (202 MHz, DMSO-d_6) δ 21.67. HRMS-ESI m/z found: 464.1623, calculated for [$C_{26}H_{26}NO_5P + H^+$]: 464.1621.

2.2.11. Diethyl (((9,10-dioxo-9,10-dihydroanthracen-1-yl)amino)(4-fluorophenyl)methyl)phosphonate (3c)

Red solid. Yield: 86 %. Melting point: 154 °C. R_f = 0.52 (Benzene/Acetonitirle) (3:1). FTIR (neat): 3236, 3078, 2985, 2886, 1667, 1632, 1590, 1501, 1404, 1361, 1307, 1277, 1251, 1217, 1165, 1120, 1048, 1010, 969, 943, 873, 844, 785, 729, 701, 664, 606, 560, 506, 421. ^{1}H NMR (500 MHz, DMSO-d_6) δ 10.60 (t, J = 8.8 Hz, 1H), 8.29 (dd, J = 7.8, 1.3 Hz, 1H), 8.13 (dd, J = 7.7, 1.5 Hz, 1H), 7.93 (td, J = 7.5, 1.5 Hz, 1H), 7.86 (td, J = 7.5, 1.4 Hz, 1H), 7.59 (t, J = 8.0 Hz, 1H), 7.59–7.52 (m, 2H), 7.49 (d, J = 7.3 Hz, 1H), 7.30 (d, J = 8.6 Hz, 1H), 7.22 (t, J = 8.7 Hz, 2H), 5.64 (dd, J = 23.6, 8.5 Hz, 1H), 4.17–4.03 (m, 2H), 4.05–3.95 (m, 1H), 3.94–3.83 (m, 1H), 1.23 (t, J = 7.0 Hz, 3H), 1.14 (t, J = 7.0 Hz, 3H). ^{13}C NMR (126 MHz, DMSO-d_6) δ 185.4 (C═O), 183.0 (C═O), 162.2 (dd, J = 244.1, 3.2 Hz, C), 150.5 (C), 150.4 (C), 136.0 (CH), 135.1 (CH), 134.6 (d, J = 1.5 Hz, C), 134.3 (CH), 132.8 (C), 132.4 (t, J = 2.8 Hz, C), 130.4 (dd, J = 8.3, 5.3 Hz, CH), 127.2 (CH), 126.8 (CH), 119.8 (CH), 116.6 (CH), 115.8 (dd, J = 21.8, 1.9 Hz, CH), 114.1 (C), 63.4 (dd, J = 6.9, 2.7 Hz, CH_2), 53.4 (NCH), 52.2 (NCH), 16.7 (d, J = 5.3 Hz, CH_3), 16.6 (d, J = 5.4 Hz, CH_3). ^{31}P NMR (202 MHz, DMSO-d_6) δ 21.36 (d, J = 4.6 Hz). HRMS-ESI m/z found: 468.1370, calculated for [$C_{25}H_{23}FNO_5P + H^+$]: 468.1371.

2.2.12. Diethyl ((((9,10-dioxo-9,10-dihydroanthracen-1-yl)amino)(4-methoxyphenyl)methyl)phosphonate (3d)

Red solid. Yield: 69 %. Melting point: 127 °C. R_f = 0.42 (Benzene/Acetonitirle) (3:1). FTIR (neat): 3245, 3076, 2982, 2939, 2907, 2841, 1657, 1630, 1575, 1505, 1465, 1404, 1364, 1253, 1211, 1170, 1105, 1014, 952, 872, 829, 801, 761, 733, 708, 662, 590, 559, 460, 413. ^{1}H NMR (500 MHz, DMSO-d_6) δ 10.58 (t, J = 8.7 Hz, 1H), 8.29 (dd, J = 7.7, 1.3 Hz, 1H), 8.14 (dd, J = 7.8, 1.4 Hz, 1H), 7.94 (td, J = 7.6, 1.4 Hz, 1H), 7.87 (td, J = 7.5, 1.4 Hz, 1H), 7.59 (dd, J = 8.6, 7.4 Hz, 1H), 7.48 (d, J = 7.4 Hz, 1H), 7.44 (dd, J = 8.8, 2.2 Hz, 2H), 7.32 (d, J = 8.6 Hz, 1H), 6.94 (d, J = 8.7 Hz, 2H), 5.50 (dd, J = 23.1, 8.5 Hz, 1H), 4.15–4.00 (m, 2H), 4.03–3.93 (m, 1H), 3.90–3.78 (m, 1H), 3.72 (s, 3H), 1.22 (t, J = 7.0 Hz, 3H), 1.13 (t, J = 7.0 Hz, 3H). ^{13}C NMR (126 MHz, DMSO-d_6) δ 185.3 (C═O), 183.1 (C═O), 159.4 (d, J = 2.7 Hz, C), 150.6 (C), 150.5 (C), 136.0 (CH), 135.1 (CH), 134.56 (d, J = 12.5 Hz, C), 134.3 (CH), 132.9 (C), 129.6 (d, J = 5.4 Hz, CH), 127.9 (d, J = 3.0 Hz, C), 127.2 (CH), 126.8 (CH), 120.0 (CH), 116.6 (CH), 114.4 (d, J = 1.8 Hz, CH), 113.9 (C), 63.2 (dd, J = 10.1, 6.9 Hz, CH_2), 55.5 ($C_{Ar}O\underline{C}H_3$), 53.6 (NCH), 52.4 (NCH), 16.8 (d, J = 5.3 Hz, CH_3), 16.6 (d, J = 5.5 Hz, CH_3). ^{31}P NMR (202 MHz, DMSO-d_6) δ 21.85. HRMS-ESI m/z found: 480.1571, calculated for [$C_{26}H_{26}NO_6P + H^+$]: 480.1571.

2.2.13. Diethyl (((9,10-dioxo-9,10-dihydroanthracen-1-yl)amino)(2-methoxyphenyl)methyl)phosphonate (3e)

Red solid. Yield: 77 %. Melting point: 140 °C. R_f = 0.45 (Benzene/Acetonitirle) (3:1). FTIR (neat): 3248, 3069, 2983, 2904, 2838, 2739, 2647, 2603, 1753, 1721, 1667, 1635, 1586, 1491, 1464, 1405, 1359, 1245, 1209, 1163, 1095, 1045, 1013, 966, 871, 828, 796, 763, 732, 704, 666, 604, 568, 529, 492, 448, 418. ^{1}H NMR (500 MHz, DMSO-d_6) δ 10.62 (t, J = 8.6 Hz, 1H), 8.29 (d, J = 7.7 Hz, 1H), 8.13 (d, J = 7.6 Hz, 1H), 7.93 (t, J = 7.5 Hz, 1H), 7.87 (t, J = 7.4 Hz, 1H), 7.62 (t, J = 8.0 Hz, 1H), 7.48 (d, J = 7.3 Hz, 1H), 7.40–7.34 (m, 1H), 7.31 (t, J = 7.8 Hz, 1H), 7.11 (d, J = 8.3 Hz, 1H), 7.03 (d, J = 8.7 Hz, 1H), 6.95 (t, J = 7.5 Hz, 1H), 5.56 (dd, J = 23.2, 8.4 Hz, 1H), 4.16–4.06 (m, 2H), 3.98–3.89 (m, 1H), 3.85–3.73 (m, 1H), 3.33 (s, 2H), 1.92 (s, 1H), 1.23 (t, J = 7.0 Hz, 3H), 1.07 (t, J = 7.0 Hz, 3H). ^{13}C NMR (126 MHz, DMSO-d_6) δ 185.2 (C═O), 183.1 (C═O), 157.3 (d, J = 5.9 Hz, C), 150.3 (C), 150.2 (C), 136.3 (CH), 135.1 (CH), 134.6 (d, J = 4.7 Hz, C), 134.3 (CH), 132.8 (C), 129.9 (d, J = 2.6 Hz, CH), 128.4 (d, J = 4.4 Hz, CH), 127.2 (CH), 126.8 (CH), 123.9 (d, J = 2.4 Hz, C), 121.2 (d, J = 2.1 Hz, CH), 118.9 (CH), 116.6 (CH), 114.1 (C), 111.7 (d, J = 1.2 Hz, CH), 63.37 (d, J = 6.9 Hz, CH_2), 63.22 (d, J = 6.9 Hz, CH_2), 56.4 ($C_{Ar}OCH_3$), 48.2 (NCH), 47.0 (NCH), 16.7 (d, J = 5.3 Hz, CH_3), 16.5 (d, J = 5.6 Hz, CH_3). ^{31}P NMR (202 MHz, DMSO-d_6) δ 21.44. HRMS-ESI m/z found: 480.1572, calculated for [$C_{26}H_{26}NO_6P + H^+$]: 480.1571.

2.2.14. Diethyl ((4-chlorophenyl)((9,10-dioxo-9,10-dihydroanthracen-1-yl)amino)methyl)phosphonate (3f)

Red solid. Yield: 72 %. Melting point: 148 °C. R_f = 0.57 (Benzene/Acetonitirle) (3:1). FTIR (neat): 3232, 3074, 2984, 2905, 1667, 1632, 1589, 1486, 1403, 1360, 1275, 1250, 1165, 1123, 1046, 1009, 957, 872, 829, 785, 754, 730, 702, 664, 603, 556, 505, 444, 414. ^{1}H NMR (500 MHz, DMSO-d_6) δ 10.59 (t, J = 8.9 Hz, 1H), 8.30 (dd, J = 7.8, 1.3 Hz, 1H), 8.15 (dd, J = 7.6, 1.4 Hz, 1H), 7.94 (td, J = 7.6, 1.5 Hz, 1H), 7.88 (td, J = 7.5, 1.4 Hz, 1H), 7.60 (dd, J = 8.6, 7.4 Hz, 1H), 7.55–7.48 (m, 3H), 7.45 (d, J = 8.5 Hz, 2H), 7.28 (d, J = 8.6 Hz, 1H), 5.65 (dd, J = 24.0, 8.5 Hz, 1H), 4.18–3.95 (m, 3H), 3.97–3.86 (m, 1H), 1.23 (t, J = 7.0 Hz, 3H), 1.15 (t, J = 7.0 Hz, 3H). ^{13}C NMR (126 MHz, DMSO-d_6) δ 185.5 (C═O), 183.1 (C═O), 150.4 (C), 150.3 (C), 136.1 (CH), 135.4 (d, J = 3.0 Hz, C), 135.1 (CH), 134.6 (C), 134.4 (CH), 133.0 (d, J = 3.6 Hz, C), 132.9 (C), 130.2 (d, J = 5.2 Hz, CH), 129.0 (d, J = 2.2 Hz, CH), 127.2 (CH), 126.8 (CH), 119.8 (CH), 116.8 (CH), 114.2 (C), 63.4 (d, J = 6.4

Hz, CH_2), 53.6 (NCH), 52.4 (NCH), 16.7 (d, J = 5.4 Hz, CH_3), 16.6 (d, J = 5.4 Hz, CH_3). ^{31}P NMR (202 MHz, DMSO-d_6) δ 21.04. HRMS-ESI *m/z* found: 484.1076, calculated for [$C_{25}H_{23}ClNO_5P + H^+$]: 484.1075.

2.2.15. Diisopropyl (((9,10-dioxo-9,10-dihydroanthracen-1-yl)amino)(phenyl)methyl)phosphonate ***(4a)***

Red solid. Yield: 84 %. Melting point: 121 °C. R_f = 0.53 (Benzene/Acetonitirle) (3:1). FTIR (neat): 3255, 3064, 3034, 2980, 2926, 2871, 2835, 1669, 1634, 1590, 1502, 1386, 1358, 1315, 1251, 1164, 1100, 975, 896, 829, 797, 752, 731, 700, 661, 595, 565, 539, 508, 477, 414. ^{1}H NMR (500 MHz, DMSO-d_6) δ 10.62 (t, J = 8.8 Hz, 1H), 8.30 (dd, J = 7.8, 1.3 Hz, 1H), 8.14 (dd, J = 7.8, 1.4 Hz, 1H), 7.94 (td, J = 7.6, 1.4 Hz, 1H), 7.87 (td, J = 7.5, 1.4 Hz, 1H), 7.58 (t, J = 7.9 Hz, 1H), 7.53 (dd, J = 7.7, 2.1 Hz, 2H), 7.48 (d, J = 7.3 Hz, 1H), 7.40–7.31 (m, 3H), 7.29 (td, J = 7.3, 1.6 Hz, 1H), 5.48 (dd, J = 23.7, 8.6 Hz, 1H), 4.65 (dq, J = 12.6, 6.2 Hz, 1H), 4.49 (dq, J = 12.7, 6.3 Hz, 1H), 1.29 (d, J = 6.1 Hz, 3H), 1.23 (d, J = 6.1 Hz, 3H), 1.16 (d, J = 6.2 Hz, 3H), 1.00 (d, J = 6.2 Hz, 3H). ^{13}C NMR (126 MHz, DMSO-d_6) δ 185.3 (C═O), 183.1 (C═O), 150.7 (C), 150.6 (C), 136.4 (d, J = 2.9 Hz, C), 136.0 (CH), 135.1 (CH), 134.6 (d, J = 8.7 Hz, C), 134.3 (CH), 132.9 (C), 128.8 (d, J = 2.1 Hz, CH), 128.6 (d, J = 5.3 Hz, CH), 128.3 (d, J = 2.6 Hz, CH), 127.2 (CH), 126.8 (CH), 119.9 (CH), 116.6 (CH), 113.9 (C), 71.9 (t, J = 7.6 Hz, $\underline{C}H(CH_3)_2$), 54.8 (NCH), 53.6 (NCH), 24.3 (d, J = 3.3 Hz, CH_3), 24.0 (d, J = 5.0 Hz, CH_3), 23.6 (d, J = 5.4 Hz, CH_3). ^{31}P NMR (202 MHz, DMSO-d_6) δ 19.69. HRMS-ESI *m/z* found: 478.1777, calculated for [$C_{27}H_{28}NO_5P + H^+$]: 478.1778.

2.2.16. Diisopropyl (((9,10-dioxo-9,10-dihydroanthracen-1-yl)amino)(p-tolyl)methyl)phosphonate ***(4b)***

Red solid. Yield: 77 %. Melting point: 107 °C. R_f = 0.52 (Benzene/Acetonitirle) (3:1). FTIR (neat): 3256, 2979, 2930, 2872, 1668, 1636, 1588, 1505, 1463, 1385, 1357, 1308, 1251, 1169, 1100, 1073, 962, 895, 867, 827, 798, 770, 704, 666, 612, 564, 501, 477, 416. ^{1}H NMR (500 MHz, DMSO-d_6) δ 10.59 (t, J = 8.8 Hz, 1H), 8.29 (dd, J = 7.8, 1.3 Hz, 1H), 8.14 (dd, J = 7.7, 1.4 Hz, 1H), 7.94 (td, J = 7.6, 1.5 Hz, 1H), 7.87 (td, J = 7.5, 1.4 Hz, 1H), 7.61–7.54 (m, 1H), 7.47 (d, J = 7.3 Hz, 1H), 7.40 (dd, J = 8.2, 2.2 Hz, 2H), 7.31 (d, J = 8.6 Hz, 1H), 7.17 (d, J = 7.8 Hz, 2H), 5.41 (dd, J = 23.5, 8.6 Hz, 1H), 4.65 (dq, J = 12.7, 6.3 Hz, 1H), 4.50 (dq, J = 12.7, 6.3 Hz, 1H), 2.27 (d, J = 1.9 Hz, 3H), 1.29 (d, J = 6.2 Hz, 3H), 1.23 (d, J = 6.2 Hz, 3H), 1.17 (d, J = 6.2 Hz, 3H), 1.03 (d, J = 6.2 Hz, 3H). ^{13}C NMR (126 MHz, DMSO-d_6) δ 185.2 (C═O), 183.1 (C═O), 150.8 (C), 150.7 (C), 137.5 (d, J = 3.0 Hz, C), 136.0 (CH), 135.1 (CH), 134.6 (d, J = 12.9 Hz, C), 134.3 (CH), 133.3 (d, J = 3.0 Hz, C), 132.9 (C), 129.4 (d, J = 2.1 Hz, CH), 128.5 (d, J = 5.3 Hz, CH), 127.1 (CH), 126.8 (CH), 120.0 (CH), 116.5 (CH), 113.8 (C), 71.8 (t, J = 6.6 Hz, $\underline{C}H(CH_3)_2$), 54.5 (NCH), 53.3 (NCH), 24.4 (d, J = 3.2 Hz, CH_3), 24.0 (d, J = 5.0 Hz, CH_3), 23.7 (d, J = 5.3 Hz, CH_3), 21.2 ($C_{Ar}\underline{C}H_3$). ^{31}P NMR (202 MHz, DMSO-d_6) δ 19.80. HRMS-ESI *m/z* found: 492.1936, calculated for [$C_{28}H_{30}NO_5P + H^+$]: 492.1934.

2.2.17. Diisopropyl (((9,10-dioxo-9,10-dihydroanthracen-1-yl)amino)(4-fluorophenyl)methyl)phosphonate ***(4c)***

Red solid. Yield: 78 %. Melting point: 152 °C. R_f = 0.50 (Benzene/Acetonitirle) (3:1). FTIR (neat): 3255, 2980, 2930, 2836, 1669, 1634, 1589, 1501, 1359, 1312, 1251, 1219, 1163, 1099, 975, 900, 867, 829, 779, 731, 703, 661, 605, 562, 521, 492, 415. ^{1}H NMR (500 MHz, DMSO-d_6) δ 10.59 (t, J = 8.8 Hz, 1H), 8.29 (d, J = 7.7 Hz, 1H), 8.15 (dd, J = 7.6, 1.3 Hz, 1H), 7.94 (td, J = 7.5, 1.4 Hz, 1H), 7.88 (td, J = 7.5, 1.4 Hz, 1H), 7.60 (t, J = 8.0 Hz, 1H), 7.58–7.54 (m, 2H), 7.49 (d, J = 7.3 Hz, 1H), 7.32 (d, J = 8.6 Hz, 1H), 7.21 (t, J = 8.7 Hz, 2H), 5.53 (dd, J = 23.7, 8.6 Hz, 1H), 4.66 (dq, J = 12.7, 6.3 Hz, 1H), 4.52 (dq, J = 12.7, 6.3 Hz, 1H), 1.29 (d, J = 6.1 Hz, 3H), 1.24 (d, J = 6.1 Hz, 3H), 1.17 (d, J = 6.2 Hz, 3H), 1.03 (d, J = 6.2 Hz, 3H). ^{13}C NMR (126 MHz, DMSO-d_6) δ 185.3 (C═O), 183.1 (C═O), 162.2 (dd, J = 243.6, 3.0 Hz, C), 150.6 (C), 150.5 (C), 136.1 (CH), 135.1 (CH), 134.6 (d, J = 2.2 Hz, C), 134.3 (CH), 132.9 (C), 132.6 (t, J = 2.7 Hz, C), 130.5 (dd, J = 8.1, 5.5 Hz, CH), 127.2 (CH), 126.8 (CH), 119.8 (CH), 116.7 (CH), 115.7 (dd, J = 21.5, 1.8 Hz, CH), 114.0 (C), 72.0 (d, J = 7.1 Hz, $\underline{C}H(CH_3)_2$), 54.0 (NCH), 52.7 (NCH), 24.3 (dd, J = 1.9, 1.4 Hz, CH_3), 24.0 (d, J = 5.0 Hz, CH_3), 23.6 (d, J = 5.2 Hz, CH_3). ^{31}P NMR (202 MHz, DMSO-d_6) δ 19.46 (d, J = 4.6 Hz). HRMS-ESI *m/z* found: 496.1683, calculated for [$C_{27}H_{27}FNO_5P + H^+$]: 496.1684.

2.2.18. Diisopropyl (((9,10-dioxo-9,10-dihydroanthracen-1-yl)amino)(4-methoxyphenyl)methyl)phosphonate ***(4d)***

Red solid. Yield: 78 %. Melting point: 150 °C. R_f = 0.45 (Benzene/Acetonitirle) (3:1). FTIR (neat): 3239, 3081, 2977, 2929, 2836, 1666, 1627, 1593, 1510, 1463, 1413, 1372, 1308, 1267, 1232, 1183, 1106, 1069, 989, 889, 842, 802, 777, 734, 708, 662, 635, 612, 572, 541, 470, 421. ^{1}H NMR (500 MHz, DMSO-d_6) δ 10.57 (t, J = 8.7 Hz, 1H), 8.29 (d, J = 7.7 Hz, 1H), 8.14 (dd, J = 7.7, 1.3 Hz, 1H), 7.94 (td, J = 7.5, 1.4 Hz, 1H), 7.87 (td, J = 7.5, 1.2 Hz, 1H), 7.59 (t, J = 8.0 Hz, 1H), 7.50–7.41 (m, 3H), 7.33 (d, J = 8.7 Hz, 1H), 6.93 (d, J = 8.5 Hz, 2H), 5.39 (dd, J = 23.2, 8.5 Hz, 1H), 4.65 (dq, J = 12.7, 6.3 Hz, 1H), 4.48 (dq, J = 12.6, 6.3 Hz, 1H), 3.72 (s, 3H), 1.29 (d, J = 6.2 Hz, 3H), 1.23 (d, J = 6.2 Hz, 3H), 1.17 (d, J = 6.1 Hz, 3H), 1.02 (d, J = 6.2 Hz, 3H). ^{13}C NMR (126 MHz, DMSO-d_6) δ 185.2 (C═O), 183.1 (C═O), 159.3 (d, J = 2.7 Hz, C), 150.8 (C), 150.7 (C), 136.0 (CH), 135.1 (CH), 134.6 (d, J = 13.6 Hz, C), 134.3 (CH), 132.9 (C), 129.7 (d, J = 5.5 Hz, CH), 128.1 (d, J = 2.7 Hz, C), 127.1 (CH), 126.8 (CH), 120.0 (CH), 116.5 (CH), 114.2 (d, J = 1.9 Hz, CH), 113.8 (C), 71.8 (dd, J = 11.7, 7.1 Hz, $\underline{C}H(CH_3)_2$), 55.5 ($C_{Ar}O\underline{C}H_3$), 54.1 (NCH), 52.9 (NCH), 24.4 (t, J = 2.8 Hz, CH_3), 24.0 (d, J = 5.0 Hz, CH_3), 23.7 (d, J = 5.3 Hz, CH_3). ^{31}P NMR (202 MHz, DMSO-d_6) δ 19.99. HRMS-ESI *m/z* found: 508.1885, calculated for [$C_{28}H_{30}NO_6P + H^+$]: 508.1884.

2.2.19. Diisopropyl (((9,10-dioxo-9,10-dihydroanthracen-1-yl)amino)(2-methoxyphenyl)methyl)phosphonate ***(4e)***

Red solid. Yield: 80 %. Melting point: 140 °C. R_f = 0.55 (Benzene/Acetonitirle) (3:1). FTIR (neat): 3263, 2977, 2933, 2841, 1666, 1632, 1586, 1490, 1465, 1404, 1362, 1312, 1280, 1246, 1177, 1102, 1070, 974, 895, 831, 803, 762, 732, 706, 666, 606, 569, 531, 503, 415. ^{1}H NMR (500 MHz, DMSO-d_6) δ 10.61 (t, J = 8.7 Hz, 1H), 8.28 (dd, J = 7.8, 1.3 Hz, 1H), 8.13 (dd, J = 7.6, 1.4 Hz, 1H), 7.93 (td, J = 7.6, 1.5 Hz, 1H), 7.86 (td, J = 7.5, 1.4 Hz, 1H), 7.62 (t, J = 8.0 Hz, 1H), 7.47 (d, J = 7.3 Hz, 1H), 7.41–7.35 (m, 1H), 7.34–7.26 (m, 1H), 7.09 (d, J = 8.3 Hz, 1H), 7.03 (d, J = 8.6 Hz, 1H), 6.95 (t, J = 7.5 Hz, 1H), 5.47 (dd, J = 23.5, 8.4 Hz, 1H), 4.69 (dq, J = 12.4, 6.2 Hz, 1H), 4.40 (dq, J = 12.6, 6.3 Hz, 1H), 3.95 (s, 3H), 1.29 (d, J = 6.1 Hz, 3H), 1.20 (dd, J = 6.2, 4.2 Hz, 6H), 0.91 (d, J = 6.2 Hz, 3H). ^{13}C NMR (126 MHz, DMSO-d_6) δ 185.2 (C═O), 183.1 (C═O), 157.3 (d, J = 6.1 Hz, C), 150.4 (C), 150.3 (C), 136.4 (CH), 135.1 (CH), 134.6 (d, J = 6.7 Hz, C), 134.3 (CH), 132.8 (C), 129.8 (d, J = 2.6 Hz, CH), 128.4 (d, J = 4.4 Hz, CH), 127.1 (CH), 126.8 (CH), 124.2 (d, J = 2.2 Hz, C), 121.2 (d, J = 2.4 Hz, CH), 118.8 (CH), 116.5 (CH), 113.9 (C), 111.6 (d, J = 1.3 Hz, CH), 71.9 (dd, J = 33.7, 7.2 Hz, $\underline{C}H(CH_3)_2$), 56.4 ($C_{Ar}O\underline{C}H_3$), 48.5 (NCH), 47.2 (NCH), 24.3 (dd, J = 12.0, 3.4 Hz, CH_3), 24.0 (d, J = 4.9 Hz, CH_3), 23.3 (d, J = 5.6 Hz, CH_3). ^{31}P NMR (202 MHz, DMSO-d_6) δ 19.83. HRMS-ESI *m/z* found: 508.1885, calculated for [$C_{28}H_{30}NO_6P + H^+$]: 508.1884.

2.2.20. Diisopropyl ((4-chlorophenyl)((9,10-dioxo-9,10-dihydroanthracen-1-yl)amino)methyl)phosphonate ***(4f)***

Red solid. Yield: 73 %. Melting point: 135 °C. R_f = 0.63 (Benzene/Acetonitirle) (3:1). FTIR (neat): 3242, 3066, 2981, 2934, 2879, 1669, 1636, 1589, 1501, 1385, 1357, 1312, 1275, 1246, 1171, 1142, 1088, 976, 870, 826, 801, 774, 732, 707, 607, 560, 522, 445, 417. ^{1}H NMR (500 MHz, DMSO-d_6) δ 10.58 (t, J = 8.9 Hz, 1H), 8.29 (dd, J = 7.8, 1.4 Hz, 1H), 8.15 (dd, J = 7.7, 1.4 Hz, 1H), 7.94 (td, J = 7.6, 1.5 Hz, 1H), 7.88 (td, J = 7.5, 1.4 Hz, 1H), 7.60 (t, J = 8.0 Hz, 1H), 7.53 (dd, J = 6.7, 2.0 Hz, 2H), 7.49 (d, J = 7.3 Hz, 1H), 7.44 (d, J = 8.3 Hz, 2H), 7.30 (d, J = 8.6 Hz, 1H), 5.54 (dd, J = 24.1, 8.5 Hz, 1H), 4.66 (dq, J = 12.6, 6.2 Hz, 1H), 4.54 (dq, J = 12.5, 6.3 Hz, 1H), 1.30 (d, J = 6.2 Hz, 3H), 1.24 (d, J

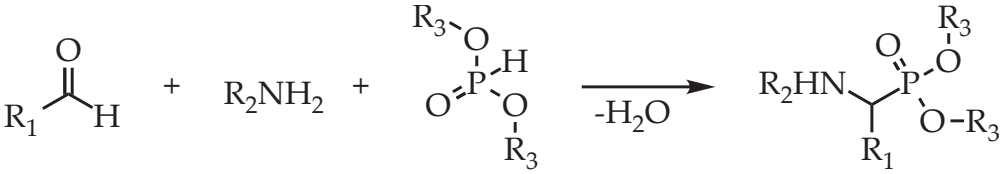

Scheme 2. Kabachnik-Fields reaction.

= 6.2 Hz, 3H), 1.18 (d, J = 6.2 Hz, 3H), 1.06 (d, J = 6.1 Hz, 3H). ^{13}C NMR (126 MHz, DMSO-d_6) δ 185.4 (C═O), 183.1 (C═O), 150.6 (C), 150.4 (C), 136.1 (CH), 135.6 (d, J = 2.8 Hz, C), 135.1 (CH), 134.6 (C), 134.3 (CH), 132.9 (d, J = 3.6 Hz, C), 132.9 (C), 130.3 (d, J = 5.2 Hz, CH), 128.8 (d, J = 2.1 Hz, CH), 127.2 (CH), 126.8 (CH), 119.8 (CH), 116.7 (CH), 114.0 (C), 72.1 (t, J = 6.9 Hz, CH(CH$_3$)$_2$), 54.1 (NCH), 52.9 (NCH), 24.3 (t, J = 3.4 Hz, CH$_3$), 24.0 (d, J = 5.0 Hz, CH$_3$), 23.7 (d, J = 5.2 Hz, CH$_3$). ^{31}P NMR (202 MHz, DMSO-d_6) δ 19.10. HRMS-ESI m/z found: 512.1387, calculated for [$C_{27}H_{27}ClNO_5P$ + H^+]: 512.1388.

2.2.21. Diisopropyl (((9,10-dioxo-9,10-dihydroanthracen-1-yl)amino)(thiophen-2-yl)methyl)phosphonate (**4g**)

Red solid. Yield: 65 %. Melting point: 133 °C. R_f = 0.60 (Benzene/Acetonitirle) (3:1). FTIR (neat): 3251, 2979, 2930, 2828, 1668, 1635, 1590, 1499, 1469, 1386, 1356, 1318, 1254, 1163, 1101, 1037, 974, 900, 860, 829, 798, 731, 702, 662, 589, 539, 508, 474, 415. ^{1}H NMR (500 MHz, DMSO-d_6) δ 10.47 (t, J = 8.3 Hz, 1H), 8.27 (dd, J = 7.7, 1.3 Hz, 1H), 8.15 (dd, J = 7.6, 1.4 Hz, 1H), 7.93 (td, J = 7.5, 1.5 Hz, 1H), 7.88 (td, J = 7.5, 1.4 Hz, 1H), 7.64 (t, J = 8.0 Hz, 1H), 7.52 (dd, J = 8.0, 5.3 Hz, 2H), 7.49–7.44 (m, 1H), 7.28–7.25 (m, 1H), 7.02 (dd, J = 5.1, 3.6 Hz, 1H), 5.87 (dd, J = 23.4, 8.7 Hz, 1H), 4.68 (dq, J = 12.7, 6.3 Hz, 1H), 4.60 (dq, J = 12.6, 6.3 Hz, 1H), 1.30 (d, J = 6.2 Hz, 3H), 1.25 (d, J = 6.1 Hz, 3H), 1.18 (d, J = 6.2 Hz, 3H), 1.10 (d, J = 6.1 Hz, 3H). ^{13}C NMR (126 MHz, DMSO-d_6) δ 185.3 (C═O), 183.1 (C═O), 150.6 (C), 150.5 (C), 139.7 (d, J = 2.6 Hz, C), 136.1 (CH), 135.1 (CH), 134.5 (d, J = 2.6 Hz, C), 134.3 (CH), 132.9 (C), 127.7 (d, J = 7.6 Hz, CH), 127.3 (d, J = 2.4 Hz, CH), 127.2 (CH), 126.8 (CH), 126.6 (d, J = 3.2 Hz, CH), 119.9 (CH), 116.9 (CH), 113.9 (C), 72.2 (d, J = 7.1 Hz, CH(CH$_3$)$_2$), 51.0 (NCH), 49.7 (NCH), 24.4 (d, J = 3.3 Hz, CH$_3$), 23.9 (d, J = 5.0 Hz, CH$_3$), 23.7 (d, J = 5.3 Hz, CH$_3$). ^{31}P NMR (202 MHz, DMSO-d_6) δ 18.13. HRMS-ESI m/z found: 484.1344, calculated for [$C_{25}H_{26}NO_5PS$ + H^+]: 484.1342.

3. Results and discussion

3.1. Synthesis

Kabachnik-Fields reaction conditions were employed to synthesize target anthraquinone α-aryl-α-aminophosphonates (Scheme 2). Quite a few reviews have described underlying mechanism and outlined varying methods for this three-component reaction, involving catalyst-free and catalyzed variants, along with the modifications of employment of microwave irradiation, ionic liquids and dehydrating agents [32,33].

Regarding anthraquinone derivatives, reaction of the 1-aminoanthraquinone with appropriate aromatic aldehydes in excess and dialkylphosphonates as both – reactants and solvents, was plumped for as the most expedient method (see **Section 2.2.1.**). This approach is conditioned by the ease of acquiring and purifying these α-aminophosphonates, where excess of an aldehyde and a dialkylphosphonate is hydrolyzed under moderately basic conditions and a pure compound is obtained via recrystallization. Thus, obtaining a variety of novel anthraquinone α-aryl-α-aminophosphonates in good yields.

3.2. Structural and spectral characterization

To confirm chemical structures of obtained compounds ***2a*** – ***4 g***, ^{1}H-, ^{13}C-, ^{31}P NMR and FTIR spectra and mass spectrometric analysis was carried out.

Structures of newly prepared derivatives were confirmed by ^{1}H NMR spectroscopy, with the corresponding signals of aromatic protons typical for anthraquinone residue, as well as phenyl and thienyl groups. Coupling of hydrogen atoms at position 2 and 4 with hydrogen atom positioned at third carbon atom of anthraquinone core results in appearance of corresponding multiplets with similar J values in the upfield region due to close proximity of amino group, as well as relatively downfield to these, doublets of doublets of hydrogen atoms at sixth and ninth position and triplets of doublets of hydrogens at positions seven and eight with essentially the same coupling constants. Hydrogens of alkyl groups of the phosphonate moiety appear as separate multiplets on account of their magnetic non-equivalence. Signals of the α-carbon hydrogens showed as doublet of doublets due to their coupling with phosphorus nuclei. Deducting these multiplets, it can be concluded that amino group hydrogen appears at approximately 10.6 ppm as a triplet. In APT NMR spectra, appropriate number of peaks of quaternary and tertiary carbon atoms in aromatic region were found. Anthraquinone carbonyl group carbons are found at around 183 and 185 ppm. Moreover, on account of carbon-phosphorous coupling and magnetic non-equivalence of carbon atoms of the phosphonate moiety, appearance of separate doublets is observed in APT spectra. In ^{31}P NMR spectra phosphorous peaks appear at around 18–24 ppm as doublets for fluorine containing compounds ***2c***, ***3c*** and ***4c***, and as singlets for the rest of the compounds (decoupled mode). The obtained results are in good correlation with the previously reported NMR data of other α-amino phosphonates and anthraquinone derivatives [34–38].

Obtained infrared spectra show two stretching vibration peaks of anthraquinone carbonyl groups (C═O) for each compound at around 1669–1627 cm^{-1}, broad aliphatic and aromatic carbon–hydrogen (C–H) stretching vibration bands around 3100–2800 cm^{-1} and broad amino group (NH) stretching vibration bands around 3263–3321 cm^{-1}.

The mass of the synthesized compounds was confirmed to be as calculated based on the results acquired from the high-resolution mass spectrometry.

3.3. Photophysical parameters

Amino substituted anthraquinones are important class of dyes with typical D-A structure [39,40]. For 1-aminoanthraquinone (***1a***), the absorption and fluorescence spectra, lifetime and fluorescence quantum yields, which are strongly affected by the solvent polarity, were measured in previously reported research [41,42]. An electron donating substituent normally enhances this ICT character, which may cause a bathochromic shift of absorption maximum.

For the purpose of examination of photophysical properties of synthesized compounds, UV–Vis absorption and fluorescence emission spectra in such solvents of varying polarity as benzene, chloroform, ethyl acetate (EtOAc), acetone, DMF(N,N-dimethylformamide), DMSO (dimethyl sulfoxide) and ethanol (EtOH) were acquired for compounds ***2a***, ***4a*** and ***4f***.

Table 2
Photophysical parameters of prepared dyes in organic solvents (concentrations: 1×10^{-5} M).

	Absorption λ_{abs} (lgε) (nm)			Fluorescence λ_{abs} (nm)			Stokes shift (cm^{-1})		
	2a	***4a***	***4f***	***2a***	***4a***	***4f***	***2a***	***4a***	***4f***
Benzene	481 (4.14)	484 (4.16)	482 (3.66)	593	591	591	3927	3741	3826
CH_3Cl	484 (4.20)	485 (4.18)	487 (3.57)	595	600	602	3854	3952	3923
EtOAc	479 (4.23)	484 (4.12)	480 (3.67)	586	595	598	3812	3854	4111
Acetone	482 (4.14)	484 (4.10)	481 (3.67)	606	617	614	4245	4454	4503
EtOH	480 (4.13)	484 (4.02)	481 (3.63)	615	615	616	4573	4401	4556
DMF	485 (4.26)	489 (4.08)	488 (3.51)	617	617	614	4411	4242	4205
DMSO	487 (4.19)	492 (4.14)	487 (3.73)	616	617	620	4300	4118	4405

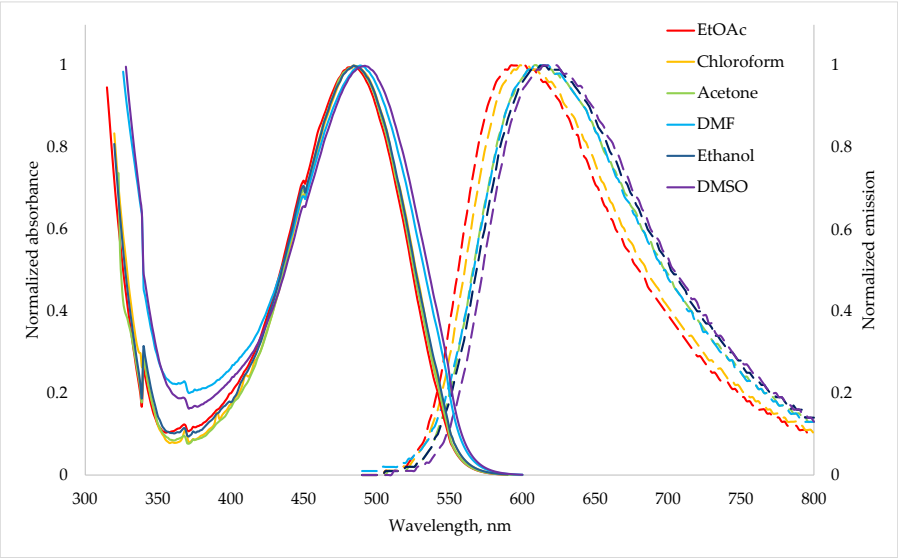

Fig. 1. The UV–Vis absorption and fluorescence emission spectra of compound ***4f*** in various organic solvents.

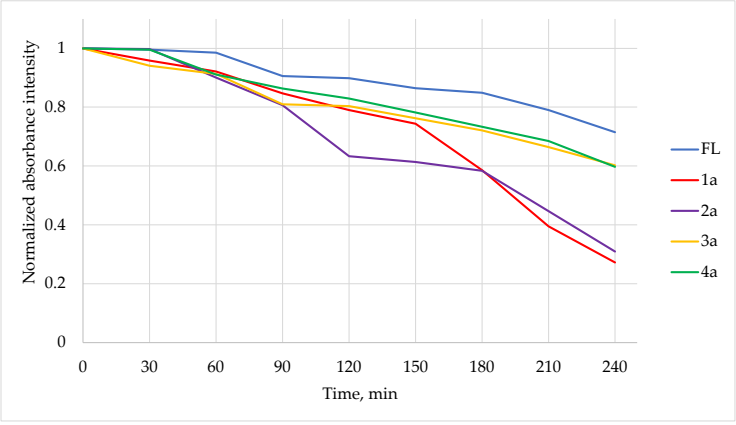

Fig. 2. Normalized absorbance intensities of fluoresceine (FL), ***1a*** and synthesized derivatives ***2a***, ***3a*** and ***4a*** as a function of irradiation time upon 365 nm excitation.

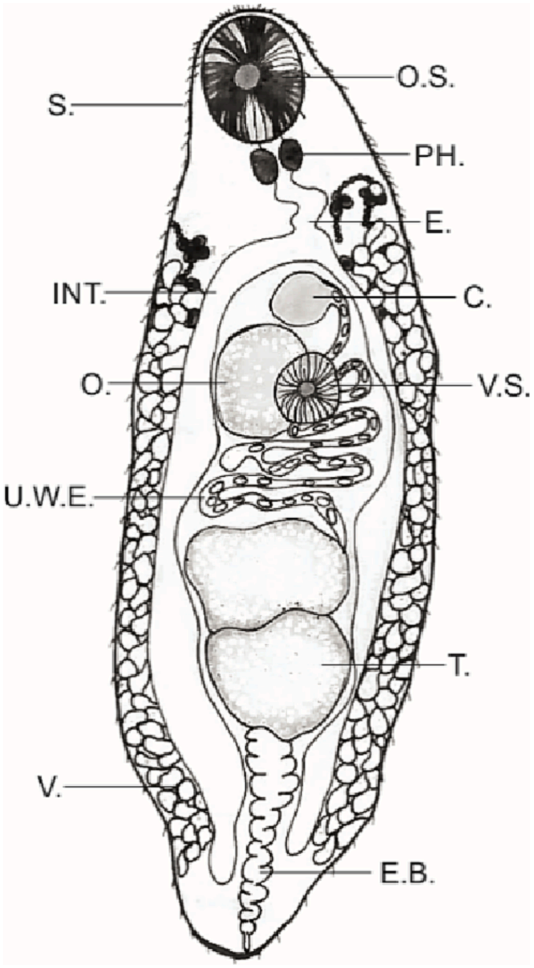

Fig. 3. Scheme of the structure of Opisthioglyphe ranae. C.-cirrus, E.B.-excretory bladder, INT.-intestine, O.-ovary, OE-oesophagus, O.S.-oral sucker, PH.-pharynx, S.-spines, T.-testis, U.W.E.-uterus with eggs, V.-vitellaria, V.S.-ventral sucker.

Absorption maxima and molar attenuation coefficients, fluorescence maxima and Stokes shifts data are summarized in Table 2. Synthesized anthraquinone dyes are fluorescent in solutions, manifesting solvatochromic properties, with emission from yellow in benzene to red in ethanol. Such solvatochromic response indicates accountable internal charge transfer (ICT) mechanism of the fluorescence phenomena during excitation from the electron donating amino group to the electron withdrawing quinone group.

The influence of phosphonate alkyl groups (methyl, ethyl or isopropyl) or substituents on the phenyl group, or the nature of the aromatic substituent on α-carbon (phenyl or thienyl) on the photophysical properties of the obtained dyes was found to be insignificant, as is seen from Table 2. Although, it must be noted that for compound ***4f***, with the chlorine atom in *para*-position on phenyl ring, lower molar attenuation coefficients were recorded, which is due to the fact that electromagnetic radiation is absorbed to a lesser extent and corresponds to the values for unsubstituted 1-aminoanthraquinone.

In instance of the studied fluorophores (Fig. 1) it is observed that in solutions anthraquinone α-aryl-α-aminophosphonates exhibit broad band absorbance with maxima at around 479–488 nm showing small bathochromic shift from benzene to DMSO solution (5–8 nm) in contrast to unsubstituted AAQ, for which the bathochromic shift of the absorption maximum between solutions in hexane and ethanol is 30 nm [42].

Studied compounds show fluorescence with maxima from 586 nm (EtOAc) to 620 nm (DMSO) thus attaining fluorescence bathochromic shifts of up to 30 nm, for 1-aminoanthraquinone this shift is 42 nm (between benzene and isopropanol solutions). The polarity effect of the medium on fluorescence is much more pronounced than on the absorption.

Among studied dyes highest Stokes shift of 4573 cm^{-1} was observed for the compound ***2a*** in ethanol. For 1-aminoanthraquinone Stokes shift is 4470 cm^{-1} (ethanol), thus, the introduction of phosphonate substituents does not significantly affect the energy loss during absorption and emission of light.

An essential requirement for the application of dyes is the high photostability. To acquire a deeper insight into photostability of new dyes, photofading behavior of obtained derivatives was determined in ethanol (at concentration 10^{-4} M) in comparison with 1-aminoanthraquinone and widely used test dye – fluorescein (FL). The experiment was carried out in quartz cells where sample solution was irradiated with a UV-lamp (365 nm) at room temperature.

The results are shown in Fig. 2. After irradiation for 4 h, fluorescein showed an absorbance of 71 % of the initial absorbance, and for ***1a***, the absorbance was only 27 % of the initial absorbance.

Of the obtained compounds, the derivatives with ethyl and isopropyl groups turned out to be the most photostable, in which the decrease in absorption is 40 %, and the less photostable is the dimethyl derivative (absorption decrease is 69 %). The data obtained show that the synthesized dyes exhibit higher photostability than the original compound ***1a***.

3.4. Confocal laser scanning microscopy imaging of trematode Opisthioglyphe ranae

With the help of luminescent dyes, it is becoming increasingly possible to visualize the biological processes within parasites and to visualize the interactions between worms and their hosts. In the present research anthraquinone dye ***4f*** was applied for bioimaging of trematode *Opisthioglyphe ranae*, a common parasite of the intestines of amphibians of Eurasia (Fig. 3).

The body was elongated in oval with broadly round posterior end, which forms a medial notch. The tegument was covered with regularly arranged flattened elongated triangle-shaped spines (Fig. 4**, A**) that covered almost the whole body.

The circular oral sucker was located on the fore end of the body. The ventral sucker was located in the slightly above the middle of the body and it was circular. Prepharynx was narrow and small. The pharynx was globular, smaller than half of the oral sucker and followed by an elongated oesophagus. The oesophagus was divided into two straight digestive intestinal caeca, ending behind the testes. Two large, elongated testes were located at the posterior end of the body, one behind the other in the transverse direction. The rounded shape ovary is located in first part of the body slightly above the ventral sucker and was placed between the digestive intestinal caeca closer to the left intestinal branch. The uterus was long, filled with globular eggs, located between the digestive intestinal caeca. The eggs had a bright fluorescence in a longer wavelength spectrum than other organs. The vitellaria was located along both edges of the body until digestive intestinal caeca, started behind the pharynx and extended until the end of the body (Fig. 4**, B** and **C**).

The anthraquinone dye is applicable for detailed imaging of detailed imaging the internal and external structure by CLSM. The digestive, reproductive, and excretory system was clearly visible; however, the dye did not perform well with muscular tissue, it was difficult to detect the

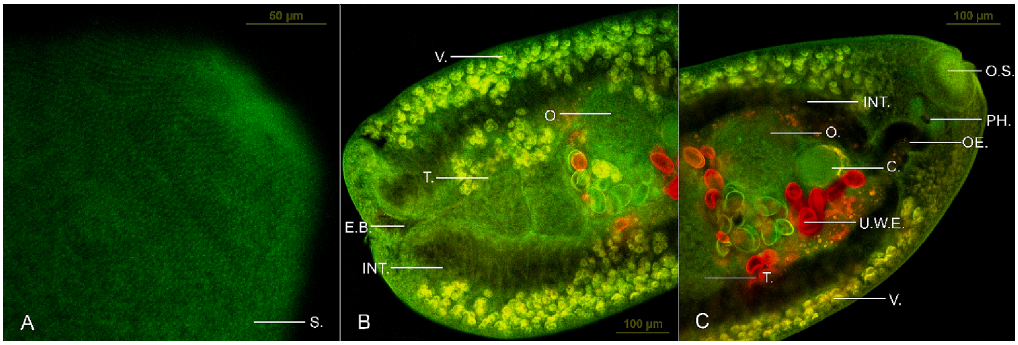

Fig. 4. Adult Opisthioglyphe ranae stained with 4f dye. C.-cirrus, E.B.-excretory bladder, INT.-intestine, O.-ovary, OE-oesophagus, O.S.-oral sucker, PH.-pharynx, S.-spines, T.-testis, U.W.E.-uterus with eggs, V.-vitellaria.

layers and structure of muscles.

4. Conclusions

In summary, a small library of new anthraquinone α-aryl-α-aminophosphonates was obtained. Structures of newly prepared chromophores were confirmed and characterized by means of ^{1}H-, ^{13}C-, ^{31}P NMR spectroscopy and high-resolution mass spectrometry. Synthesized compounds were found to be fluorescent in various solutions with maxima from 586 nm (EtOAc) to 620 nm (DMSO), showing solvatochromic response to the environment with emission of light upon excitation from yellow to red, attaining bathochromic shift of 30 nm and Stokes shift of more than 4570 cm^{-1}. Photofading behavior of obtained derivatives was determined in solutions of ethanol in comparison with 1-aminoanthraquinone and fluorescein, and were found to retain up to 60 % of absorbance intensity after irradiation for 4 h. These photophysical properties enable to apply newly obtained anthraquinone α-aryl-α-amino phosphonates as dyes for detailed and rapid bioimaging of trematode *Opisthioglyphe ranae* using confocal laser scanning microscopy and visualize its digestive, reproductive and excretory system. Taking into consideration copious amounts of applications of α-aminophosphonates, further research could be aimed at investigation of potential utilization of the synthesized compounds in other areas too. In addition, as it is the first report of utilization of α-aryl-α-aminophosphonates as dyes for CLSM, other fluorophores that are functionalized with α-aminophosphonate moiety could be analyzed as prospective dyes in CLSM for not only trematodes, but other organisms as well.

CRediT authorship contribution statement

Armands Maļeckis: Methodology, Validation, Formal analysis, Investigation, Writing – original draft, Project administration, Funding acquisition. **Marija Cvetinska:** Methodology, Validation, Investigation. **Evans Griškjāns:** Methodology, Validation, Investigation. **Ligita Mežaraupe:** Validation, Investigation. **Muza Kirjušina:** Validation, Investigation. **Veronika Pavlova:** Validation, Investigation. **Elena Kirilova:** Methodology, Resources, Writing – review & editing, Supervision.

Declaration of Competing Interest

The authors declare that they have no known competing financial interests or personal relationships that could have appeared to influence the work reported in this paper.

Data availability

Data will be made available on request.

Acknowledgments

This publication was supported by Riga Technical University's Doctoral Grant programme.

Appendix A. Supplementary material

Supplementary data to this article can be found online at https://doi.org/10.1016/j.jphotochem.2023.114918.

References

[1] S. Mukherjee, P. Thilagar, Organic white-light emitting materials, Dyes Pigm. 110 (2014) 2–27, https://doi.org/10.1016/j.dyepig.2014.05.031.
[2] R. Chen, Y. Guan, H. Wang, Y. Zhu, X. Tan, P. Wang, et al., Organic Persistent Luminescent Materials: Ultralong Room-Temperature Phosphorescence and Multicolor-Tunable Afterglow, ACS Appl. Mater. Interfaces 13 (2021) 41131–41139, https://doi.org/10.1021/acsami.1c12249.
[3] J.M. Ha, S.H. Hur, A. Pathak, J.-E. Jeong, H.Y. Woo, Recent advances in organic luminescent materials with narrowband emission, NPG Asia Mater. 13 (2021) 53, https://doi.org/10.1038/s41427-021-00318-8.
[4] J. Yang, M. Fang, Z. Li, Organic luminescent materials: The concentration on aggregates from aggregation-induced emission, Aggregate 1 (2020) 6–18, https://doi.org/10.1002/agt2.2.
[5] Q. Zang, J. Yu, W. Yu, J. Qian, R. Hu, B.Z. Tang, Red-emissive azabenzanthrone derivatives for photodynamic therapy irradiated with ultralow light power density and two-photon imaging, Chem. Sci. 9 (2018) 5165–5171, https://doi.org/10.1039/C8SC00633D.
[6] Z. Wu, A.C. Midgley, D. Kong, D. Ding, Organic persistent luminescence imaging for biomedical applications, Mater Today Bio 17 (2022), 100481, https://doi.org/10.1016/j.mtbio.2022.100481.
[7] É. Whelan, F.W. Steuber, T. Gunnlaugsson, W. Schmitt, Tuning photoactive metal–organic frameworks for luminescence and photocatalytic applications, Coord. Chem. Rev. 437 (2021), 213757, https://doi.org/10.1016/j.ccr.2020.213757.
[8] S. Jaswal, J. Kumar, Review on fluorescent donor–acceptor conjugated system as molecular probes, Mater. Today:. Proc. 26 (2020) 566–580, https://doi.org/10.1016/j.matpr.2019.12.161.
[9] Y. Li, J.-Y. Liu, Y.-D. Zhao, Y.-C. Cao, Recent advancements of high efficient donor–acceptor type blue small molecule applied for OLEDs, Mater. Today 20 (2017) 258–266, https://doi.org/10.1016/j.mattod.2016.12.003.
[10] S. Benkhaya, S. M'rabet, A. el Harfi, A review on classifications, recent synthesis and applications of textile dyes, Inorg. Chem. Commun. 115 (2020), 107891, https://doi.org/10.1016/j.inoche.2020.107891.
[11] Q. Zhang, H. Kuwabara, W.J. Potscavage, S. Huang, Y. Hatae, T. Shibata, et al., Anthraquinone-Based Intramolecular Charge-Transfer Compounds: Computational Molecular Design, Thermally Activated Delayed Fluorescence, and Highly Efficient Red Electroluminescence, J. Am. Chem. Soc. 136 (2014) 18070–18081, https://doi.org/10.1021/ja510144h.
[12] N. Kaur, Gauri, Anthraquinone appended chemosensors for fluorescence monitoring of anions and/or metal ions, Inorganica Chim Acta 536 (2022), 120917, https://doi.org/10.1016/j.ica.2022.120917.

[13] P. Zhang, H. Huang, Y. Chen, J. Wang, L. Ji, H. Chao, Ruthenium(II) anthraquinone complexes as two-photon luminescent probes for cycling hypoxia imaging in vivo, Biomaterials 53 (2015) 522–531, https://doi.org/10.1016/j.biomaterials.2015.02.126.
[14] Z. Fu, Y. Cui, F. Cui, G. Zhang, Modeling techniques and fluorescence imaging investigation of the interactions of an anthraquinone derivative with HSA and ctDNA, Spectrochim. ActaA Mol Biomol Spectrosc 153 (2016) 572–579, https://doi.org/10.1016/j.saa.2015.09.011.
[15] M.S. Malik, R.I. Alsantali, R.S. Jassas, A.A. Alsimaree, R. Syed, M.A. Alsharif, et al., Journey of anthraquinones as anticancer agents – a systematic review of recent literature, RSC Adv. 11 (2021) 35806–35827, https://doi.org/10.1039/D1RA05686G.
[16] E.M. Malik, C.E. Müller, Anthraquinones As Pharmacological Tools and Drugs, Med. Res. Rev. 36 (2016) 705–748, https://doi.org/10.1002/med.21391.
[17] A. Mucha, P. Kafarski, Ł. Berlicki, Remarkable Potential of the α-Aminophosphonate/Phosphinate Structural Motif in Medicinal Chemistry, J. Med. Chem. 54 (2011) 5955–5980, https://doi.org/10.1021/jm200587f.
[18] P. Kafarski, B. Lejczak, Biological activity of aminophosphonic acids, Phosphorus Sulfur Silicon Relat. Elem. 63 (1991) 193–215, https://doi.org/10.1080/10426509108029443.
[19] S. Li, R. Liu, X. Han, C. Ge, X. Zhang, Diethyl α-aminophosphonate containing lubricating additives synthesized from (3-aminophenyl)boronic acid pinacol ester, Inorg. Chem. Commun. 140 (2022), 109477, https://doi.org/10.1016/j.inoche.2022.109477.
[20] N.B. Reddy, C.S. Sundar, B.S. Krishna, S. Santhisudha, P. Sreelakshmi, S.K. Nayak, et al., Cellulose-SO3H catalyzed synthesis of bis(α-aminophosphonates) and their antioxidant activity, Organic Commun. 10 (2017) 46–55, https://doi.org/10.25135/acg.oc.8.16.06.422.
[21] S.R. Fouda, I.E. El-Sayed, N.F. Attia, M.M. Abdeen, A.A.H. Abdel Aleem, I. F. Nassar, et al., Mechanistic study of Hg(II) interaction with three different α-aminophosphonate adsorbents: Insights from batch experiments and theoretical calculations, Chemosphere 304 (2022), 135253, https://doi.org/10.1016/j.chemosphere.2022.135253.
[22] E.A. Imam, A.I. Hashem, A.A. Tolba, M.G. Mahfouz, I.-E.-T. El-Sayed, A.I. El-Tantawy, et al., Effect of mono- vs. bi-functionality of aminophosphonate derivatives on the enhancement of U(VI) sorption: physicochemical properties and sorption performance, J. Environ. Chem. Eng. 11 (2023), 109951, https://doi.org/10.1016/j.jece.2023.109951.
[23] R.R. Neiber, A.A. Galhoum, I. El-Tantawy El Sayed, E. Guibal, J. Xin, X. Lu, Selective lead (II) sorption using aminophosphonate-based sorbents: Effect of amine linker, characterization and sorption performance, Chem. Eng. J. 442 (2022), 136300, https://doi.org/10.1016/j.cej.2022.136300.
[24] O. Moumeni, M. Mehri, R. Kerkour, A. Boublia, F. Mihoub, K. Rebai, et al., Experimental and detailed DFT/MD simulation of α-aminophosphonates as promising corrosion inhibitor for XC48 carbon steel in HCl environment, J. Taiwan Inst. Chem. Eng. 147 (2023), 104918, https://doi.org/10.1016/j.jtice.2023.104918.
[25] M. Górny vel Górniak, P. Kafarski, Preparation of the library of fluorescent aromatic aminophosphonate phenyl and benzyl esters, Phosphorus Sulfur Silicon Relat. Elem. 191 (2016) 511–519, https://doi.org/10.1080/10426507.2015.1094658.
[26] A. Kuśnierz, E. Chmielewska, Synthesis of fluorescent aminophosphonates by green chemistry procedures, Phosphorus Sulfur Silicon Relat. Elem. 192 (2017) 700–705, https://doi.org/10.1080/10426507.2017.1308934.
[27] M.G. Górniak vel, A. Czernicka, P. Młynarz, W. Balcerzak, P. Kafarski, Synthesis of fluorescent (benzyloxycarbonylamino) (aryl)methylphosphonates, Beilstein J. Org. Chem. 10 (2014) 741–745, https://doi.org/10.3762/bjoc.10.68.
[28] Q.-M. Wang, W. Gao, J.-L. Song, Y. Liu, H. Qi, X.-H. Tang, Synthesis, X-Ray Crystallographic Analysis and BSA Interaction of a New α-Aminophosphonate, J. Appl. Spectrosc. 83 (2016) 703–709, https://doi.org/10.1007/s10812-016-0351-9.
[29] J. Lewkowski, M. Rodriguez Moya, A. Wrona-Piotrowicz, J. Zakrzewski, R. Kontek, G. Gajek, Synthesis, fluorescence properties and the promising cytotoxicity of pyrene–derived aminophosphonates, Beilstein J. Org. Chem. 12 (2016) 1229–1235, https://doi.org/10.3762/bjoc.12.117.
[30] I. Kraicheva, E. Vodenicharova, E. Tashev, T. Tosheva, I. Tsacheva, K. Troev, Synthesis and NMR Characterization of Two Novel Anthracene-Derived BIS-Aminophosphonates. Basic Hydrolysis of Some Aminophosphonate Derivatives, Phosphorus Sulfur Silicon Relat. Elem. 187 (2012) 660–667, https://doi.org/10.1080/10426507.2011.638349.
[31] A. Maļeckis, E. Griškjāns, M. Cvetinska, M. Savicka, S. Belyakov, E. Kirilova, Synthesis, characterization, spectroscopic studies and evaluation of toxicological effect on growth of wheat sprouts (Triticum aestivum) of new benzanthrone α-aryl-α-aminophosphonates, J. Mol. Struct. 1277 (2023), 134838, https://doi.org/10.1016/j.molstruc.2022.134838.
[32] A. Amira, Z. Aouf, H. K'tir, Y. Chemam, R. Ghodbane, R. Zerrouki, et al., Recent Advances in the Synthesis of α-Aminophosphonates: A Review, ChemistrySelect 6 (2021) 6137–6149, https://doi.org/10.1002/slct.202101360.
[33] P.R. Varga, G. Keglevich, Synthesis of α-Aminophosphonates and Related Derivatives; The Last Decade of the Kabachnik-Fields Reaction, Molecules 26 (2021) 2511, https://doi.org/10.3390/molecules26092511.
[34] A. Balakrishna, C. Suresh Reddy, S.K. Naik, M. Manjunath, R.C. Naga, Synthesis, characterization and bio-activity of some new aminophosphonates, Bull. Chem. Soc. Ethiop. (2009) 23, https://doi.org/10.4314/bcse.v23i1.21300.
[35] B. Litim, A. Djahoudi, S. Meliani, A. Boukhari, Synthesis and potential antimicrobial activity of novel α-aminophosphonates derivatives bearing substituted quinoline or quinolone and thiazole moieties, Med. Chem. Res. 31 (2022) 60–74, https://doi.org/10.1007/s00044-021-02815-5.
[36] G.W. Francis, D.W. Aksnes, Ø. Holt, Assignment of the1H and13C NMR spectra of anthraquinone glycosides fromRhamnus frangula, Magn. Reson. Chem. 36 (1998) 769–772, https://doi.org/10.1002/(SICI)1097-458X(1998100)36:10<769::AID-OMR361>3.0.CO;2-E.
[37] B. Sui, X. Fu, The copper(I) iodide accelerated synthesis of mono- and bisbenzyl substituted 1- and 2-aminoanthraquinones, Dyes Pigm. 83 (2009) 1–6, https://doi.org/10.1016/j.dyepig.2009.01.004.
[38] F. Serigne Abdou Khadir, S. Boukhssas, S. Achamlale, Y. Aouine, A. Nakkabi, H. Faraj, et al. Synthesis and Characterization of the Structure of Diethyl [(4-{(1H-Benzo[d]Imidazol-1-yl)Methyl}-1H-1,2,3-Triazol-1-yl)(Benzamido)Methyl] Phosphonate Using 1D and 2D NMR Experiments. Eur. J. Adv. Chem. Res. 2021; 2: 1–7. https://doi.org/10.24018/ejchem.2021.2.1.42.
[39] S. Sun, C. Qin, H. Liu, C. Jiang, Excitation wavelength dependent ICT character and ISC efficiency in a photocleavage agent of 1-aminoanthraquinone, Spectrochim. ActaA Mol Biomol Spectrosc 234 (2020), 118200, https://doi.org/10.1016/j.saa.2020.118200.
[40] Y. Zhao, M. Wang, P. Zhou, S. Yang, Y. Liu, C. Yang, et al., Mechanism of Fluorescence Quenching by Acylamino Twist in the Excited State for 1-(Acylamino) anthraquinones, Chem. A Eur. J. 122 (2018) 2864–2870, https://doi.org/10.1021/acs.jpca.7b11675.
[41] D.A. Navas, Absorption and emission spectroscopy and photochemistry of 1,10-anthraquinone derivatives: a review, J. Photochem. Photobiol. A Chem. 53 (1990) 141–167, https://doi.org/10.1016/1010-6030(90)87120-Z.
[42] T.P. Smith, K.A. Zaklika, K. Thakur, P.F. Barbara, Excited state intramolecular proton transfer in 1-(acylamino)anthraquinones, J. Am. Chem. Soc. 113 (1991) 4035–4036, https://doi.org/10.1021/ja00010a079.

3. pielikums
Appendix III

Maļeckis, A.; Cvetinska, M.; Puckins, A.; Osipovs, S.; Sirokova, J.; Belyakov, S.; Kirilova, E.

Synthesis and Properties of New 3-Heterylamino-Substituted 9-Nitrobenzanthrone Derivatives

Molecules ***2023****, 28 (13), 5171.*

https://doi.org/10.3390/molecules28135171

molecules

MDPI

Article

Synthesis and Properties of New 3-Heterylamino-Substituted 9-Nitrobenzanthrone Derivatives

Armands Maļeckis [1], Marija Cvetinska [1], Aleksandrs Puckins [2], Sergejs Osipovs [2], Jelizaveta Sirokova [2], Sergey Belyakov [3] and Elena Kirilova [2,*]

[1] Institute of Technology of Organic Chemistry, Faculty of Materials Science and Applied Chemistry, Riga Technical University, P. Valdena Str. 3, LV-1048 Riga, Latvia
[2] Department of Applied Chemistry, Institute of Life Sciences and Technology, Daugavpils University, LV-5401 Daugavpils, Latvia
[3] Latvian Institute of Organic Synthesis, Aizkraukles Str. 21, LV-1006 Riga, Latvia; serg@osi.lv
* Correspondence: jelena.kirilova@du.lv

Abstract: In the present study, new fluorophores based on disubstituted benzanthrone derivatives were designed starting from 9-nitro-3-bromobenzanthrone with nucleophilic substitution of the bromine atom with some secondary cyclic amines. It has been found that this reaction is positively affected by the presence of a nitro group in comparison with 3-bromobenzanthrone. The new compounds exhibit intense absorption and pronounced luminescent properties in various organic solvents. In this regard, their photophysical properties were evaluated with an experimental study of the solvatochromic behavior of the obtained compounds in various solvents. It has recently been found that the addition of an electron-withdrawing nitro group to the benzanthrone core increases its first- and second-order hyperpolarizability. Such dyes can be used in the fabrication of optical limiter devices. Therefore, the developed fluorescent molecules have a potential prospect for extensive application in optoelectronics.

Keywords: benzanthrone; heterocycle; substituted amines; nitro derivative; fluorescence; solvatochromism; crystal structure

Citation: Maļeckis, A.; Cvetinska, M.; Puckins, A.; Osipovs, S.; Sirokova, J.; Belyakov, S.; Kirilova, E. Synthesis and Properties of New 3-Heterylamino-Substituted 9-Nitrobenzanthrone Derivatives. *Molecules* **2023**, *28*, 5171. https://doi.org/10.3390/molecules28135171

Academic Editors: Michal Szostak, Guangchen Li and Changan Wang

Received: 7 June 2023
Revised: 29 June 2023
Accepted: 30 June 2023
Published: 2 July 2023

1. Introduction

Fluorescence is known as a phenomenon where a substance absorbs light and promptly emits it at a longer wavelength—the process taking place within nanoseconds. The emitted light has a lower energy compared to the absorbed light, which results in a spectral shift towards longer wavelengths [1]. There are several characteristics that make an organic compound a good fluorophore. Such a compound should have a high absorption coefficient—the more efficiently the molecule can be excited, the brighter the emitted fluorescence [2]. A Stokes shift, the difference between the excitation and emission wavelengths, should be large enough to minimize reabsorption and maximize sensitivity [3]. An efficient fluorophore should also have a high quantum yield, indicating that most of the absorbed energy is converted into emitted light rather than the absorbed energy being transformed into other competing non-radiative processes and should be photostable so that it will not degrade or lose its fluorescent properties over time or with repeated exposure to light [4,5].

In the anthrone family of fluorescent dyes, a four-cyclic condensed aromatic ketone, benzanthrone, has been confirmed to display the excellent above-mentioned characteristics, which prompts the synthesis of new derivatives and their study [6,7]. Previously, benzanthrone compounds have found utilization as fluorescent bioimaging probes, which can aid in the visualization of parasitic trematodes and nematodes [8–10], as well as in the identification of callus embryos of different plant species through the use of confocal laser scanning microscopy imaging [11]. Moreover, these substances can be selectively deployed to identify amyloid fibrils [12,13]. Benzanthrone derivatives also have the potential to

be utilized in liquid crystal displays [14,15], polymeric materials [16,17] and as probes to determine the pH levels and presence of cations in solutions [18–20]. These multiple benefits of these compounds have shown them to be a potential tool for various industries and research fields.

Previous studies have shown a significant effect of the substituent in the third position of the aromatic system on the photophysical properties of benzanthrone dyes [21–23]. This is explained by the ability of benzanthrone compounds to form a state based on the intramolecular charge transfer (ICT) between the electron-donating substituent and the electron-withdrawing carbonyl moiety, which leads to a significant charge redistribution upon excitation and, as a consequence, to pronounced fluorosolvatochromism.

The influence of such electron-donating groups as amino, amidino, alkoxy and other groups is described in the literature, showing the highest ICT character of the first transition for derivatives with the strongest donor group [22].

Over the last few decades, 3-aminobenzanthrone derivatives (including alkylamines and imines [6,15,24], amides [25–27], amidines [28] and aminophosphonates [29]) have become the subject of significant attention. Among these many derivatives, substituted 3-piperazinyl derivatives of benzanthrone [30,31], as well as 3-(4-(diphenylamino)phenyl)benzanthrone and perylenediimide–benzanthrone dyads, were recently found to exhibit nonlinear optical (NLO) properties [32,33], which propels their design and use not only for imaging and sensing but also for applications in laser technology and optical communications.

In the latest research, it has been found that the introduction of a nitro group at position 9 of the benzanthrone core increases the efficiency of the charge transfer, which results in a stronger NLO response [33]. Thus, considering all of the information mentioned above, we have chosen to share our knowledge on previously unreported nitrated benzanthrone derivatives. In this paper, we detail the synthesis of these newly obtained compounds and provide a comprehensive comparison of their photophysical properties.

2. Results and Discussion

2.1. Synthesis

The first representative of benzanthrone derivatives with a nitro group and a substituted amino group (morpholine residue) was previously synthesized and showed interesting optical properties [34]. Therefore, we continued the study of such substances using a similar synthesis technique to obtain them. The target compounds were synthesized with the reaction of the nucleophilic aromatic substitution of aryl bromide with an addition–elimination mechanism in the previously obtained 3–bromo-9-nitrobenzanthrone (**1**) by heating with an appropriate heterocyclic secondary amine in 1-methyl-2-pyrrolidone as a solvent (see Scheme 1). The starting nitro derivative **1** was obtained with nitration of 3-bromobenzanthrone according to the procedure described in [35].

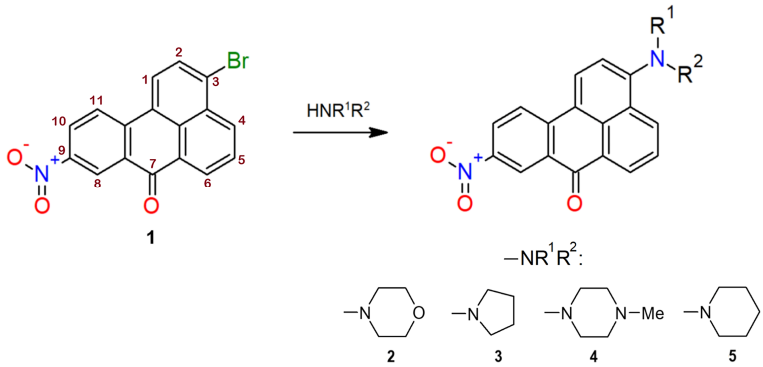

Scheme 1. Synthetic route for the preparation of the target substances.

In contrast to the analogous nucleophilic substitution reaction in 3-bromobenzanthrone, the bromine atom in nitro derivative **1** is replaced faster and at a lower temperature. This is obviously due to the strong electron-withdrawing effect of the nitro group, as a result of which the electron density at the third carbon atom is significantly reduced and the attack of the nucleophile is facilitated. Therefore, the yields of target products **2**–**5** are higher than those of similar derivatives that do not contain a nitro group. The obtained substances are deeply colored dark red solids and have an intense luminescence in solutions.

2.2. NMR Spectra Analysis

Structures of the obtained compounds were confirmed with ^{1}H and APT NMR spectra (see Figures S1–S10); chemical shifts for tertiary carbon atoms and attached hydrogens were assigned on the basis of COSY and HSQC spectra (see Figures S11–S24, Table 1).

Table 1. ^{1}H and ^{13}C chemical shifts for compounds **2**–**6** in $CDCl_3$.

	δ, ppm									
	2		**3**		**4**		**5**		**6**	
	^{1}H	^{13}C	^{1}H	^{13}C	^{1}H	^{13}C	^{1}H	^{13}C	^{1}H	^{13}C
C-8	9.19, d	123.72	9.21, d	124.07	9.14, d	123.77	9.13, d	123.76	8.67, d	127.97
C-4	8.55, d	131.65	8.65, d	133.24	8.51, dd	131.88	8.48, d	132.21	8.46, d	131.26
C-6	8.75, d	130.86	8.78, d	130.99	8.72, dd	130.81	8.70, d	130.74	8.38, d	129.76
C-10	8.39, d	126.82	8.33, dd	126.42	8.34, dd	126.80	8.31, dd	126.68	7.58, ddd	133.16
C-1	8.38, d	127.46	8.26, d	128.92	8.31, d	127.56	8.27, d	127.70	8.21, d	125.14
C-11	8.30, d	123.94	8.20, d	123.11	8.23, d	123.89	8.20, d	123.76	8.12, d	122.53
C-5	7.76, dd	126.29	7.63, dd	123.72	7.73, dd	126.10	7.71, dd	125.85	7.65, dd	125.49
C-2	7.21, d	115.10	6.83, d	108.86	7.18, d	115.10	7.12, d	114.82	7.06, d	114.88
C-7		182.17		–		182.26		182.30		184.15
C-9									7.38, ddd	127.16

It was of interest to compare the chemical shifts of protons and carbon atoms in monosubstituted amino derivatives and nitrated amines in order to evaluate the effect of the nitro group on the NMR spectra of the substances under study.

For comparison, a pair of derivatives with a piperidine residue containing a nitro group (**5**) and a previously synthesized non-nitrated derivative (**6**) were analyzed. In the example of benzanthrone derivative **5**, as indicated by ^{1}H and COSY NMR spectra, signals of H-C(1) and H-C(2) appear as doublets at 8.27 and 7.12 ppm, respectively, with a coupling constant of 8 Hz. H-C(4) (doublet at 8.48 ppm) and H-C(6) (doublet at 8.70 ppm) are not chemically equal, and while the signal of H-C(5) in the ^{1}H NMR spectrum shows up as an apparent triplet, it is in fact a masked doublet of doublets with similar splitting; COSY NMR spectra confirms coupling of both H-C(4) and H-C(6) with H-C(5). Deshielded H-C(8), situated next to both the carbonyl group and nitro group, appears as a doublet downfield at 9.13 ppm. It is observed that there is coupling of H-C(8) with H-C(10), which is attested with the COSY NMR spectrum and equal *J* values of 2.5 Hz. H-C(10) is also split by neighboring H-C(11) (doublet at 8.20 ppm), which makes H-C(10) appear as a doublet of doublets. The same patterns are applicable to the rest of the synthesized derivatives **2**–**4**.

Multiplicity and chemical shifts of the obtained compound **5** can be contrasted with previously reported non-nitrated compound **6**. It is noteworthy to mention that, as validated with HMBC NMR spectra, while H-C(6) is positioned downfield relative to H-C(4) for compound **5**, the opposite is true for non-nitrated compound **6**. Moreover, besides an additional signal of H-C(9), there is a change in relative position and multiplicity for H-C(10), both of which are masked doublets of doublets of doublets that appear as triplets in the ^{1}H NMR spectrum. Obtained results fully correlate with previous NMR studies of benzanthrone derivatives [36–38].

2.3. X-ray Crystallographic Study

Synthesized compound **3** crystallizes from dichloromethane in the form of dark red crystals, the structure of which was determined in this work with an X-ray diffraction analysis of single crystals (see Figure 1 and Tables S1–S6).

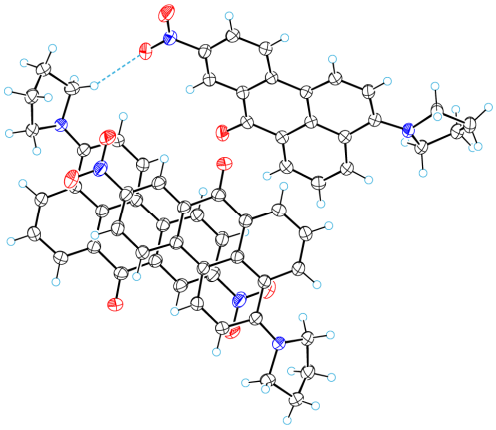

Figure 1. A fragment of molecular packing of **3** showing N–O···H–C hydrogen bonds.

Obtained compound **5** crystallizes from toluene in the form of red luminescent crystals, the structure of which was determined with an X-ray diffraction analysis of single crystals in this research (see Tables S7–S12).

A characteristic feature of the crystal structure of **5** is the fact that there are two independent molecules (A and B) in the asymmetric unit (see Figure 2). These molecules are slightly distinguished by the conformation (the rotation of the piperidine cycles relative to the benzanthrone systems). The torsion angles of C2–C3–N18–C19 are equal to −16.0(1) and −20.3(1)° for molecules A and B, respectively. In both molecules, the piperidine cycles are a chair conformation. The nitro groups of these molecules lie almost in the planes of the benzanthrone systems.

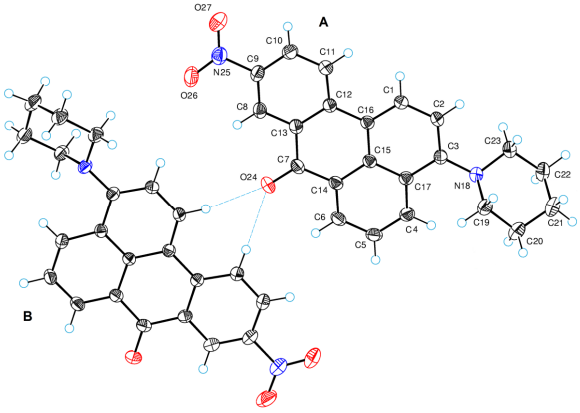

Figure 2. ORTEP diagrams for the asymmetric unit with the labels of atoms and molecules for compound **5**.

Molecules are connected to each other through weak intermolecular bifurcated hydrogen bonds of the CH···O type. Oxygen atom O24(A) forms C1(B)–H1(B)···O24(A) and C11(B)–

H11(B)···O24(A) hydrogen bonds with lengths of 3.293(2) and 3.314(2) Å (H1(B)···O24(A) = 2.38 Å, C1(B)–H1(B)···O24(A) = 160°; H11(B)···O24(A) = 2.41 Å, C11(B)–H11(B)···O24(A) = 159°). In turn, O24(B) forms hydrogen bonds C1(A)–H1(A)···O24(B) (with parameters C1(A)···O24(B) = 3.368(2) Å, H1(A)···O24(B) = 2.47 Å, C1(A)–H1(A)···O24(B) = 157°) and C11(A)–H11(A)···O24(B) (C11(A)···O24(B) = 3.242(2) Å, H11(A)···O24(B) = 2.32 Å, C11(A)–H11(A)···O24(B) = 164°). By means of these hydrogen bonds, molecular chains (bands) are formed in the crystal structure, approximately parallel to the crystallographic plane ($\bar{2}$ 2 1).

In the crystal structure, π–π stacking interactions between benzanthrone systems are observed. Due to these interactions, the molecular stacks are formed in the crystal lattice. The rows of these stacks are arranged parallel to the crystallographic direction [1 $\bar{1}$ 0]. Each stack contains both molecules A and molecules B. Figure 3 shows such a stack. The shortest intermolecular atom–atomic contacts in the stacks are C9(A)···C8(B) (3.361(2) Å) and C4(A)···C10(A) (3.431(2) Å).

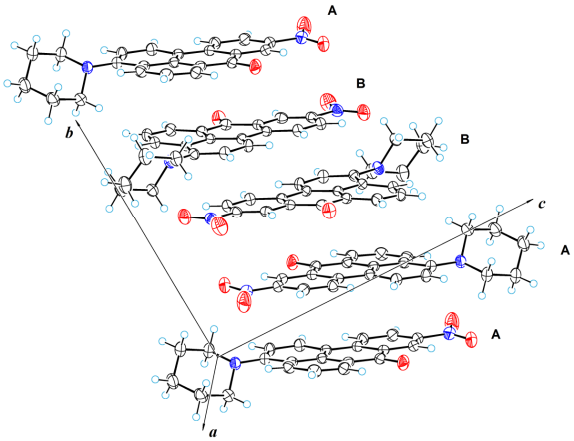

Figure 3. A perspective view of molecular stack with the labels of molecule **5**.

2.4. Spectroscopic Properties

The synthesized dyes exhibit pronounced luminescent properties in various organic solvents. In this regard, the photophysical properties of the obtained derivative were evaluated, recording the absorption and emission spectra in the seven organic solvents with a wide range of polarities (see Figures S36–S38).

The obtained spectral data are summarized in Tables 2–4 in comparison with the characteristics of the previously studied unnitrated 3-piperidinobenzanthrone (**6**) and 3-pyrrolidinobenzanthrone (**7**) (see Scheme 2). The photophysical properties of morpholine derivatives have been analyzed in a recent study [34].

Table 2. Absorption maxima λ_{abs} (lgε) of nitrated and non-nitrated amines in various organic solvents.

	λ_{abs} max, nm (lgε)					
Solvent	**3**	**7**	**2**	**4**	**5**	**6**
Benzene	498 (3.94)	525 (4.16)	447 (4.47)	453 (4.26)	460 (4.55)	447 (4.16)
Chloroform	505 (4.01)	541 (4.21)	449 (4.56)	462 (4.26)	474 (4.62)	454 (4.15)
EtOAc	493 (3.92)	527 (4.24)	447 (4.49)	454 (4.15)	459 (4.53)	445 (4.13)
Acetone	512 (4.08)	542 (4.31)	448 (4.60)	462 (4.11)	467 (4.51)	448 (4.12)
EtOH	526 (3.97)	542 (4.21)	449 (4.49)	455 (3.99)	471 (4.50)	457 (4.09)
DMF	519 (4.18)	548 (4.35)	460 (4.54)	467 (4.17)	475 (4.50)	448 (4.11)
DMSO	531 (4.06)	558 (4.31)	466 (4.43)	472 (4.11)	478 (4.49)	463 (4.11)

Table 3. Emission maxima λ_{em} of nitrated and non-nitrated amines in various organic solvents.

	λ_{em} max, nm					
Solvent	**3**	**7**	**2**	**4**	**6**	**5**
Benzene	584	577	570	574	582	578
Chloroform	613	602	592	598	617	606
EtOAc	598	593	592	592	602	598
Acetone	621	632	612	612	628	620
EtOH	661	652	652	645	675	661
DMF	630	645	624	622	635	632
DMSO	641	645	650	634	665	643

Table 4. Stokes shifts (in cm^{-1}) of nitrated and non-nitrated amines in various organic solvents.

	$(\nu_{abs} - \nu_{em})$ (cm^{-1})					
Solvent	**3**	**7**	**2**	**4**	**6**	**5**
Benzene	2957	1716	4564	4653	5189	4438
Chloroform	3489	1873	4827	4923	5819	4596
EtOAc	3562	2112	5380	5135	5861	5064
Acetone	3428	2627	5479	5305	6398	5284
EtOH	3882	3113	5981	6474	7067	6103
DMF	3395	2744	6935	5336	6573	5230
DMSO	3231	2417	5713	5413	6561	5368

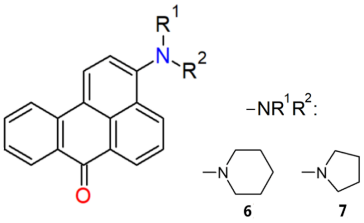

Scheme 2. Structure of compounds **6** and **7** with the corresponding substituents R^1 and R^2.

Amines **4** and **5** absorb light at 450–480 nm, while derivative **3** with a pyrrolidine fragment has a longer wavelength absorption band at 525–560 nm and also exhibits a larger bathochromic shift from nonpolar benzene to polar DMSO (33 nm) than derivatives **4** and **5** (18–19 nm). The pyrrolidine derivative **7** obtained earlier [39] exhibits absorption in the longest wavelength range compared to all other studied compounds, both monosubstituted and disubstituted. It is known that the main process that determines the photophysical properties in substituted amino derivatives of benzanthrone is the transfer of electron density from the amino nitrogen to the benzanthrone ring, the degree of which may also depend on other substituents [21–23].

Obviously, in the case of compound **7**, there is a stronger interaction between the donor and acceptor groups, which leads to a lower electronic transition energy and an increase in the charge transfer upon absorption of a light quantum. The addition of an electronegative nitro group to the molecule of compound **3** leads to competition between this substituent and the carbonyl group of the molecule and, consequently, to a new electron density distribution in the ground state. The hypsochromic shift of the absorption band in derivative **3** and the low sensitivity of the absorption maxima to the polarity of the solvent indicate a decrease in the ICT character of the electronic transition.

Compared to unnitrated amines, compounds **3**–**5** have more intense absorption. For the synthesized compounds, the bathochromic shift of luminescence maxima (from benzene to DMSO) is comparable to the bathochromic shift of unnitrated derivatives and is 60–85 nm.

Nitrated compounds **3** and **5** show a bathochromic shift of absorption maxima by 15–35 nm compared to non-nitrated derivatives **7** and **6**, but their emission maxima demonstrate a hypsochromic shift by 3–14 nm relative to the luminescence spectra of monosubstituted derivatives. As a result, the Stokes shifts of the spectra of nitro derivatives become smaller than those of non-nitrated derivatives (see Table 4).

3. Materials and Methods

3.1. Materials and Basic Measurements

All reagents were of an analytical grade (Aldrich Chemical Company, Munich, Germany) and were used as received. The progress of the chemical reactions and the purity of products were monitored with TLC on silica gel plates (Fluka F60254, 20*10, 0.2 mm, ready-to-use), using C_6H_6-CH_3CN (3:1) as an eluent, and visualization under UV light. Column chromatography on silica gel was carried out on Merck Kieselgel (230–240 mesh) with dichloromethane as an eluent. Melting points were determined on an MP70 Melting Point System apparatus and were not corrected.

^{1}H-, COSY-, APT-, HMBC- and HSQC-NMR spectra were recorded on a Bruker Avance 500 MHz (Bruker Corporation, Billerica, MA, USA) in $CDCl_3$ at an ambient temperature, using solvent peaks as the internal reference. Chemical shift (δ) values are reported in ppm. High-resolution accurate mass measurements were performed employing Orbitrap Exploris 120 (Thermo Fisher Scientific, 168 Third Avenue, Waltham, MA, USA) operating at the Full Scan mode at a 120,000 resolution. The IR spectrum was recorded on a Thermo Scientific Nicolet iS50 Spectrometer (ATR accessory; no. of scans: 64; resolution: 4; data spacing: 0.482 cm^{-1}).

3.2. Synthesis and Characterization

General Procedure for synthesis of derivatives **2**–**5**:

In a 25 mL round bottom flask, a mixture of 0.3 g (0.8 mmol) of 3-bromo-9-nitrobenzan throne, 0.5 g of the corresponding heterocycle and 5 mL of 1-methyl-2-pyrrolidone was heated at 90–100 °C for 2–3 h. After cooling, a mixture of 5 mL of ethanol and 10 mL of water was added; the precipitate was filtered off and dried. The resulting solid was dissolved in dichloromethane and purified with column chromatography on silica gel 40/100 as an eluent using toluene.

3-Morpholino-9-nitro-7H-benzo[de]anthracen-7-one (**2**), Obtained as a red compound in a 58% yield with an m.p. of 229–230 °C. R_f = 0.63 (eluent C_6H_6-CH_3CN, *v/v* 3:1). ^{1}H NMR (500 MHz, $CDCl_3$) δ 9.19 (d, *J* = 2.4 Hz, 1H, (8)), 8.75 (d, *J* = 7.3 Hz, 1H, (6)), 8.55 (d, *J* = 8.3 Hz, 1H, (4)), 8.39 (d, *J* = 6.8 Hz, 1H, (10)), 8.38 (d, *J* = 6.5 Hz, 1H, (1)), 8.30 (d, *J* = 8.9 Hz, 1H, (11)), 7.76 (t, *J* = 7.8 Hz, 1H, (5)), 7.21 (d, *J* = 8.1 Hz, 1H, (2)), 3.98 (t, *J* = 4.5 Hz, 4H, (2′, 6′)), 3.21 (t, *J* = 4.5 Hz, 4H, (3′, 5′)). ^{13}C NMR (126 MHz, $CDCl_3$) δ 182.17 (C=O), 154.28 (C), 146.61 (C), 141.30 (C), 131.65 (CH, (4)), 130.86 (CH, (6)), 130.46 (C), 129.76 (C), 128.57 (C), 127.88 (C), 127.46 (CH, (1)), 126.82 (CH, (10)), 126.29 (CH, (5), 123.94 (CH, (11)), 123.72 (CH, (8)), 119.77 (C), 115.10 (CH, (2)), 67.08 (CH_2, (2′, 6′)), 53.79 (CH_2, (3′, 5′)). FTIR (neat): 655, 649, 709, 744, 756, 768, 794, 804, 833, 872, 903, 925, 945, 954, 979, 1024, 1040, 1052, 1067, 1081, 1092, 1126, 1157, 1179, 1212, 1249, 1278, 1303, 1319, 1361, 1385, 1407, 1439, 1460, 1477, 1506, 1569, 1582, 1595, 1646, 2885, 2991, 3054. ESI-FTMS: calculated for [$C_{21}H_{16}N_2O_4$ + H^+]: 361.1183, found: 361.1181.

9-Nitro-3-(pyrrolidin-1-yl)-7H-benzo[de]anthracen-7-one (**3**), Obtained as a red compound in a 63% yield with an m.p. of 257–258 °C. R_f = 0.73 (eluent C_6H_6-CH_3CN, *v/v* 3:1). ^{1}H NMR (500 MHz, $CDCl_3$) δ 9.21 (d, *J* = 2.6 Hz, 1H, (8)), 8.78 (d, *J* = 7.3 Hz, 1H, (6)), 8.65 (d, *J* = 8.4 Hz, 1H, (4)), 8.33 (dd, *J* = 8.9, 2.6 Hz, 1H, (10)), 8.26 (d, *J* = 8.7 Hz, 1H, (1)), 8.20 (d, *J* = 8.9 Hz, 1H, (11)), 7.63 (dd, *J* = 7.9 Hz, 1H, (5)), 6.83 (d, *J* = 8.7 Hz, 1H, (2)), 3.76–3.70 (m, 4H, (2′, 5′)), 2.09–2.03 (m, 4H, (3′, 4′)). ^{13}C NMR (126 MHz, $CDCl_3$) δ 133.24 (CH, (4)), 130.99 (CH, (6)), 128.92 (CH, (1)), 126.42 (CH, (10)), 124.07 (CH, (8)), 123.72 (CH, (5)), 123.11 (CH, (11)), 108.86 (CH, (2)), 53.48 (CH_2, (2′, 5′)), 26.10 (CH_2, (3′, 4′)). FTIR (neat): 661, 675, 696, 743, 761, 768, 796, 818, 841, 861, 875, 890, 921, 966, 1007, 1039, 1072, 1100, 1113, 1146,

1169, 1213, 1242, 1266, 1290, 1312, 1344, 1405, 1444, 1497, 1524, 1556, 1567, 1582, 1603, 1644, 2847, 2959, 3083. ESI-FTMS: calculated for [$C_{21}H_{16}N_2O_3$ + H^+]: 345.1234, found: 345.1232.

3-(4-Methylpiperazin-1-yl)-9-nitro-7H-benzo[de]anthracen-7-one (**4**), Obtained as a red compound in a 59% yield with an m.p. of 271–273 °C. R_f = 0.02 (eluent C_6H_6-CH_3CN, *v/v* 3:1). ^{1}H NMR (500 MHz, $CDCl_3$) δ 9.14 (d, J = 2.5 Hz, 1H, (8)), 8.72 (dd, J = 7.3, 1.4 Hz, 1H, (6)), 8.51 (dd, J = 8.3, 1.4 Hz, 1H, (4)), 8.34 (dd, J = 8.9, 2.6 Hz, 1H, (10)), 8.31 (d, J = 8.2 Hz, 1H, (1)), 8.23 (d, J = 9.0 Hz, 1H, (11)), 7.73 (dd, J = 8.3, 7.3 Hz, 1H, (5)), 7.18 (d, J = 8.2 Hz, 1H, (2)), 3.24 (t, J = 4.8 Hz, 4H, CH_2), 2.71 (brs, 4H, CH_2), 2.40 (s, 3H, CH_3). ^{13}C NMR (126 MHz, $CDCl_3$) δ 182.26 (C=O), 154.66, 146.53, 141.43, 131.88 (CH, (4)), 130.81 (CH, (6)), 130.39, 129.75, 128.52, 127.93, 127.56 (CH, (1)), 126.80 (CH, (10)), 126.10 (CH, (5)), 123.89 (CH, (11)), 123.77 (CH, (8)), 119.33, 115.10 (CH, (2)), 77.28, 77.03, 76.77, 55.26, 53.35, 46.19. FTIR (neat): 402, 479, 505, 596, 654, 699, 749, 777, 828, 889, 925, 956, 1010, 1073, 1141, 1169, 1242, 1287, 1328, 1372, 1453, 1503, 1575, 1651, 2692, 2786, 2833, 2939, 3090. ESI-FTMS: calculated for [$C_{22}H_{19}N_3O_3$ + H^+]: 374.1499, found: 374.1485.

9-Nitro-3-(piperidin-1-yl)-7H-benzo[de]anthracen-7-one (**5**), Obtained as a red compound in a 60% yield with an m.p. of 251–252 °C. R_f = 0.92 (eluent C_6H_6-CH_3CN, *v/v* 3:1). ^{1}H NMR (500 MHz, $CDCl_3$) δ 9.13 (d, *J* = 2.5 Hz, 1H, (8)), 8.70 (d, *J* = 7.3 Hz, 1H, (6)), 8.48 (d, *J* = 8.3 Hz, 1H, (4)), 8.31 (dd, *J* = 8.9, 2.6 Hz, 1H, (10)), 8.27 (d, *J* = 8.2 Hz, 1H, (1)), 8.20 (d, *J* = 8.9 Hz, 1H, (11)), 7.71 (dd, *J* = 7.8 Hz, 1H), 7.11 (d, *J* = 8.2 Hz, 1H), 3.16 (s, 4H), 1.84 (p, *J* = 5.6 Hz, 4H), 1.67 (p, *J* = 5.8 Hz, 2H). ^{13}C NMR (126 MHz, $CDCl_3$) δ 182.30 (C=O), 156.09 (C), 146.32 (C), 141.57 (C), 132.21 (CH, (4)), 130.74 (CH, (6)), 130.23 (C), 129.76 (C), 128.44 (C), 128.05 (C), 127.70 (CH, (1)), 126.68 (CH, (10)), 125.85 (CH, (5)), 123.76 (CH, (11)), 123.76 (CH, (8)), 118.54 (C), 114.82 (CH, (2)), 54.93 (CH_2, (2′, 6′)), 26.31 (CH_2, (3′, 5′)), 24.39 (CH_2, (4′)). FTIR (neat): 406, 452, 478, 530, 586, 619, 666, 697, 743, 774, 824, 888, 921, 952, 989, 1025, 1068, 1128, 1169, 1229, 1273, 1329, 1376, 1440, 1505, 1570, 1645, 2662, 2702, 2738, 2818, 2852, 2919, 3066, 3109, 3997. ESI-FTMS: calculated for [$C_{22}H_{18}N_2O_3$ + H^+]: 359.1390, found: 359.1381.

3-(Piperidin-1-yl)-7H-benzo[de]anthracen-7-one (**6**), Obtained from 3-bromobenzanthrone at 120–130 °C for 6–7 h as an orange compound in a 48% yield with an m.p. of 165–166 °C. R_f = 0.94 (eluent C_6H_6-CH_3CN, *v/v* 3:1). ^{1}H NMR (500 MHz, $CDCl_3$) δ 8.67 (d, J = 7.3 Hz, 1H, (8)), 8.46 (d, J = 8.3 Hz, 1H, (4)), 8.38 (d, J = 7.9 Hz, 1H, (6)), 8.21 (d, J = 8.1 Hz, 1H, (1)), 8.12 (d, J = 8.2 Hz, 1H, (11)), 7.65 (dd, J = 7.8 Hz, 1H, (5)), 7.58 (dd, J = 7.6 Hz, 1H, (10)), 7.38 (dd, J = 7.5 Hz, 1H, (9)), 7.06 (d, J = 8.0 Hz, 1H, (2)), 3.05 (brs, 4H, (2′, 6′)), 1.79 (p, J = 5.6 Hz, 4H, (3′, 5′)), 1.61 (brs, 2H, (4′)). ^{13}C NMR (126 MHz, $CDCl_3$) δ 184.15 (C=O), 153.93 (C), 136.60 (C), 133.16 (CH, (10)), 131.26 (CH, (4)), 130.24 (C), 129.76 (CH, (6)), 129.24 (C), 129.00 (C), 128.35 (C), 127.97 (CH, (8)), 127.16 (CH, (9)), 125.49 (CH, (5)), 125.14 (CH, (1)), 122.53 (CH, (11)), 120.97 (C), 114.88 (CH, (2)), 55.01 (CH_2, (2′, 6′)), 26.46 (CH_2, (3′, 5′)), 24.48 (CH_2, (4′)). FTIR (neat): 410, 450, 473, 507, 581, 625, 653, 703, 772, 842, 878, 939, 961, 1027, 1060, 1101, 1168, 1206, 1277, 1375, 1463, 1511, 1573, 1643, 2668, 2704, 2737, 2808, 2847, 2930, 3064. ESI-FTMS: calculated for [$C_{22}H_{19}NO$ + H^+]: 314.1539, found: 314.1530.

3.3. Spectroscopic Measurements

The spectral properties of the investigated compound were measured in benzene (C_6H_6), chloroform ($CHCl_3$), ethyl acetate (EtOAc), acetone, ethanol (EtOH), dimethyl sulfoxide (DMSO) and dimethylformamide (DMF) with concentrations of 10^{-5} M at an ambient temperature in 10 mm quartz cuvettes. All solvents were of a p.a. or analytical grade. The absorption spectra were obtained using the UV-visible spectrophotometer SPECORD® 80 (Analytik Jena AG, Jena, Germany). The fluorescence emission spectra were recorded on a FLSP920 (Edinburgh Instruments Ltd., Edinburgh, UK) spectrofluorometer in the visible range 500–800 nm.

3.4. Single Crystal X-ray Diffraction Analysis

Single crystals of $C_{21}H_{16}N_2O_3$ (**3**) were investigated on a Rigaku, XtaLAB Synergy, Dualflex, HyPix diffractometer. The crystal was kept at 140.0(1) K during data collection.

Using Olex2 [40], the structure was solved with the ShelXT [41] structure solution program using Intrinsic Phasing and refined with the olex2.refine [42] refinement package using Levenberg–Marquardt minimization. Crystal data for **3** are as follows: orthorhombic, space group *Pbca* (no. 61), a = 14.4599(2) Å, b = 7.1736(2) Å, c = 29.6287(6) Å, V = 3073.4(1) Å^3, Z = 8, T = 140.0(1) K, μ(Cu Kα) = 0.822 mm^{-1}, *Dcalc* = 1.4884 g/cm^3, 19,757 measured reflections (2Θ ≤ 160°) and 3342 unique (R_{int} = 0.0356, R_{sigma} = 0.0343) that were used in all calculations. The final R_1 was 0.0430 ($I > 2\sigma(I)$) and wR_2 was 0.1216 (all data).

Diffraction data of compound **5** were collected at 150 K on a Rigaku, XtaLAB Synergy, Dualflex, HyPix diffractometer using CuKα radiation (λ = 1.54184 Å). The crystal structure was solved with direct methods [43] and refined using Gauss–Newton minimization with the help of a software package [42]. Crystal data for **5** are as follows: triclinic; a = 9.0593(1), b = 12.1264(2), c = 15.8953(2) Å, α = 87.867(1), β = 76.570(1), γ = 86.651(1)°; V = 1695.05(4) Å3, Z = 4, μ = 0.766 mm^{-1} and Dcalc = 1.404 g·cm^{-3}; space group is P $\bar{1}$; R[F2 > 2σ(F2)] = 0.0417. For further details, see crystallographic data for **5** deposited at the Cambridge Crystallographic Data Centre as the Supplementary Publication Number CCDC 2,233,481. Copies of the data can be obtained, free of charge, on application to CCDC, 12 Union Road, Cambridge CB2 1EZ, UK.

4. Conclusions

In the present research, a synthetic method for preparing new disubstituted heterylaminobenzanthrones was implemented from 9-nitro-3-bromobenzanthrone. The synthesized derivatives were obtained with 59–63% yields as crystalline deeply colored substances with an intense luminescence in organic solvents.

The obtained compounds absorb at 450–560 nm with large extinction coefficients and emit at 570–660 nm. The results obtained indicate that emission of the aimed derivatives is sensitive to the solvent polarity showing positive fluorosolvatochromism.

Taking into account the fact that the addition of an electron-withdrawing nitro group to the benzanthrone molecule increases its first- and second-order hyperpolarizability, it can be assumed that the developed fluorescent compounds have a potential prospect for application in optoelectronics.

Supplementary Materials: The following supporting information can be downloaded at: https://www.mdpi.com/article/10.3390/molecules28135171/s1, ^{1}H, APT, HMBC, HSQC NMR, FTIR spectra; FTMS (ESI) and RSA data; UV-Vis absorption and fluorescence spectra.

Author Contributions: Methodology, E.K., S.B. and A.M.; validation, A.M. and A.P.; investigation, A.M., M.C., J.S. and S.O.; resources, E.K.; writing—original draft preparation, A.M. and S.B.; writing—review and editing, E.K.; supervision, E.K.; funding acquisition, A.M. and E.K. All authors have read and agreed to the published version of the manuscript.

Funding: This research was funded by Daugavpils University Research Project. Project No. 14-95/2023/10.

Institutional Review Board Statement: Not applicable.

Informed Consent Statement: Not applicable.

Data Availability Statement: Data are contained within this article or Supplementary Material.

Acknowledgments: Rūdolfs Beļaunieks is acknowledged for the advice on the NMR analysis.

Conflicts of Interest: The authors declare no conflict of interest.

Sample Availability: Samples of the compounds are available from the authors.

References

1. Zacharioudaki, D.-E.; Fitilis, I.; Kotti, M. Review of Fluorescence Spectroscopy in Environmental Quality Applications. *Molecules* **2022**, *27*, 4801. [CrossRef]
2. Yang, Q.; Ma, H.; Liang, Y.; Dai, H. Rational Design of High Brightness NIR-II Organic Dyes with S-D-A-D-S Structure. *Acc. Mater. Res.* **2021**, *2*, 170–183. [CrossRef]

3. Mohd Yusof Chan, N.N.; Idris, A.; Zainal Abidin, Z.H.; Tajuddin, H.A.; Abdullah, Z. White Light Employing Luminescent Engineered Large (Mega) Stokes Shift Molecules: A Review. *RSC Adv.* **2021**, *11*, 13409–13445. [CrossRef]
4. Wünsch, U.J.; Murphy, K.R.; Stedmon, C.A. Fluorescence Quantum Yields of Natural Organic Matter and Organic Compounds: Implications for the Fluorescence-Based Interpretation of Organic Matter Composition. *Front. Mar. Sci.* **2015**, 2. [CrossRef]
5. Zheng, Q.; Juette, M.F.; Jockusch, S.; Wasserman, M.R.; Zhou, Z.; Altman, R.B.; Blanchard, S.C. Ultra-Stable Organic Fluorophores for Single-Molecule Research. *Chem. Soc. Rev.* **2014**, *43*, 1044–1056. [CrossRef]
6. Altaf, Y.; Ullah, S.; Khan, F.A.; Maalik, A.; Rubab, S.L.; Hashmi, M.A. Finding New Precursors for Light Harvesting Materials: A Computational Study of the Fluorescence Potential of Benzanthrone Dyes. *ACS Omega* **2021**, *6*, 32334–32341. [CrossRef] [PubMed]
7. Grabchev, I.; Bojinov, V.; Moneva, I. The synthesis and application of fluorescent dyes based on 3-amino benzanthrone. *Dyes Pigment.* **2001**, *48*, 143–150. [CrossRef]
8. Tsiko, U.; Sych, G.; Volyniuk, D.; Bezvikonnyi, O.; Keruckiene, R.; Lazauskas, A.; Grazulevicius, J.V. Self-recovering mechanochromic luminescence of the derivatives of benzanthrone and carbazole: Towards damage-resistive information recording and security probes. *Dyes Pigment.* **2022**, *199*, 110082. [CrossRef]
9. Gavarane, I.; Kirilova, E.; Rubenina, I.; Mežaraupe, L.; Osipovs, S.; Deksne, G.; Pučkins, A.; Kokina, I.; Bulanovs, A.; Kirjušina, M. A Simple and Rapid Staining Technique for Sex Determination of Trichinella Larvae Parasites by Confocal Laser Scanning Microscopy. *Microsc. Microanal.* **2019**, *25*, 1491–1497. [CrossRef] [PubMed]
10. Rubenina, I.; Gavarane, I.; Kirilova, E.; Mezaraupe, L.; Kirjusina, M. Comparison of the Benzanthrone Luminophores: They Are Not Equal for Rapid Examination of Parafasciolopsis Fasciolaemorpha (Trematoda: Digenea). *Biomolecules* **2021**, *11*, 598. [CrossRef]
11. Kirilova, E.; Mickevica, I.; Mezaraupe, L.; Puckins, A.; Rubenina, I.; Osipovs, S.; Kokina, I.; Bulanovs, A.; Kirjusina, M.; Gavarane, I. Novel Dye for Detection of Callus Embryo by Confocal Laser Scanning Fluorescence Microscopy. *Luminescence* **2019**, *34*, 353–359. [CrossRef] [PubMed]
12. Vus, K.; Trusova, V.; Gorbenko, G.; Sood, R.; Kirilova, E.; Kirilov, G.; Kalnina, I.; Kinnunen, P. Fluorescence Investigation of Interactions Between Novel Benzanthrone Dyes and Lysozyme Amyloid Fibrils. *J. Fluoresc.* **2014**, *24*, 493–504. [CrossRef]
13. Tarabara, U.; Kirilova, E.; Kirilov, G.; Vus, K.; Zhytniakivska, O.; Trusova, V.; Gorbenko, G. Benzanthrone Dyes as Mediators of Cascade Energy Transfer in Insulin Amyloid Fibrils. *J. Mol. Liq.* **2021**, *324*, 115102. [CrossRef]
14. Grabchev, I.; Moneva, I.; Wolarz, E.; Bauman, D. Fluorescent 3-Oxy Benzanthrone Dyes in Liquid Crystalline Media. *Dyes Pigm* **2003**, *58*, 1–6. [CrossRef]
15. Grabtchev, I.K.; Bojinov, V.B.; Moneva, I.T. Functional Properties of Azomethine Substituted Benzanthrone Dyes for Use in Nematic Liquid Crystals. *J. Mol. Struct.* **1998**, *471*, 19–25. [CrossRef]
16. Konstantinova, T.; Bojadgieva, J. On the Polymerization of Styrene in the Presence of Some Benzanthrone Dyes. *Angew. Makromolek. Chem.* **1993**, *205*, 91–95. [CrossRef]
17. Konstantinova, T.N. The Synthesis of Some Benzanthrone Derivatives for Use as Dyes for Polymeric Materials. *Dyes Pigment.* **1989**, *10*, 63–67. [CrossRef]
18. Staneva, D.; Vasileva-Tonkova, E.; Grabchev, I. PH Sensor Potential and Antimicrobial Activity of a New PPA Dendrimer Modified with Benzanthrone Fluorophores in Solution and on Viscose Fabric. *J. Photochem. Photobiol. A Chem.* **2019**, *375*, 24–29. [CrossRef]
19. Maļeckis, A.; Avotiņa, L.; Ķizāne, G.; Pučkins, A.; Osipovs, S.; Kirilova, E. New Fluorescent Heterocyclic Compounds Derived From 3-Cyanobenzanthrone. *Polycycl. Aromat. Compd.* **2022**, *42*, 5508–5520. [CrossRef]
20. Adam, A.M.A.; Altalhi, T.A.; El-Megharbel, S.M.; Saad, H.A.; Refat, M.S.; Grabchev, I.; Althobaiti, R.A. Capturing of Environment Polluting Metal Ions Co^{2+}, Ni^{2+}, Cu^{2+}, and Zn^{2+} Using a 3-Azomethine Benzanthrone-Based Fluorescent Dye: Its Synthesis, Structural, and Spectroscopic Characterizations. *Russ. J. Gen. Chem.* **2020**, *90*, 2394–2399. [CrossRef]
21. Bentley, P.; McKellar, J.F.; Phillips, G.O. The photochemistry of benz[de]anthracen-7-ones. Part I. Electronic absorption and emission spectroscopy. *J. Chem. Soc. Perkin Trans. 2* **1974**, *5*, 523–526. [CrossRef]
22. Nepraš, M.; Machalický, O.; Šeps, M.; Hrdina, R.; Kapusta, P.; Fidler, V. Structure and properties of fluorescent reactive dyes: Electronic structure and spectra of some benzanthrone derivatives. *Dyes Pigment.* **1997**, *35*, 31–44. [CrossRef]
23. Kapusta, P.; Machalicky, O.; Hrdina, R.; Nepras, M.; Zimmt, B.M.; Fidler, V. Photophysics of 3-substituted benzanthrones: Substituent and solvent control of intersystem crossing. *J. Phys. Chem.* **2003**, *107*, 9740–9746. [CrossRef]
24. Orlova, N.; Nikolajeva, I.; Pučkins, A.; Belyakov, S.; Kirilova, E. Heterocyclic Schiff Bases of 3-Aminobenzanthrone and Their Reduced Analogues: Synthesis, Properties and Spectroscopy. *Molecules* **2021**, *26*, 2570. [CrossRef] [PubMed]
25. Staneva, D.; Vasileva-Tonkova, E.; Grabchev, I. A New Bioactive Complex between Zn(II) and a Fluorescent Symmetrical Benzanthrone Tripod for an Antibacterial Textile. *Materials* **2019**, *12*, 3473. [CrossRef]
26. Staneva, D.; Vasileva-Tonkova, E.; Makki, M.S.; Sobahi, T.R.; Abdel-Rahman, R.M.; Asiri, A.M.; Grabchev, I. Synthesis, photophysical and antimicrobial activity of new water soluble ammonium quaternary benzanthrone in solution and in polylactide film. *J. Photochem. Photobiol. B* **2015**, *143*, 44–51. [CrossRef] [PubMed]
27. Kirilova, E.M.; Nikolaeva, I.D.; Romanovska, E.; Pučkins, A.I.; Belyakov, S.V. The Synthesis of Novel Heterocyclic 3-Acetamide Derivatives of Benzanthrone. *Chem. Heterocycl. Compd.* **2020**, *56*, 192–198. [CrossRef]
28. Kirilova, E.M.; Puckins, A.I.; Romanovska, E.; Fleisher, M.; Belyakov, S.V. Novel Amidine Derivatives of Benzanthrone: Effect of Bromine Atom on the Spectral Parameters. *Spectrochim. Acta A Mol. Biomol. Spectrosc.* **2018**, *202*, 41–49. [CrossRef]

29. Maļeckis, A.; Griškjāns, E.; Cvetinska, M.; Savicka, M.; Belyakov, S.; Kirilova, E. Synthesis, Characterization, Spectroscopic Studies and Evaluation of Toxicological Effect on Growth of Wheat Sprouts (Triticum Aestivum) of New Benzanthrone α-Aryl-α-Aminophosphonates. *J. Mol. Struct.* **2023**, *1277*, 134838. [CrossRef]
30. Thomas, A.; Patil, P.S.; Siddlingeshwar, B.; Manohara, S.R.; Gummagol, N.B.; Krishna Chaitanya, G.; M.Kirilova, E. Nonlinear Optical Properties of Benzanthrone Derivatives with N′-Methylpiperazin-1-Yl and N′-Phenylpiperazin-1-Yl Substituents: Experimental and Quantum Chemical Study. *Opt. Laser Technol.* **2022**, *156*, 108616. [CrossRef]
31. Thomas, A.; Kirilova, E.M.; Nagesh, B.V.; Manohara, S.R.; Siddlingeshwar, B.; Belyakov, S.V. Synthesis, Solvatochromism and DFT Study of Pyridine Substituted Benzanthrone with ICT Characteristics. *J. Mol. Struct.* **2022**, *1262*, 132971. [CrossRef]
32. Cao, L.; Zhang, D.; Xu, L.; Fang, Z.; Jiang, X.-F.; Lu, F. Perylenediimide-Benzanthrone Dyad: Organic Chromophores with Enhanced Third-Order Nonlinear-Optical Activities. *Eur. J. Org. Chem.* **2017**, *2017*, 2495–2500. [CrossRef]
33. Cao, L.; Xu, L.; Zhang, D.; Zhou, Y.; Zheng, Y.; Fu, Q.; Jiang, X.-F.; Lu, F. D-A Dyad and D-A-D Triad Incorporating Triphenylamine, Benzanthrone and Perylene Diimide: Synthesis, Electrochemical, Linear and Nonlinear Optical Properties. *Chem. Phys. Lett.* **2017**, *682*, 133–139. [CrossRef]
34. Thomas, A.; Kirilova, E.M.; Nagesh, B.V.; Krishna Chaitanya, G.; Philip, R.; Manohara, S.R.; Sudeeksha, H.C.; Siddlingeshwar, B. Influence of Nitro Group on Solvatochromism, Nonlinear Optical Properties of 3-Morpholinobenzanthrone: Experimental and Theoretical Study. *J. Photochem. Photobiol. A Chem.* **2023**, *437*, 114434. [CrossRef]
35. Day, F.H. Nitration of the 13-halogenobenzanthrones. *J. Chem. Soc.* **1940**, 1474–1475. [CrossRef]
36. Rao, A.V.R.; Vaidyanathan, A. The 1H NMR Spectrum of Benzanthrone. *Spectrochim. Acta A* **1981**, *37*, 145–146. [CrossRef]
37. Takekawa, M.; Aoki, J.; Iwashima, S.; Ueda, T. Complete Assignment Of1H And13C NMR Spectra of Chlorobenzanthrones. *Magn. Reson. Chem.* **1994**, *32*, 87–92. [CrossRef]
38. Sakamoto, Y.; Ohshima, S.; Enya, T.; Suzuki, H.; Hisamatsu, Y. NMR Spectroscopy and Molecular Orbital Calculations to Interpret the Mutagenicity of Nitrobenzanthrones. *Polycycl. Aromat. Compd.* **2001**, *19*, 73–81. [CrossRef]
39. Kirilova, E.M.; Belyakov, S.V.; Kirilov, G.K.; Kalnina, I.; Gerbreder, V. Luminescent properties and crystal structure of novel benzanthrone dyes. *J. Luminesc.* **2009**, *129*, 1827–1830. [CrossRef]
40. Dolomanov, O.V.; Bourhis, L.J.; Gildea, R.J.; Howard, J.A.K.; Puschmann, H. OLEX2: A complete structure solution, refinement and analysis program. *J. Appl. Crystallogr.* **2009**, *42*, 339–341. [CrossRef]
41. Sheldrick, G.M. SHELXT—Integrated space-group and crystal-structure determination. *Acta Crystallogr. A Found. Adv.* **2015**, *71*, 3–8. [CrossRef] [PubMed]
42. Bourhis, L.J.; Dolomanov, O.V.; Gildea, R.J.; Howard, J.A.K.; Puschmann, H. The anatomy of a comprehensive constrained, restrained refinement program for the modern computing environment—Olex2 dissected. *Acta Crystallogr. A Found. Adv.* **2015**, *71*, 59–75. [CrossRef] [PubMed]
43. Burla, M.C.; Caliandro, R.; Camalli, M.; Carrozzini, B.; Cascarano, G.L.; De Caro, L.; Giacovazzo, C.; Polidori, G.; Siliqi, D.; Spagna, R. IL MILIONE: A suite of computer programs for crystal structure solution of proteins. *J. Appl. Cryst.* **2007**, *40*, 609–613. [CrossRef]

4. pielikums
Appendix IV

Maļeckis, A.; Cvetinska, M.; Griškjāns, E.; Dmitrijevs, K.; Traskovskis, K.; Belyakov, S.; Kirilova, E.

Benzanthrone Sulfides: Synthesis, Solvatochromism Characterization and Analysis of Experimental Photophysical Parameters and Theoretical Calculations

Dyes and Pigments ***2023****, 219, 111599.*

https://doi.org/10.1016/j.dyepig.2023.111599

Dyes and Pigments 219 (2023) 111599

Contents lists available at ScienceDirect

Dyes and Pigments

journal homepage: www.elsevier.com/locate/dyepig

Benzanthrone sulfides: synthesis, solvatochromism characterization and analysis of experimental photophysical parameters and theoretical calculations

Armands Maļeckis [a,*], Marija Cvetinska [a], Evans Griškjāns [a], Kirills Dmitrijevs [b], Kaspars Traskovskis [b], Sergey Belyakov [c], Elena Kirilova [d]

[a] Institute of Technology of Organic Chemistry, Faculty of Materials Science and Applied Chemistry, Riga Technical University, P. Valdena Str. 3, LV-1048, Riga, Latvia
[b] Institute of Applied Chemistry, Faculty of Materials Science and Applied Chemistry, Riga Technical University, P. Valdena Str. 3, LV-1048, Riga, Latvia
[c] Latvian Institute of Organic Synthesis, Aizkraukles Str. 21, LV-1006, Riga, Latvia
[d] Department of Applied Chemistry, Institute of Life Sciences and Technology, Daugavpils University, Parades Str. 1A, LV-5401, Daugavpils, Latvia

ARTICLE INFO

Keywords:
Benzanthrone: fluorescence
Sulfides
Solvatochromism: aromatic substitution
DFT calculations

ABSTRACT

In this paper the synthesis, characterization, and photophysical properties of benzanthrone-derived sulfides are discussed. The compounds were synthesized using a practical method of nucleophilic aromatic substitution reactions of 3-bromobenzanthrone with thiols. Structural characterization was conducted using nuclear magnetic resonance (NMR) and Fourier-transform (FTIR) spectroscopy and high-resolution mass spectrometry, confirming the chemical structures. The crystal structure of a compound was determined via X-ray diffraction, revealing π-π stacking interactions and intermolecular hydrogen bonding. Photophysical analysis showed solvatochromic effects (emission of light upon excitation from 507 nm in benzene to 591 nm in ethanol) and attributed fluorescence to intramolecular charge transfer. Computational analysis using DFT calculations provided further insights into the compounds' properties, including excited state energies and the potential for efficient intersystem crossing. Overall, the research provides a comprehensive understanding of the newly synthesized benzanthrone alkyl and aryl sulfides as well as a phenylselanyl derivative. The photophysical properties, charge transfer characteristics observed in the compounds and the solvatochromic effects exhibited by the compounds suggest their potential to be utilized for developing sensors for detecting environmental changes, chemical substances or biological targets.

1. Introduction

Fluorescent dyes have gained significant importance in both industrial and scientific domains. The phenomenon of fluorescence arises from the unique properties of molecules in their excited state, primarily due to the presence of conjugated pi-systems. The effectiveness of fluorescence emission is influenced by various factors, such as the molecular structure and the surrounding solvent environment.

Fluorescent molecules possess several key characteristics that determine their practicality in various applications. Useful fluorescent molecules should have a high fluorescence quantum yield, which measures the efficiency of fluorescence emission compared to other competing processes [1]. Another important characteristic is the Stokes shift, which represents the difference between the excitation and emission wavelengths. It indicates the extent of relaxation that occurs in the excited state before fluorescence emission. A larger Stokes shift suggests a higher degree of relaxation and implies a more efficient fluorescence emission process [2]. Furthermore, the photostability of a fluorescent organic compound is a pivotal factor to consider. A photostable compound will experience minimal deterioration or loss of fluorescence intensity over time, ensuring accurate and consistent data acquisition [3]. These features render them valuable for a wide array of applications.

Benzanthrone derivatives with donor–π–acceptor (D–π–A) architecture, belonging to the anthrone dye family, have garnered significant interest due to their remarkable luminescent properties. These compounds exhibit exceptional characteristics such as photostability, significant Stokes shifts, noticeable solvatochromism, and fluorescence

* Corresponding author.
E-mail address: armands5maleckis@inbox.lv (A. Maļeckis).

https://doi.org/10.1016/j.dyepig.2023.111599
Received 25 May 2023; Received in revised form 1 August 2023; Accepted 1 August 2023
Available online 3 August 2023

emission spanning from green to red, controllable through molecular substitutions and the properties of the surrounding solvent [4–6]. These features make them useful in a variety of functional materials. In former studies it has been shown that benzanthrone derivatives as fluorescent probes can be used to selectively detect amyloid fibrils of the lysozyme enzyme [7,8] and enable the diagnosis of plant species' callus embryos [9], parasitic trematodes and nematodes through confocal laser scanning microscopy imaging [10–12], sensing of oxygen [13], as well as probes for the pH of solutions [14] and cations [15]. Utility of benzanthrone dyes in polymeric materials [16–19] and liquid crystal displays [20,21], and non-linear properties [22–25] have also been demonstrated previously.

Sulfur-containing compounds are gaining widespread interest in the scientific community. For instance, pyrene derivatives of vinyl sulfides and sulfoxides [26], dithiafulvene moiety containing compounds [27], rhodamine sulfones as NIR fluorescent probes in biological systems [28], 1,5-bis-(4-alkylphenylthio) anthraquinone dyes with potential for liquid crystal systems [29,30], triarylcyclopentadiene with thiophene ring and dibenzothiophene group were used for production of blue OLEDs [31] and many more such compounds and their applications were comprehensively reviewed in recently published paper [32].

While 3-mercaptobenzanthrone [33] was reported previously and 14*H*-anthra[2,1,9-*m*,*n*,*a*]thioxanthen-14-one was examined as semiconducting compound [34], and phenothiazine-based benzanthrone compounds with thermally activated delayed fluorescence were described earlier [35], due to the scarcity of available data regarding thioalkyl and thiophenyl derivatives of benzanthrone, we have made the decision to undertake the synthesis and analysis of benzanthrone compounds containing sulfur and selenium with the aim to expand the knowledge base in this area.

2. Experimental

2.1. Materials and general measurements

All of the reagents and solvents were obtained commercially and used without any additional purification.

The assessment of the progress of reactions and purity of the synthesized compounds was performed by TLC on MERCK Silica gel 60 F_{254} plates in hexane/acetone (3:1) as an eluent and visualized under UV light. Melting points were determined on METTLER TOLEDO™ Melting Point System MP70 apparatus. ^{1}H- and APT-NMR spectra were recorded on a Bruker Avance 500 MHz (Bruker Corporation, Billerica, MA, USA) in $CDCl_3$ at ambient temperature, using solvent peaks as the internal reference. Chemical shift (δ) values are reported in ppm. High-resolution accurate mass measurements were performed employing Orbitrap Exploris 120 (Thermo Fischer Scientific) operating at Full Scan mode at 120,000 resolution.

Single crystals of compound ***2b*** were investigated on a Rigaku, XtaLAB Synergy, Dualflex, HyPix diffractometer. The crystal was kept at 150.0(1) K during data collection. Using Olex2 [36], the structure was solved with the ShelXT [37] structure solution program using Intrinsic Phasing and refined with the olex2.refine [38] refinement package using Gauss-Newton minimization.

The spectral properties of the investigated compound were measured at an ambient temperature in 10 mm quartz cuvettes in hexane, benzene, chloroform, ethyl acetate (EtOAc), acetone, ethanol (EtOH), dimethyl sulfoxide (DMSO) and dimethylformamide (DMF) with concentrations 10^{-5} M. All solvents were of p.a. or analytical grade. The fluorescence emission spectra were recorded on a FLSP920 (Edinburgh Instruments Ltd, UK) spectrofluorometer in the visible range 450–800 nm and the absorption spectra were obtained using the UV–visible spectrophotometer SPECORD® 80 (Analytik Jena AG, Germany). PL lifetime measurements were performed with QuantaMaster 40 spectrofluorometer (Photon Technology International, Inc.) using a 410 nm diode laser excitation source. Low temperature measurements of Zeonex film sample were performed in liquid-nitrogen filled quartz dewar.

Density functional theory (DFT) calculations for ground state geometry optimization and time-dependent DFT (TD-DFT) calculations for excited state energies and S_1 geometries were performed using Schrödinger Jaguar software package (release 2022–1) [39]. Geometry optimization and TD-DFT calculations employed PBE0-D3 functional and 6–31g* basis [40]. Dispersion forces were accounted for using dispersion correction (D3). Tamm–Dancoff approximation (TDA) was used for TD-DFT. Ground state geometry was optimized in vacuum, while conductor-like polarizable continuum model (CPCM) was used to simulate surrounding medium in TD-DFT calculations [41]. SOC matrix elements for $S_1 \rightarrow T_n$ transitions were calculated using Orca program package [42]. For this SOC-TD-DFT method was employed at PBE0/ZORA-DEF2-TZVP level.

2.2. Synthesis of compounds *2a – 2e, 3a – 3d* and *4a*

As mentioned earlier in the introduction, in the context of materials chemistry, aromatic sulfides serve as valuable building blocks due to their versatile chemical properties. Numerous review articles have formerly comprehensively detailed the mechanism and synthesis of aliphatic and aromatic sulfides through nucleophilic aromatic substitution reactions [43–45]. This study presents a practical method for synthesizing benzanthrone sulfides through nucleophilic aromatic substitution reaction by employing 3-bromobenzanthrone as the key electrophile and thiols as nucleophilic sulfur sources, the reactions were carried out under basic conditions (NaOH) in *N*-methyl-2-pyrrolidone (NMP). 3-(Phenylselanyl)-7*H*-benzo[*de*]anthracen-7-one (**4a**) was synthesized in the same fashion as aliphatic and aromatic sulfides from sodium benzeneselenolate in the absence of base in accordance with the previously reported procedure [46].

Target compounds were synthesized according to Scheme 1 and structures of the obtained compounds are summarized in Table 1.

2.3. General methodology

A 25 mL flask was charged with 3-bromobenzanthrone (618 mg, 2 mmol) and NaOH (84 mg, 2,02 mmol). The flask was then evacuated and filled with argon. NMP and corresponding thiol (2,1 mmol) was added through septum, followed with heating at 80 °C for 2 h. Upon completion (TLC control), reaction mixture was poured into water and stirred for 15 min. Precipitate was then vacuum filtered and dried at room temperature in desiccator. Finally, product was recrystallized from chlorobenzene to produce pure compound.

2.3.1. 3-(methylthio)-7H-benzo[de]anthracen-7-one (2a)

Orange solid. Yield: 59%. Melting point: 153 °C. $R_f = 0.45$ (Hexane/Acetone; 3:1). IR, λ_{max} (neat) cm^{-1}: 656, 685, 697, 743, 772, 842, 944, 1040, 1051, 1081, 1095, 1124, 1157, 1188, 1215, 1249, 1277, 1303, 1314, 1359, 1381, 1408, 1431, 1460, 1479, 1506, 1568,1580, 1597, 1645, 2990, 3055.^{1}H NMR (500 MHz, $CDCl_3$) δ 8.74 (d, $J = 7.3$ Hz, 1H), 8.54 (d, $J = 8.3$ Hz, 1H), 8.45 (d, $J = 7.9$ Hz, 1H), 8.17 (dd, $J = 13.1$, 8.1 Hz, 2H), 7.74 (t, $J = 7.8$ Hz, 1H), 7.68 (t, $J = 7.6$ Hz, 1H), 7.50 (t, $J = 7.5$ Hz, 1H), 7.32 (d, $J = 8.0$ Hz, 1H), 2.63 (s, 3H). ^{13}C NMR (126 MHz, $CDCl_3$) δ 183.53 (C=O), 140.28 (C), 136.11 (C), 133.29 (CH), 130.72 (CH), 130.67 (C), 130.43 (C), 129.98 (CH), 128.82 (C), 128.05 (C), 128.00 (CH), 127.80 (CH), 126.27 (CH), 123.92 (CH), 123.48 (C), 122.61 (CH), 122.17 (CH), 15.50 (CH_3). FTMS (ESI) *m/z*: [M + H]+ calculated for $C_{18}H_{12}OS$: 277.0682, found: 277.0680.

2.3.2. 3-(isopropylthio)-7H-benzo[de]anthracen-7-one (2b)

Yellow solid. Yield: 67%. Melting point: 131 °C. $R_f = 0.49$ (Hexane/Acetone; 3:1). IR, λ_{max} (neat) cm^{-1}: 697, 752, 776, 805, 840, 879, 902, 931, 944, 956, 1043, 1051, 1070, 1083, 1096, 1156, 1174, 1193, 1210, 1278, 1304, 1320, 1358, 1366, 1383, 1407, 1461, 1479, 1507, 1567, 1581, 1596, 1607, 1646, 2863, 2897, 2913, 2924, 2954, 2973, 3007,

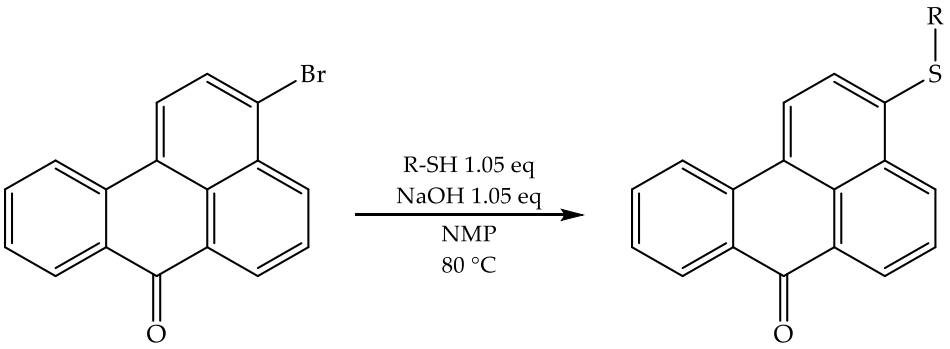

Scheme 1. Synthesis of reported benzanthrone sulfides.

Table 1
The summary of structures of the obtained compounds.

Compound	Structure	Yield, %	Compound	Structure	Yield, %
2a	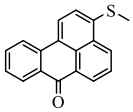	59	**3a**	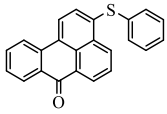	70
2b	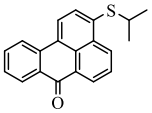	67	**3b**	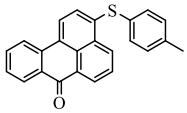	73
2c	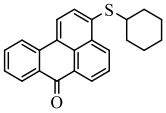	69	**3c**	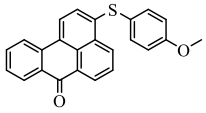	54
2d	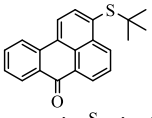	70	**3d**	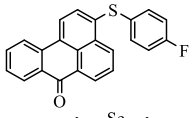	61
2e	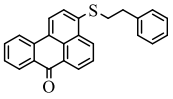	86	**4a**	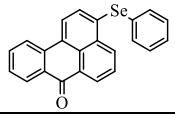	60

3067.^{1}H NMR (500 MHz, $CDCl_3$) δ 8.78 (dd, J = 8.4, 1.3 Hz, 1H), 8.71 (dd, J = 7.3, 1.3 Hz, 1H), 8.40 (dd, J = 7.8, 1.5 Hz, 1H), 8.26 (d, J = 7.9 Hz, 1H), 8.20 (d, J = 8.1 Hz, 1H), 7.73 (t, J = 7.7 Hz, 1H), 7.68 (d, J = 7.9 Hz, 1H), 7.67–7.62 (m, 1H), 7.49–7.42 (m, 1H), 3.47 (hept, J = 6.7 Hz, 1H), 1.31 (d, J = 6.7 Hz, 6H). ^{13}C NMR (126 MHz, $CDCl_3$) δ 183.67 (C=O), 137.32 (C), 136.00 (C), 133.42 (CH), 133.29 (C), 132.57 (CH), 130.76 (C), 130.15 (CH), 129.84 (CH), 128.98 (C), 128.57 (C), 128.25 (CH), 128.13 (CH), 126.70 (CH), 125.69 (C), 123.71 (CH), 122.93 (CH), 38.89 ($\underline{C}H(CH_3)_2$), 23.21 ($CH(\underline{C}H_3)_2$). FTMS (ESI) *m/z*: $[M + H]^+$ calculated for $C_{20}H_{16}OS$: 305.0995, found: 305.0992.

2.3.3. 3-(cyclohexylthio)-7H-benzo[de]anthracen-7-one (2c)

Yellow solid. Yield: 69%. Melting point: 181 °C. R_f = 0.53 (Hexane/Acetone; 3:1). IR, λ_{max} (neat) cm^{-1}: 686, 698, 748, 769, 803, 819, 835, 943, 999, 1026, 1041, 1052, 1082, 1096, 1128, 1172, 1198, 1216, 1255, 1279, 1303, 1317, 1357, 1381, 1451, 1479, 1507, 1567, 1580, 1596, 1606, 1646, 2844, 2886, 2927, 2939, 2990, 3053.^{1}H NMR (500 MHz, $CDCl_3$) δ 8.74 (d, J = 8.3 Hz, 1H), 8.66 (d, J = 7.2 Hz, 1H), 8.36 (dd, J = 7.9, 1.1 Hz, 1H), 8.16 (d, J = 7.9 Hz, 1H), 8.12 (d, J = 8.1 Hz, 1H), 7.69 (t, J = 7.8 Hz, 1H), 7.64–7.56 (m, 2H), 7.41 (t, J = 7.5 Hz, 1H), 3.17 (tt, J = 10.6, 3.7 Hz, 1H), 2.01–1.89 (m, 2H), 1.77–1.67 (m, 2H), 1.58–1.50 (m, 1H), 1.46–1.34 (m, 2H), 1.31–1.14 (m, 3H). ^{13}C NMR (126 MHz, $CDCl_3$) δ 183.59 (C=O), 136.92 (C), 135.97 (C), 133.35 (CH), 133.32 (C), 132.59 (CH), 130.68 (C), 130.07 (CH), 129.76 (CH), 128.90 (C), 128.51 (C), 128.16 (CH), 128.06 (CH), 126.61 (CH), 125.50 (C), 123.66 (CH), 122.87 (CH), 47.18 (CH), 33.39 (CH_2), 26.03 (CH_2), 25.74 (CH_2). FTMS (ESI) *m/z*: $[M + H]^+$ calculated for $C_{23}H_{20}OS$: 345.1308, found: 345.1304.

2.3.4. 3-(tert-butylthio)-7H-benzo[de]anthracen-7-one (2d)

Yellow solid. Yield: 70%. Melting point: 163 °C. R_f = 0.54 (Hexane/Acetone; 3:1). IR, λ_{max} (neat) cm^{-1}: 655, 697, 751, 781, 803, 847, 863, 880, 901, 942, 960, 1025, 1040, 1051, 1076, 1092, 1163, 1194, 1205, 1220, 1276, 1304, 1316, 1367, 1383, 1459, 1469, 1503, 1565, 1581,

1596, 1654, 2862, 2895, 2925, 2957, 2977, 3065.^{1}H NMR (500 MHz, $CDCl_3$) δ 9.03 (dd, J = 8.4, 1.4 Hz, 1H), 8.67 (dd, J = 7.2, 1.4 Hz, 1H), 8.37 (dd, J = 7.9, 1.5 Hz, 1H), 8.24 (d, J = 7.7 Hz, 1H), 8.18 (d, J = 8.1 Hz, 1H), 7.86 (d, J = 7.7 Hz, 1H), 7.72 (dd, J = 8.4, 7.2 Hz, 1H), 7.62 (ddd, J = 8.4, 7.2, 1.5 Hz, 1H), 7.45 (t, J = 7.5 Hz, 1H), 1.24 (s, 9H). ^{13}C NMR (126 MHz, $CDCl_3$) δ 183.60 (C=O), 137.53 (CH), 136.29 (C), 135.71 (C), 134.67 (CH), 134.15 (C), 133.41 (CH), 130.97 (C), 130.09 (CH), 128.78 (C), 128.65 (CH), 128.57 (C), 128.10 (CH), 127.92 (C), 126.81 (CH), 123.20 (CH), 123.15 (CH), 48.40 ($\underline{C}(CH_3)_3$), 31.38 (C($\underline{C}H_3)_3$). FTMS (ESI) m/z: $[M + H]^+$ calculated for $C_{21}H_{18}OS$: 319.1151, found: 319.1149.

2.3.5. 3-(phenethylthio)-7H-benzo[de]anthracen-7-one (2e)

Orange solid. Yield: 86%. Melting point: 180 °C. R_f = 0.43 (Hexane/Acetone; 3:1). IR, λ_{max} (neat) cm^{-1}: 655, 695, 733, 747, 775, 804, 839, 874, 904, 943, 959, 1029, 1041, 1051, 1081, 1094, 1126, 1166, 1204, 1277, 1305, 1316, 1356, 1380, 1405, 1453, 1478, 1497, 1505, 1564, 1579, 1597, 1641, 2847, 2926, 3030, 3060.^{1}H NMR (500 MHz, $CDCl_3$) δ 8.80 (d, J = 7.2 Hz, 1H), 8.73 (d, J = 8.3 Hz, 1H), 8.50 (d, J = 7.8 Hz, 1H), 8.31 (d, J = 7.9 Hz, 1H), 8.27 (d, J = 8.1 Hz, 1H), 7.80 (t, J = 7.8 Hz, 1H), 7.73 (t, J = 7.5 Hz, 1H), 7.63 (d, J = 7.9 Hz, 1H), 7.55 (t, J = 7.5 Hz, 1H), 7.35 (t, J = 7.4 Hz, 2H), 7.32–7.24 (m, 3H), 3.36 (t, J = 7.8 Hz, 2H), 3.06 (t, J = 7.8 Hz, 2H). ^{13}C NMR (126 MHz, $CDCl_3$) δ 183.61 (C=O), 139.79 (C), 138.22 (C), 136.04 (C), 133.41 (CH), 131.96 (C), 131.68 (CH), 130.64 (C), 130.17 (CH), 128.98 (C), 128.64 (CH), 128.56 (CH), 128.46 (C), 128.12 (CH), 126.70 (CH), 126.60 (CH), 126.02 (CH), 124.80 (C), 123.84 (CH), 122.82 (CH), 35.33 (CH_2), 35.12 (CH_2). FTMS (ESI) m/z: $[M + H]^+$ calculated for $C_{25}H_{18}OS$: 367.1151, found: 367.1146.

2.3.6. 3-(phenylthio)-7H-benzo[de]anthracen-7-one (3a)

Yellow solid. Yield: 70%. Melting point: 186 °C. R_f = 0.55 (Hexane/Acetone; 3:1). IR, λ_{max} (neat) cm^{-1}: 654, 685, 698, 746, 769, 792, 811, 834, 875, 902, 944, 1018, 1040, 1050, 1079, 1125, 1178,1193, 1209, 1249, 1277, 1303, 1316, 1359, 1380, 1400, 1459, 1477, 1488, 1505, 1567, 1579, 1593, 1646, 1696, 2913, 3053.^{1}H NMR (500 MHz, $CDCl_3$) δ 8.69 (t, J = 6.6 Hz, 2H), 8.39 (d, J = 7.7 Hz, 1H), 8.19 (d, J = 7.9 Hz, 1H), 8.15 (d, J = 8.0 Hz, 1H), 7.71 (t, J = 7.8 Hz, 1H), 7.62 (t, J = 7.4 Hz, 1H), 7.51–7.42 (m, 2H), 7.31–7.23 (m, 5H). ^{13}C NMR (126 MHz, $CDCl_3$) δ 183.56 (C=O), 136.75 (C), 135.84 (C), 134.69 (C), 133.48 (CH), 132.24 (C), 132.15 (CH), 131.28 (CH), 130.79 (C), 130.28 (CH), 130.16 (CH), 129.54 (CH), 129.00 (C), 128.66 (C), 128.43 (CH), 128.16 (CH), 127.57 (CH), 127.09 (CH), 126.40 (C), 123.95 (CH), 122.99 (CH). FTMS (ESI) m/z: $[M + H]^+$ calculated for $C_{23}H_{14}OS$: 339.0838, found: 339.0836.

2.3.7. 3-(p-tolylthio)-7H-benzo[de]anthracen-7-one (3b)

Yellow solid. Yield: 73%. Melting point: 219 °C. R_f = 0.50 (Hexane/Acetone; 3:1). IR, λ_{max} (neat) cm^{-1}: 655, 671, 698, 729, 744, 778, 800, 826, 836, 869, 891, 919, 956, 993, 1023, 1047, 1071, 1111, 1133, 1170, 1186, 1207, 1229, 1247, 1261, 1274, 1298, 1311, 1333, 1369, 1439, 1448, 1461, 1506, 1521, 1572, 1584, 1600, 1646, 2841, 2859, 2894, 2963, 3079.^{1}H NMR (500 MHz, $CDCl_3$) δ 8.69 (dd, J = 10.8, 7.8 Hz, 2H), 8.38 (d, J = 7.9 Hz, 1H), 8.13 (dd, J = 10.4, 8.0 Hz, 2H), 7.71 (t, J = 7.8 Hz, 1H), 7.61 (t, J = 7.7 Hz, 1H), 7.44 (t, J = 7.5 Hz, 1H), 7.33 (d, J = 7.9 Hz, 1H), 7.26 (d, J = 7.7 Hz, 2H), 7.10 (d, J = 7.8 Hz, 2H), 2.29 (s, 3H). ^{13}C NMR (126 MHz, $CDCl_3$) δ 183.66 (C=O), 138.44 (C), 138.31 (C), 136.00 (C), 133.47 (CH), 132.56 (CH), 131.86 (CH), 131.73 (C), 130.73 (C), 130.46 (CH), 130.27 (CH), 130.01 (C), 128.99 (C), 128.58 (C), 128.45 (CH), 128.26 (CH), 128.17 (CH), 126.91 (CH), 125.62 (C), 124.00 (CH), 122.90 (CH), 21.21 (CH_3). FTMS (ESI) m/z: $[M + H]^+$ calculated for $C_{24}H_{16}OS$: 353.0995, found: 353.0993.

2.3.8. 3-((4-methoxyphenyl)thio)-7H-benzo[de]anthracen-7-one (3c)

Yellow solid. Yield: 54%. Melting point: 235 °C. R_f = 0.46 (Hexane/Acetone; 3:1). IR, λ_{max} (neat) cm^{-1}: 685, 698, 746, 770, 800, 813, 829, 875, 901, 944, 988, 1006, 1030, 1049, 1080, 1102, 1125, 1170, 1188, 1209, 1249, 1277, 1290, 1299, 1316, 1360, 1380, 1407, 1451, 1477, 1488, 1506, 1567, 1579, 1589, 1646, 1664, 2840, 2898, 2938, 2960, 3011, 3062, 3077.^{1}H NMR (500 MHz, $CDCl_3$) δ 8.83 (d, J = 7.3 Hz, 1H), 8.79 (d, J = 8.3 Hz, 1H), 8.50 (d, J = 7.9 Hz, 1H), 8.23 (dd, J = 8.2, 3.5 Hz, 2H), 7.84 (t, J = 7.8 Hz, 1H), 7.72 (t, J = 7.6 Hz, 1H), 7.54 (t, J = 7.5 Hz, 1H), 7.51 (d, J = 8.3 Hz, 2H), 7.26 (d, J = 7.9 Hz, 1H), 6.99 (d, J = 8.3 Hz, 2H), 3.88 (s, 3H). ^{13}C NMR (126 MHz, $CDCl_3$) δ 183.71 (C=O), 140.34 (C), 136.13 (C), 135.80 (CH), 133.45 (CH), 131.36 (CH), 130.99 (C), 130.66 (C), 130.27 (CH), 128.99 (C), 128.47 (C), 128.16 (CH), 128.09 (CH), 126.73 (CH), 126.27 (CH), 126.10 (C), 124.77 (C), 124.06 (CH), 122.80 (CH), 122.64 (C), 115.46 (CH), 55.46 (-O-$\underline{C}H_3$). FTMS (ESI) m/z: $[M + H]^+$ calculated for $C_{24}H_{16}O_2S$: 369.0944, found: 369.0938.

2.3.9. 3-((4-fluorophenyl)thio)-7H-benzo[de]anthracen-7-one (3d)

Yellow solid. Yield: 61%. Melting point: 210 °C. R_f = 0.46 (Hexane/Acetone; 3:1). IR, λ_{max} (neat) cm^{-1}: 655, 686, 696, 744, 767, 794, 844, 872, 902, 945, 982, 1013, 1050, 1081, 1091, 1126, 1157, 1174, 1217, 1278, 1303, 1319, 1361, 1383, 1461, 1486, 1507, 1568, 1583, 1594, 1645, 3034.^{1}H NMR (500 MHz, $CDCl_3$) δ 8.68 (d, J = 7.2 Hz, 1H), 8.63 (d, J = 8.3 Hz, 1H), 8.37 (d, J = 7.8 Hz, 1H), 8.12 (dd, J = 12.3, 7.9 Hz, 2H), 7.70 (t, J = 7.8 Hz, 1H), 7.61 (t, J = 7.5 Hz, 1H), 7.44 (t, J = 7.5 Hz, 1H), 7.40–7.29 (m, 3H), 6.99 (t, J = 8.4 Hz, 2H). ^{13}C NMR (126 MHz, $CDCl_3$) δ 183.57 (C=O), 162.69 (d, J = 248.7 Hz, C), 137.59 (C), 135.85 (C), 134.28 (d, J = 8.2 Hz, CH), 133.53 (CH), 131.74 (CH), 130.77 (C), 130.75 (C), 130.33 (CH), 129.04 (C), 129.01 (C), 128.87 (CH), 128.64 (C), 128.43 (CH), 128.20 (CH), 127.08 (CH), 126.12 (C), 123.94 (CH), 122.96 (CH), 116.95 (CH), 116.78 (CH). FTMS (ESI) m/z: $[M + H]^+$ calculated for $C_{23}H_{13}FOS$: 357.0744, found: 357.0742.

2.3.10. 3-(phenylselanyl)-7H-benzo[de]anthracen-7-one (4a)

Yellow solid. Yield: 60%. Melting point: 190 °C. R_f = 0.47 (Hexane/Acetone; 3:1). IR, λ_{max} (neat) cm^{-1}: 654, 670, 691, 740, 750, 767, 792, 840, 941, 998, 1022, 1038, 1046, 1064, 1081, 1122, 1170, 1215, 1277, 1304, 1317, 1359, 1382, 1438, 1469, 1476, 1506, 1565, 1581, 1595, 1608, 1646, 2989, 3052.^{1}H NMR (500 MHz, $CDCl_3$) δ 8.69 (d, J = 7.3 Hz, 1H), 8.62 (d, J = 8.3 Hz, 1H), 8.39 (d, J = 7.9 Hz, 1H), 8.15 (dd, J = 8.1, 4.7 Hz, 2H), 7.70 (t, J = 7.8 Hz, 1H), 7.66 (d, J = 7.8 Hz, 1H), 7.63 (t, J = 7.6 Hz, 1H), 7.46 (t, J = 7.5 Hz, 1H), 7.43–7.38 (m, 2H), 7.24–7.16 (m, 3H). ^{13}C NMR (126 MHz, $CDCl_3$) δ 183.50 (C=O), 135.90 (C), 134.41 (C), 134.24 (CH), 133.49 (CH), 133.21 (CH), 132.53 (CH), 130.84 (C), 130.33 (C), 130.26 (CH), 129.68 (CH), 129.03 (C), 128.66 (C), 128.47 (CH), 128.16 (CH), 127.83 (CH), 127.18 (CH), 126.83 (C), 124.04 (CH), 122.99 (CH). FTMS (ESI) m/z: $[M + H]^+$ calculated for $C_{23}H_{14}OSe$: 387.0284, found: 387.0283.

3. Results and discussion

3.1. Structural and spectral characterization

^{1}H-, APT-NMR (attached proton test NMR), FTIR spectra and high-resolution mass spectrometric analysis confirmed chemical structures of newly prepared compounds.

The collected infrared spectra indicate that the benzanthrone carbonyl group (C=O) vibration band has peaks ranging from 1645 to 1654 cm^{-1} and bands of aliphatic and aromatic carbon–hydrogen (C–H) vibrations around 2840–3100 cm^{-1}.

The NMR spectroscopy was used to detect the doublets (d), doublets of doublets (dd), doublets of doublets of doublets (ddd), triplets (t), triplets of triplets (tt) and multiplets (m) of the aromatic protons (δ 9.05–7.05 ppm) that are commonly found in phenyl groups and benzanthrone residue. The APT NMR spectra revealed the characteristic peaks of the benzanthrone carbonyl group carbon at approximately 183–184 ppm, as well as the peaks of both aromatic and aliphatic carbon atoms. These results were found to be consistent with previous NMR

studies on other benzanthrone derivatives [47–50].

The molecular weight of the produced compounds was confirmed to be as calculated based on the results acquired from the high-resolution mass spectrometry.

3.2. Crystal structure analysis

Fig. 1 gives a perspective view of molecule **2b** respectively with thermal ellipsoids and the atom-numbering scheme. Table 2 gives the principal torsion angles characterizing the conformation of the isopropylthio group. The values of the C1–C2–C3–S18, C17–C3–S18–C19 and C3–S18–C19–C21 angles close to the flat angle indicate that all atoms of the molecule (with the exception of C20) lie in the plane of the benzanthrone system. Table 3 lists the main crystallographic parameters for the crystals of **2b**.

In the crystal structure of **2b** there are π-π stacking interactions between benzanthrone systems. Fig. 2 illustrates these interactions. The shortest interatomic contact in these interactions is C9···C17 with length of 3.338(2) Å. By means of these interactions the molecules associate into centrosymmetric dimers in the crystal structure. Among other shortened contacts, the C21···O22 contact with a length of 3.484(2) Å should be distinguished. This contact can be interpreted as a weak intermolecular hydrogen bond of the CH···O type (see Fig. 2). The angle of C21–H21b···O22 is 155°, the H21b···O22 length is equal 2.57 Å.

3.3. Photophysical properties

3.3.1. Absorption and emission

To investigate the photophysical properties of newly synthesized compounds **2a** – **2e, 3a** – **3d** and **4a**, absorbance and emission spectra were acquired in seven solvents with varying polarity, specifically, in benzene (PhH), chloroform, ethyl acetate (EtOAc), acetone, DMF (*N*,*N*-dimethylformamide), DMSO (dimethyl sulfoxide) and ethanol.

All of the dyes examined in this study exhibited fluorescence and displayed notable solvatochromic effect (Fig. 3), emitting light that ranged from blue-green in solvents of lower polarity to orange in higher polarity solvents. The observed solvatochromic properties of these benzanthrone derivatives, evident from both – their fluorescence and absorption spectra in solutions, provide compelling evidence supporting the notion that their fluorescence originates from the ICT (intramolecular charge transfer) mechanism, which occurs during excitation from the electron-donating thiol group to the electron-withdrawing carbonyl group.

Table 4 – 6provide a summary of the data for absorption maxima and molar extinction coefficients, as well as fluorescence maxima and Stokes shifts.

The benzanthrone alkyl and aryl sulfides, as well as 3-(phenylselanyl)benzanthrone in solutions were observed to have absorption band in the range of 403–448 nm with a shift towards longer wavelengths of 10–20 nm between the maxima in benzene and DMSO. In comparison to absorption, the influence of solvent polarity on fluorescence is more conspicuous. Both alkyl and aryl sulfides emit light upon excitation from around 507 nm in benzene to 591 nm in ethanol (Fig. 4). Substitution of sulfur atom with larger – selenium – atom, slightly shifts emission bathochromically and somewhat increases Stokes shifts, while extinction coefficients and absorption maxima are practically unaffected. Despite the high electron-donating ability of selenium, its introduction into the 3rd position of benzanthrone significantly reduces the emission quantum yields of the compound, especially in polar solvents.

To better understand how electronic properties of the obtained compounds respond to changes in solvent polarity, the Lippert-Mataga plots (Fig. 5) were charted for compounds **2a**, **3a** and **4a**, providing insights into the molecule-solvent interactions. The relationship between the Stokes shift of studied molecules' electronic transition and the

Table 2
Selected torsion angles in **2b**.

Angle	Value (°)
C1–C2–C3–S18	179.5(1)
C17–C3–S18–C19	−167.9(1)
C3–S18–C19–C20	67.7(2)
C3–S18–C19–C21	−170.4(2)

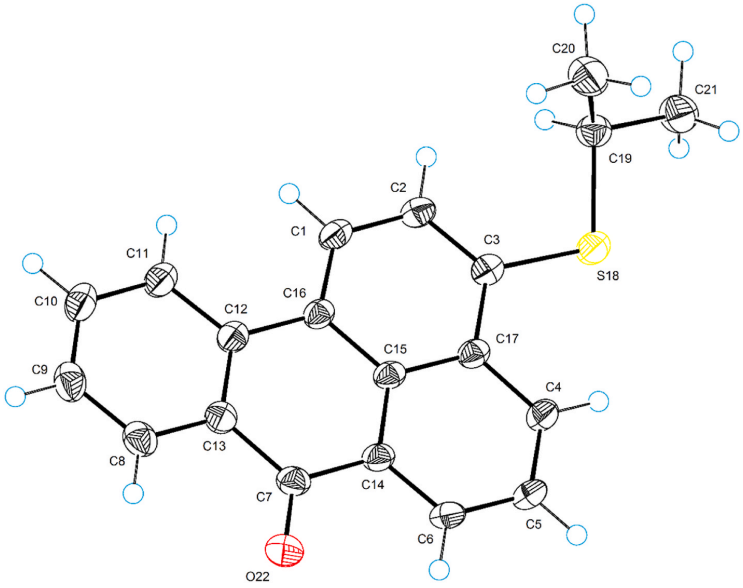

Fig. 1. ORTEP diagram for molecule **2b**.

Table 3
Crystal data and structure refinement of the compound **2b**.

	2b
Empirical formula	$C_{20}H_{16}OS$
Formula weight	304.42
Temperature/K	150.0(1)
Crystal system	monoclinic
a (Å)	8.13153(6)
b (Å)	11.23841(8)
c (Å)	16.13048(13)
α (°)	90
β (°)	92.0316(7)
γ (°)	90
Volume (Å^3)	1473.164(19)
Z	4
μ (mm^{-1})	1.923
Density (calculated) (g/cm^3)	1.3724
Space group	$P2_1/c$
F(000)	643.0
Radiation	Cu Kα (λ = 1.54184 Å)
2Θ max. for data collection/°	160
Index ranges	$-10 \leq h \leq 10$, $-11 \leq k \leq 14$, $-20 \leq l \leq 20$
Reflections collected	17,086
Independent reflections	3229 [$R_{int} = 0.0184$, $R_{sigma} = 0.0139$]
Data/restraints/parameters	3229/0/205
Goodness-of-fit on F^2	1.038
Final *R* indexes [$I > 2\sigma(I)$]	$R_1 = 0.0321$, $wR_2 = 0.0911$
Final *R* indexes [all data]	$R_1 = 0.0328$, $wR_2 = 0.0921$
Largest diff. peak/hole/e Å^{-3}	0.23/-0.33
CCDC number	2,261,465

Lippert-Mataga solvent parameter is not a simple, direct proportionality. This implies that there are more complex interactions between these molecules and solvents, which may include specific solute-solvent interactions, solvent effects on the molecule's electronic structure, or even changes in conformation of molecules. The non-linearity in the plot could also arise from the presence of multiple electronic transitions contributing to the observed spectra, each having different sensitivities to solvent polarity. It may indicate the existence of specific solvent binding sites or highlight the significance of dipole-dipole, hydrogen bonding, or other types of interactions.

The absorption spectra of benzanthrone amidines previously examined exhibit wavelengths ranging from 410 to 495 nm and the absorption spectra of 3-substituted benzanthrone amino derivatives fall within the range of 430–520 nm [51–54]. Regarding the 3-methoxy and 3-phenoxy derivatives of benzanthrone, their absorption spectra range from 417 to 436 nm [20,55,56]. Notably, the peaks of emission and absorption are shifted towards shorter wavelengths in sulfur and selenium derivatives, indicating a slightly weaker donating effect compared to nitrogen and oxygen-containing species. In general, the photophysical properties of these compounds are similar to those of previously investigated derivatives of benzanthrone that contain oxygen and nitrogen.

3.3.2. Fluorescence lifetime

For compounds **2a**, **3a** and **4a** PL decays were measured in benzene, $CHCl_3$, DMF and EtOH solutions (Figs. 6–9). In all cases the obtained curves can be approximated with a monoexponential decay function, yielding PL lifetimes in the range of 1.0–10.7 ns (Table 7). The nanosecond-scale light emission process and calculated radiative rate constants (k_r) on order of 10^7 s^{-1} are indicative of fluorescence mechanism. Interestingly, k_r for **2a** is about twice higher than for the other two compounds. This suggests that the attachment of alkylthio fragment to the benzanthrone core increases the oscillator strength of the emissive S_1 excited state, if compared to the structural analogues, which bear phenylthio and phenylselanyl substituents. In all cases the non-radiative rate constants (k_{nr}) substantially exceed those of the radiative process, in accordance with the observed low-to-moderate Φ_F values. Non-radiative constants are notably higher for **3a** and **4a**, suggesting more pronounced non-emissive excitation relaxation pathways for the respective compounds. Regarding the surrounding medium impact, it is apparent that

Fig. 3. Solutions of compound **2a** in ultraviolet light in different organic solvents (from left to right: in benzene, chloroform, EtOAc, acetone, ethanol, DMF and DMSO).

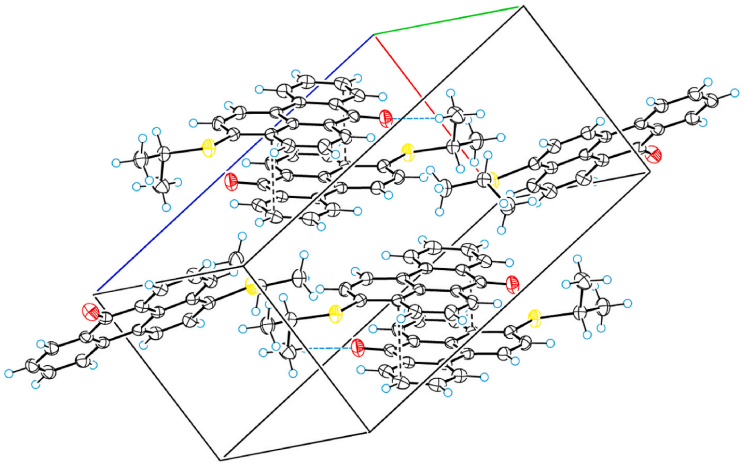

Fig. 2. Molecular packing in the unit cell of **2b** showing the intermolecular shortened contacts.

Table 4
Absorption maxima of prepared dyes in organic solvents (concentration 10^{-5} M).

	Absorption λ_{abs} (lgε) (nm)									
	2a	**2b**	**2c**	**2d**	**2e**	**3a**	**3b**	**3c**	**3d**	**4a**
Benzene	429 (4.18)	414 (4.01)	416 (3.83)	411 (4.26)	422 (4.42)	413 (4.16)	426 (4.10)	432 (3.90)	418 (4.27)	416 (4.14)
$CHCl_3$	444 (4.16)	420 (4.02)	421 (3.82)	403 (4.30)	430 (4.40)	421 (4.18)	436 (4.04)	447 (3.94)	424 (4.25)	423 (4.14)
EtOAc	431 (4.17)	411 (4.03)	412 (3.81)	406 (4.16)	424 (4.38)	410 (4.14)	423 (4.07)	430 (3.95)	414 (4.25)	412 (4.14)
Acetone	443 (4.19)	413 (3.97)	414 (3.84)	407 (4.27)	430 (4.39)	413 (4.11)	425 (4.04)	438 (3.92)	415 (4.20)	416 (4.16)
DMF	446 (4.06)	422 (3.98)	422 (3.83)	411 (4.27)	445 (4.21)	417 (4.15)	431 (4.02)	443 (3.92)	422 (4.23)	419 (4.11)
DMSO	448 (4.19)	426 (4.00)	425 (3.70)	412 (4.21)	446 (4.06)	420 (4.07)	430 (3.91)	447 (3.92)	424 (4.10)	423 (3.93)
EtOH	448 (4.15)	423 (3.96)	422 (3.79)	405 (4.27)	442 (4.31)	423 (4.09)	442 (4.03)	447 (3.90)	425 (4.21)	423 (4.04)

Table 5
Emission maxima of prepared dyes in organic solvents (concentration 10^{-5} M).

	Emission λ_{em} (nm)									
	2a	**2b**	**2c**	**2d**	**2e**	**3a**	**3b**	**3c**	**3d**	**4a**
Benzene	508	507	521	503	505	504	523	520	501	510
$CHCl_3$	533	539	544	538	538	538	545	537	533	543
EtOAc	519	518	515	514	518	516	518	517	514	543
Acetone	541	536	538	540	537	533	545	562	538	560
DMF	552	546	548	544	547	541	555	563	543	562
DMSO	565	555	557	553	560	552	563	565	555	569
EtOH	587	584	585	582	586	583	591	573	580	595

Table 6
Stokes shift of prepared dyes in organic solvents (concentration 10^{-5} M).

	Stokes shift (cm^{-1})									
	2a	**2b**	**2c**	**2d**	**2e**	**3a**	**3b**	**3c**	**3d**	**4a**
Benzene	3625	4431	4845	4450	3895	4372	4354	3917	3963	4431
$CHCl_3$	3761	5257	5371	6227	4668	5166	4587	3749	4823	5224
EtOAc	3934	5026	4854	5175	4280	5010	4336	3913	4699	5856
Acetone	4089	5556	5567	6052	4634	5451	5181	5037	5509	6181
DMF	4306	5382	5449	5949	4190	5497	5184	4811	5280	6073
DMSO	4622	5456	5576	6189	4564	5694	5494	4672	5567	6066
EtOH	5286	6517	6603	7509	5560	6488	5704	4919	6288	6834

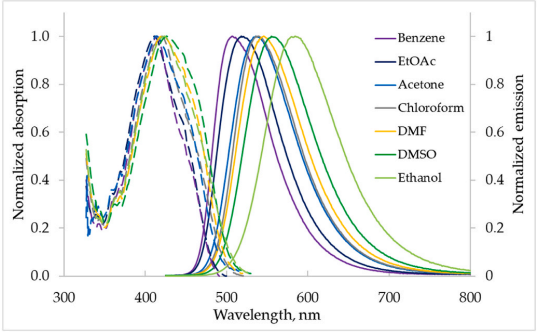

Fig. 4. The UV–Vis absorption and fluorescence emission spectra of compound **3a** in various organic solvents.

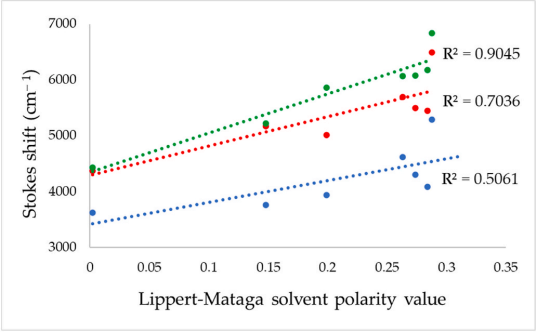

Fig. 5. Stoke shift versus solvent Lippert-Mataga polarity parameter for compounds **2a** (blue), **3a** (red) and **4a** (green) in selected solvents.

an increase in solvent polarity leads to a slight drop in both k_r and k_{nr} constants. The decrease in non-radiative rate exceeds that of k_r, generally resulting in Φ_F rise in more polar solvents. The exception is compound **4a**, for which an opposite trend is observed, as PL efficiency dramatically drops.

3.4. Computational analysis

In order to gain a better understanding about the photophysical properties of the synthesized compounds a series of DFT calculations were performed for **2a**, **3a** and **4a**. The optimization of ground-state geometries yielded structures, where the bonds at sulfur or selenium atom are located in the plane of benzanthrone ring system, in agreement with the previously discussed X-ray structure of **2b**. The bonds between benzanthrone and heteroatom are slightly shortened (e.g., 1.77 and 1.78 Å for **2a** and **3a**), indicating a partial delocalization of heteroatom lone pair electrons in the neighboring electron deficient ring system. The calculated frontier molecular orbitals of the compounds are presented in

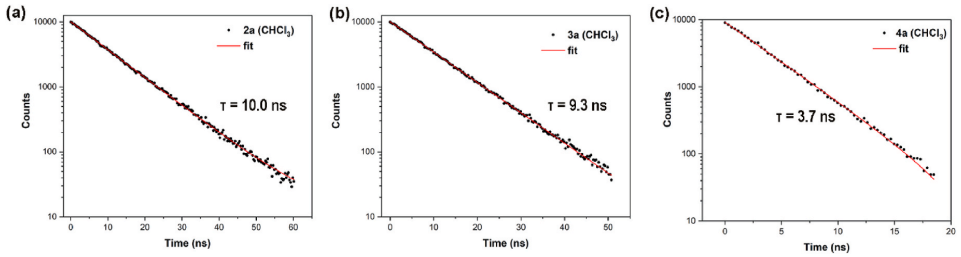

Fig. 6. Emission decay curves of **2a** (a), **3a** (b) and **4a** (c) measured in $CHCl_3$ solution.

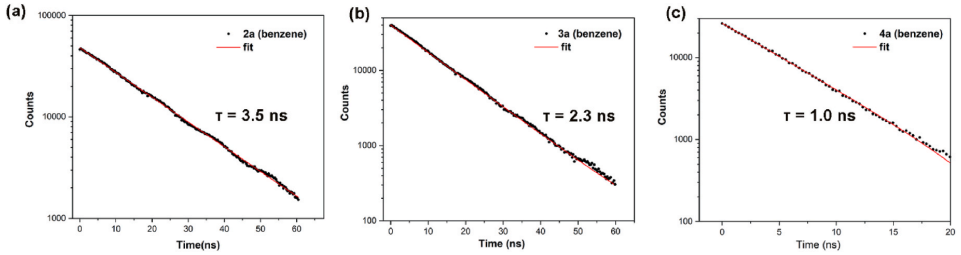

Fig. 7. Emission decay curves of **2a** (a), **3a** (b) and **4a** (c) measured in benzene solution.

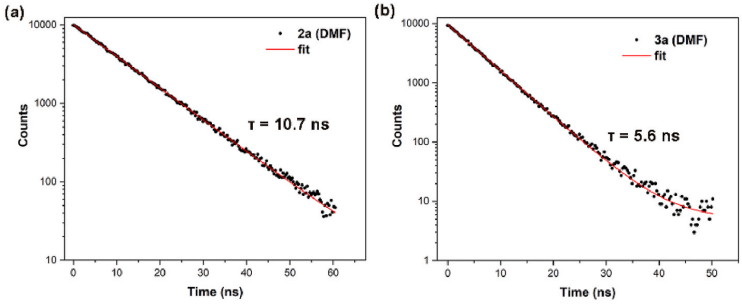

Fig. 8. Emission decay curves of **2a** (a) and **3a** (b) measured in DMF solution.

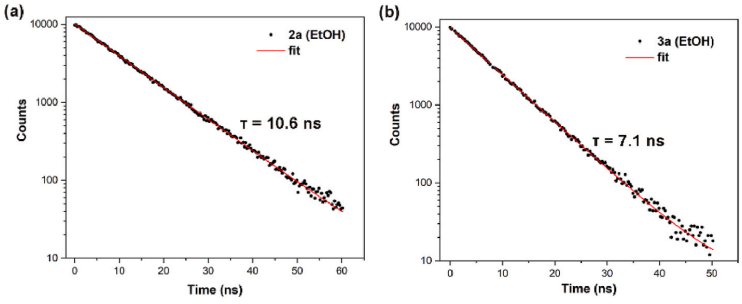

Fig. 9. Emission decay curves of **2a** (a) and **3a** (b) measured in EtOH solution.

Table 8. Highest occupied molecular orbital (HOMO) predominantly resides on the sulfur or selenium atoms and on the neighboring benzene ring. Lowest unoccupied molecular orbital (LUMO), on other hand, is shifted towards the carbonyl-bearing electron deficient aromatic ring of benzanthrone. The structural variance in the investigated compounds shows a little impact on the calculated HOMO and LUMO energy level

Table 7
Fluorescence quantum yield (Φ_F), PL lifetime values and radiative and non-radiative rate constants of compounds **2a**, **3a** and **4a** in different polarity solvents.

Compound	Φ_F	τ, ns	χ^2 [a]	k_r, [b] $1{\cdot}10^7$ s^{-1}	k_{nr}, [c] $1{\cdot}10^7$ s^{-1}
PhH					
2a	0.31	3.5	1.35	8.9	19.7
3a	0.08	2.3	1.18	3.3	38.3
4a	0.05	1.0	1.26	4.5	86.4
$CHCl_3$					
2a	0.52	10.0	1.29	5.2	4.8
3a	0.24	9.3	1.23	2.6	8.1
4a	0.07	3.7	1.28	1.9	25.1
DMF					
2a	0.40	10.7	1.32	3.7	5.6
3a	0.14	5.6	1.19	2.5	15.4
4a	0.001	-[d]	–	–	–
EtOH					
2a	0.32	10.6	1.35	3.0	6.4
3a	0.11	7.1	1.18	1.5	12.4
4a	0.001	-[d]	–	–	–

[a] Reduced chi-squared value of PL decay fit.
[b] $k_r = \Phi_{PL}/\tau$.
[c] $k_{nr} = (1\text{-}\Phi_{PL})/\tau$.
[d] Value could not be determined due to low PL intensity.

values (Table 8), except for the selenium containing compound **4a**, for which a slight destabilization for both frontier orbitals is evident. TD-DFT calculations were sequentially performed to predict excited state energy levels. The calculated S_1 excitation energies (3.00–2.95 eV) and oscillator strength (*f*) parameters are fairly similar and compare well with the experimental measurements. The analysis of natural transition orbitals (NTOs) (Table 9) reveals that $S_0 \rightarrow S_1$ transition predominantly involves an electron transfer between HOMO and LUMO orbitals and thus possess an intramolecular charge transfer (ICT) character. ICT nature of the singlet transition is also evident in the performed solvatochromic simulations. For reference, in solvent series benzene, DCM and DMSO compound **4a** exhibits solvent polarity induced S_1 level stabilization with the corresponding values 2.95, 2.92 and 2.90 eV. A similar trend can be seen in experimental measurements (Fig. 4). The lowest energy triplet state (T_1) is significantly stabilized (by approximately 1 eV) in relation to S_1 level. T_2 state, on the other hand is situated relatively closely to the lowest energy singlet, suggesting a possible pathway for efficient intersystem crossing (ISC) process. To closer investigate the probability of this hypothetical photophysical mechanism the optimization of geometries of S_1 excited state were performed for the molecules and the corresponding spin-orbit coupling (SOC) matrix elements for $S_1 \rightarrow T_1$ and $S_1 \rightarrow T_2$ transitions ($\langle S_n|H_{SO}|T_n\rangle$) were calculated (Table 8). It can be seen that for **4a** a significant increase in SOC parameter can be observed due to a heavy atom effect, arising from the presence of selenium [57]. By taking into consideration the fact that **4a** exhibits the lowest Φ_F value among the investigated compound series, it can be proposed that upon the photoexcitation an efficient ISC to dark triplet states takes place, limiting the light emission efficiency of the compound. In order to test this assumption and detect possible triplet state-related emissive processes in more rigid media, a Zeonex film bearing 5 wt% of **4a** was prepared. At room temperature conditions the sample exhibited very weak emission, which showed no increase in intensity upon a placement under nitrogen atmosphere. Further, the Zeonex film was cooled to 77 K and time-resolved PL spectra were acquired (Fig. 10). As it can be seen, the sample does not exhibit any long-lived emissive process, typical for metal-free phosphorescent compounds, as no PL can be detected in 1000–5000 μs interval after the excitation. Instead, the observed PL can be attributed to fluorescence, as indicated by the nanosecond scale PL decay of the cooled sample (Fig. 11). In comparison to the measurements in solvents, the shape of the PL band in cooled Zeonex film exhibits structured features, associated with vibrational sublevels of the excited singlet emissive state, which become apparent due to a restricted thermal motion of the **4a** molecules. Considering theses results, the triplet excited states of the examined compounds can be considered as non-emissive due to very efficient non-radiative relaxation processes, which cannot be suppressed even at low-temperature conditions in rigid polymer host (see Table 10).

It is worth noting that for the optimized S_1 geometries the thio- or seleno-substituents change their conformation from being in the plane of benzanthrone to being perpendicular, indicative of a formation of twisted intramolecular charge transfer state [58]. However, the energy difference between planar and twisted states are very small. For example, the calculated energy difference between these two

Table 9
Calculated HOMO and LUMO wavefunctions for compounds **2a**, **3a** and **4a**.

Compound	HOMO	LUMO
2a	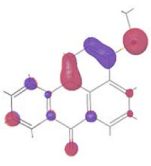	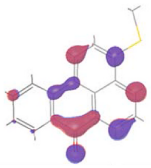
3a	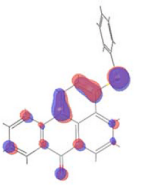	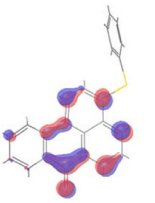
4a	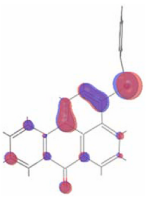	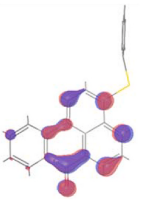

Table 8
Results of DFT calculations (PBE0, 6–31g* theory level).

	HOMO, eV	LUMO, eV	S_1,[a] eV (exp.)[b]	$f_{S0\rightarrow S1}$	T_1,[a] eV	T_2,[a] eV	S_1,[a,c] eV (exp)[d]	$\langle S_1\|H_{SO}\|T_1\rangle$[a,c], cm^{-1}	$\langle S_1\|H_{SO}\|T_2\rangle$[a,c], cm^{-1}
2a	−5.78	−2.21	3.00 (2.89)	0.457	2.10	2.93	2.69 (2.44)	13.0	2.3
3a	−5.77	−2.21	2.99 (3.00)	0.498	2.08	2.91	2.46 (2.46)	6.5	1.6
4a	−5.72	−2.19	2.95 (2.98)	0.497	2.09	2.91	2.35 (2.43)	36.4	13.4

[a] Calculated in benzene.
[b] Experimentally measured λ_{abs} values.
[c] Calculated at S_1 geometry.
[d] Experimentally measured λ_{em} values.

Table 10
Natural transition orbitals (NTOs) of the $S_0 \rightarrow S_1$, $S_0 \rightarrow T_1$ and $S_0 \rightarrow T_2$ transitions for **2a**, **3a** and **4a**. Blue color represents the hole, while red color the particle.

Compound	$S_0 \rightarrow S_1$	$S_0 \rightarrow T_1$	$S_0 \rightarrow T_2$
2a	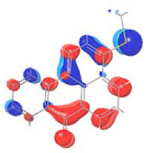	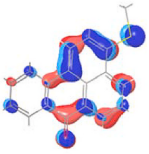	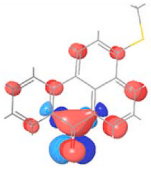
3a	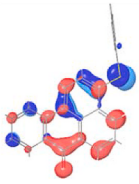	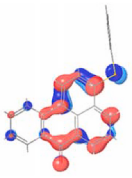	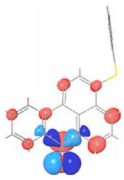
4a	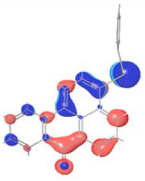		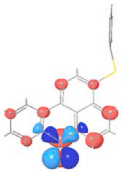

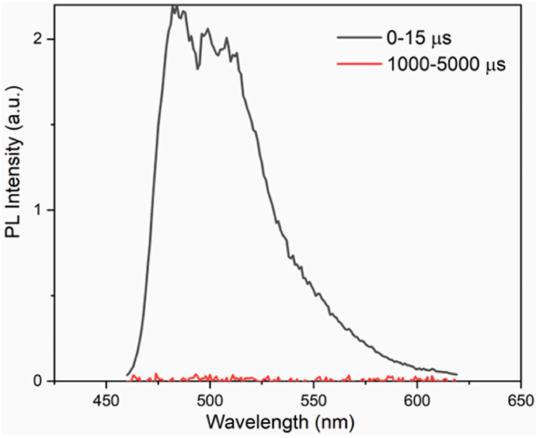

Fig. 10. Time-resolved PL measurements of a doped Zeonex film containing 5 wt% of compound **4a** at 77 K temperature showing PL intensity in 0–15 μs and 1000–5000 μs intervals.

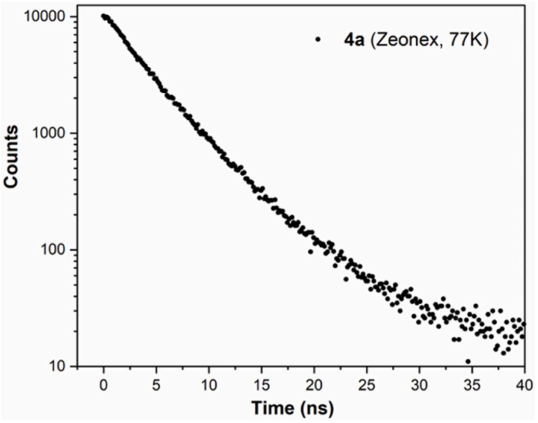

Fig. 11. PL decay of a doped Zeonex film containing 5 wt% of compound 4a at 77 K temperature measured at 500 nm (excitation 410 nm).

conformations for compound **2a** is only 0.001 eV (Fig. 12), meaning that they both are freely accessible at room temperature conditions. Considering the fact that the twisted conformations possess very small *f* values (e.g., 0.0016 for **2a**), but the experimental radiative rates are relatively high, it can be assumed that the fluorescence in the investigated compounds proceed predominantly from the planar conformation.

4. Conclusions

In conclusion, this paper has discussed the synthesis, characterization, and photophysical properties of benzanthrone-derived sulfides. The compounds were successfully synthesized through a practical method of nucleophilic aromatic substitution reactions. Structural characterization using various spectroscopic techniques confirmed their chemical structures, and the crystal structure of one compound was determined through X-ray diffraction, revealing π-π stacking interactions between benzanthrone systems and intermolecular hydrogen bonds. Photophysical analysis demonstrated solvatochromic effects and attributed fluorescence to intramolecular charge transfer. Computational analysis using DFT calculations provided additional insights into the properties of the compounds including excited state energies and potential for efficient intersystem crossing. Overall, this research has provided a comprehensive understanding of the newly synthesized benzanthrone sulfides and their phenylselanyl derivative. The observed photophysical properties, charge transfer characteristics and the solvatochromic effects exhibited by the compounds suggest their potential

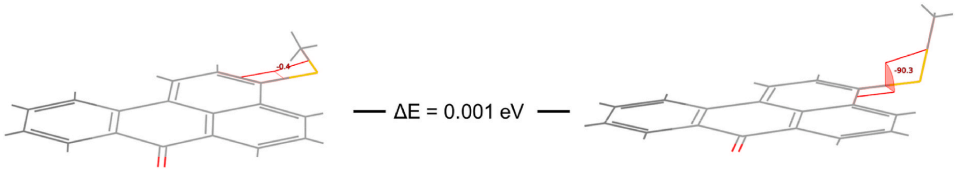

Fig. 12. Optimized geometries of two conformations of S_1 excited state of **2a**. Dihedral angle between the plane of benzanthrone and -SMe bond are shown.

utility in developing sensors for detecting environmental changes, chemical substances, or biological targets.

CRediT authorship contribution statement

Armands Maļeckis: Methodology, Investigation, Writing – original draft, Project administration, Funding acquisition. **Marija Cvetinska:** Methodology, Investigation. **Evans Griškjāns:** Methodology, Investigation, Visualization. **Kirills Dmitrijevs:** Investigation. **Kaspars Traskovskis:** Investigation, Writing – original draft, Visualization. **Sergey Belyakov:** Investigation, Validation, Formal analysis. **Elena Kirilova:** Validation, Resources, Writing – review & editing, Supervision.

Declaration of competing interest

The authors declare that they have no known competing financial interests or personal relationships that could have appeared to influence the work reported in this paper.

Data availability

Data will be made available on request.

Acknowledgments

This work has been supported by the European Social Fund within the Project No 8.2.2.0/20/I/008 «Strengthening of PhD students and academic personnel of Riga Technical University and BA School of Business and Finance in the strategic fields of specialization» of the Specific Objective 8.2.2 «To Strengthen Academic Staff of Higher Education Institutions in Strategic Specialization Areas» of the Operational Programme « Growth and Employment».

Appendix A. Supplementary data

Supplementary data to this article can be found online at https://doi.org/10.1016/j.dyepig.2023.111599.

References

[1] Hu J, Zhang C. Simple and accurate quantification of quantum yield at the single-molecule/particle level. Anal Chem 2013;85. https://doi.org/10.1021/ac3036487. 2000–4.
[2] Ren T-B, Xu W, Zhang W, Zhang X-X, Wang Z-Y, Xiang Z, et al. A general method to increase Stokes shift by introducing alternating vibronic structures. J Am Chem Soc 2018;140:7716–22. https://doi.org/10.1021/jacs.8b04404.
[3] Zheng Q, Lavis LD. Development of photostable fluorophores for molecular imaging. Curr Opin Chem Biol 2017;39:32–8. https://doi.org/10.1016/j.cbpa.2017.04.017.
[4] Tsiko U, Sych G, Volyniuk D, Bezvikonnyi O, Keruckiene R, Lazauskas A, et al. Self-recovering mechanochromic luminescence of the derivatives of benzanthrone and carbazole: towards damage-resistive information recording and security probes. Dyes Pigments 2022;199:110082. https://doi.org/10.1016/j.dyepig.2022.110082.
[5] Thomas A, Kirilova EM, Nagesh BV, Manohara SR, Siddlingeshwar B, Belyakov SV. Synthesis, solvatochromism and DFT study of pyridine substituted benzanthrone with ICT characteristics. J Mol Struct 2022;1262:132971. https://doi.org/10.1016/j.molstruc.2022.132971.
[6] Maļeckis A, Griškjāns E, Cvetinska M, Kirilova E. 3-(Phenylethynyl)-7H-benzo[de]anthracen-7-one. Molbank 2022;2022:M1442. https://doi.org/10.3390/M1442.
[7] Vus K, Trusova V, Gorbenko G, Sood R, Kirilova E, Kirilov G, et al. Fluorescence investigation of interactions between novel benzanthrone dyes and lysozyme amyloid fibrils. J Fluoresc 2014;24:493–504. https://doi.org/10.1007/s10895-013-1318-3.
[8] Gorbenko G, Trusova V, Kirilova E, Kirilov G, Kalnina I, Vasilev A, et al. New fluorescent probes for detection and characterization of amyloid fibrils. Chem Phys Lett 2010;495:275–9. https://doi.org/10.1016/j.cplett.2010.07.005.
[9] Kirilova E, Mickevica I, Mezaraupe L, Puckins A, Rubenina I, Osipovs S, et al. Novel dye for detection of callus embryo by confocal laser scanning fluorescence microscopy. Luminescence 2019;34:353–9. https://doi.org/10.1002/bio.3616.
[10] Kirilova EM, Kecko S, Mežaraupe L, Gavarāne I, Pučkins A, Mickeviča I, et al. Novel luminescent dyes for confocal laser scanning microscopy used in parasite Trematoda diagnostics. Acta Biochim Pol 2018;65. https://doi.org/10.18388/abp.2018_2574.
[11] Gavarane I, Kirilova E, Rubeniņa I, Mežaraupe L, Osipovs S, Deksne G, et al. A simple and rapid staining technique for sex determination of Trichinella larvae parasites by confocal laser scanning microscopy. Microsc Microanal 2019;25:1491–7. https://doi.org/10.1017/S1431927619015046.
[12] Rubenina I, Gavarane I, Kirilova E, Mezaraupe L, Kirjusina M. Comparison of the benzanthrone luminophores: they are not equal for rapid examination of parafasciolopsis fasciolaemorpha (trematoda: digenea). Biomolecules 2021;11:598. https://doi.org/10.3390/biom11040598.
[13] Tsiko U, Bezvikonnyi O, Volyniuk D, Minaev BF, Keruckas J, Cekaviciute M, et al. TADF quenching properties of phenothiazine or phenoxazine-substituted benzanthrones emitting in deep-red/near-infrared region towards oxygen sensing. Dyes Pigments 2022;197:109952. https://doi.org/10.1016/j.dyepig.2021.109952.
[14] Maļeckis A, Avotiņa L, Ķizāne G, Pučkins A, Osipovs S, Kirilova E. New fluorescent heterocyclic compounds derived from 3-Cyanobenzanthrone. Polycycl Aromat Comp 2022;42:5508–20. https://doi.org/10.1080/10406638.2021.1939068.
[15] Staneva D, Grabchev I. Heterogeneous sensors for ammonia, amines and metal ions based on a dendrimer modified fluorescent viscose fabric. Dyes Pigments 2018;155:164–70. https://doi.org/10.1016/j.dyepig.2018.03.044.
[16] Konstantinova T, Lazarova R. Synthesis of some polymerizable triazinylaminobenzotriazole stabilizers and benzanthrone dyes containing a stabilizer fragment. Dyes Pigments 2007;74:208–14. https://doi.org/10.1016/j.dyepig.2006.01.035.
[17] Grabchev I, Bojinov V, Moneva I. The synthesis and application of fluorescent dyes based on 3-amino benzanthrone. Dyes Pigments 2001;48:143–50. https://doi.org/10.1016/S0143-7208(00)00098-X.
[18] Konstantinova TN. The synthesis of some benzanthrone derivatives for use as dyes for polymeric materials. Dyes Pigments 1989;10:63–7. https://doi.org/10.1016/0143-7208(89)85040-5.
[19] Bojinov VB, Konstantinova TN. A new method for the synthesis of 3-alkoxybenzanthrones as luminophore dyes for polymers. Dyes Pigments 1996;32:151–7. https://doi.org/10.1016/0143-7208(96)00027-7.
[20] Grabchev I, Moneva I, Wolarz E, Bauman D. Fluorescent 3-oxy benzanthrone dyes in liquid crystalline media. Dyes Pigments 2003;58:1–6. https://doi.org/10.1016/S0143-7208(03)00033-0.
[21] Grabchev I, Moneva I. Synthesis and properties of benzanthrone derivatives as luminophore dyes for liquid crystals. Dyes Pigments 1998;37:155–64. https://doi.org/10.1016/S0143-7208(97)00050-8.
[22] Cao L, Zhang D, Xu L, Fang Z, Jiang X-F, Lu F. Perylenediimide-benzanthrone dyad: organic chromophores with enhanced third-order nonlinear-optical activities. Eur J Org Chem 2017;2017:2495–500. https://doi.org/10.1002/ejoc.201700094.
[23] Thomas A, Kirilova EM, Nagesh BV, Krishna Chaitanya G, Philip R, Manohara SR, et al. Influence of nitro group on solvatochromism, nonlinear optical properties of 3-morpholinobenzanthrone: experimental and theoretical study. J Photochem Photobiol Chem 2023;437:114434. https://doi.org/10.1016/j.jphotochem.2022.114434.
[24] Cao L, Xu L, Zhang D, Zhou Y, Zheng Y, Fu Q, et al. D-A dyad and D-A-D triad incorporating triphenylamine, benzanthrone and perylene diimide: synthesis, electrochemical, linear and nonlinear optical properties. Chem Phys Lett 2017;682:133–9. https://doi.org/10.1016/j.cplett.2017.06.015.
[25] Th, omas A, Patil PS, Siddlingeshwar B, Manohara SR, Gummagol NB, Krishna Chaitanya G, et al. Nonlinear optical properties of benzanthrone derivatives with N'-methylpiperazin-1-yl and N'-phenylpiperazin-1-yl substituents: experimental and quantum chemical study. Opt Laser Technol 2022;156:108616. https://doi.org/10.1016/j.optlastec.2022.108616.
[26] Monçalves M, Zanotto GM, Toldo JM, Rampon DS, Schneider PH, Gonçalves PFB, et al. Dipolar vinyl sulfur fluorescent dyes. Synthesis and photophysics of sulfide, sulfoxide and sulfone based D–π–A compounds. RSC Adv 2017;7:8832–42. https://doi.org/10.1039/C6RA27989A.

[27] Rachi Y, Yamakado R, Okada S. Synthesis of dyes with a sulfur-containing heterocyclic donor and a pyrroline-type acceptor. Dyes Pigments 2018;159:345–51. https://doi.org/10.1016/j.dyepig.2018.06.032.
[28] Liu J, Sun Y-Q, Zhang H, Shi H, Shi Y, Guo W. Sulfone-rhodamines: a new class of near-infrared fluorescent dyes for bioimaging. ACS Appl Mater Interfaces 2016;8:22953–62. https://doi.org/10.1021/acsami.6b08338.
[29] Cowling SJ, Ellis C, Goodby JW. Anthraquinone Liquid crystal dichroic dyes – a new form of chromonic dye? Liq Cryst 2011;38:1683–98. https://doi.org/10.1080/02678292.2011.620181.
[30] Sims MT, Abbott LC, Cowling SJ, Goodby JW, Moore JN. Molecular design parameters of anthraquinone dyes for guest–host liquid-crystal applications: experimental and computational studies of spectroscopy, structure, and stability. J Phys Chem C 2016;120:11151–62. https://doi.org/10.1021/acs.jpcc.6b03607.
[31] Ye J, Gao Y, He L, Tan T, Chen W, Liu Y, et al. Efficient blue-emitting molecules by incorporating sulfur-containing moieties into triarylcyclopentadiene: synthesis, crystal structures and photophysical properties. Dyes Pigments 2016;124:145–55. https://doi.org/10.1016/j.dyepig.2015.09.018.
[32] Liu Y, Yu Y, Zhao Q, Tang C, Zhang H, Qin Y, et al. Fluorescent probes based on nucleophilic aromatic substitution reactions for reactive sulfur and selenium species: recent progress, applications, and design strategies. Coord Chem Rev 2021;427:213601. https://doi.org/10.1016/j.ccr.2020.213601.
[33] Vaidyanathan T, Seshadri S. Nucleophilic substitution reactions on 3-bromo- and 3-nitrobenzanthrones. Dyes Pigments 1984;5:431–6. https://doi.org/10.1016/0143-7208(84)80035-2.
[34] Melville OA, Rice NA, Therrien I, Lessard BH. Organic thin-film transistors incorporating a commercial pigment (Hostasol Red GG) as a low-cost semiconductor. Dyes Pigments 2018;149:449–55. https://doi.org/10.1016/j.dyepig.2017.10.034.
[35] Tsiko U, Bezvikonnyi O, Volyniuk D, Minaev BF, Keruckas J, Cekaviciute M, et al. TADF quenching properties of phenothiazine or phenoxazine-substituted benzanthrones emitting in deep-red/near-infrared region towards oxygen sensing. Dyes Pigments 2022;197:109952. https://doi.org/10.1016/j.dyepig.2021.109952.
[36] Dolomanov OV, Bourhis LJ, Gildea RJ, Howard JAK, Puschmann H. OLEX2: a complete structure solution, refinement and analysis program. J Appl Crystallogr 2009;42:339–41. https://doi.org/10.1107/S0021889808042726.
[37] Sheldrick GM. Shelxt – Integrated space-group and crystal-structure determination. Acta Crystallogr A Found Adv 2015;71:3–8. https://doi.org/10.1107/S2053273314026370.
[38] Bourhis LJ, Dolomanov OV, Gildea RJ, Howard JAK, Puschmann H. The anatomy of a comprehensive constrained, restrained refinement program for the modern computing environment – olex2 dissected. Acta Crystallogr A Found Adv 2015;71:59–75. https://doi.org/10.1107/S2053273314022207.
[39] Bochevarov AD, Harder E, Hughes TF, Greenwood JR, Braden DA, Philipp DM, et al. Jaguar: a high-performance quantum chemistry software program with strengths in life and materials sciences. Int J Quant Chem 2013;113:2110–42. https://doi.org/10.1002/qua.24481.
[40] Adamo C, Barone V. Toward reliable density functional methods without adjustable parameters: the PBE0 model. J Chem Phys 1999;110:6158–70. https://doi.org/10.1063/1.478522.
[41] Grimme S, Antony J, Ehrlich S, Krieg H. A consistent and accurate ab initio parametrization of density functional dispersion correction (DFT-D) for the 94 elements H-Pu. J Chem Phys 2010;132:154104. https://doi.org/10.1063/1.3382344.
[42] Neese F, Wennmohs F, Becker U, Riplinger C. The ORCA quantum chemistry program package. J Chem Phys 2020;152:224108. https://doi.org/10.1063/5.0004608.
[43] Campodónico PR, Alarcón-Espósito J, Olivares B. Kinetics and reaction mechanism of biothiols involved in SNAr reactions: an experimental study. Front Chem 2022;10. https://doi.org/10.3389/fchem.2022.854918.
[44] Montanari S, Paradisi C, Scorrano G. Thiol anions in nucleophilic aromatic substitution reactions with activated aryl halides. Attack on carbon vs attack on halogen. J Org Chem 1993;58:5628–31. https://doi.org/10.1021/jo00073a020.
[45] Rohrbach S, Smith AJ, Pang JH, Poole DL, Tuttle T, Chiba S, et al. Concerted nucleophilic aromatic substitution reactions. Angew Chem Int Ed 2019;58:16368–88. https://doi.org/10.1002/anie.201902216.
[46] Henriksen L, Stuhr-Hansen N. Rapid and precise preparation of reactive benzeneselenolate solutions by reduction of diphenyl diselenide with hydrazine–sodium methanolate. J Chem Soc Perkin 1999;1. https://doi.org/10.1039/a903686e. 1915–6.
[47] Vaidyanathan A. The carbon-13 NMR spectra of benzanthrone and its derivatives. Dyes Pigments 1982;3:243–8. https://doi.org/10.1016/0143-7208(82)80026-0.
[48] Sakamoto Y, Ohshima S, Enya T, Suzuki H, Hisamatsu Y. NMR spectroscopy and molecular orbital calculations to interpret the mutagenicity of nitrobenzanthrones. Polycycl Aromat Comp 2001;19:73–81. https://doi.org/10.1080/10406630008034723.
[49] Takekawa M, Aoki J, Iwashima S, Ueda T. Complete assignment of1H and13C NMR spectra of chlorobenzanthrones. Magn Reson Chem 1994;32:87–92. https://doi.org/10.1002/mrc.1260320205.
[50] Rao AVR, Vaidyanathan A. The 1H NMR spectrum of benzanthrone. Spectrochim Acta 1981;37:145–6. https://doi.org/10.1016/0584-8539(81)80102-X.
[51] Konstantinova A, Avotiņa L, Ķizāne G, Pučkins A, Osipovs S, Kirilova E. Amino acid functionalized benzanthrone dyes: synthesis and photophysical study. Dyes Pigments 2022;204:110363. https://doi.org/10.1016/j.dyepig.2022.110363.
[52] Kirilova EM, Puckins AI, Romanovska E, Fleisher M, Belyakov SV. Novel amidine derivatives of benzanthrone: effect of bromine atom on the spectral parameters. Spectrochim Acta Mol Biomol Spectrosc 2018;202:41–9. https://doi.org/10.1016/j.saa.2018.05.029.
[53] Gonta S, Utinans M, Kirilov G, Belyakov S, Ivanova I, Fleisher M, et al. Fluorescent substituted amidines of benzanthrone: synthesis, spectroscopy and quantum chemical calculations. Spectrochim Acta Mol Biomol Spectrosc 2013;101:325–34. https://doi.org/10.1016/j.saa.2012.09.104.
[54] Olipova M, Maļeckis A, Pučkins A, Kirilova A, Romanovska E, Kirilova E. Spectroscopic investigation of new benzanthrone luminescent dyes. Bulg Chem Commun 2022;54:253–7.
[55] Nepraš M, Machalický O, Šeps M, Hrdina R, Kapusta P, Fidler V. Structure and properties of fluorescent reactive dyes: electronic structure and spectra of some benzanthrone derivatives. Dyes Pigments 1997;35:31–44. https://doi.org/10.1016/S0143-7208(96)00092-7.
[56] Grabchev I, Moneva I, Wolarz E, Bauman D. Fluorescent 3-oxy benzanthrone dyes in liquid crystalline media. Dyes Pigments 2003;58:1–6. https://doi.org/10.1016/S0143-7208(03)00033-0.
[57] Drummond BH, Hoover GC, Gillett AJ, Aizawa N, Myers WK, McAllister BT, et al. Selenium substitution enhances reverse intersystem crossing in a delayed fluorescence emitter. J Phys Chem C 2020;124:6364–70. https://doi.org/10.1021/acs.jpcc.0c01499.
[58] Grabowski ZR, Rotkiewicz K, Rettig W. Structural changes accompanying intramolecular electron transfer: focus on twisted intramolecular charge-transfer states and structures. Chem Rev 2003;103:3899–4032. https://doi.org/10.1021/cr940745l.

5. pielikums
Appendix V

Maļeckis, A.; Cvetinska, M.; Kirjušina, M.; Mežaraupe, L.; Kecko, S.; Gavarāne, I.; Kiyan, V.; Lider, L.; Pavlova, V.; Savicka, M.; Belyakov, S.; Kirilova, E.

A Comparative Study of New Fluorescent Anthraquinone and Benzanthrone α-Aminophosphonates: Synthesis, Spectroscopy, Toxicology, X-Ray Crystallography, and Microscopy of *Opisthorchis Felineus*

Molecules ***2024****, 29 (5), 1143.*

https://doi.org/10.3390/molecules29051143

molecules

MDPI

Article

A Comparative Study of New Fluorescent Anthraquinone and Benzanthrone α-Aminophosphonates: Synthesis, Spectroscopy, Toxicology, X-ray Crystallography, and Microscopy of *Opisthorchis felineus*

Armands Maļeckis [1,*], Marija Cvetinska [1], Muza Kirjušina [2], Ligita Mežaraupe [2], Sanita Kecko [2], Inese Gavarāne [2], Vladimir Kiyan [3], Lyudmila Lider [4], Veronika Pavlova [2], Marina Savicka [2], Sergey Belyakov [5] and Elena Kirilova [6]

[1] Institute of Chemistry and Chemical Technology, Faculty of Natural Sciences and Technology, Riga Technical University, P. Valdena Str. 3, LV-1048 Riga, Latvia
[2] Department of Ecology, Institute of Life Sciences and Technology, Daugavpils University, LV-5401 Daugavpils, Latvia
[3] Laboratory of Biodiversity and Genetic Resources, National Center for Biotechnology, 13/5 Kurgalzhynskoye Road, Astana 010000, Kazakhstan
[4] Faculty of Veterinary Medicine and Animal Husbandry Technology, S. Seifullin Kazakh Agro Technical Research University, 62 Zhenis Avenue, Astana 010011, Kazakhstan
[5] Latvian Institute of Organic Synthesis, Aizkraukles Str. 21, LV-1006 Riga, Latvia
[6] Department of Environment and Technologies, Faculty of Natural Sciences and Healthcare, Daugavpils University, LV-5401 Daugavpils, Latvia
* Correspondence: armands5maleckis@inbox.lv

check for updates

Citation: Maļeckis, A.; Cvetinska, M.; Kirjušina, M.; Mežaraupe, L.; Kecko, S.; Gavarāne, I.; Kiyan, V.; Lider, L.; Pavlova, V.; Savicka, M.; et al. A Comparative Study of New Fluorescent Anthraquinone and Benzanthrone α-Aminophosphonates: Synthesis, Spectroscopy, Toxicology, X-ray Crystallography, and Microscopy of *Opisthorchis felineus*. *Molecules* **2024**, *29*, 1143. https://doi.org/10.3390/molecules29051143

Academic Editor: Ana Margarida Gomes da Silva

Received: 6 February 2024
Revised: 28 February 2024
Accepted: 1 March 2024
Published: 4 March 2024

Abstract: In this research, we explore the synthesis of and characterize α-aminophosphonates derived from anthraquinone and benzanthrone, focusing on their fluorescence properties and potential applications in confocal laser scanning microscopy (CLSM). The synthesized compounds exhibit notable solvatochromic behavior, emitting fluorescence from green to red across various solvents. Spectroscopic analysis, including ^{1}H-, ^{13}C-, and ^{31}P-NMR, FTIR, and mass spectrometry, confirms the chemical structures. The compounds' toxicity is evaluated using etiolated wheat sprouts, revealing varying degrees of impact on growth and oxidative damage. Furthermore, the study introduces these α-aminophosphonates for CLSM imaging of the parasitic flatworm *Opisthorchis felineus*, demonstrating their potential in visualizing biological specimens. Additionally, an X-ray crystallographic study of an anthraquinone α-aminophosphonate provides valuable structural insights.

Keywords: fluorescence; solvatochromism; aminophosphonate; benzanthrone; anthraquinone; Kabachnik–Fields reaction; one-pot reaction; crystal structure; toxicology; confocal laser scanning microscopy

1. Introduction

Fluorescence is a phenomenon wherein a substance absorbs light and promptly releases it at a longer wavelength, occurring within nanoseconds and resulting in a spectral shift towards longer wavelengths. An effective organic fluorophore possesses specific characteristics. A crucial factor is a high absorption coefficient, ensuring efficient molecule excitation and, consequently, brighter emitted fluorescence. The Stokes shift, representing the difference between excitation and emission wavelengths, should be sufficiently large to minimize reabsorption and maximize sensitivity. Additionally, an efficient fluorophore exhibits a high quantum yield, signifying that most absorbed energy is converted into emitted light rather than being redirected into competing non-radiative processes. Photostability is equally vital in order to prevent degradation or loss of fluorescent properties over time or

with repeated exposure to light. These key attributes collectively define an optimal organic compound for fluorescence applications [1].

In our prior investigation of α-aminophosphonates, we explored derivatives belonging to the anthrone dye family, specifically focusing on anthraquinone and benzanthrone derivatives [2,3]. These compounds, characterized by a donor–π–acceptor architecture, have attracted considerable attention owing to the noteworthy properties mentioned earlier.

While both anthraquinone and benzanthrone derivatives have held a crucial position in advancing the dye industry and are typically employed in vat dyeing techniques [4,5], various other applications have arisen. For anthraquinones, these include: serving as emitters in organic light-emitting diodes (OLEDs) [6,7], detecting ionic species in chemosensory processes [8,9], contributing to cellular imaging [10,11], and finding utility in the medical field as agents with fungicidal, antibacterial, insecticidal, antiparasitic, antiviral, and anticancer properties [12]. On the other hand, benzanthrones are suited for diverse uses: in liquid crystal displays [13,14], polymeric materials [15], as probes for the pH of solutions and cations [16,17], selective detectors of amyloid fibrils of the lysozyme enzyme [18], and visualization of parasitic trematodes and nematodes through confocal laser scanning microscopy imaging [19].

α-aminophosphonates, analogues of amino acids, possess the ability to inhibit various enzymes involved in amino acid metabolism, thus acting as antagonists and displaying a diverse range of biological activities such as antifungal, antimicrobial, antiviral, anticancer, herbicidal, and neuromodulatory effects [20,21]. Additionally, these compounds, both natural and synthetic, have been extensively studied for their potential applications as lubricating additives [22], antioxidants [23], sorbents [24,25], and corrosion inhibitors [26,27]. Furthermore, α-aminophosphonates derived from aromatic amines, including benzene, naphthalene, anthracene, pyrene, and phenanthrene, as well as bis-aminophosphonates with anthracene rings, have been explored for their fluorescent properties [28–33].

In our previous research, we have independently explored some benzanthrone and anthraquinone α-aminophosphonates. The difference between these compounds has not been explored yet. In this study, we synthesize novel derivatives by utilizing aldehydes featuring previously unreported substituents and bridge the gap by comparing their synthesis processes; luminescent properties; toxicological aspects, which have not been previously analyzed for anthraquinone derivatives; and applicability for confocal laser scanning microscopy, an aspect overlooked in studies of benzanthrone derivatives. An X-ray crystallographic study of an anthraquinone α-aminophosphonate, absent in earlier research, and benzanthrone α-aminophosphonate was performed as well.

2. Results and Discussion

2.1. Synthesis

The synthesis of target compounds was carried out using the Kabachnik–Fields reaction conditions. Numerous reviews have elucidated the mechanism and summarized diverse approaches for this three-component reaction [34–37]. These approaches encompass catalyzed and catalyst-free variations, as well as synthesis involving the use of ionic liquids, dehydrating agents, and microwave irradiation. We utilized our previously outlined synthetic procedure wherein an aromatic amine reacts at an elevated temperature with suitable aromatic aldehyde in excess, employing a dimethylphosphonate as both the reactant and the solvent. This one-pot, solvent-free approach is also influenced by the convenience of the subsequent extraction and purification of α-aminophosphonates. An excess of an aldehyde and a dimethylphosphonate undergo hydrolysis under moderately basic conditions, leading to the isolation of a pure compound through simple recrystallization. Compounds were obtained, on average, in 65% yields. Although the substrate has no significant impact on the reaction yield, the reaction with 4-bromobenzaldehyde, on average, yielded more than 70%. In contrast, the reaction with 4-(methylthio)benzaldehyde resulted in a slightly lower yield of 66%, and the lowest yield of 57% was achieved with 3-cyano-4-fluorophenylbenzaldehyde. Compounds were synthesized according to Figure 1.

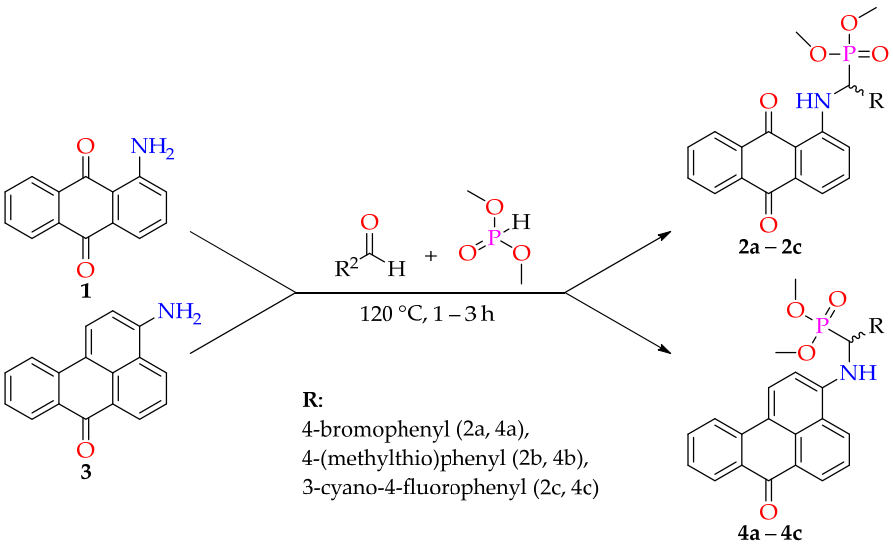

Figure 1. Synthesis of target α-aminophosphonates.

2.2. Spectroscopy

2.2.1. Structure

To validate the chemical structures of the acquired compounds, ^{1}H-, ^{13}C-, ^{31}P-NMR, and FTIR spectroscopy, as well as mass spectrometry, were performed.

The obtained infrared spectra showed broad amino group (NH) stretching vibration bands around 3225–3237 cm^{-1} for anthraquinone derivatives and around 3297–3484 cm^{-1} for benzanthrone derivatives; two stretching vibration peaks of anthraquinone carbonyl groups (C=O) and one for benzanthrone carbonyl group at around 1630–1669 cm^{-1}; and broad aliphatic and aromatic carbon–hydrogen (C–H) stretching vibration bands around 2848–3077 cm^{-1}.

The confirmation of the obtained compounds' structures was achieved through ^{1}H-NMR spectroscopy. The characteristic signals of aromatic protons were identified. The α-carbon hydrogen signal manifested as a doublet of doublets, arising from coupling with phosphorus. Hydrogens within the methyl groups of the phosphonate moiety appeared as distinct multiplets due to their magnetic non-equivalence. In APT NMR spectra, identifiable peaks of carbonyl group carbons emerged at approximately 184 ppm. Furthermore, the APT spectra exhibited distinct doublets due to carbon–phosphorus coupling and the magnetic non-equivalence of carbon atoms within the phosphonate moiety. In ^{31}P-NMR spectra, phosphorus peaks appeared as singlets at around 23 ppm (decoupled mode) and as doublets for fluorine-containing compounds **2c** and **4c**. The acquired data align well with previously reported NMR results for analogous compounds: benzanthrones [38,39], anthraquinones [40], and α-aminophosphonates [41–43].

The mass of the synthesized compounds, determined through the results obtained from high-resolution mass spectrometry, was verified to match the calculated values.

2.2.2. Photophysical Properties

To investigate the photophysical characteristics of the synthesized compounds, UV–Vis absorption and fluorescence emission spectra in solvents of varying polarity (benzene, chloroform, ethyl acetate (EtOAc), acetone, DMF (*N*,*N*-dimethylformamide), DMSO (dimethyl sulfoxide), and ethanol (EtOH)) were acquired.

The examined dyes demonstrated fluorescence and exhibited significant solvatochromic behavior, emitting light ranging from green in hexane to red in ethanol. The solvatochromic

properties of these derivatives indicate that the fundamental mechanism governing fluorescence was internal charge transfer during excitation, specifically from the electron-donating amino group to the electron-withdrawing carbonyl groups. Tables 1–3 provide a summary of data representing absorption maxima, molar attenuation coefficients, fluorescence maxima, fluorescence quantum yields, and Stokes shifts.

Table 1. Absorption maxima (and extinction coefficients) of synthesized dyes in organic solvents (concentration: 10^{-5} M).

Solvent	λ_{abs} Max, nm (lgε)					
	2a	**2b**	**2c**	**4a**	**4b**	**4c**
Hexane	471 (3.99)	475 (3.84)	465 (3.60)	454 (4.35)	457 (4.13)	447 (3.76)
Benzene	478 (4.00)	481 (3.89)	471 (3.87)	465 (4.38)	467 (4.27)	459 (4.00)
Chloroform	480 (3.95)	483 (3.81)	448 (3.95)	476 (4.37)	467 (4.24)	465 (4.00)
EtOAc	477 (4.04)	480 (3.86)	472 (3.83)	470 (4.40)	472 (4.21)	465 (4.00)
Acetone	478 (4.02)	478 (3.85)	472 (3.84)	477 (4.42)	478 (4.26)	476 (4.00)
DMF	481 (4.04)	486 (3.86)	478 (3.83)	490 (4.37)	491 (4.27)	486 (4.04)
DMSO	484 (4.03)	488 (3.88)	479 (3.85)	497 (4.40)	498 (4.25)	491 (4.08)
EtOH	480 (3.92)	478 (3.93)	473 (3.83)	489 (4.23)	488 (4.23)	483 (4.04)

Table 2. Fluorescence maxima (and quantum yields) of synthesized dyes in organic solvents (concentration: 10^{-5} M).

Solvent	λ_{em} Max, nm					
	2a	**2b**	**2c**	**4a**	**4b**	**4c**
Hexane	585 (0.05)	-	-	516 (0.49)	555 (0.48)	562 (0.08)
Benzene	584 (0.11)	580 (0.17)	572 (0.03)	552 (0.47)	555 (0.57)	542 (0.18)
Chloroform	596 (0.07)	595 (0.09)	550 (0.14)	571 (0.41)	589 (0.48)	574 (0.22)
EtOAc	597 (0.08)	592 (0.07)	582 (0.02)	588 (0.48)	578 (0.53)	566 (0.18)
Acetone	599 (0.01)	604 (0.08)	593 (0.02)	591 (0.43)	597 (0.56)	587 (0.15)
DMF	605 (0.06)	604 (0.03)	606 (0.01)	601 (0.45)	611 (0.48)	610 (0.13)
DMSO	610 (0.04)	617 (0.03)	616 (<0.01)	614 (0.36)	620 (0.42)	619 (0.12)
EtOH	614 (0.02)	628 (0.05)	609 (<0.01)	633 (0.19)	636 (0.23)	629 (0.10)

Table 3. Stokes shift of synthesized dyes in organic solvents (concentration: 10^{-5} M).

Solvent	$\nu_{abs} - \nu_{em}$, cm^{-1}					
	2a	**2b**	**2c**	**4a**	**4b**	**4c**
Hexane	4137	-	-	2647	3864	4578
Benzene	3797	3549	3749	3389	3395	3336
Chloroform	4055	3897	4140	3495	4435	4084
EtOAc	4214	3941	4004	4270	3885	3838
Acetone	4226	4364	4323	4044	4170	3973
DMF	4261	4020	4419	3769	4000	4183
DMSO	4268	4284	4643	3834	3951	4212
EtOH	4547	4997	4721	4652	4769	4806

In solutions, anthraquinone α-aminophosphonates **2a**, **2b**, and **2c** exhibit broad band absorbance around 465–488 nm and fluorescence from 584 nm (benzene) to 628 nm (ethanol) (Figure 2), whereas benzanthrone α-aminophosphonates **4a**, **4b**, and **4c** absorb around 447–498 nm and fluorescence from 516 nm (hexane) to 636 nm (ethanol) (Figure 3).

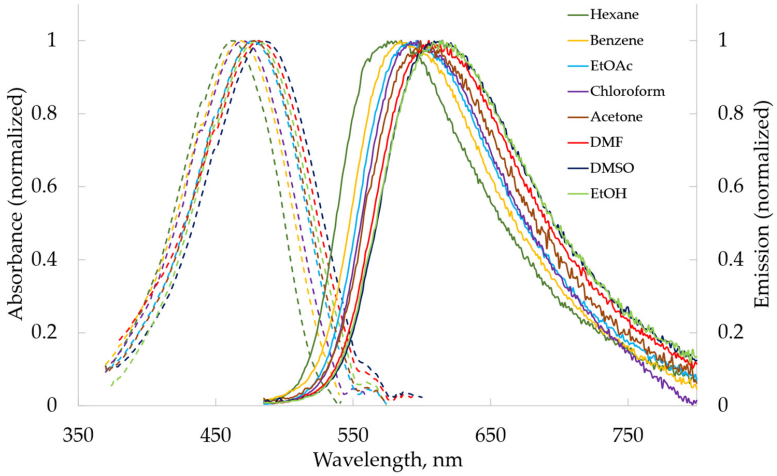

Figure 2. The UV–Vis absorption and fluorescence emission spectra of compound **2a** in various organic solvents.

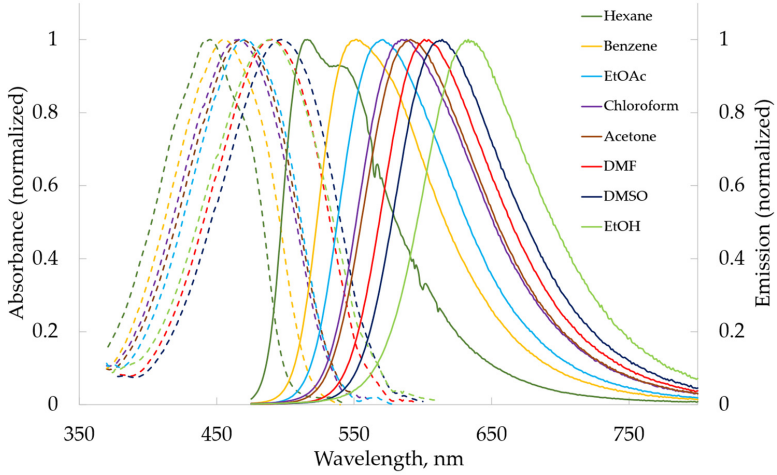

Figure 3. The UV–Vis absorption and fluorescence emission spectra of compound **4a** in various organic solvents.

While extinction coefficients, on average, were slightly higher for benzanthrone compounds than anthraquinone ones with the same substituents on the phenyl ring, fluorescence quantum yields were considerably higher, indicating a more efficient conversion of absorbed photons into emitted fluorescence. Because of the diminished fluorescence intensity of the examined anthraquinone dyes, the emission spectra exhibited noise. The polarity effect of the medium on fluorescence was more pronounced than on the absorption for both substrates. Among the studied dyes, the highest Stokes shift of 4997 cm^{-1}

was observed for the anthraquinone derivative **2c** in ethanol. The introduction of strong electron-accepting groups (**2c** and **4c**) significantly decreased both the extinction coefficients and quantum yields. The absorption spectra of the recently examined benzanthrone alkyl and aryl sulfides spanned from 403 to 448 nm [44], and amidines absorbed in the range of 410 to 495 nm [45,46], whereas 3-substituted benzanthrone amino derivatives exhibited absorption between 430 and 520 nm [47]. For 3-amino-9-nitrobenzanthrone derivatives, absorption occurred in the range of 450 to 560 nm [48]. This suggests that the benzanthrone amino group, when attached to a phosphoryl group, demonstrates a stronger donating effect compared to amidino and thiol groups, albeit to a slightly lesser degree than an alkyl amino group.

The molecular–microscopic solvent polarity parameter (E_T^N) considers the molecular aspects of the solvent structure that contribute to its overall polarity. Plots (Figure 4) show how changes in solvent polarity affected the emission wavelength maxima of compounds **2a** (anthraquinone derivative) and **4a** (benzanthrone derivative). As the polarity of the solvent rose, there was a corresponding lengthening of the emission wavelength. The linear correlation observed between the E_T^N parameter and emission maxima suggests the presence of general solute–solvent interactions, including H-bonding interactions, in the majority of solvents. The influence of polarity on the emission wavelength maxima was more pronounced for compound **4a** compared to **2a**.

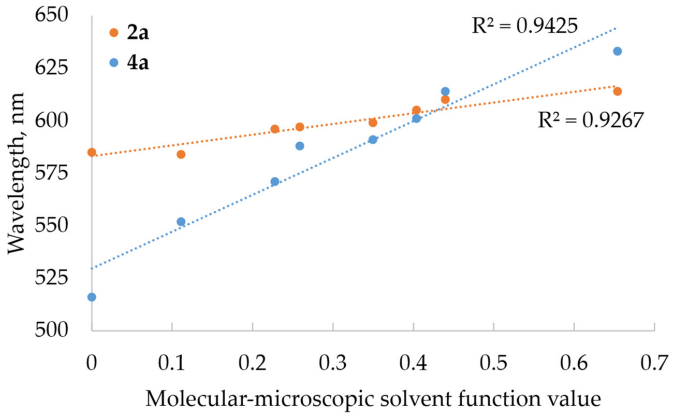

Figure 4. Emission wavelength maxima versus molecular–microscopic solvent polarity parameter (E_T^N) for compounds **2a** and **4a** in selected solvents; dotted lines represent linearity trend.

2.3. Toxicity Assessment

For the evaluation of the toxicity of compounds **2a** and **4a**, 6×10^{-5} M and 3×10^{-6} M solutions were prepared. Within 24 h, the etiolated wheat sprouts of the cultivar "Fenomen" were grown in a dark chamber at a temperature of 26 °C on moist filter paper. Wheat is a convenient object for research in plant physiology and biochemistry because the development of cereals is synchronous throughout ontogeny [49]. The first leaf and coleoptile were used because the first leaf is a developing organ of wheat, but the coleoptile is a senescent organ of wheat, and the processes which occur in these organs are different. A morphology test on filter paper was carried out in plastic dishes with three layers of paper on the bottom. Each dish contained 5 mL of dye solution or 5 mL of distilled water (control) and 30 seeds, which were covered by a lid. Dishes containing seeds were incubated for 5 days in a dark chamber at 26 ± 1 °C. The lengths of the first leaf and coleoptile were measured in millimeters (mm). Data are presented taking into consideration the standard error (SE) of three replicates.

The highest concentration of both dyes had a significant toxicological effect on the growth of the wheat leaves and coleoptiles (Figure 5); thus, an evaluation of the toxicity of

compounds **2a** and **4a** on the wheat seedlings was performed using only 3×10^{-6} M dye concentration. As a result, the phytotoxicity of the **2a** on the first leaf and coleoptile was higher than that of the **4a** (Table 4). We used this method to assess oxidative damage in wheat grown at lower concentrations as well (Table 5). The MDA levels were raised in the wheat leaves and coleoptile with both dyes compared to the control. This increase suggests that the cell membranes in wheat leaves and coleoptiles were experiencing oxidative damage, leading to lipid peroxidation. Nevertheless, the electrolyte leakage was decreased in the wheat sprouts. The decrease in electrolyte leakage suggests that the cell membrane's integrity was maintained or repaired to some extent, possibly due to the plant's defense mechanisms. The increase in MDA levels and the decrease in electrolyte leakage are indicative of complex cellular responses to oxidative stress due to dye toxicity.

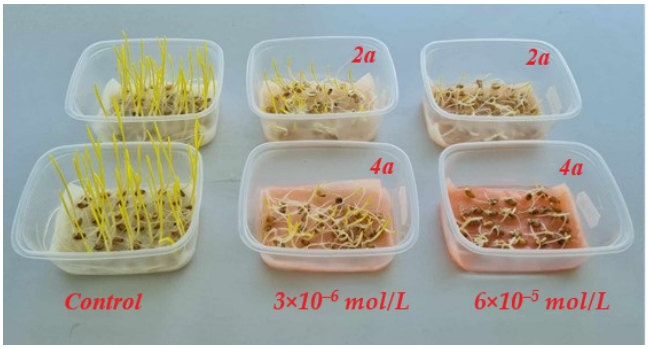

Figure 5. Wheat seedlings cultivated in the presence of dyes **2a** and **4a**, with concentrations 0 M, 6×10^{-5} M, 3×10^{-6} M.

Table 4. Morphology of the wheat sprouts cultivated in the presence of dyes **2a** and **4a**.

	Length of First Leaf (mm)	Length of Coleoptile (mm)	Phytotoxicity on the First Leaf (%)	Phytotoxicity on the Coleoptile (%)
Control	68.26	34.52	-	-
2a (3×10^{-6} M)	20.52	12.70	70	63
4a (3×10^{-6} M)	24.24	14.76	64	57

Table 5. Electrolyte leakage and MDA assay of the wheat sprouts cultivated in the presence of dyes **2a** and **4a**.

	Electrolyte Leakage		MDA Assay	
	First Leaf	Coleoptile	First Leaf	Coleoptile
Control	41	15	31.9	15.1
2a (3×10^{-6} M)	29	23	63.8	40.9
4a (3×10^{-6} M)	20	21	67.0	46.5

Both dyes were found to cause significant oxidative damage to wheat seedlings, as evidenced by elevated levels of malondialdehyde (as the indicator of oxidative stress) content and electrolyte leakage compared to control wheat sprouts.

The results thus show that the toxic properties of the studied substances differed: the anthraquinone derivative **2a** was more toxic to plants than analogous benzanthrone one **4a**. This may arise from the quinone nature of **2a**, which, when reacting with antioxidants, leads to the release of reactive oxygen species (ROS) [50].

Similar data were obtained for benzanthrone derivatives with the thiophene and unsubstituted phenyl group [2].

2.4. Confocal Laser Scanning Microscopy Imaging of Trematode Opisthorchis Felineus

Opisthorchis felineus is a parasitic flatworm, commonly known as the cat liver fluke, that primarily infects the livers and bile ducts of various mammals, including humans. The life cycle of *O. felineus* involves several stages and includes both intermediate and definitive hosts. Adult flukes residing in the bile ducts release eggs, which are then excreted with the host's feces. Embryonated eggs release miracidia upon reaching the external environment. Miracidia penetrate specific freshwater snails (e.g., *Radix* spp.) for further development [51]. Within the snail host, miracidia transform into sporocysts and then rediae, undergoing asexual reproduction. Cercariae, free-swimming larvae, are released from the snails. Cercariae infect freshwater fish, the second intermediate hosts [52]. Cercariae encyst in the muscles of fish, becoming metacercariae, the infective stage for the definitive host. Definitive hosts, including mammals and humans, become infected by consuming raw or undercooked fish containing metacercariae [53]. The life cycle is completed when adult flukes release eggs into the bile ducts, restarting the cycle. *Opisthorchis felineus* is endemic in regions around the Baltic Sea, Caspian Sea, and Black Sea [54]. Various estimates suggest that the current infection rate with these liver flukes potentially affects up to 40 million people, while a substantial risk group of approximately 600–750 million people exists in Eurasian countries [55]. These parasites are expanding their colonization into previously unreported regions in Eurasia [56]. Opisthorchiasis in humans is associated with chronic liver disease and an increased risk of cholangiocarcinoma [57]. Moreover, *O. felineus* can also infect domestic and wild mammals, which serve as reservoir hosts and contribute to the persistence of the parasite in certain ecosystems [58]. To bring all of this together, *O. felineus* poses a significant public health concern. Thus, understanding the life cycle and epidemiology of *O. felineus* is crucial for implementing effective control strategies and public health interventions in endemic areas.

Among the synthesized anthrone-based dyes investigated in this study, four specific compounds were subjected to testing with *Opisthorchis felineus*. Two of these compounds, namely, **4b** and **4c**, were benzanthrone dyes, which have pronounced lipophilic properties, while the remaining two, **2b** and **2c**, were anthraquinone dyes, exhibiting comparatively lower hydrophobic characteristics. According to the initial data, **4b** and **4c** dyes showed the structure and muscle of the parasite *O. felineus* slightly more clearly (see Figures 6 and 7). Thus, it can be concluded that benzanthrone dyes are better for visualizing *Opisthorchis felineus* flukes. The obviously hydrophilic nature of the dye has a significant impact on the visualization of these biological objects. Overall, all tested dyes demonstrated promising initial outcomes, prompting us to undertake a more comprehensive examination of these dyes in subsequent studies.

2.5. X-ray Crystallographic Study

Figure 8 shows a perspective view of molecule **2a** with thermal ellipsoids, and the atom-numbering scheme follows in the text. In the molecular structure, the planar anthraquinone and phenyl systems form a dihedral angle of 84.3(8)°. The torsion angle of C1–N11–C12–C19 is equal to 73.2(7)°. The coordination polyhedron of the phosphorus atom is a tetrahedron in which the central atom (P13) deviates by 0.463(6) Å from the plane of the base (O14, O15, O17). The molecular structure is stabilized by a strong intramolecular hydrogen bond of NH···O type between the amino group and the quinone oxygen O26; the parameters of this bond are as follows: N11···O26 = 2.636(7) Å, H11···O26 = 1.93(6) Å, N11–H11···O26 = 146(4)°.

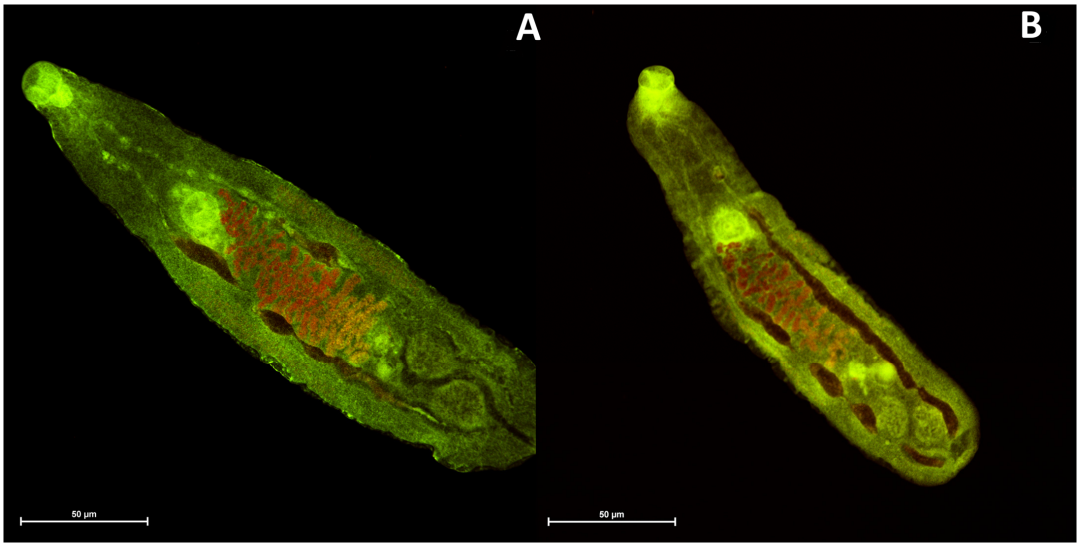

Figure 6. Adult *Opisthorchis felineus* stained with the examined dyes: (**A**)—**2b**; (**B**)—**2c**.

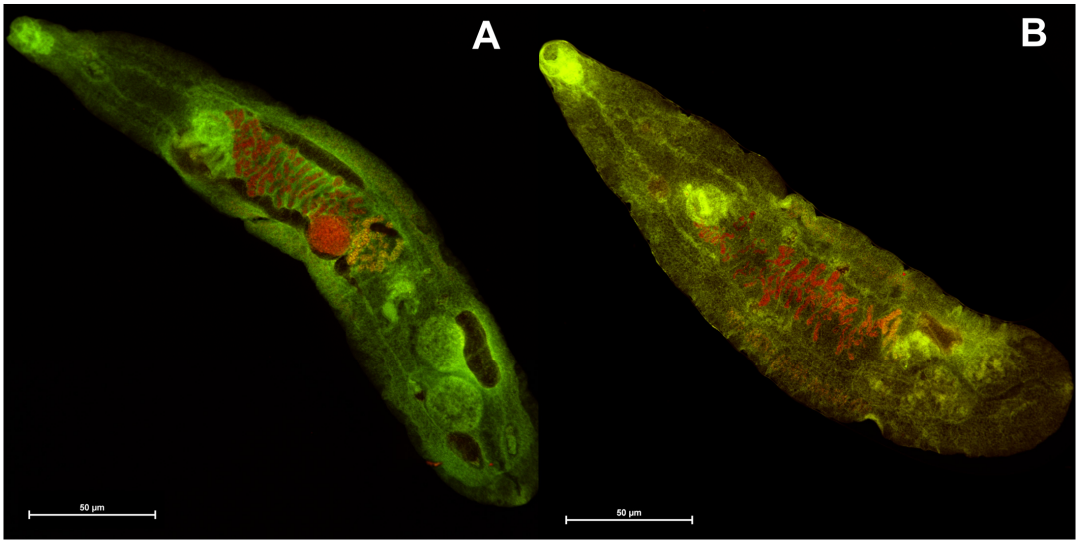

Figure 7. Adult *Opisthorchis felineus* stained with the examined dyes: (**A**)—**4b**; (**B**)—**4c**.

The crystal structure of **2a** is achiral (space group is $P\bar{1}$); thus, despite the asymmetric carbon atom (C12), the substance represents a true racemate. A characteristic feature of the crystal structure of **2a** is the fact that there is a strong π–π stacking interaction between anthraquinone systems; the shortest intermolecular atom–atomic contact (C9a···C10) is equal to 3.332(8) Å. By means of these interactions, molecular stacks are formed in the crystal structure along the crystallographic direction [0 1 0] (Figure 9). The amino group is involved in the strong intramolecular H-bond; therefore, it does not form intermolecular H-bonds. However, there are carbon atoms with as increased electronegativity; first of all, these are carbons of methyl groups bonded to oxygen atoms. This is why mod-

erated intermolecular H-bonds of CH···O type are formed in the crystal structure. The parameters of these bonds are as follows: C16···O27 = 3.292(9) Å, H16B···O27 = 2.31 Å, C16–H16B···O27 = 178°; C18···O17 = 3.244(9) Å, H18A···O17 = 2.50 Å, C16–H16B···O27 = 132°. It is also worth highlighting a rather strong halogen bond between bromine atoms with a length of 3.449(5) Å. Through this bond, the molecules in the crystal structure combine to form centrosymmetric dimers.

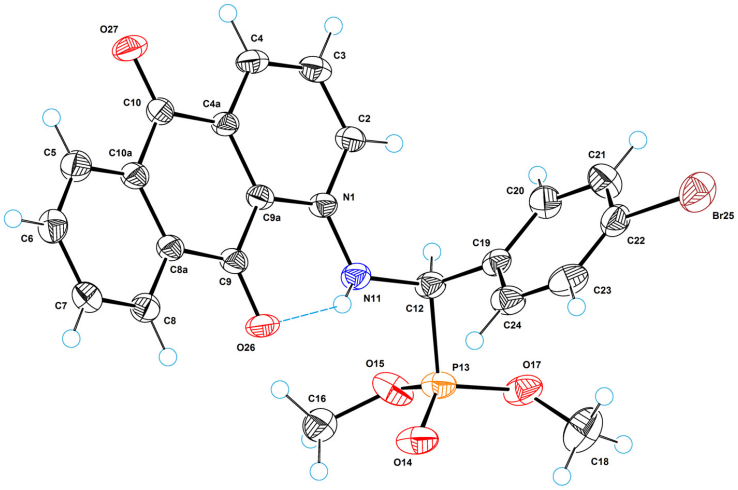

Figure 8. ORTEP diagram with the labels of atoms for **2a**.

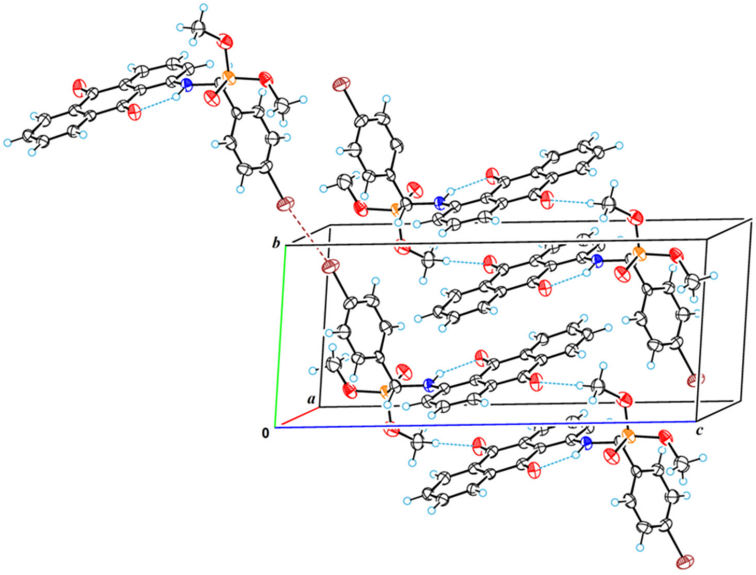

Figure 9. A fragment of the crystal structure of **2a**, showing hydrogen and halogen bonds. Red—oxygen, blue—nitrogen, orange—phosphorous, brown—bromine. Brown dashed line represents halogen bond between bromine atoms and blue dotted line represents hydrogen bonding.

Figure 10 illustrates a perspective view of molecule **4a**, with thermal ellipsoids and the atom-numbering scheme following in the text. A characteristic feature of the crystal structure is static disorder of the dimethyl phosphonate group: In the crystals, there are two molecular forms of **4a**, which differ in the conformation of the dimethyl phosphonate group. The occupancy g-factors of these forms are 0.65 and 0.35; Figure 10 shows the form with the largest g-factor.

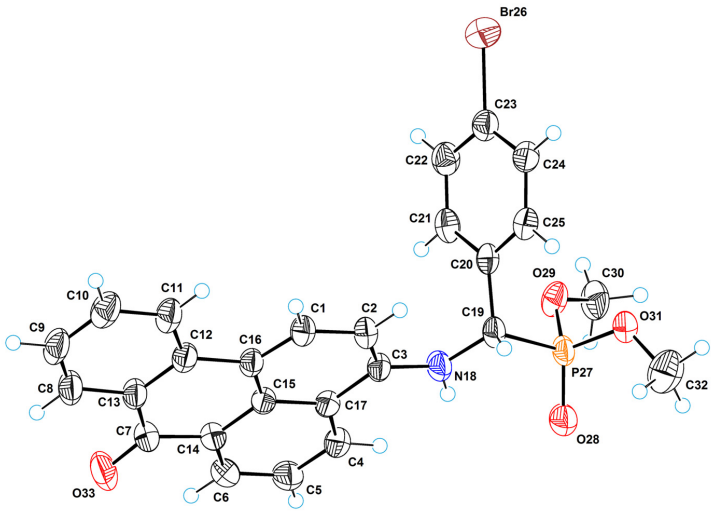

Figure 10. ORTEP diagrams with labels of atoms for **4a**. Red—oxygen, blue—nitrogen, orange—phosphorous, brown—bromine.

The peculiarity of the molecular structure is a fairly strong intramolecular hydrogen bond of NH···O type between the amino group and dimethylphosphonate. The parameters of this bond are as follows: N18···O28 = 2.947(4) Å, H11···O26 = 2.44(3) Å, N18−H18···O28 = 121(3)°. By means of this bond, an additional five-membered cycle is formed in the structure of **4a** molecules (see Figure 11). The H-bond stabilizes the molecular structure; through it, the oxygen atom O28 is not disordered, unlike the other atoms of the dimethyl phosphonate group.

The torsion angle of C3−N18−C19−C20 is equal to −66.8(3)°. In the molecular structure, the planar benzanthrone and phenyl systems form a dihedral angle of 73.7(3)°.

The crystal structure of **4a** is less dense than **2a**. The packing index for **4a**, calculated using Kitaigorodsky's approach [59], is equal to 0.693, while for **2a**, it is 0.708. In the crystal structure **4a**, there is no halogen bond; only a weak intermolecular hydrogen bond of CH···O type with a length of 3.263(5) Å occurs between the C24−H24 group and oxygen atom O28. Numerous weak intermolecular CH···π interactions are also present, the strongest of which is C4−H4···C_s (H4···C_s = 3.14 Å), where C_s represents the centroid of the phenyl ring. Figure 12 shows this interaction along with hydrogen bonds. In addition to **2a**, the crystal structure of **4a** is achiral (space group is $P2_1/c$); thus, despite the asymmetric carbon atom (C19), the substance represents a true racemate.

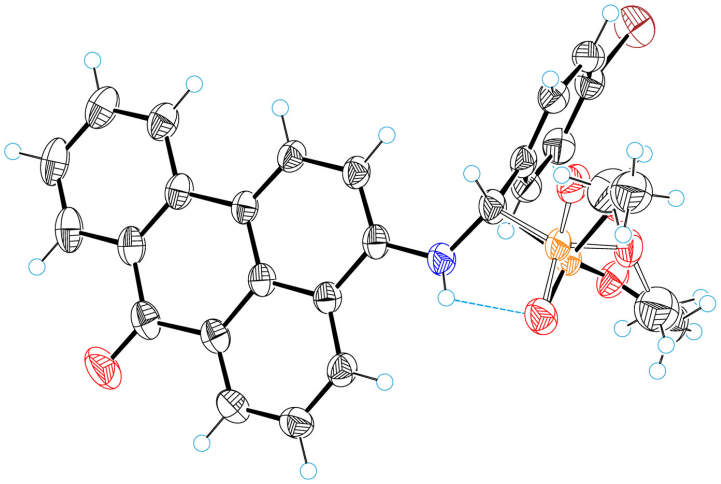

Figure 11. H-bond formation and disorder of the dimethyl phosphonate group in **4a**. Red—oxygen, blue—nitrogen, orange—phosphorous, brown—bromine.

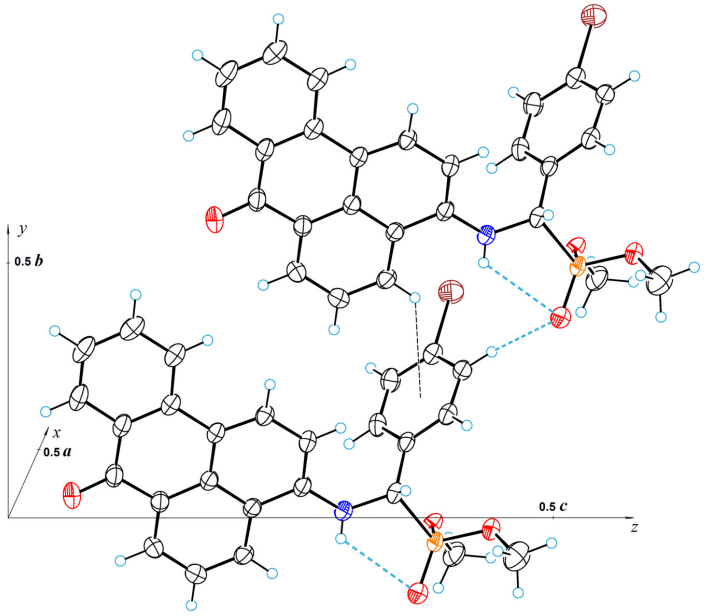

Figure 12. A fragment of the crystal structure of 4a, showing hydrogen and C4−H4···π bonds. Red—oxygen, blue—nitrogen, orange—phosphorous, brown—bromine.

3. Materials and Methods

3.1. Materials and Measurments

All of the reagents and solvents were obtained commercially and used without any additional purification. The assessment of the progress of reactions and purity of the synthesized compounds was performed using TLC on MERCK Silica gel 60 F254 plates, with hexane/acetone (1:2) as an eluent, and visualized under UV light. Melting points were

determined using a METTLER TOLEDO™ Melting Point System MP70 apparatus. The IR spectrum was recorded on a Thermo Scientific Nicolet iS50 Spectrometer (ATR accessory; no. of scans: 64; resolution: 4; data spacing: 0.482 cm^{-1}). ^{1}H-, ^{13}C-, and ^{31}P-NMR were captured using a Bruker Avance 500 MHz (Bruker Corporation, Billerica, MA, USA) in $CDCl_3$ at room temperature. Solvent peaks were used as the internal reference. Chemical shift (δ) values are reported in ppm. Accurate high-resolution mass measurements were conducted using the Orbitrap Exploris 120 (Thermo Fisher Scientific, Waltham, MA, USA), operating in Full Scan mode at a resolution of 120,000. The FLSP920 spectrofluorometer (Edinburgh Instruments Ltd., Livingston, UK) captured fluorescence emission spectra within the visible range of 450–800 nm, while the absorption spectra were acquired using the UV-visible spectrophotometer SPECORD® 80 (Analytik Jena AG, Jena, Germany).

3.2. Synthesis and Characterization

General procedure for synthesis of derivatives **2a**–**2c** and **4a**–**4c**:

In a 10 mL round-bottom flask fitted with a magnetic stirrer bar, 2 mmol of an amine, 6 mmol of an aldehyde, and 5 mL of dimethylphosphonate were combined. The mixture was stirred at 120 °C for 1 to 3 h, with progress monitored using TLC. After the completion of the reaction, the mixture was poured into 100 mL of concentrated sodium bicarbonate ($NaHCO_3$) solution and left overnight while being stirred until a solid product was formed. The precipitate was then filtered, thoroughly washed with water, and dried. Purification of the product was achieved through multi-solvent recrystallization using xylenes and hexane.

Dimethyl ((4-bromophenyl)((9,10-dioxo-9,10-dihydroanthracen-1-yl)amino)methyl)phosphonate (**2a**) was obtained as an orange compound in a 71% yield with a m.p. of 166 °C. R*f* = 0.72 (hexane-acetone, *v*/*v* 1:2). ^{1}H NMR (500 MHz, *Chloroform-d*) δ 10.64 (dd, J = 10.4, 7.4 Hz, 1H, NH), 8.31 (dd, J = 7.7, 1.6 Hz, $1H_{Ar}$), 8.18 (dd, J = 7.6, 1.6 Hz, $1H_{Ar}$), 7.73 (td, J = 7.5, 1.5 Hz, $1H_{Ar}$), 7.68 (td, J = 7.5, 1.5 Hz, $1H_{Ar}$), 7.59 (d, J = 7.4 Hz, $1H_{Ar}$), 7.44 (d, J = 8.1 Hz, $2H_{Ar}$), 7.38 (t, J = 8.0 Hz, $1H_{Ar}$), 7.36–7.30 (m, $2H_{Ar}$), 6.75 (d, J = 8.6 Hz, $1H_{Ar}$), 4.92 (dd, J = 24.0, 7.3 Hz, 1H, NCH), 3.70 (ddd, J = 18.9, 10.7, 1.4 Hz, 6H, OCH_3). ^{13}C NMR (126 MHz, *Chloroform-d*) δ 185.86 (C=O), 183.41 (C=O), 149.92 (d, J = 13.5 Hz, C), 135.41 (CH), 134.82 (C), 134.67 (C), 134.12 (CH), 134.01 (d, J = 3.7 Hz, C), 133.44 (CH), 132.98 (C), 132.12 (d, J = 2.8 Hz, CH), 129.37 (d, J = 5.2 Hz, CH), 127.13 (CH), 126.85 (CH), 122.46 (d, J = 4.2 Hz, C), 118.24 (CH), 117.16 (CH), 114.82 (C), 54.60 (d, J = 152.5 Hz, NCH), 54.39 (d, J = 7.2 Hz, OCH_3), 54.09 (d, J = 7.1 Hz, OCH_3). ^{31}P NMR (202 MHz, *Chloroform-d*) δ 22.38. FTIR (neat): 1631 and 1668 (C=O); 2852, 2905, 2952 and 3067 (CH); 3225 (NH). ESI-FTMS: calculated for $[C_{23}H_{19}BrNO_5P]$: 500.0257, found: 500.0254.

*Dimethyl (((9,10-dioxo-9,10-dihydroanthracen-1-yl)*amino*)(4-(methylthio)phenyl)methyl)phosphonate* (**2b**) was obtained as an orange compound in 63% yield with a m.p. of 154 °C. R*f* = 0.69 (hexane-acetone, *v*/*v* 1:2). ^{1}H NMR (500 MHz, *Chloroform-d*) δ 10.63 (dd, J = 10.2, 7.4 Hz, 1H, NH), 8.31 (dd, J = 7.6, 1.6 Hz, $1H_{Ar}$), 8.18 (dd, J = 7.6, 1.6 Hz, $1H_{Ar}$), 7.72 (td, J = 7.5, 1.6 Hz, $1H_{Ar}$), 7.67 (td, J = 8.2, 6.7 Hz, $1H_{Ar}$), 7.58 (d, J = 7.4 Hz, $1H_{Ar}$), 7.41–7.33 (m, $3H_{Ar}$), 7.17 (d, J = 8.4 Hz, $2H_{Ar}$), 6.80 (d, J = 8.5 Hz, $1H_{Ar}$), 4.92 (dd, J = 23.6, 7.5 Hz, 1H, NCH), 3.71 (d, J = 10.6 Hz, 2H, OCH_3), 3.66 (d, J = 10.7 Hz, 2H, OCH_3), 2.39 (s, 3H, SCH_3), 1.56 (d, J = 3.5 Hz, 2H, OCH_3). ^{13}C NMR (126 MHz, *Chloroform-d*) δ 185.75 (C=O), 183.49 (C=O), 150.16 (C), 150.06 (C), 138.99 (d, J = 3.8 Hz, C), 135.34 (CH), 134.75 (d, J = 3.6 Hz, C), 134.09 (CH), 133.36 (CH), 132.99 (C), 131.33 (d, J = 4.0 Hz, C), 128.14 (d, J = 5.3 Hz, CH), 127.12 (CH), 126.81 (CH), 126.67 (d, J = 2.7 Hz, CH), 118.44 (CH), 117.00 (CH), 114.70 (C), 54.65 (d, *J* = 153.0 Hz, NCH), 54.33 (d, J = 7.1 Hz, OCH_3), 54.05 (d, J = 7.1 Hz, OCH_3), 15.50 (SCH_3). ^{31}P NMR (202 MHz, *Chloroform-d*) δ 22.97. FTIR (neat): 1630 and 1669 (C=O); 2848, 2950, 2998 and 3077 (CH); 3237 (NH). ESI-FTMS: calculated for $[C_{24}H_{22}SNO_5P+H^+]$: 468.1029, found: 468.1017.

Dimethyl ((3-cyano-4-fluorophenyl)((9,10-dioxo-9,10-dihydroanthracen-1-yl)amino)methyl)phosphonate (**2c**) was obtained as an orange solid in a 59% yield with a m.p. of 205 °C. R*f* = 0.71 (hexane-acetone, *v*/*v* 1:2). ^{1}H NMR (500 MHz, *Chloroform-d*) δ 10.63 (dd, *J* = 10.7, 7.4 Hz, 1H, NH), 8.31 (d, *J* = 7.6 Hz, $1H_{Ar}$), 8.20 (d, *J* = 7.5 Hz, $1H_{Ar}$), 7.78–7.69 (m, $2H_{Ar}$), 7.69 (t, *J* = 4.0 Hz, $2H_{Ar}$), 7.64 (d, *J* = 7.4 Hz, $1H_{Ar}$), 7.42 (t, *J* = 8.0 Hz, $1H_{Ar}$), 7.16 (d, *J* = 8.4 Hz, $1H_{Ar}$), 6.68 (d, *J* = 8.5

Hz, 1H$_{Ar}$), 4.95 (dd, *J* = 24.3, 7.3 Hz, 1H, NCH), 3.76 (dd, *J* = 12.9, 10.8 Hz, 6H, OCH$_3$). ^{13}C NMR (126 MHz, *Chloroform-d*) δ 186.14 (C=O), 183.23 (C=O), 163.94 (d, *J* = 3.3 Hz, C), 161.85 (C), 149.42 (d, J = 13.4 Hz, C), 135.59 (CH), 135.00 (C), 134.52 (C), 134.30 (dd, J = 8.5, 4.7 Hz, CH), 134.22 (CH), 133.66 (CH), 132.94 (C), 132.60 (C), 132.46 (d, J = 5.3 Hz, CH), 127.18 (CH), 126.93 (CH), 117.72 (CH), 117.58 (CH), 117.15 (dd, J = 20.0, 2.5 Hz, CH), 115.13 (C), 113.51 (C), 54.53 (d, J = 7.2 Hz, OCH$_3$), 54.20 (d, J = 7.0 Hz, OCH$_3$), 53.80 (d, J = 153.0 Hz, NCH). ^{31}P NMR (202 MHz, *Chloroform-d*) δ 21.54 (d, J = 7.4 Hz). FTIR (neat): 1630 and 1667 (C=O); 2236 (C≡N); 2857, 2904, 2960 and 3046 (CH); 3235 (NH). ESI-FTMS: calculated for [$C_{24}H_{22}SNO_5P$+H$^+$]: 465.1010, found: 465.0996.

Dimethyl ((4-bromophenyl)((7-oxo-7H-benzo[de]anthracen-3-yl)amino)methyl)phosphonate (**4a**) was obtained as a red solid in a 75% yield with a m.p. of 207 °C. R*f* = 0.68 (hexane-acetone, *v*/*v* 1:2). ^{1}H NMR (500 MHz, *Chloroform-d*) δ 8.77 (dd, J = 7.3, 1.2 Hz, 1HAr), 8.37 (td, J = 7.9, 1.4 Hz, 2HAr), 8.09 (d, J = 8.3 Hz, 1H$_{Ar}$), 8.04 (d, J = 8.2 Hz, 1H$_{Ar}$), 7.75 (t, J = 7.8 Hz, 1H$_{Ar}$), 7.61–7.54 (m, 1H$_{Ar}$), 7.45 (d, J = 8.5 Hz, 2H$_{Ar}$), 7.39–7.32 (m, 3H$_{Ar}$), 6.42 (d, J = 8.3 Hz, 1H$_{Ar}$), 5.87 (dd, J = 10.5, 6.7 Hz, 1H, NH), 4.93 (dd, J = 24.0, 6.6 Hz, 1H, NCH), 3.77 (d, J = 10.8 Hz, 3H, OCH$_3$), 3.53 (d, J = 10.7 Hz, 3H, OCH$_3$). ^{13}C NMR (126 MHz, *Chloroform-d*) δ 184.01 (C=O), 143.65 (d, J = 14.3 Hz, C), 136.80 (C), 133.87 (d, J = 3.9 Hz, C), 133.25 (CH), 132.22 (d, J = 2.8 Hz, CH), 130.13 (CH), 129.67 (C), 129.23 (CH), 129.19 (CH), 129.16 (C), 128.75 (C), 127.98 (CH), 126.67 (CH), 126.05 (CH), 125.58 (CH), 123.40 (C), 122.53 (d, J = 4.2 Hz, C), 122.05 (CH), 117.48 (C), 106.92 (CH), 55.23 (d, *J* = 151.1 Hz, NCH), 54.28 (d, J = 7.0 Hz, OCH$_3$), 54.08 (d, J = 7.0 Hz, OCH$_3$). ^{31}P NMR (202 MHz, *Chloroform-d*) δ 23.60. FTIR (neat): 1638 (C=O); 2849, 2952 and 3050 (CH); 3401 (NH). ESI-FTMS: calculated for [$C_{26}H_{21}BrNO_4P$–H+]: 520.0318, found: 521.0320.

Dimethyl ((4-(methylthio)phenyl)((7-oxo-7H-benzo[de]anthracen-3-yl)amino)methyl)phosphonate (**4b**) was obtained as a red solid in a 68% yield with a m.p. of 123 °C. Rf = 0.77 (hexane-acetone, *v*/*v* 1:2). ^{1}H NMR (500 MHz, *Chloroform-d*) δ 8.77 (dd, J = 7.1, 0.8 Hz, 1H$_{Ar}$), 8.41–8.35 (m, 2H$_{Ar}$), 8.10 (d, J = 8.3 Hz, 1H$_{Ar}$), 8.05 (d, J = 8.2 Hz, 1H$_{Ar}$), 7.75 (t, J = 7.8 Hz, 1H$_{Ar}$), 7.61–7.54 (m, 1H$_{Ar}$), 7.42–7.32 (m, 3H$_{Ar}$), 7.18 (d, J = 7.8 Hz, 2H$_{Ar}$), 6.48 (d, J = 8.3 Hz, 1H$_{Ar}$), 5.90 (s, 1H, NH), 4.94 (d, J = 23.8 Hz, 1H, NCH), 3.76 (d, J = 10.8 Hz, 3H, OCH$_3$), 3.50 (d, J = 10.6 Hz, 3H, OCH$_3$), 2.39 (s, 3H, SCH$_3$). ^{13}C NMR (126 MHz, *Chloroform-d*) δ 184.04 (C=O), 143.94 (d, J = 14.4 Hz, C), 139.20 (C), 136.89 (C), 133.22 (CH), 131.15 (d, J = 3.9 Hz, C), 130.10 (CH), 129.64 (C), 129.12 (C), 128.74 (C), 128.02 (CH), 127.97 (d, J = 1.6 Hz, CH), 126.78 (CH), 126.69 (d, J = 2.7 Hz, CH), 126.56 (CH), 126.19 (CH), 125.48 (CH), 123.41 (C), 122.02 (CH), 117.20 (C), 106.91 (CH), 55.24 (d, J = 151.8 Hz, NCH), 54.29 (d, J = 7.0 Hz, OCH$_3$), 53.97 (d, J = 7.1 Hz, OCH$_3$), 15.46 (SCH$_3$). ^{31}P NMR (202 MHz, *Chloroform-d*) δ 24.16. FTIR (neat): 1630 (C=O); 2851, 2914, 2951, 2982 and 3059 (CH); 3484 (NH). ESI-FTMS: calculated for [$C_{27}H_{24}NO_4PS$+H+]: 490.1236, found: 490.1221.

Dimethyl ((3-cyano-4-fluorophenyl)((7-oxo-7H-benzo[de]anthracen-3-yl)amino)methyl)phosphonate (**4c**) was obtained as a red solid in a 55% yield with a m.p. of 120 °C. Rf = 0.66 (hexane-acetone, *v*/*v* 1:2). ^{1}H NMR (500 MHz, *Chloroform-d*) δ 8.79 (d, J = 7.3 Hz, 1H$_{Ar}$), 8.38 (d, J = 7.9 Hz, 1H$_{Ar}$), 8.35 (d, J = 8.3 Hz, 1H$_{Ar}$), 8.10 (d, J = 8.2 Hz, 1H$_{Ar}$), 8.06 (d, J = 8.2 Hz, 1H$_{Ar}$), 7.81–7.70 (m, 2H$_{Ar}$), 7.60 (t, J = 7.7 Hz, 1H$_{Ar}$), 7.38 (t, J = 7.5 Hz, 1H$_{Ar}$), 7.13–7.05 (m, 2H$_{Ar}$), 6.36 (d, J = 8.2 Hz, 1H$_{Ar}$), 5.81 (dd, J = 10.9, 6.3 Hz, 1H, NH), 4.97 (dd, J = 24.0, 5.9 Hz, 1H, NCH), 3.80 (d, J = 10.8 Hz, 3H, OCH$_3$), 3.65 (d, J = 10.8 Hz, 3H, OCH$_3$). ^{13}C NMR (126 MHz, *Chloroform-d*) δ 183.94 (C=O), 161.89 (C), 159.30 (C), 143.01 (d, J = 13.7 Hz, C), 136.60 (C), 133.98 (dd, J = 8.4, 4.8 Hz, CH), 133.36 (CH), 132.44 (C), 132.43 (d, J = 5.2 Hz, CH), 130.26 (CH), 129.75 (C), 129.24 (C), 129.05 (CH), 128.83 (C), 128.24 (CH), 128.03 (CH), 126.72 (d, J = 55.9 Hz, CH), 125.80 (d, J = 16.5 Hz, CH), 123.42 (C), 122.12 (CH), 118.21 (C), 117.26 (dd, J = 20.0, 2.5 Hz, CH), 113.46 (C), 106.88 (CH), 54.56 (d, J = 151.5 Hz, NCH), 54.39 (d, J = 7.1 Hz, OCH$_3$), 54.21 (d, J = 7.0 Hz, OCH$_3$). ^{31}P NMR (202 MHz, *Chloroform-d*) δ 22.74 (d, J = 5.2 Hz). FTIR (neat): 1648 (C=O); 2236 (C≡N); 2851, 2962, 3023 and 3067 (CH); 3297 (NH). ESI-FTMS: calculated for [$C_{27}H_{20}FN_2O_4P$+H+]: 487.1218, found: 487.1200.

3.3. Toxicology

For toxicological study, ethanol solutions of the obtained compounds **2a** and **4a**, at concentrations of 3×10^{-3} M, were prepared. Then, 10 mL of this solution was diluted with water to 500 mL to obtain a finely dispersed suspension with a resulting concentration of 6×10^{-5} M. Then, by means of dilution, a suspension with a concentration of 3×10^{-6} M was prepared. Within 24 h, the etiolated wheat sprouts of the cultivar "Fenomen" were grown in a dark chamber at a temperature of 26 °C on moist filter paper. A morphology test on filter paper was carried out in plastic dishes with three layers of paper on the bottom. Each dish contained 5 mL of dye solution or 5 mL of distilled water (control) and 30 seeds, covered by a lid. Dishes containing seeds were incubated for 5 days in a dark chamber at 26 ± 1 °C.

3.3.1. Quantification of Malondialdehyde

The MDA content was determined by the thiobarbituric acid (TBA) reaction as described previously by Ali et al., with slight modifications [60]. Wheat germ, the first leaves, and the coleoptiles were homogenized in 0.1% trichloroacetic acid solution (1/10) and centrifuged for 15 min (14,000 rpm). After centrifugation, 2.5 mL of 0.5% thiobarbituric acid (in 20% trichloroacetic acid solution) was added to 1 mL of the upper fraction, and the solution was incubated in hot water (95 °C) for 30 min. The solution was cooled immediately to stop the reaction and centrifuged for 30 min (14,000 rpm). The optical density of the solution was determined at 532 nm and 600 nm wavelengths using a UV/VIS spectrophotometer, and the MDA concentration was calculated by subtracting the non-specific absorbance (600 nm) from the absorbance at a wavelength of 532 nm (ϵ = 155 $mM^{-1}cm^{-1}$).

3.3.2. Electrolyte Leakage Measurements

The electrolyte leakage was determined as described previously by Guo et al. [61]. Organs of four seedlings (the first leaves, coleoptiles) were immersed in 15 mL deionized water (24 h, room temperature). After 24 h, the initial conductivity of the wheat germ organs was determined using a conductometer. The test tubes with the samples were placed into boiling water for 15 min, and after cooling to room temperature, the conductivity of the samples was again determined.

3.4. Imaging

Adult *Opisthorchis felineus* trematodes were collected within the framework of the project AP05131132, "PCR test for the detection and differential diagnosis of pathogens of opisthorchiasis and metorchiasis". This research was approved by the Animal Ethics Committee of Veterinary Medicine Faculty of KATU (Ethical approval letter, No: 1, 9 November 2017).

An ethanol solution of the synthesized dyes with a molar concentration of 10^{-4} M was used for staining of the parasite sample for 10 min. Then, the dye was washed out three times with 70% ethanol. Further, the sample was placed into ethanol–xylene solution (1:1) for 10 min. Finally, the specimens were mounted on Canada balsam and covered with coverslips (24 × 24 mm).

A CLSM Eclipse Ti-E microscope, outfitted with a digital sight DS-U3 camera and configured with a high-speed multiphoton A1R MP confocal system and motorized stage (Nikon, Japan) was used. The CLSM images underwent processing using the NIS Elements Advanced Research 3.2 64-bit software (Nikon, Tokyo, Japan). Two lasers were employed to visualize the parasite: a 488 nm laser with a FITC filter (500–550 nm) and a 638 nm laser with a Cy5 filter (662–737 nm). The fluorescence signal registration was conducted using an internal spectral detector. The registration process began with a start wavelength set 20 nm higher than the excitation wavelength, extending to the edge of the red visible spectrum. No passive cutoff filters were inserted into the optical path. Images were captured as Z stacks with a 2.0 μm Z step size.

3.5. Single-Crystal X-ray Diffraction Analysis

The studied single crystals were grown from dichloromethane via slow evaporation. Diffraction data were collected at 160 K on a Rigaku, XtaLAB Synergy, Dualflex, HyPix diffractometer using monochromated Cu-Kα radiation (λ = 1.54184 Å).

For the compound **2a**, the crystal structure was solved using the heavy-atom method [62], and for the compound **4a**, the crystal structure was solved with the SIR2011 [63] structure solution program using Direct Methods Refined with the ShelXL [64] refinement package and least squares minimization. All nonhydrogen atoms were refined in anisotropic approximation. The hydrogen atoms involved in the formation of H-bonds were refined isotopically; all other H-atoms were refined using a riding model with Uiso(H) = 1.2Ueq(C).

Crystal Data for **2a** ($C_{23}H_{19}BrNO_5P$; M = 500.27 g/mol): triclinic, space group $P\,\bar{1}$ (no. 2), a = 7.5626(2) Å, b = 7.7876(2) Å, c = 18.0152(5) Å, α = 85.582(2)°, β = 78.626(2)°, γ = 85.643(2)°, V = 1035.07(5) Å^3, Z = 2, T = 150.0(3) K, μ(CuKα) = 3.759 mm^{-1}, *Dcalc* = 1.605 g/cm^3, 17,799 reflections measured (2Θ ≤ 160°), and 4456 unique (R_{int} = 0.0343, R_{sigma} = 0.0246) were used in all calculations. The final R_1 was 0.0770 ($I > 2\sigma(I)$), and wR_2 was 0.2016 (all data). For further details, see the crystallographic data for this compound deposited at the Cambridge Crystallographic Data Centre. Deposition number CCDC 2314862 contains the supplementary crystallographic data for this paper.

Crystal Data for **4a** ($C_{26}H_{21}BrNO_4P$; M = 520.03 g/mol): monoclinic, space group $P2_1/c$ (no.14), a = 10.8242(3) Å, b = 8.2331(3) Å, c = 24.9042(5) Å, β = 93.006(2)°, V = 2216.3(1) Å^3, Z = 4, T = 160.0(2) K, μ(CuKα) = 3.450 mm^{-1}, *Dcalc* = 1.517 g/cm^3, 22,314 reflections measured (2Θ ≤ 160°), and 4782 unique (R_{int} = 0.0738, R_{sigma} = 0.0629) were used in all calculations. The final R_1 was 0.0541 ($I > 2\sigma(I)$), and wR_2 was 0.1480 (all data). For further details, see the crystallographic data for this compound deposited at the Cambridge Crystallographic Data Centre. Deposition number (https://www.ccdc.cam.ac.uk/services/structures (accessed on 6 December 2023)) CCDC 2333330 contains the supplementary crystallographic data for this paper.

4. Conclusions

In conclusion, this study presents a comprehensive investigation into the synthesis, characterization, and potential applications of α-aminophosphonates derived from anthraquinone and benzanthrone. The synthesized compounds exhibited notable fluorescence properties with solvatochromic behavior, making them suitable for diverse applications. The spectroscopic analysis confirms the chemical structures, and the compounds' luminescent properties are thoroughly explored in various solvents. The toxicity assessment on etiolated wheat sprouts reveals varying degrees of impact on growth and oxidative damage. Importantly, the research introduces these α-aminophosphonates as promising candidates for CLSM imaging of the parasitic flatworm *Opisthorchis felineus*, showcasing their potential in visualizing biological specimens. The X-ray crystallographic study of an anthraquinone α-aminophosphonate contributes valuable information regarding the compound's molecular arrangement and intermolecular interactions. Overall, the synthesized compounds demonstrate potential for versatile applications, particularly in the investigation of parasitic organisms.

Supplementary Materials: The following supporting information can be downloaded at: https://www.mdpi.com/article/10.3390/molecules29051143/s1, ^{1}H, APT, ^{31}P NMR, FTIR spectra; FTMS (ESI) and RSA data [65].

Author Contributions: A.M. and E.K. formulated research goals and aims; M.C. and V.P. synthesized compounds; L.M. and S.K. performed sample preparation, staining for CLSM investigation, microscopy of slides, and imaging; M.K. and I.G. wrote Section 2.4 and were involved in analysis of images on page 13, Section 3.4; S.B. performed single-crystal X-ray diffraction analysis and wrote Section 2.5; M.S. performed toxicology investigation and wrote Section 2.3; V.K. and L.L. provided samples and fluke species identification; A.M. analyzed, managed, and visualized data of NMR, FTIR, FTMS, and UV-Vis spectra and wrote the rest of the manuscript; E.K. obtained UV-Vis spectral data,

coordinated responsibility for the research activity planning and execution, and acquired the financial support for the project. All authors have read and agreed to the published version of the manuscript.

Funding: This work is supported by fundamental and applied research projects of the Latvian Council of Science. Project No. lzp-2022/1-0436 "Novel fluorescent anthrone-derived functional materials for bioimaging applications".

Institutional Review Board Statement: Not applicable.

Informed Consent Statement: Not applicable.

Data Availability Statement: Data is contained within the article or Supplementary Materials.

Conflicts of Interest: The authors declare no conflicts of interest.

References

1. Lakowicz, J.R. Introduction to Fluorescence. In *Principles of Fluorescence Spectroscopy*; Springer: Boston, MA, USA, 2006; pp. 1–26.
2. Maļeckis, A.; Griškjāns, E.; Cvetinska, M.; Savicka, M.; Belyakov, S.; Kirilova, E. Synthesis, Characterization, Spectroscopic Studies and Evaluation of Toxicological Effect on Growth of Wheat Sprouts (Triticum Aestivum) of New Benzanthrone α-Aryl-α-Aminophosphonates. *J. Mol. Struct.* **2023**, *1277*, 134838. [CrossRef]
3. Maļeckis, A.; Cvetinska, M.; Griškjāns, E.; Mežaraupe, L.; Kirjušina, M.; Pavlova, V.; Kirilova, E. Novel Anthraquinone α-Aryl-α-Aminophosphonates: Synthesis, Spectroscopy and Imaging by Confocal Laser Scanning Microscopy of Trematode Opisthioglyphe Ranae. *J. Photochem. Photobiol. A Chem.* **2023**, *444*, 114918. [CrossRef]
4. Langhals, H. Color Chemistry. Synthesis, Properties and Applications of Organic Dyes and Pigments. 3rd Revised Edition. By Heinrich Zollinger. *Angew. Chem. Int. Ed.* **2004**, *43*, 5291–5292. [CrossRef]
5. Christie, R. *Colour Chemistry*; The Royal Society of Chemistry: London, UK, 2014; ISBN 978-1-84973-328-1.
6. Huang, B.; Ji, Y.; Li, Z.; Zhou, N.; Jiang, W.; Feng, Y.; Lin, B.; Sun, Y. Simple Aggregation–Induced Delayed Fluorescence Materials Based on Anthraquinone Derivatives for Highly Efficient Solution–Processed Red OLEDs. *J. Lumin.* **2017**, *187*, 414–420. [CrossRef]
7. Yin, C.; Liu, R.; Zhang, D.; Duan, L. Indeno-Anthraquinone Hosts with Thermally Activated Delayed Fluorescence for Deep-Red OLEDs. *J. Mater. Chem. C Mater.* **2022**, *10*, 4668–4673. [CrossRef]
8. Kaur, N.; Gauri. Anthraquinone Appended Chemosensors for Fluorescence Monitoring of Anions and/or Metal Ions. *Inorganica Chim. Acta* **2022**, *536*, 120917. [CrossRef]
9. Ghosh, A.; Jose, D.A.; Kaushik, R. Anthraquinones as Versatile Colorimetric Reagent for Anions. *Sens. Actuators B Chem.* **2016**, *229*, 545–560. [CrossRef]
10. Ma, Z.; Zhang, D.; Guo, J.; Li, M.; Wang, T.; Yin, H.; Wang, H.; Liu, J. An Anthraquinone-Based "Turn-on" Fluorescence Probe for Hg^{2+} Detection and Its Application in Cell Imaging. *Inorg. Chem. Commun.* **2021**, *130*, 108753. [CrossRef]
11. Fu, Z.; Cui, Y.; Cui, F.; Zhang, G. Modeling Techniques and Fluorescence Imaging Investigation of the Interactions of an Anthraquinone Derivative with HSA and CtDNA. *Spectrochim. Acta A Mol. Biomol. Spectrosc.* **2016**, *153*, 572–579. [CrossRef]
12. Malik, E.M.; Müller, C.E. Anthraquinones as Pharmacological Tools and Drugs. *Med. Res. Rev.* **2016**, *36*, 705–748. [CrossRef]
13. Grabchev, I.; Moneva, I.; Wolarz, E.; Bauman, D. Fluorescent 3-Oxy Benzanthrone Dyes in Liquid Crystalline Media. *Dye. Pigment.* **2003**, *58*, 1–6. [CrossRef]
14. Grabchev, I.; Moneva, I. Synthesis and Properties of Benzanthrone Derivatives as Luminophore Dyes for Liquid Crystals. *Dye. Pigment.* **1998**, *37*, 155–164. [CrossRef]
15. Konstantinova, T.N. The Synthesis of Some Benzanthrone Derivatives for Use as Dyes for Polymeric Materials. *Dye. Pigment.* **1989**, *10*, 63–67. [CrossRef]
16. Maļeckis, A.; Avotiņa, L.; Ķizāne, G.; Pučkins, A.; Osipovs, S.; Kirilova, E. New Fluorescent Heterocyclic Compounds Derived From 3-Cyanobenzanthrone. *Polycycl. Aromat. Compd.* **2022**, *42*, 5508–5520. [CrossRef]
17. Adam, A.M.A.; Altalhi, T.A.; El-Megharbel, S.M.; Saad, H.A.; Refat, M.S.; Grabchev, I.; Althobaiti, R.A. Capturing of Environment Polluting Metal Ions Co^{2+}, Ni^{2+}, Cu^{2+}, and Zn^{2+} Using a 3-Azomethine Benzanthrone-Based Fluorescent Dye: Its Synthesis, Structural, and Spectroscopic Characterizations. *Russ. J. Gen. Chem.* **2020**, *90*, 2394–2399. [CrossRef]
18. Vus, K.; Trusova, V.; Gorbenko, G.; Kirilova, E.; Kirilov, G.; Kalnina, I.; Kinnunen, P. Novel Aminobenzanthrone Dyes for Amyloid Fibril Detection. *Chem. Phys. Lett.* **2012**, *532*, 110–115. [CrossRef]
19. Rubenina, I.; Gavarane, I.; Kirilova, E.; Mezaraupe, L.; Kirjusina, M. Comparison of the Benzanthrone Luminophores: They Are Not Equal for Rapid Examination of Parafasciolopsis Fasciolaemorpha (Trematoda: Digenea). *Biomolecules* **2021**, *11*, 598. [CrossRef]
20. Mucha, A.; Kafarski, P.; Berlicki, Ł. Remarkable Potential of the α-Aminophosphonate/Phosphinate Structural Motif in Medicinal Chemistry. *J. Med. Chem.* **2011**, *54*, 5955–5980. [CrossRef]
21. Kafarski, P.; Lejczak, B. Biological Activity of Aminophosphonic Acids. *Phosphorus Sulfur Silicon Relat. Elem.* **1991**, *63*, 193–215. [CrossRef]
22. Li, S.; Liu, R.; Han, X.; Ge, C.; Zhang, X. Diethyl α-Aminophosphonate Containing Lubricating Additives Synthesized from (3-Aminophenyl)Boronic Acid Pinacol Ester. *Inorg. Chem. Commun.* **2022**, *140*, 109477. [CrossRef]

23. Reddy, N.B.; Sundar, C.S.; Krishna, B.S.; Santhisudha, S.; Sreelakshmi, P.; Nayak, S.K.; Reddy, C.S. Cellulose-SO3H Catalyzed Synthesis of Bis(α-Aminophosphonates) and Their Antioxidant Activity. *Org. Commun.* **2017**, *10*, 46–55. [CrossRef]
24. Rashad, M.M.; El-Sayed, I.E.; Galhoum, A.A.; Abdeen, M.M.; Mira, H.I.; Elshehy, E.A.; Zhang, S.; Lu, X.; Xin, J.; Guibal, E. Synthesis of α-Aminophosphonate Based Sorbents—Influence of Inserted Groups (Carboxylic vs. Amine) on Uranyl Sorption. *Chem. Eng. J.* **2021**, *421*, 127830. [CrossRef]
25. Neiber, R.R.; Galhoum, A.A.; El-Tantawy El Sayed, I.; Guibal, E.; Xin, J.; Lu, X. Selective Lead (II) Sorption Using Aminophosphonate-Based Sorbents: Effect of Amine Linker, Characterization and Sorption Performance. *Chem. Eng. J.* **2022**, *442*, 136300. [CrossRef]
26. Moumeni, O.; Mehri, M.; Kerkour, R.; Boublia, A.; Mihoub, F.; Rebai, K.; Khan, A.A.; Erto, A.; Darwish, A.S.; Lemaoui, T.; et al. Experimental and Detailed DFT/MD Simulation of α-Aminophosphonates as Promising Corrosion Inhibitor for XC48 Carbon Steel in HCl Environment. *J. Taiwan Inst. Chem. Eng.* **2023**, *147*, 104918. [CrossRef]
27. Deyab, M.A.; Abdeen, M.M.; Hussien, M.; El-Sayed, I.E.; Galhoum, A.; El-Shamy, O.A.A.; Abd Elfattah, M. Novel Corrosion Inhibitor for Carbon Steel in Acidic Solutions Based on α-Aminophosphonate (Chemical, Electrochemical, and Quantum Studies). *Molecules* **2023**, *28*, 4962. [CrossRef]
28. Górny vel Górniak, M.; Kafarski, P. Preparation of the Library of Fluorescent Aromatic Aminophosphonate Phenyl and Benzyl Esters. *Phosphorus Sulfur Silicon Relat. Elem.* **2016**, *191*, 511–519. [CrossRef]
29. Kuśnierz, A.; Chmielewska, E. Synthesis of Fluorescent Aminophosphonates by Green Chemistry Procedures. *Phosphorus Sulfur Silicon Relat. Elem.* **2017**, *192*, 700–705. [CrossRef]
30. vel Górniak, M.G.; Czernicka, A.; Młynarz, P.; Balcerzak, W.; Kafarski, P. Synthesis of Fluorescent (Benzyloxycarbonylamino)(Aryl)Methylphosphonates. *Beilstein J. Org. Chem.* **2014**, *10*, 741–745. [CrossRef]
31. Wang, Q.-M.; Gao, W.; Song, J.-L.; Liu, Y.; Qi, H.; Tang, X.-H. Synthesis, X-ray Crystallographic Analysis and BSA Interaction of a New α-Aminophosphonate. *J. Appl. Spectrosc.* **2016**, *83*, 703–709. [CrossRef]
32. Lewkowski, J.; Rodriguez Moya, M.; Wrona-Piotrowicz, A.; Zakrzewski, J.; Kontek, R.; Gajek, G. Synthesis, Fluorescence Properties and the Promising Cytotoxicity of Pyrene–Derived Aminophosphonates. *Beilstein J. Org. Chem.* **2016**, *12*, 1229–1235. [CrossRef]
33. Kraicheva, I.; Vodenicharova, E.; Tashev, E.; Tosheva, T.; Tsacheva, I.; Troev, K. Synthesis and NMR Characterization of Two Novel Anthracene-Derived BIS-Aminophosphonates. Basic Hydrolysis of Some Aminophosphonate Derivatives. *Phosphorus Sulfur Silicon Relat. Elem.* **2012**, *187*, 660–667. [CrossRef]
34. Amira, A.; Aouf, Z.; K'tir, H.; Chemam, Y.; Ghodbane, R.; Zerrouki, R.; Aouf, N. Recent Advances in the Synthesis of A-Aminophosphonates: A Review. *ChemistrySelect* **2021**, *6*, 6137–6149. [CrossRef]
35. Sravya, G.; Balakrishna, A.; Zyryanov, G.V.; Mohan, G.; Reddy, C.S.; Bakthavatchala Reddy, N. Synthesis of α-Aminophosphonates by the Kabachnik-Fields Reaction. *Phosphorus Sulfur Silicon Relat. Elem.* **2021**, *196*, 353–381. [CrossRef]
36. Keglevich, G.; Bálint, E. The Kabachnik–Fields Reaction: Mechanism and Synthetic Use. *Molecules* **2012**, *17*, 12821–12835. [CrossRef]
37. Varga, P.R.; Keglevich, G. Synthesis of α-Aminophosphonates and Related Derivatives; The Last Decade of the Kabachnik–Fields Reaction. *Molecules* **2021**, *26*, 2511. [CrossRef]
38. Rao, A.V.R.; Vaidyanathan, A. The 1H NMR Spectrum of Benzanthrone. *Spectrochim. Acta A* **1981**, *37*, 145–146. [CrossRef]
39. Vaidyanathan, A. The Carbon-13 NMR Spectra of Benzanthrone and Its Derivatives. *Dye. Pigment.* **1982**, *3*, 243–248. [CrossRef]
40. Francis, G.W.; Aksnes, D.W.; Holt, Ø. Assignment of the 1H and 13C NMR Spectra of Anthraquinone Glycosides from Rhamnus Frangula. *Magn. Reson. Chem.* **1998**, *36*, 769–772. [CrossRef]
41. Balakrishna, A.; Suresh Reddy, C.; Naik, S.K.; Manjunath, M.; Naga Raju, C. Synthesis, Characterization and Bio-Activity of Some New Aminophosphonates. *Bull. Chem. Soc. Ethiop.* **2009**, *23*, 69–75. [CrossRef]
42. Litim, B.; Djahoudi, A.; Meliani, S.; Boukhari, A. Synthesis and Potential Antimicrobial Activity of Novel α-Aminophosphonates Derivatives Bearing Substituted Quinoline or Quinolone and Thiazole Moieties. *Med. Chem. Res.* **2022**, *31*, 60–74. [CrossRef]
43. Serigne Abdou Khadir, F.; Boukhssas, S.; Achamlale, S.; Aouine, Y.; Nakkabi, A.; Faraj, H.; Alami, A. Synthesis and Characterization of the Structure of Diethyl [(4-{(1H-Benzo[d]Imidazol-1-Yl)Methyl}-1H-1,2,3-Triazol-1-Yl)(Benzamido)Methyl]Phosphonate Using 1D and 2D NMR Experiments. *Eur. J. Adv. Chem. Res.* **2021**, *2*, 1–7. [CrossRef]
44. Maļeckis, A.; Cvetinska, M.; Griškjāns, E.; Dmitrijevs, K.; Traskovskis, K.; Belyakov, S.; Kirilova, E. Benzanthrone Sulfides: Synthesis, Solvatochromism Characterization and Analysis of Experimental Photophysical Parameters and Theoretical Calculations. *Dye. Pigment.* **2023**, *219*, 111599. [CrossRef]
45. Gonta, S.; Utinans, M.; Kirilov, G.; Belyakov, S.; Ivanova, I.; Fleisher, M.; Savenkov, V.; Kirilova, E. Fluorescent Substituted Amidines of Benzanthrone: Synthesis, Spectroscopy and Quantum Chemical Calculations. *Spectrochim. Acta A Mol. Biomol. Spectrosc.* **2013**, *101*, 325–334. [CrossRef]
46. Olipova, M.; Maleckis, A.; Puckins, A.; Kirilova, A.; Romanovska, E.; Kirilova, E. Spectroscopic Investigation of New Benzanthrone Luminescent Dyes. *Bulg. Chem. Commun.* **2022**, *54*, 253–257.
47. Grabchev, I.; Bojinov, V.; Moneva, I. The Synthesis and Application of Fluorescent Dyes Based on 3-Amino Benzanthrone. *Dye. Pigment.* **2001**, *48*, 143–150. [CrossRef]
48. Maļeckis, A.; Cvetinska, M.; Puckins, A.; Osipovs, S.; Sirokova, J.; Belyakov, S.; Kirilova, E. Synthesis and Properties of New 3-Heterylamino-Substituted 9-Nitrobenzanthrone Derivatives. *Molecules* **2023**, *28*, 5171. [CrossRef]

49. Zamyatnina, V.A.; Bakeeva, L.E.; Aleksandrushkina, N.I.; Vanyushin, B.F. Apoptosis in the Initial Leaf of Etiolated Wheat Seedlings: Influence of the Antioxidant Ionol (BHT) and Peroxides. *Biochemistry* **2002**, *67*, 212–221. [CrossRef]
50. Kishikawa, N.; El-Maghrabey, M.; Nagamune, Y.; Nagai, K.; Ohyama, K.; Kuroda, N. A Smart Advanced Chemiluminescence-Sensing Platform for Determination and Imaging of the Tissue Distribution of Natural Antioxidants. *Anal. Chem.* **2020**, *92*, 6984–6992. [CrossRef]
51. Bogitsh, B.J.; Carter, C.E.; Oeltmann, T.N. Visceral Flukes. In *Human Parasitology*; Elsevier: Amsterdam, The Netherlands, 2019; pp. 175–191.
52. Chai, J.-Y.; Jung, B.-K. Fishborne Zoonotic Heterophyid Infections: An Update. *Food Waterborne Parasitol.* **2017**, *8–9*, 33–63. [CrossRef] [PubMed]
53. Pozio, E.; Armignacco, O.; Ferri, F.; Gomez Morales, M.A. Opisthorchis Felineus, an Emerging Infection in Italy and Its Implication for the European Union. *Acta Trop.* **2013**, *126*, 54–62. [CrossRef]
54. Pozio, E. Epidemiology and Control Prospects of Foodborne Parasitic Zoonoses in the European Union. *Parassitologia* **2008**, *50*, 17–24.
55. Keiser, J.; Utzinger, J. Food-Borne Trematodiases. *Clin. Microbiol. Rev.* **2009**, *22*, 466–483. [CrossRef]
56. Mordvinov, V.A.; Furman, D.P. The Digenea Parasite Opisthorchis Felineus: A Target for the Discovery and Development of Novel Drugs. *Infect. Disord. Drug Targets* **2010**, *10*, 385–401. [CrossRef]
57. Sripa, B.; Tangkawattana, S.; Laha, T.; Kaewkes, S.; Mallory, F.F.; Smith, J.F.; Wilcox, B.A. Toward Integrated Opisthorchiasis Control in Northeast Thailand: The Lawa Project. *Acta Trop.* **2015**, *141*, 361–367. [CrossRef]
58. Fedorova, O.S.; Fedotova, M.M.; Zvonareva, O.I.; Mazeina, S.V.; Kovshirina, Y.V.; Sokolova, T.S.; Golovach, E.A.; Kovshirina, A.E.; Konovalova, U.V.; Kolomeets, I.L.; et al. Opisthorchis Felineus Infection, Risks, and Morbidity in Rural Western Siberia, Russian Federation. *PLoS Negl. Trop. Dis.* **2020**, *14*, e0008421. [CrossRef]
59. Kitaigorodsky, A. *Molecular Crystals and Molecules*; Academic Press: Cambridge, MA, USA, 1973.
60. Ali, M.B.; Hahn, E.-J.; Paek, K.-Y. Effects of Light Intensities on Antioxidant Enzymes and Malondialdehyde Content during Short-Term Acclimatization on Micropropagated Phalaenopsis Plantlet. *Environ. Exp. Bot.* **2005**, *54*, 109–120. [CrossRef]
61. Guo, Z.; Ou, W.; Lu, S.; Zhong, Q. Differential Responses of Antioxidative System to Chilling and Drought in Four Rice Cultivars Differing in Sensitivity. *Plant Physiol. Biochem.* **2006**, *44*, 828–836. [CrossRef]
62. Sheldrick, G.M. A Short History of SHELX. *Acta Crystallogr. A* **2008**, *64*, 112–122. [CrossRef]
63. Burla, M.C.; Caliandro, R.; Camalli, M.; Carrozzini, B.; Cascarano, G.L.; De Caro, L.; Giacovazzo, C.; Polidori, G.; Siliqi, D.; Spagna, R. IL MILIONE: A Suite of Computer Programs for Crystal Structure Solution of Proteins. *J. Appl. Crystallogr.* **2007**, *40*, 609–613. [CrossRef]
64. Sheldrick, G.M. Crystal Structure Refinement with SHELXL. *Acta Crystallogr. C Struct. Chem.* **2015**, *71*, 3–8. [CrossRef]
65. Dolomanov, O.V.; Bourhis, L.J.; Gildea, R.J.; Howard, J.A.K.; Puschmann, H. OLEX2: A complete structure solution, refinement and analysis program. *J. Appl. Cryst.* **2009**, *42*, 339–341. [CrossRef]

6. pielikums
Appendix VI

Maļeckis, A.; Cvetinska, M.; Griškjāns, E.; Kirilova, E.

Exploring Dual Solvatochromic Traits in Novel Fluorescent Benzanthrone Ethynyl Derivatives

J. Solution. Chem. ***2024***.

https://doi.org/10.1007/s10953-024-01363-x

Journal of Solution Chemistry
https://doi.org/10.1007/s10953-024-01363-x

Exploring Dual Solvatochromic Traits in Novel Fluorescent Benzanthrone Ethynyl Derivatives

Armands Maļeckis[1] · Marija Cvetinska[1] · Evans Griškjāns[1] · Elena Kirilova[2]

Received: 1 November 2023 / Accepted: 7 January 2024

Abstract

Motivated by the scarcity of prior research, in this study we report the synthesis and photophysical characteristics of newly obtained benzanthrone ethynyl derivatives. Fourier-transform infrared spectroscopy, ^{1}H and ^{13}C nuclear magnetic resonance spectroscopy and high-resolution mass spectrometry elucidated the structures of the compounds. To study photophysical characteristics, absorbance and emission spectra were measured in solvents with different polarities. Photofading proved high stability of the synthesized compounds (up to 96% of initial absorption after irradiation for 4 h). The analyzed compounds are fluorescent (quantum yields from 0.01 to 0.74 in ethanol) with a significant solvatochromic effect (from 466 nm in benzene to 720 nm in dimethyl sulfoxide). Based on these findings, there is a correlation between the electronic nature of substituents and photophysical parameters. Hence, these compounds could find applications as probes in fluorescence microscopy and sensors to detect polarity variations.

Graphical Abstract

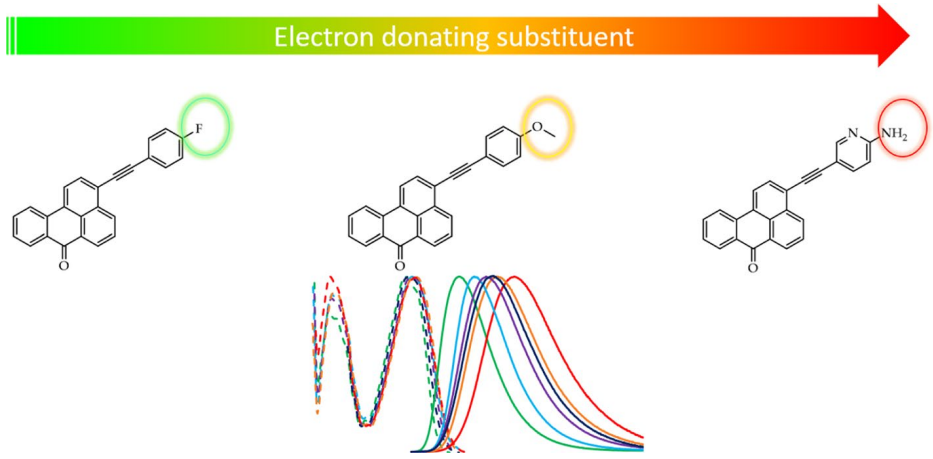

Keywords Benzanthrone · Alkyne · Fluorescence · Sonogashira coupling

Extended author information available on the last page of the article

Published online: 05 March 2024

1 Introduction

Fluorescent organic compounds have become an increasingly important class of compounds in recent years, owing to their unique optical properties and their potential applications in a wide range of fields. Fluorescence is a result of the excited-state properties of the molecules and is typically attributed to the presence of conjugated pi-systems within the molecules. The efficiency of fluorescence emission depends on several factors, including the molecular structure and the solvent environment [1].

A well-designed fluorescent molecule should possess a high fluorescence quantum yield—a measure of the efficiency of fluorescence emission relative to other competing pathways [2]. Stokes shift—defined as the difference between the excitation and emission wavelengths—is another important property that characterizes the fluorescence emission of a molecule, which reflects the degree of relaxation that occurs in the excited state before fluorescence emission. A larger Stokes shift indicates a greater degree of relaxation and can be indicative of a more efficient fluorescence emission process [3, 4]. The photostability of a fluorescent organic compound is also an important consideration; a photostable compound will exhibit minimal degradation or loss of fluorescence intensity over time, ensuring that accurate and reproducible data can be obtained [5–7]. The spectral properties of a fluorescent compound, including the position and shape of the fluorescence emission spectrum, can be tailored to suit specific applications. For example, a red-shifted emission spectrum may be desirable in biological imaging applications to reduce background fluorescence, while a narrow emission peak may be useful in sensing applications to improve the specificity of detection [8–10]. Overall, a complex interplay of molecular structure, solvent environment, and competing decay pathways determine the fluorescence properties of organic compounds. By carefully designing and optimizing these properties, fluorescent organic compounds can be tailored to suit a wide range of scientific and commercial applications.

The optical properties of fluorescent organic compounds make them useful tools in a variety of scientific applications. As described before, they are commonly used in biological imaging, where they can be used to visualize specific biological targets with high spatial and temporal resolution. They are also used as sensing agents, where their fluorescence can be used to detect the presence of specific chemical species [11–14]. The unique optical properties of fluorescent organic compounds make them also attractive for a wide range of optoelectronic applications, including OLED displays [15–17], organic photovoltaics [18–20], nonlinear optical devices [21–26], and ultrafast lasers [27–29]. Development of new materials and device architectures is likely to expand even further the potential applications of fluorescent organic compounds.

Benzanthrone derivatives—polycyclic aromatic compounds—as part of anthrone dye family have gained attention for their excellent abovementioned luminescent properties: photostability, sizable Stokes shifts, noticeable solvatochromism and tuneable fluorescence emission that ranges from green to red depending on the substituents of the molecule and solvent properties [30–32]. These features make them useful in a variety of technological applications. For example, they can be used as fluorescent probes for parasitic trematodes and nematodes [33, 34], to diagnose plant species' callus embryos using confocal laser scanning microscopy imaging [35], and to detect amyloid fibrils of the lysozyme enzyme selectively [36–38]. They also have applications in liquid crystal displays [39, 40], polymeric materials [41], and as probes for the pH of solutions and cations [42, 43].

Numerous theoretical and practical studies show that directly attaching phenylacetylene groups to luminescent molecules modifies photophysical parameters and improves fluorescent properties. These molecules include: pyrene, carbazole, anthraquinone, naphthalimide, and quninolylthiazole [44–48]. Additionally, research suggests that introducing of electron-donating or electron-withdrawing groups to the phenyl rings of phenylacetylene groups and adjusting the length of π-conjugation can alter fluorescence yields, the size of Stokes shifts, and absorption and emission maxima [49]. Beyond their impressive fluorescence, phenylacetylene derivatives have potential as valuable precursors for various other compounds and materials [50, 51]. Given the results, we have opted to share our knowledge about previously unreported phenylacetylene derivatives of benzanthrone. This report details the synthesis and photophysical characteristics of obtained compounds.

2 Experimental

2.1 Materials and General Measurements

2-Amino-5-ethynylpyridine was synthesized according to the previously reported procedure [52]. The rest of reagents and solvents were obtained commercially and used without any additional purification. The progress of reactions and the assessment of the purity of the synthesized compounds was performed by TLC on MERCK Silica gel F254 plates in hexane/chloroform/acetone (4:2:1, volume ratios) system as an eluent and visualized under UV light.

MP70 Melting Point System apparatus was used for the determination of the melting points and were uncorrected. ^{1}H- and ^{13}C-NMR spectra were recorded on a Bruker Avance 500 MHz (Bruker Corporation, Billerica, MA, USA) at ambient temperature, using peaks of solvents as the internal reference. Chemical shift (δ) values are reported in ppm. IR spectra were recorded in KBr tablets with a Perkin–Elmer Spectrum BX FTIR spectrometer (4000–450 cm^{-1}). Wavelengths are given in cm^{-1}. The high-resolution mass spectrum was recorded on an Agilent 1290 Infinity series UPLC connected to an Agilent 6230 TOF mass spectrometer.

The fluorescence emission spectra were recorded on a FLSP920 (Edinburgh Instruments Ltd, UK) spectrofluorometer in the visible range 450–800 nm and the absorption spectra were obtained using the UV–visible spectrophotometer SPECORD® 80 (Analytik Jena AG, Germany). The spectral properties of the investigated compound were measured at an ambient temperature in 10 mm quartz cuvettes in benzene, chloroform, ethyl acetate (EtOAc), acetone, ethanol (EtOH), dimethyl sulfoxide (DMSO) and dimethylformamide (DMF) with concentrations of 10^{-5} mol•L^{-1}. All solvents had a purity of at least 99%. The quantum yields were measured relative to 3-methoxybenzanthrone ($Q_S = 0.56$ in acetone) [53]. The photofading were carried out in quartz cells where sample solution (with concentration 10^{-4} mol•L^{-1}) in ethanol was irradiated with UV-lamp (365 nm, maximum power 15 W) at room temperature. The distance between the cells and the lamp was 10 cm. The bleaching of the dyes at the absorption maximum was monitored as a function of time every 30 min.

2.2 General Synthesis Methodology for Compounds 2a–2e

3-Bromobenzanthrone (309 mg, 1 mmol), an ethynyl derivative (1.05 mmol), $PdCl_2(PPh_3)_2$ (18 mg, 0.025 mmol) and CuI (4 mg, 0.025 mmol) are placed in a 20 mL round-bottom flask under argon atmosphere, followed by the addition of 10 mL

of dry *N*,*N*-dimethylacetamide (DMAc) and 5 mL of triethylamine (Et_3N). The reaction mixture is heated at 80 °C for 1–3 h (TLC control). When the reaction is complete, the mixture is then poured into 20 mL of water. The resulting precipitate is well mixed for 30 min, filtered and dried. Purified by means of recrystallization from chlorobenzene to obtain a desired compound.

3 3-((4-Fluorophenyl)Ethynyl)-7 H-benzo[de]Anthracen-7-one (2a)

Bright yellow solid. Yield: 60%. Melting point: 207 °C. R_f = 0.70 (hexane/chloroform/acetone; 4:2:1). IR, λ_{max} (KBr) cm^{-1}: 1657 (C=O), 2203 (C≡C). ^{1}H NMR (500 MHz, $CDCl_3$) δ 8.72–8.64 (m, $2H_{Ar}$), 8.40 (d, J = 7.8 Hz, $1H_{Ar}$), 8.27 (d, J = 7.7 Hz, $1H_{Ar}$), 8.19 (d, J = 8.1 Hz, $1H_{Ar}$), 7.80–7.73 (m, $2H_{Ar}$), 7.64 (t, J = 7.6 Hz, $1H_{Ar}$), 7.60–7.54 (m, $2H_{Ar}$), 7.47 (t, J = 7.5 Hz, $1H_{Ar}$), 7.05 (t, J = 8.4 Hz, $2H_{Ar}$). ^{13}C NMR (126 MHz, $CDCl_3$) δ 183.60 (C=O), 162.90 (d, J = 250.8 Hz, C), 135.65 (C), 133.70 (d, J = 8.4 Hz, CH), 133.46 (CH), 133.28 (CH), 132.73 (C), 130.92 (C), 130.71 (CH), 130.23 (CH), 128.75 (C), 128.64 (CH), 128.20 (CH), 127.79 (C), 127.20 (CH), 127.16 (C), 123.45 (CH), 123.24 (CH), 123.14 (C), 118.98 (d, J = 3.4 Hz, C), 115.94 (d, J = 22.1 Hz, CH), 95.88 (C≡C), 86.79 (C≡C). HRMS (ESI): *m*/*z* calculated for $[C_{25}H_{13}FO + H^+]$ 349.1023, found 349.1031.

4 3-((Trimethylsilyl)Ethynyl)-7 H-benzo[de]Anthracen-7-one (2b)

Light brown solid. Yield: 57%. Melting point: 145 °C. R_f = 0.76 (hexane/chloroform/acetone; 4:2:1). IR, λ_{max} (KBr) cm^{-1}: 1653 (C=O), 2146 (C≡C). ^{1}H NMR (500 MHz, $CDCl_3$) δ 8.45 (dd, J = 7.2, 1.4 Hz, $1H_{Ar}$), 8.39 (dd, J = 8.3, 1.4 Hz, $1H_{Ar}$), 8.18 (dd, J = 7.9, 1.5 Hz, $1H_{Ar}$), 7.95 (d, J = 7.8 Hz, $1H_{Ar}$), 7.90 (d, J = 8.1 Hz, $1H_{Ar}$), 7.55 (t, J = 7.7 Hz, $1H_{Ar}$), 7.51 (d, J = 7.7 Hz, $1H_{Ar}$), 7.42 (td, J = 8.0, 7.6, 1.5 Hz, $1H_{Ar}$), 7.27 (t, J = 7.4 Hz, $1H_{Ar}$), 0.18 (s, 9 H, $Si(CH_3)_3$). ^{13}C NMR (126 MHz, $CDCl_3$) δ 183.33 (C=O), 135.38 (C), 133.22 (CH), 132.70 (C), 130.99 (CH), 130.72 (C), 129.97 (CH), 128.47 (CH), 128.43 (C), 127.97 (CH), 127.41 (C), 127.06 (CH), 123.10 (CH), 123.10 (CH), 122.91 (C), 102.53 (C, C≡C), 102.30 (C, C≡C), 0.00 (CH_3, Si–($\underline{C}H_3$)$_3$). HRMS (ESI): *m*/*z* calculated for $[C_{22}H_{18}OSi + H^+]$ 327.1200, found 327.1185.

5 4-((7-Oxo-7 H-benzo[de]Anthracen-3-yl)Ethynyl)Benzaldehyde (2c)

Yellow solid. Yield: 43%. Melting point: 237 °C. R_f = 0.57 (hexane/chloroform/acetone; 4:2:1). IR, λ_{max} (KBr) cm^{-1}: 1656 (C=O) (benzanthrone core), 1698 (C=O) (aldehyde), 2120 (C≡C). ^{1}H NMR (500 MHz, Acetone-d_6) δ 10.00 (s, 1H, CHO), 8.86 (d, J = 8.2 Hz, $1H_{Ar}$), 8.67 (dd, J = 7.5, 4.2 Hz, $2H_{Ar}$), 8.52 (d, J = 8.1 Hz, $1H_{Ar}$), 8.32 (d, J = 8.0 Hz, $1H_{Ar}$), 8.01 (d, J = 7.8 Hz, $1H_{Ar}$), 7.99–7.90 (m, $3H_{Ar}$), 7.87 (d, J = 7.8 Hz,

$2H_{Ar}$), 7.77 (t, J = 8.0 Hz, $1H_{Ar}$), 7.57 (t, J = 7.6 Hz, $1H_{Ar}$). HRMS (ESI): *m*/*z* calculated for [$C_{26}H_{14}O_2 + H^+$] 359.1067, found 359.1065.

6 3-((4-Methoxyphenyl)Ethynyl)-7 H-benzo[de]Anthracen-7-one (2d)

Bright orange solid. Yield: 89%. Melting point: 241 °C. R_f = 0.61 (hexane/chloroform/acetone; 4:2:1). IR, λ_{max} (KBr) cm^{-1}: 1260 (Ar–O–C), 1651 (C=O), 2199 (C≡C). ^1H NMR (500 MHz, DMF-d_7) δ 9.18 (d, J = 8.2 Hz, $1H_{Ar}$), 9.05 (d, J = 7.8 Hz, $1H_{Ar}$), 8.97 (d, J = 7.2 Hz, $1H_{Ar}$), 8.90 (d, J = 8.1 Hz, $1H_{Ar}$), 8.62 (d, J = 7.8 Hz, $1H_{Ar}$), 8.28 (t, J = 7.4 Hz, $2H_{Ar}$), 8.12 (t, J = 7.6 Hz, $1H_{Ar}$), 7.98 (d, J = 8.5 Hz, $2H_{Ar}$), 7.90 (t, J = 7.5 Hz, $1H_{Ar}$), 7.32 (d, J = 8.5 Hz, $2H_{Ar}$), 3.72 (s, 3 H, CH_3). HRMS (ESI): *m*/*z* calculated for [$C_{26}H_{16}O_2 + H^+$] 361.1223, found 361.1209.

7 3-((6-Aminopyridin-3-yl)Ethynyl)-7 H-benzo[de]Anthracen-7-one (2e)

Orange solid. Yield: 69%. Melting point: 273 °C. R_f = 0.75 (acetone). IR, λ_{max} (KBr) cm^{-1}: 1652 (C=O), 2196 (C≡C), 3453 and 3294 (NH_2). ^1H NMR (500 MHz, $CDCl_3$) δ 8.85 (d, J = 7.8 Hz, $2H_{Ar}$), 8.54 (d, J = 7.8 Hz, $1H_{Ar}$), 8.50–8.44 (m, $2H_{Ar}$), 8.38 (d, J = 8.2 Hz, $1H_{Ar}$), 7.97–7.89 (m, $2H_{Ar}$), 7.80 (t, J = 7.6 Hz, $1H_{Ar}$), 7.77–7.71 (m, $1H_{Ar}$), 7.61 (t, J = 7.5 Hz, $1H_{Ar}$), 6.58 (d, J = 8.4 Hz, $1H_{Ar}$), 4.72 (s, 2 H, NH_2). HRMS (ESI): *m*/*z* calculated for [$C_{24}H_{14}N_2O + H^+$] 347.1179, found 347.1180.

8 Results and Discussion

8.1 Synthesis

Sonogashira coupling reaction, named after the Japanese chemist, Kenkichi Sonogashira, who first reported the reaction in 1975 is a cross-coupling reaction used to synthesize alkynes [54]. It involves the reaction between a terminal alkyne with a palladium catalyst, a copper(I) co-catalyst and an aryl (or vinyl) halide. The reaction proceeds through a series of steps, starting with oxidative addition of the palladium catalyst to the aryl or vinyl halide and results in reductive elimination of the desired alkyne product. The copper(I) co-catalyst plays a key role in facilitating the transmetalation step. The reaction was initially slow and required high temperatures and pressure. However, over the years, the reaction conditions were optimized, and various modifications were made to improve its efficiency, selectivity and scope of the reaction, which allowed for the use of less reactive substrates [55–57].

To date, within the context of palladium-catalysed reactions, to the best of our knowledge the sole documented approaches for the synthesis of novel derivatives of benzanthrone involved aryl cyanation and Buchwald–Hartwig amination reactions [43, 58]. However, our group has recently reported a new synthesis strategy for 3-(phenylethynyl)-*7 H*-benzo[*de*] anthracen-7-one [59]. In this research we have decided to explore the scope of these slightly modified reaction conditions for different alkynes (Table 1) and study effects on photophysical parameters of substitution nature (Scheme 1).

Table 1 Structures of synthesized compounds

	Structure	R_f[a]	Melting point, °C	Reaction yield, %
2a	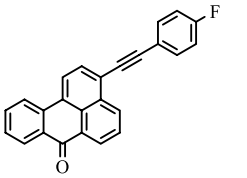	0.70	207	60
2b	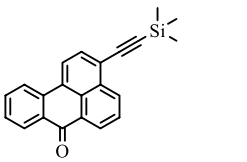	0.76	145	57
2c	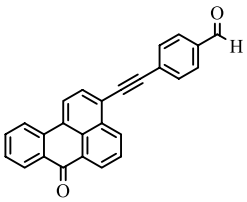	0.57	237	43
2d	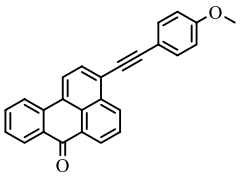	0.61	241	89
2e	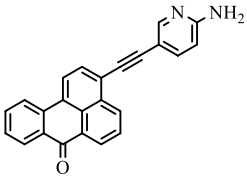	0.75	273	69

[a]Retention factor (hexane/CH_3Cl/acetone; 4:2:1)

8.2 Structural and Spectral Characterization

The mass of the synthesized compounds was validated using high-resolution mass spectrometry Figures S1–S5 (see Supplementary material).

The confirmation of the structures of the obtained compounds was achieved through ^{1}H-nuclear magnetic resonance (NMR) spectroscopy, which identified the respective doublets (d), triplets (t), and multiplets (m) of aromatic protons (δ 9.05–7.05 ppm) typical for the phenyl groups and benzanthrone residue. In the APT NMR spectra, the relevant peaks of the benzanthrone carbonyl group carbon at around 183 ppm, peaks of acetylene carbon atoms with a chemical shift of approximately 87–103 ppm, and peaks of aromatic and aliphatic carbon atoms were found Figures S6 – S11 (see Supplementary material). The obtained data shows a strong correlation with NMR studies previously reported for other

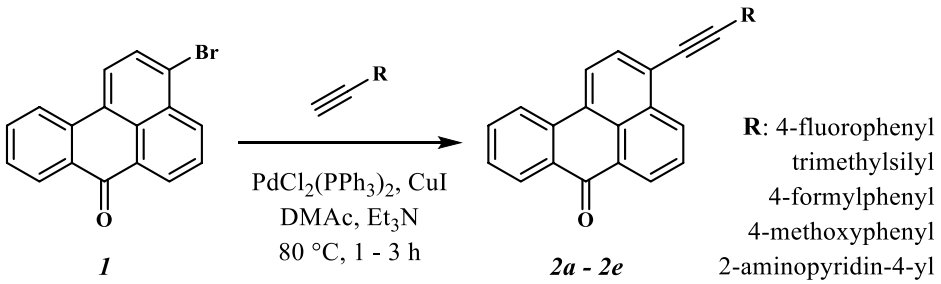

Scheme 1 Synthesis of benzanthrone ethynyl derivatives

derivatives of benzanthrone [60, 61]. Although, low solubility of certain compounds limited the acquisition of spectra to only ^{1}H NMR.

The infrared spectra obtained show characteristic peaks corresponding to the benzanthrone carbonyl group (C=O) vibrations at approximately 1655 cm^{-1}, as well as carbon-carbon triple-bond (C≡C) vibrations at around 2120–2203 cm^{-1}, which are typically observed in alkynes.

8.3 Photophysical Properties

The 3-substituted derivatives of benzanthrones are the most widely utilized luminescent dyes among their various substituted counterparts. This is attributed to the conjugation between the substituent in the third position and the carbonyl group, resulting in the formation of intramolecular charge transfer compounds that possess donor-acceptor type architectures.

To investigate the photophysical characteristics of recently synthesized compounds, absorbance and emission spectra of *2a–2e* were measured in solvents with different polarities, specifically, in benzene, ethyl acetate (EtOAc), chloroform, acetone, *N*,*N*-dimethylformamide (DMF), dimethyl sulfoxide (DMSO) and ethanol (EtOH). Tables 2, 3 and 4 display fundamental absorption and fluorescence properties.

All investigated dyes exhibit fluorescence and demonstrate a significant solvatochromic effect. Figure 1 represents UV–Vis absorption and fluorescence emission spectra of compound *2d* in various organic solvents. In solutions, benzanthrone alkynes exhibit two absorption bands around 310–330 nm and 420–450 nm, showing a bathochromic shift of 12–30 nm for the long wavelength absorption band between the maxima in benzene and DMSO. The impact of the polarity of solvents on fluorescence is more prominent than on absorbance. Synthesized compounds are fluorescent with emission from 462 nm (derivative *2c*, EtOAc) to 701 nm (derivative *2e*, EtOH).

Obtained compounds display dual solvatochromism—not only emission peak of each individual compound is influenced by solvent polarity, but a strong correlation between electronic nature of substituents and photophysical parameters is evident as well; electron-withdrawing 4-fluorophenyl substituent shifts emission hypsochromically and strong electron-donating 6-aminopyridinyl substituent—bathocromically in the same solvent (Fig. 2). The electronic properties of the substituents significantly influence the emission efficiency of the studied substances. Derivatives with electron-withdrawing groups (*2a* and *2e*) have a higher luminescence quantum yield in ethanol compared with

Table 2 Absorption data of the studied derivatives *2a–2e*

Solvent	Absorption λ_{abs} ($lg\varepsilon$) (nm)				
	2*a*	2*b*	2*c*	2*d*	2*e*
Benzene	423 (4.55)	423 (4.24)	416 (4.65)	427 (4.51)	432 (4.32)
EtOAc	416 (4.56)	419 (4.29)	412 (4.68)	425 (4.51)	437 (4.29)
$CHCl_3$	425 (4.52)	427 (4.22)	420 (4.72)	436 (4.46)	438 (4.49)
Acetone	419 (4.55)	419 (4.27)	414 (4.65)	432 (4.49)	445 (4.41)
DMF	423 (4.58)	422 (4.25)	419 (4.71)	437 (4.48)	455 (4.54)
DMSO	435 (4.50)	424 (4.26)	422 (4.68)	440 (4.42)	462 (4.55)
EtOH	429 (4.57)	419 (4.19)	430 (4.25)	442 (4.45)	446 (4.36)

Table 3 Fluorescence emission data of the studied derivatives *2a–2e*

Solvent	Fluorescence λ_{em} (Q) (nm)				
	2*a*	2*b*	2*c*	2*d*	2*e*
Benzene	466 (0.02)	482 (0.03)	463 (0.02)	502 (0.20)	530 (0.32)
EtOAc	473 (0.05)	479 (0.02)	462 (0.01)	510 (0.25)	576 (0.33)
$CHCl_3$	498 (0.41)	491 (0.09)	479 (0.24)	534 (0.64)	574 (0.40)
Acetone	492 (0.09)	488 (0.04)	475 (0.05)	565 (0.31)	641 (0.19)
DMF	497 (0.12)	495 (0.05)	481 (0.07)	553 (0.30)	691 (0.02)
DMSO	506 (0.20)	494 (0.06)	489 (0.22)	570 (0.27)	720 (0.01)
EtOH	531 (0.74)	495 (0.18)	515 (0.67)	598 (0.20)	701 (0.01)

Table 4 Stokes shifts of the studied derivatives *2a–2e*

Solvent	Stokes shift (cm^{-1})				
	2*a*	2*b*	2*c*	2*d*	2*e*
Benzene	2181	2894	2440	3499	4280
EtOAc	2897	2990	2627	3922	5522
$CHCl_3$	3449	3053	2933	4209	5409
Acetone	3541	3375	3102	5449	6871
DMF	3520	3495	3076	4800	7506
DMSO	3226	3342	3247	5183	7756
EtOH	4478	3664	3838	5902	8156

less polar solvents. In contrast, derivatives with donor groups luminesce more intensely in chloroform than in ethanol. In turn, the presence of a trimethylsilyl group leads to a dramatic drop in emission efficiency. The alteration of photophysical parameters also has an impact on Stokes shifts. Specifically, the range of Stokes shifts varies from 2181 cm to 1 for compound *2a* in a less polar solvent (benzene) to 8156 cm^{-1} for compound *2e* in a polar solvent (ethanol). Thus, the presence of an electron-donating substituent leads to a larger Stokes shift, as large as in derivatives with thio, amino and amidino groups

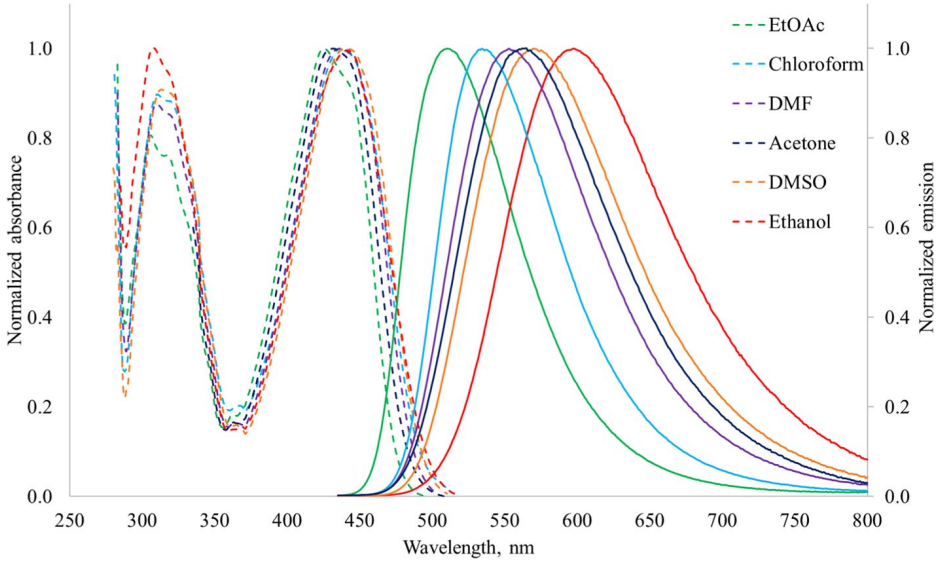

Fig. 1 UV–Vis absorption and fluorescence emission spectra of compound *2d* in various organic solvents

in the 3rd position of the benzanthrone core [62–67]. Dual solvatochromic nature and unique chemical structures of obtained ethynyl derivatives might offer advantages such as enhanced sensitivity or specific binding capabilities, making them valuable for applications where detecting subtle polarity variations, such as cellular membrane changes or environmental conditions, is crucial for diagnostic or research purposes.

The molecular-microscopic solvent polarity parameter (E_T^N) considers the molecular aspects of the solvent structure that contributes to its overall polarity. Plots (Fig. 3) show how changes in solvent polarity affect the electronic properties of compounds *2a*, *2d* and *2e*. An increase in solvent polarity leads to a redshift (longer wavelength) in the

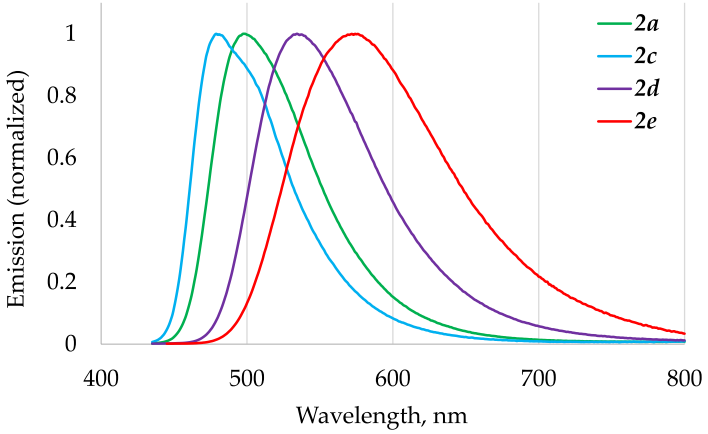

Fig. 2 Fluorescence emission spectra of compound *2a*, *2c*, *2d* and 2e in chloroform

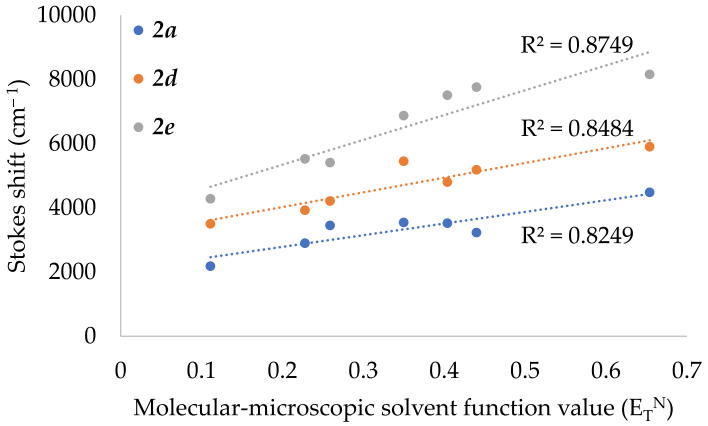

Fig. 3 Stoke shift versus molecular-microscopic solvent polarity parameter (E_T^N) for compounds *2a*, *2d* and *2e* in selected solvents; dotted line represents linearity trend

emission as a more polar solvent stabilizes the excited state of the molecule. The linear correlation between the molecular-microscopic solvent polarity parameter and Stokes shift indicates the existence of general solute-solvent interactions, along with H-bonding interactions, in the majority of the solvents.

An essential requirement for the application of dyes is high photostability. To acquire a deeper insight into photostability of new dyes, photofading process of synthesized derivatives was performed in ethanol (at concentration 10^{-4} mol•L^{-1}) in comparison with widely used test dye (fluorescein). The experiment was carried out in quartz cells where sample solution was irradiated with a UV-lamp (365 nm) at room temperature (Table 5).

The results are shown in Fig. 4. After irradiation for 4 h, fluorescein showed an absorbance of 0.71 of the initial absorbance. Out of the obtained compounds, the derivative with fluorine atom (*2a*) turned out to be the most photostable, showing 96% of the initial absorption. The next most stable derivative is the compound *2c* with a formyl group (0.82). The least stable substance is the derivative with a methoxy group (*2d*), which lost more than half of its absorption (57%) after 4 h of irradiation.

The data show that three of the synthesized substances (*2a*, *2b* and *2c*) have higher photostability than fluorescein.

Table 5 Absorbance intensities of fluoresceine and synthesized compounds *2a–2e* upon 365 nm excitation

	Fluorescein	2*a*	2*b*	2*c*	2*d*	2*e*
Initial	2.6054	2.7631	1.6571	2.9489	2.0007	2.0364
30 min	2.5944	2.7616	1.6512	2.9323	1.7710	2.0084
60 min	2.5680	2.7295	1.6506	2.9143	1.4812	1.9603
90 min	2.3586	2.7351	1.5596	2.8276	1.2187	1.8817
120 min	2.3413	2.7210	1.4919	2.7515	1.1417	1.6979
150 min	2.2524	2.6993	1.3999	2.6323	1.0182	1.5950
180 min	2.2127	2.6901	1.3705	2.6148	0.9959	1.5710
210 min	2.0572	2.6860	1.3481	2.5071	0.9047	1.5237
240 min	1.8615	2.6639	1.2881	2.4067	0.8662	1.4462

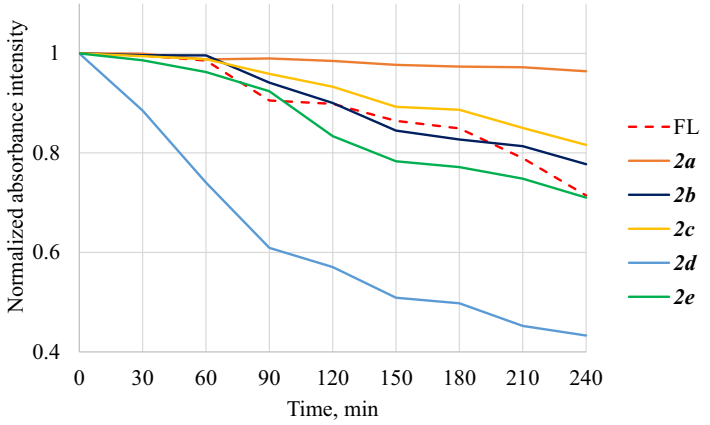

Fig. 4 Normalized absorbance intensities of fluoresceine (FL) and synthesized compounds *2a–2e* as a function of irradiation time upon 365 nm excitation

9 Conclusions

As a result, synthesis and photophysical characteristics of newly obtained benzanthrone ethynyl derivatives were studied. A set of analytical techniques, such as ^{1}H, ^{13}C NMR and FTIR spectroscopy, and high-resolution mass spectrometry analysis confirmed the structures of the new compounds. The photophysical characteristics of the synthesized compounds were studied by measuring absorbance and emission spectra and quantum yields in solvents of varying polarities. The findings indicate that the investigated compounds exhibit fluorescence and a significant solvatochromic effect. Furthermore, the electronic nature of substituents correlates with photophysical parameters. This research has the potential to be extended by employing other alkynes with electron-donating and withdrawing groups and study of non-linear optical properties of these compounds. The photophysical parameters of the newly obtained compounds, including solvatochromism, photostability, quantum yields, tunability and large Stokes shifts, indicate their potential for use in an exceptionally extensive range of scientific and industrial applications.

Supplementary Information The online version contains supplementary material available at https://doi.org/10.1007/s10953-024-01363-x.

Acknowledgements This publication was supported by Riga Technical University's Doctoral Grant programme.

Author Contributions A. M.: Methodology, Investigation, Writing—original draft, Project administration. M. C.: Methodology, Investigation. E. G.: Methodology, Investigation, Visualization. E. K.: Validation, Resources, Writing—review and editing, Supervision.

Declarations

Competing Interests The authors declare that they have no known competing financial interests or personal relationships that could have appeared to influence the work reported in this paper.

References

1. Barman, D., Narang, K., Parui, R., Zehra, N., Khatun, M.N., Adil, L.R., Iyer, P.K.: Review on recent trends and prospects in π-conjugated luminescent aggregates for biomedical applications. Aggregate **3**(5), e172 (2022). https://doi.org/10.1002/agt2.172
2. Wünsch, U.J., Murphy, K.R., Stedmon, C.A.: Fluorescence quantum yields of natural organic matter and organic compounds: implications for the fluorescence-based interpretation of organic matter composition. Front. Mar. Sci. **2**, 98 (2015). https://doi.org/10.3389/fmars.2015.00098
3. Czaplińska, B., Malarz, K., Mrozek-Wilczkiewicz, A., Slodek, A., Korzec, M., Musiol, R.: Theoretical and experimental investigations of large Stokes Shift Fluorophores based on a Quinoline Scaffold. Molecules. **25**, 2488 (2020). https://doi.org/10.3390/molecules25112488
4. Ren, T.-B., Xu, W., Zhang, W., Zhang, X.-X., Wang, Z.-Y., Xiang, Z., Yuan, L., Zhang, X.-B.: A General Method to increase Stokes Shift by Introducing Alternating Vibronic structures. J. Am. Chem. Soc. **140**, 7716–7722 (2018). https://doi.org/10.1021/jacs.8b04404
5. Lee, Y.U., Li, S., Bopp, S.E., Zhao, J., Nie, Z., Posner, C., Yang, S., Zhang, X., Zhang, J., Liu, Z.: Unprecedented fluorophore photostability enabled by low-loss Organic hyperbolic materials. Adv. Mater. **33**, 2006496 (2021). https://doi.org/10.1002/adma.202006496
6. Zheng, Q., Lavis, L.D.: Development of photostable fluorophores for molecular imaging. Curr. Opin. Chem. Biol. **39**, 32–38 (2017). https://doi.org/10.1016/j.cbpa.2017.04.017
7. Gong, W., Das, P., Samanta, S., Xiong, J., Pan, W., Gu, Z., Zhang, J., Qu, J., Yang, Z.: Redefining the photo-stability of common fluorophores with triplet state quenchers: Mechanistic insights and recent updates. Chem. Commun. **55**, 8695–8704 (2019). https://doi.org/10.1039/C9CC02616A
8. Li, Y., Chen, Q., Pan, X., Lu, W., Zhang, J.: Development and challenge of fluorescent probes for Bioimaging Applications: From visualization to diagnosis. Top. Curr. Chem. **380**, 22 (2022). https://doi.org/10.1007/s41061-022-00376-8
9. Wu, J., Shi, Z., Zhu, L., Li, J., Han, X., Xu, M., Hao, S., Fan, Y., Shao, T., Bai, H., Peng, B., Hu, W., Liu, X., Yao, C., Li, L., Huang, W.: The design and bioimaging applications of NIR fluorescent Organic dyes with high brightness. Adv. Opt. Mater. **10**, 2102514 (2022). https://doi.org/10.1002/adom.202102514
10. Yang, I., Lee, J.W., Hwang, S., Lee, J.E., Lim, E., Lee, J., Hwang, D., Kim, C.H., Keum, Y.-S., Kim, S.K.: Live bio-imaging with fully bio-compatible organic fluorophores. J. Photochem. Photobiol B. **166**, 52–57 (2017). https://doi.org/10.1016/j.jphotobiol.2016.11.009
11. Wu, D., Sedgwick, A.C., Gunnlaugsson, T., Akkaya, E.U., Yoon, J., James, T.D.: Fluorescent chemosensors: The past, present and future. Chem. Soc. Rev. **46**, 7105–7123 (2017). https://doi.org/10.1039/C7CS00240H
12. Carter, K.P., Young, A.M., Palmer, A.E.: Fluorescent sensors for Measuring Metal ions in Living systems. Chem. Rev. **114**, 4564–4601 (2014). https://doi.org/10.1021/cr400546e
13. Goshisht, M.K., Tripathi, N.: Fluorescence-based sensors as an emerging tool for anion detection: Mechanism, sensory materials and applications. J. Mater. Chem. C Mater. **9**, 9820–9850 (2021). https://doi.org/10.1039/D1TC01990B
14. Yan, Z., Cai, Y., Zhang, J., Zhao, Y.: Fluorescent sensor arrays for metal ions detection: A review. Measurement. **187**, 110355 (2022). https://doi.org/10.1016/j.measurement.2021.110355
15. Ha, J.M., Hur, S.H., Pathak, A., Jeong, J.-E., Woo, H.Y.: Recent advances in organic luminescent materials with narrowband emission. NPG Asia Mater. **13**, 53 (2021). https://doi.org/10.1038/s41427-021-00318-8
16. Lee, J.: Lifetime modeling for organic light-emitting diodes: A review and analysis. J. Inform. Disp. **24**, 57–70 (2023). https://doi.org/10.1080/15980316.2022.2126018
17. Hong, G., Gan, X., Leonhardt, C., Zhang, Z., Seibert, J., Busch, J.M., Bräse, S.: A brief history of OLEDs—Emitter Development and Industry milestones. Adv. Mater. **33**, 2005630 (2021). https://doi.org/10.1002/adma.202005630
18. He, Q., Kafourou, P., Hu, X., Heeney, M.: Development of non-fullerene electron acceptors for efficient organic photovoltaics. SN Appl. Sci. **4**, 247 (2022). https://doi.org/10.1007/s42452-022-05128-3
19. Rwenyagila, E.R.: A review of Organic photovoltaic energy source and its technological designs. Int. J. Photoenergy. **2017**, 1656512 (2017). https://doi.org/10.1155/2017/1656512
20. Li, Y., Huang, W., Zhao, D., Wang, L., Jiao, Z., Huang, Q., Wang, P., Sun, M., Yuan, G.: Recent progress in Organic Solar cells: A review on materials from acceptor to Donor. Molecules. **27**, 1800 (2022). https://doi.org/10.3390/molecules27061800

21. Yahya, M., Nural, Y., Seferoğlu, Z.: Recent advances in the nonlinear optical (NLO) properties of phthalocyanines: A review. Dyes Pigm. **198**, 109960 (2022). https://doi.org/10.1016/j.dyepig.2021.109960
22. Wu, J., Li, Z., Luo, J., Jen, A.K.-Y.: High-performance organic second- and third-order nonlinear optical materials for ultrafast information processing. J. Mater. Chem. C Mater. **8**, 15009–15026 (2020). https://doi.org/10.1039/D0TC03224G
23. Semin, S., Li, X., Duan, Y., Rasing, T.: Nonlinear Optical Properties and Applications of Fluorenone Molecular materials. Adv. Opt. Mater. **9**, 2100327 (2021). https://doi.org/10.1002/adom.202100327
24. Thomas, A., Patil, P.S., Siddlingeshwar, B., Manohara, S.R., Gummagol, N.B., Krishna Chaitanya, G.: .Kirilova, nonlinear optical properties of benzanthrone derivatives with N'-methylpiperazin-1-yl and N'-phenylpiperazin-1-yl substituents: Experimental and quantum chemical study. Opt. Laser Technol. **156**, 108616 (2022). https://doi.org/10.1016/j.optlastec.2022.108616
25. Cao, L., Zhang, D., Xu, L., Fang, Z., Jiang, X.-F., Lu, F.: Perylenediimide-Benzanthrone Dyad: Organic chromophores with enhanced third-order nonlinear-optical activities. Eur. J Org Chem. **2017**, 2495–2500 (2017). https://doi.org/10.1002/ejoc.201700094
26. Shivraj, A., Thomas, E.M., Kirilova, I., Nikolajeva, B., Siddlingeshwar: Influence of Solvent Environment on Photophysical properties of 3-(Piperidin-1-yl)-4H-benzo[de]anthracen-7(11bH)-one. J Solut. Chem. **45**, 1391–1413 (2016). https://doi.org/10.1007/s10953-016-0508-4
27. Orazi, L., Romoli, L., Schmidt, M., Li, L.: Ultrafast laser manufacturing: From physics to industrial applications. CIRP Ann. **70**, 543–566 (2021). https://doi.org/10.1016/j.cirp.2021.05.007
28. Daskalakis, K.S., Väkeväinen, A.I., Martikainen, J.-P., Hakala, T.K., Törmä, P.: Ultrafast Pulse Generation in an Organic nanoparticle-array laser. Nano Lett. **18**, 2658–2665 (2018). https://doi.org/10.1021/acs.nanolett.8b00531
29. Kuehne, A.J.C., Gather, M.C.: Organic lasers: Recent developments on materials, device geometries, and fabrication techniques. Chem. Rev. **116**, 12823–12864 (2016). https://doi.org/10.1021/acs.chemrev.6b00172
30. Thomas, A., Kirilova, E.M., Nagesh, B.V., Manohara, S.R., Siddlingeshwar, B., Belyakov, S.V.: Synthesis, solvatochromism and DFT study of pyridine substituted benzanthrone with ICT characteristics. J. Mol. Struct. **1262**, 132971 (2022). https://doi.org/10.1016/j.molstruc.2022.132971
31. Altaf, Y., Ullah, S., Khan, F.A., Maalik, A., Rubab, S.L., Hashmi, M.A.: Finding New precursors for light harvesting materials: A computational study of the fluorescence potential of Benzanthrone Dyes. ACS Omega. **6**, 32334–32341 (2021). https://doi.org/10.1021/acsomega.1c05849
32. Maļeckis, A., Griškjāns, E., Cvetinska, M., Savicka, M., Belyakov, S., Kirilova, E.: Synthesis, characterization, spectroscopic studies and evaluation of toxicological effect on growth of wheat sprouts (Triticum aestivum) of new benzanthrone α-aryl-α-aminophosphonates. J. Mol. Struct. **1277**, 134838 (2023). https://doi.org/10.1016/j.molstruc.2022.134838
33. Gavarane, I., Kirilova, E., Rubeniņa, I., Mežaraupe, L., Osipovs, S., Deksne, G., Pučkins, A., Kokina, I., Bulanovs, A., Kirjušina, M.: A simple and rapid staining technique for sex determination of trichinella larvae parasites by confocal laser scanning microscopy. Microsc. Microanal. **25**, 1491–1497 (2019). https://doi.org/10.1017/S1431927619015046
34. Rubenina, I., Gavarane, I., Kirilova, E., Mezaraupe, L., Kirjusina, M.: Comparison of the Benzanthrone luminophores: They are not equal for Rapid Examination of Parafasciolopsis fasciolaemorpha (Trematoda: Digenea). Biomolecules. **11**, 598 (2021). https://doi.org/10.3390/biom11040598
35. Kirilova, E., Mickevica, I., Mezaraupe, L., Puckins, A., Rubenina, I., Osipovs, S., Kokina, I., Bulanovs, A., Kirjusina, M., Gavarane, I.: Novel dye for detection of callus embryo by confocal laser scanning fluorescence microscopy. Luminescence. **34**, 353–359 (2019). https://doi.org/10.1002/bio.3616
36. Tarabara, U., Kirilova, E., Kirilov, G., Vus, K., Zhytniakivska, O., Trusova, V., Gorbenko, G.: Benzanthrone dyes as mediators of cascade energy transfer in insulin amyloid fibrils. J. Mol. Liq. **324**, 115102 (2021). https://doi.org/10.1016/j.molliq.2020.115102
37. Gorbenko, G., Trusova, V., Kirilova, E., Kirilov, G., Kalnina, I., Vasilev, A., Kaloyanova, S., Deligeorgiev, T.: New fluorescent probes for detection and characterization of amyloid fibrils. Chem. Phys. Lett. **495**, 275–279 (2010). https://doi.org/10.1016/j.cplett.2010.07.005
38. Vus, K., Trusova, V., Gorbenko, G., Sood, R., Kirilova, E., Kirilov, G., Kalnina, I., Kinnunen, P.: Fluorescence investigation of interactions between Novel Benzanthrone dyes and Lysozyme amyloid fibrils. J. Fluoresc. **24**, 493–504 (2014). https://doi.org/10.1007/s10895-013-1318-3
39. Grabchev, I., Moneva, I., Wolarz, E., Bauman, D.: Fluorescent 3-oxy benzanthrone dyes in liquid crystalline media. Dyes Pigm. **58**, 1–6 (2003). https://doi.org/10.1016/S0143-7208(03)00033-0

40. Grabchev, I., Moneva, I.: Synthesis and properties of benzanthrone derivatives as luminophore dyes for liquid crystals. Dyes Pigm. **37**, 155–164 (1998). https://doi.org/10.1016/S0143-7208(97)00050-8
41. Konstantinova, T.N.: The synthesis of some benzanthrone derivatives for use as dyes for polymeric materials. Dyes Pigm. **10**, 63–67 (1989). https://doi.org/10.1016/0143-7208(89)85040-5
42. Kirilova, E., Bulanovs, A., Puckins, A., Romanovska, E., Kirilov, G.: Spectral and structural characterization of chromium(III) complexes bearing 7-oxo-7H-benzo[de]anthracen-3-yl-amidines ligand. Polyhedron. **157**, 107–115 (2019). https://doi.org/10.1016/j.poly.2018.09.072
43. Maļeckis, A., Avotiņa, L., Ķizāne, G., Pučkins, A., Osipovs, S., Kirilova, E.: New fluorescent heterocyclic compounds derived from 3-Cyanobenzanthrone. Polycycl. Aromat. Compd. **42**, 5508–5520 (2022). https://doi.org/10.1080/10406638.2021.1939068
44. Maeda, H., Maeda, T., Mizuno, K., Fujimoto, K., Shimizu, H., Inouye, M.: Alkynylpyrenes as Improved Pyrene-based Biomolecular Probes with the Advantages of High Fluorescence Quantum Yields and long Absorption/Emission wavelengths. Chem.---Eur. J. **12**, 824–831 (2006). https://doi.org/10.1002/chem.200500638
45. Chen, M., Wei, J., Zhang, Y., Wu, L., Tan, L., Shi, S., Shi, J., Ji, L.: 2,7-Carbazole derived organoboron compounds: synthesis and molecular fluorescence. Front. Chem. **9**, 754298 (2021). https://doi.org/10.3389/fchem.2021.754298
46. Yang, J., Dass, A., Rawashdeh, A.-M.M., Sotiriou-Leventis, C., Panzner, M.J., Tyson, D.S., Kinder, J.D., Leventis, N.: Arylethynyl substituted 9,10-Anthraquinones: Tunable Stokes shifts by Substitution and Solvent Polarity. Chem. Mater. **16**, 3457–3468 (2004). https://doi.org/10.1021/cm049590g
47. Yang, J.-X., Wang, X.-L., Wang, X.-M., Xu, L.-H.: The synthesis and spectral properties of novel 4-phenylacetylene-1,8-naphthalimide derivatives. Dyes Pigm. **66**, 83–87 (2005). https://doi.org/10.1016/j.dyepig.2004.07.015
48. Bai, J.-Y., Xie, Y.-Z., Wang, C.-J., Fang, S.-Q., Cao, L.-N., Wang, L.-L., Jin, J.-Y.: A quninolylthiazole derivatives as an ICT-Based fluorescent probe of hg(II) and its application in ratiometric imaging in live HeLa cells. J. Fluoresc. **28**, 795–800 (2018). https://doi.org/10.1007/s10895-018-2241-4
49. Yamaguchi, Y., Matsubara, Y., Ochi, T., Wakamiya, T., Yoshida, Z.: How the π conjugation length affects the fluorescence Emission Efficiency. J. Am. Chem. Soc. **130**, 13867–13869 (2008). https://doi.org/10.1021/ja8040493
50. Piskunov, A.V., Moroz, A.A., Shvartsberg, M.S.: Nucleophilic addition of secondary mines to acetylenylakthraquinones. Bull. Acad. Sci. USSR Div. Chem. Sci. **35**, 785–790 (1986). https://doi.org/10.1007/BF00954230
51. Wang, T., Zhang, N., Bai, W., Bao, Y.: Fluorescent chemosensors based on conjugated polymers with N-heterocyclic moieties: Two decades of progress. Polym. Chem. **11**, 3095–3114 (2020). https://doi.org/10.1039/D0PY00336K
52. Okamura, H., Trinh, G.H., Dong, Z., Fan, W., Nagatsugi, F.: Synthesis of 6-Alkynylated purine-containing DNA via On-Column Sonogashira Coupling and Investigation of their Base-Pairing properties. Molecules. **28**, 1766 (2023). https://doi.org/10.3390/molecules28041766
53. Kapusta, P., Machalický, O., Hrdina, R., Nepraš, M., Zimmt, M.B., Fidler, V.: Photophysics of 3-Substituted benzanthrones: Substituent and Solvent Control of Intersystem Crossing. J. Phys. Chem. A. **107**, 9740–9746 (2003). https://doi.org/10.1021/jp035610a
54. Sonogashira, K., Tohda, Y., Hagihara, N.: A convenient synthesis of acetylenes: Catalytic substitutions of acetylenic hydrogen with bromoalkenes, iodoarenes and bromopyridines. Tetrahedron Lett. **16**, 4467–4470 (1975). https://doi.org/10.1016/S0040-4039(00)91094-3
55. Chinchilla, R., Nájera, C.: The Sonogashira reaction: A booming methodology in Synthetic Organic Chemistry. Chem. Rev. **107**, 874–922 (2007). https://doi.org/10.1021/cr050992x
56. Chinchilla, R., Nájera, C.: Recent advances in Sonogashira reactions. Chem. Soc. Rev. **40**, 5084 (2011). https://doi.org/10.1039/c1cs15071e
57. Kanwal, I., Mujahid, A., Rasool, N., Rizwan, K., Malik, A., Ahmad, G., Shah, S.A.A., Rashid, U., Nasir, N.M.: Palladium and Copper Catalyzed Sonogashira cross Coupling an Excellent Methodology for C–C Bond Formation over 17 Years: A Review. Catalysts **10**(4), 443 (2020). https://doi.org/10.3390/catal10040443
58. Tsiko, U., Sych, G., Volyniuk, D., Bezvikonnyi, O., Keruckiene, R., Lazauskas, A., Grazulevicius, J.V.: Self-recovering mechanochromic luminescence of the derivatives of benzanthrone and carbazole: Towards damage-resistive information recording and security probes. Dyes Pigm. **199**, 110082 (2022). https://doi.org/10.1016/j.dyepig.2022.110082
59. Maļeckis, A., Griškjāns, E., Cvetinska, M., Kirilova, E.: 3-(Phenylethynyl)-7H-benzo[de]anthracen-7-one. Molbank **2022**(3), M1442 (2022). https://doi.org/10.3390/M1442

60. Rao, A.V.R., Vaidyanathan, A.: The 1H NMR spectrum of benzanthrone. Spectrochim Acta A. **37**, 145–146 (1981). https://doi.org/10.1016/0584-8539(81)80102-X
61. Vaidyanathan, A.: The carbon-13 NMR spectra of benzanthrone and its derivatives. Dyes Pigm. **3**, 243–248 (1982). https://doi.org/10.1016/0143-7208(82)80026-0
62. Olipova, M., Maļeckis, A., Pučkins, A., Kirilova, A., Romnovska, E., Kirilova, E.: Spectroscopic investigation of new benzanthrone luminescent dyes. Bul. Chem. Commun. **54**, 253–257 (2022)
63. Orlova, N., Nikolajeva, I., Pučkins, A., Belyakov, S., Kirilova, E.: Heterocyclic Schiff bases of 3-Aminobenzanthrone and their reduced analogues: Synthesis, properties and Spectroscopy. Molecules. **26**, 2570 (2021). https://doi.org/10.3390/molecules26092570
64. Maļeckis, A., Cvetinska, M., Puckins, A., Osipovs, S., Sirokova, J., Belyakov, S., Kirilova, E.: Synthesis and Properties of New 3-Heterylamino-substituted 9-Nitrobenzanthrone derivatives. Molecules. **28**, 5171 (2023). https://doi.org/10.3390/molecules28135171
65. Maļeckis, A., Cvetinska, M., Griškjāns, E., Dmitrijevs, K., Traskovskis, K., Belyakov, S., Kirilova, E.: Benzanthrone sulfides: Synthesis, solvatochromism characterization and analysis of experimental photophysical parameters and theoretical calculations. Dyes Pigm. **219**, 111599 (2023). https://doi.org/10.1016/j.dyepig.2023.111599
66. Cao, L., Xu, L., Zhang, D., Zhou, Y., Zheng, Y., Fu, Q., Jiang, X.-F., Lu, F.: D-A dyad and D-A-D triad incorporating triphenylamine, benzanthrone and perylene diimide: Synthesis, electrochemical, linear and nonlinear optical properties. Chem. Phys. Lett. **682**, 133–139 (2017). https://doi.org/10.1016/j.cplett.2017.06.015
67. Staneva, D., Vasileva-Tonkova, E., Kukeva, R., Stoyanova, R., Grabchev, I.: Synthesis, spectral characteristics and microbiological activity of benzanthrone derivatives and their Cu(II) complexes. J. Mol. Struct. **1197**, 576–582 (2019). https://doi.org/10.1016/j.molstruc.2019.07.087

Authors and Affiliations

Armands Maļeckis[1] · Marija Cvetinska[1] · Evans Griškjāns[1] · Elena Kirilova[2]

✉ Armands Maļeckis
armands5maleckis@inbox.lv

[1] Institute of Chemistry and Chemical Technology, Faculty of Natural Sciences and Technology, Riga Technical University, P. Valdena Str. 3, Riga LV-1048, Latvia

[2] Department of Environment and Technologies, Faculty of Natural Sciences and Healthcare, Daugavpils University, Parades Str. 1A, Daugavpils LV-5401, Latvia

Armands Maļeckis dzimis 1997. gadā Daugavpilī. Rīgas Tehniskajā universitātē ieguvis inženierzinātņu akadēmisko bakalaura grādu ķīmijas tehnoloģijā (2019), Daugavpils Universitātē (DU) – dabaszinātņu maģistra grādu ķīmijā (2021). 10 oriģinālpublikāciju līdzautors, astoņām no tām – korespondējošais autors. Patlaban ir organisko vielu ķīmiķis uzņēmumā "*Enamine Ltd*" un pētnieks DU, kur turpina pētījumus fluorescento vielu ķīmijā.

Armands Maļeckis was born in 1997 in Daugavpils. He obtained an academic Bachelor's degree in Engineering Sciences in Chemical Technology from Riga Technical University (2019) and a Master's degree in Natural Sciences in Chemistry from Daugavpils University (2021). He is a co-author of ten original publications, serving as the corresponding author for eight of them. Currently, he is an organic chemist at Enamine Ltd and continues his research in the chemistry of fluorescent compounds at Daugavpils University as a researcher.